Inflammatory mechanisms after ischaemic stroke: characterisation of central nervous system (CNS) border-associated macrophages (BAMs) and dimethylarginine dimethylaminohydrolase (DDAH2)

Gabriela Gerganova (MSci, MRes)

Submitted in fulfilment of the degree

Doctor of Philosophy

School of Cardiovascular and Metabolic Health

College of Medical, Veterinary and Life Sciences

University of Glasgow

April 2025

Total words: 45,656

Author's Declaration

I declare that this thesis was written by myself and provides a record of research performed by myself. For certain experiments, others were involved in practical aspects of the work:

- Dr Alyson Miller conducted my training for the *in vivo* surgical model and performed stroke surgeries for Chapter 3 and Chapter 5 with anaesthetic assistance from me.

- Dr Alyson Miller, Dr Alexandra Riddell, Dr Arun Flynn, Mrs Jawzaa Sulaiman S Alenazi and Ms Nicola Gilroy have supported surgical preparation, anaesthesia, and, on occasion, post-stroke animal monitoring.

- Dr Ashton Bernard, Dr Arun Flynn and Dr Emily Gallen performed flow cytometry data collection for a pilot study used for power calculations (Table 3-5) and for myeloid cells quantification for the 24-hour timepoint assessment (Figure 3-9).

- Stroke surgeries for immunofluorescent analyses for Chapter 3 have been performed by Dr Alyson Miller and Dr Arun Flynn. Cryo-sectioning has been conducted by Dr Arun Flynn (Figure 3-18-23).

- Stroke surgeries for Western blot analysis for Chapter 4 have been performed by Dr Alyson Miller and Dr Arun Flynn. Brain tissue harvest and protein extraction for has been conducted by Dr Arun Flynn (Figure 4-12).

- Ms Nicola Gilroy performed sample preparation for flow cytometric analysis (Figure 5-8, Figure 5-9, Figure 5-9) under my lab supervision. Madihah Hussain prepared samples for magnetic activated cell sorting (Figure 4-6, Figure 4-7) under my lab supervision.

- Ms Diane Vaugh and Ms Alana Hamilton performed cell sorting for myeloid cells (Figure 4-10) and have supported me to troubleshoot instrument and software failures during immunophenotyping.

- Genotyping of DDAH2 deficient mice was conducted by myself, Dr Alexandra Riddell or Mrs Elaine Friel (Figure 4-5).

- Dr Alexandra Riddell performed mouse brain cryosectioning for infarct and oedema volume analysis (Figure 5-2, Figure 5-13, Figure 5-14).

Contributions from others have been clearly stated where relevant in the thesis. For data generated with sample preparation help from others, data analysis, interpretation and presentation were conducted by myself. All research was

conducted in the BHF Glasgow Cardiovascular Research Centre and in the Sir Graeme Davies Building. This work has not been submitted previously for a higher degree and was supervised by Dr Alyson Miller and Prof James Leiper.

Impact Statement: COVID-19 and Personal Injury

The experimental work presented in this thesis commenced in October 2020, during the aftermath of the most stringent restrictions during the global COVID-19 pandemic. Local laboratory and animal facility restrictions and the ongoing need for isolation upon close contact with a seropositive person persisted into the middle of 2021. This notably affected *in vivo* surgical training, which underpins findings presented in Chapter 3 and Chapter 5 for the initial 6 months. Then in October 2022 I suffered a personal injury during an accident, which required me to undergo surgery and rehabilitation, and further slowed the progress of my experimental work for another 3-4 months. Together, these factors contributed to a reduced research output during the experimental phase of this project.

Acknowledgements

I am grateful to the British Heart Foundation for their financial support in conducting the research for this thesis.

Thank you to my supervisors Alyson Miller and James Leiper for everything you have done to support this research. Alyson, thank you for the laughter during the long days of surgeries and for all the guidance, even when I didn't take heed and made you climb a wall. I have learnt so much from you! James, thank you for always invigorating scientific curiosity in me.

Thank you, Laura Dowsett, Fiona Leiper, and Alex Riddell, for the unwavering support throughout my PhD and particularly towards the end when I was struggling the most. Laura, thank you for inviting me to write in your office and practically taking me under your wing.

Thank you to the lab group members, past and present: Nic, Jawzaa, Arun, Ashton, Emily, Erika, Corey, Erin, Zaniah, Noha, Sarah, thank you for all the conversations. You have all shaped the science that is presented here.

Thank you to my fellow PhD colleagues, SCMH staff and friends. Caitlin, Nic, Corey, Dora, Iain, Lara, Stelios, Manshi, thank you for the fun days and the annual pilgrimage to Belfast. Marianne, Cara, Rebecca, and Will (aka the SCMH running club), thank you for all the runs together and opportunities to vent about science doing science things. Erin, thank you for the numerous conversations about science, cats, gym, and life. Parisa, thank you for all the kind words of support and gym sessions together. Alice Main, I have you to blame for embarking on this journey back in 2018, for your encouragement to apply to the BHF programme and relentless enthusiasm to help me along the way. There is a huge number of people I want to extend my words of gratitude towards, for their pastoral and scientific support: Wendy, Josie, Nic, Wai, Blessy, Ryszard, Emma, Diane, Alana, Lorraine, Eleanor, Del, Martin, Alisha, Antoniya, Simon, Eleni, Jocelyn, Eilidh, Alex, Aisling, Jim, Marianne, Seonagh, Max. Enormous thank you all for being good listeners when things were not going my way and for all the laughter.

Thank you to my friends, Crinan, Amber, Seren, Roosa, Hanna, Simon, Hannah, Kirsten, Miriam, for all the fun times together and apologies for subjecting you to my research mishaps. I could not have written this thesis without having those days.

A huge thank you to my Mum for her love and incessant support, even when she wasn't sure the stress was worth it. Thank you to my grandmother Binka, my aunt Borislava, and my uncle Svet for nudging me along the way with ample support. Thank you to Mary & Alan Jeans for treating me like your daughter throughout this journey. Thank you to Anne Gallanagh for inviting us into her home for a year. I will never forget the generosity and kindness you have all shown me.

Thank you to the loved ones I lost during this journey: my grandfather Georgi, for teaching me how to ride a bike, so I can commute to the lab every day, and for all the small things; my great aunt Janka, for encouraging me to pursue a PhD and for the huge support whilst in Switzerland; my Dad, who I lost just shortly before I finished this thesis.

Michael, thank you for believing in me when I didn't believe in myself, and for waiting patiently for me to finish this, so we can both move on with our lives. You'll be relieved to see the back of this book almost as much as me. This thesis is dedicated to you.

List of publications, awards and presentations

- Gerganova, G., Riddell, A. & Miller, A. A. 2022. CNS border-associated macrophages in the homeostatic and ischaemic brain. Pharmacology & Therapeutics 240, 108220, doi: 10.1016/j.pharmthera.2022.108220.

- "To BAM or not to BAM?" People's Choice Award for the University of Glasgow's 2022 Three Minute Thesis.

- "Accumulation of CD206+LYVE1+ brain-associated macrophages beyond the period of infarct development after experimental ischaemic stroke in mice" Oral presentation on 3rd June 2022 at the British Heart Foundation's 4-Year PhD Programme Student Conference, Leeds, United Kingdom.

- "Evidence that CD206+LYVE1+ border-associated macrophages accumulate beyond the period of infarct development after ischaemic stroke" Oral presentation and poster during 29th May – 1st June 2022 at the International Brain and Brain PET Conference, Scottish Event Campus, Glasgow, United Kingdom.

- "Characterisation of CNS border-associated macrophages (BAMs) after ischaemic stroke" Poster presentation on 26th October 2023 at the Early Career Life Scientists' Symposium in Vascular Brain Health, The Mazumdar-Shaw Advanced Research Centre, University of Glasgow, United Kingdom.

“Anything more is not necessary, anything less is not enough”

Abstract

Central nervous system (CNS) border-associated macrophages (BAMs) are a rare and specialised population of immune cells in the brain with emerging functions in ischaemic stroke. Preliminary work from our group has identified BAMs as $CD45^{+high}CD11b^{+}CD206^{+}Lyve1^{+}$ cells by flow cytometry and indicated increased numbers of BAMs 24 hours following stroke in a mouse model of focal ischaemic stroke (transient middle cerebral artery occlusion, tMCAo). Work presented in this thesis establishes the accumulation of BAMs beyond the period of infarct development. The numbers of BAMs in the ipsilateral hemisphere after tMCAo increased in the acute phase after stroke, peaked one week later and subsequently declined in the chronic stages. BAMs were identified in perivascular and in meningeal spaces as $CD206^{+}\alpha SMA^{+}$ and $CD206^{+}Lyve1^{+}$ cells and their localisation with respect to the infarct and peri-infarct zones was investigated.

The signalling molecule nitric oxide (NO) has deleterious roles in ischaemic stroke and macrophages are an immune cell source of inducible nitric oxide synthase (iNOS)-produced NO. Work from Prof Leiper's lab has shown that dimethylarginine dimethylaminohydrolase (DDAH2) enzymatically regulates NO signalling in hypoxic and septic conditions and thereby controls macrophage function. Work presented here demonstrates that *Ddah2* mRNA expression increased following oxygen and glucose deprivation in RAW264 macrophage cell line, while DDAH2 protein levels remained unchanged after tMCAo in C57BL6/J mice. The expression of the pro-inflammatory genes *Il-1β, Tnfα, Il-6* and *Ccl2* was reduced in peritoneal macrophages from naïve monocytes/macrophages specific *Ddah2* knockout mice, indicating that DDAH2 may regulate the inflammatory phenotype of these cells.

To explore the potential implications of DDAH2-mediated altered macrophage phenotype on ischaemic stroke outcomes, a study was conducted in monocytes/macrophages specific *Ddah2* knockout mice. Preliminary evidence suggests that infarct and oedema volume did not differ between knockout and control mice. There was a slight reduction in neurological deficit and reduced levels of apoptosis in knockout mice after tMCAo. The rate of immune cell infiltration into the brain after tMCAo was not altered, as the numbers of total leukocytes, myeloid cells and lymphocytes were comparable between genotypes.

This thesis reinforces the emerging significance of BAMs in the pathophysiology of ischaemic stroke. Through detailed characterisation and temporal mapping, it establishes BAMs as dynamic responders that accumulate during the acute and subacute phases of stroke and recede in the chronic stages. Although modulation of nitric oxide signalling via DDAH2 showed limited impact on infarct size and immune infiltration, subtle improvements in neurological deficits and reduced apoptosis suggest that DDAH2 may fine-tune the inflammatory profile of macrophages in ways that are neuroprotective. These findings open a window into targeted immune modulation as a therapeutic avenue in stroke recovery.

This work points to a paradigm shift in how we understand neuroimmune regulation in stroke. Far from being passive residents at CNS borders, BAMs may play active, time-sensitive roles in brain injury and repair. By linking BAM behaviour with nitric oxide signalling and the regulatory role of DDAH2, the thesis lays groundwork for future exploration into cell-specific interventions—aimed not at altering infarct size, but at refining the inflammatory environment to promote neurological resilience. The immune landscape of the brain is more intricate than previously assumed, and the key to healing might lie not in suppressing inflammation broadly, but in sculpting it precisely.

Table of Contents

List of Tables

List of Figures

Definitions/Abbreviations

7-AAD	7-aminoactinomycin d
ADMA	Asymmetric dimethylarginine
ANOVA	Analysis of variance
APC	Allophycocyanin
APC-Cy7	Allophycocyanin-cyanine 7
ARG-1	Arginase-1
ATP	Adenosine triphosphate
BAM	Central nervous system (CNS) border-associated macrophages
BBB	Blood-brain barrier
BDNF	Brain-derived growth factor
BMDM	Bone-marrow derived macrophages
BV785	Brilliant violet 785
CBF	Cerebral blood flow
CCR2	C-c chemokine receptor type 2
CD	Cluster of differentiation
CD11b	Integrin alpha m (itgam) or macrophage antigen-1 (mac-1)
CD19	Cluster of differentiation 19, b-lymphocyte surface antigen b4
CD206	Mannose receptor c type 1
CD3	Protein complex and T cell co-receptor involved in activating T cells
CD45	Protein tyrosine phosphatase receptor type c (ptprc) or leukocyte-common antigen
CNS	Central nervous system
CSF	Cerebrospinal fluid
CSF1	Colony stimulating factor 1
CSF1R	Macrophage colony-stimulating factor-1 receptor
CX3CR1	Cx3c motif chemokine receptor 1
DAMP	Damage-associated molecular pattern
DAPI	4′,6-diamidino-2-phenylindole
DDAH2	Dimethylarginine dimethylaminohydrolase 2
DMEM	Dulbecco's modified eagle medium
EDTA	Ethylenediaminetetraacetic acid
ERK	Extracellular signal-regulated kinase
EVT	Endovascular thrombectomy
FACS	Fluorescence activated cell sorting
FBS	Foetal bovine serum
FITC	Fluorescein isothiocyanate
HIF-1α	Hypoxia-inducible factor-1 alpha
HSC	Haematopoietic stem cell
ICAM-1	Intercellular adhesion molecule-1
IL-10	Interleukin-10
IL-1ß	Interleukin-1 beta
IL-6	Interleukin-6
iNOS	Inducible nitric oxide synthase

IVT	Intravenous thrombolysis
Ly6C	Lymphocyte antigen 6 complex
Ly6G	Lymphocyte antigen 6 complex, locus g
LYVE1	Lymphatic vessel endothelial hyaluronan receptor 1
Lyz2	Lysozyme c-2 precursor
MACS	Magnetic activated cell sorting
MCA	Middle cerebral artery
MCAo	Middle cerebral artery occlusion
mGluR	Metabotropic glutamate receptors
MHCII	Major histocompatibility complex class ii
MMP	Matrix metalloproteases
mNSS	Modified neurological severity score
NF-κB	nuclear factor kappa-light-chain-enhancer of activated B cells
NMDAR	N-methyl-d-aspartate receptors
NO	Nitric oxide
NOS	Nitric oxide synthase
OGD	Oxygen glucose deprivation
OXPHOS	Oxidative phosphorylation
PBS	Phosphate buffered saline
PE	Phycoerythrin
PE-Cy7	Phycoerythrin-cyanine 7
PerCP-Cy5.5	Peridinin chlorophyll protein-cyanine 5.5
PFA	Paraformaldehyde
PPARγ	Peroxisome proliferator-activated receptor-γ
PVS	Perivascular space
qRT-PCR	Quantitative real-time polymerase chain reaction
RT	Room temperature
scRNAseq	single cell RNA sequencing
SDS	Sodium dodecyl sulfate
SEM	Standard error of the mean
STAT	Signal transducer and activator of transcription
TBS	Tris buffered saline
TGF-ß	Transforming growth factor beta
tMCAo	Transient middle cerebral artery occlusion
TNF-α	Tumour necrosis factor alpha
TUNEL	Terminal deoxynucleotidyl transferase dutp nick end labelling
V500	Violet 500
VEGF	Vascular endothelial growth factor
αSMA	smooth muscle actin

1 Chapter 1: General Introduction

1.1 Vascular anatomy of the brain

The brain is perfused by a network of arteries, veins, arterioles, venules, and a dense capillary network. Arterial supply to the brain is extracranially supported by the common carotid arteries (CCA) and basilar arteries (BA), which feed oxygenated blood to the Circle of Willis, a ring-like intracranial structure consisting of the anterior and posterior communicating arteries, that supplies blood to the brain and creates redundancy if the internal carotid artery (ICA) or BA are occluded. The anterior (ACA), posterior (PCA) and middle cerebral arteries (MCA) each perfuse specific cerebral territories. The common carotid arteries bifurcate into external (ECA) and internal (ICA) branches. The distal portion of the ICA is located within the cranium and gives rise to the proximal branches of the MCA (Figure 1-1). The MCA supplies the lateral surface of the cortex and mid-brain territories, such as the dorsal striatum, the caudate putamen, the thalamus and hypothalamus with oxygenated blood and consists of several consecutively smaller branches (Patel et al., 2008).

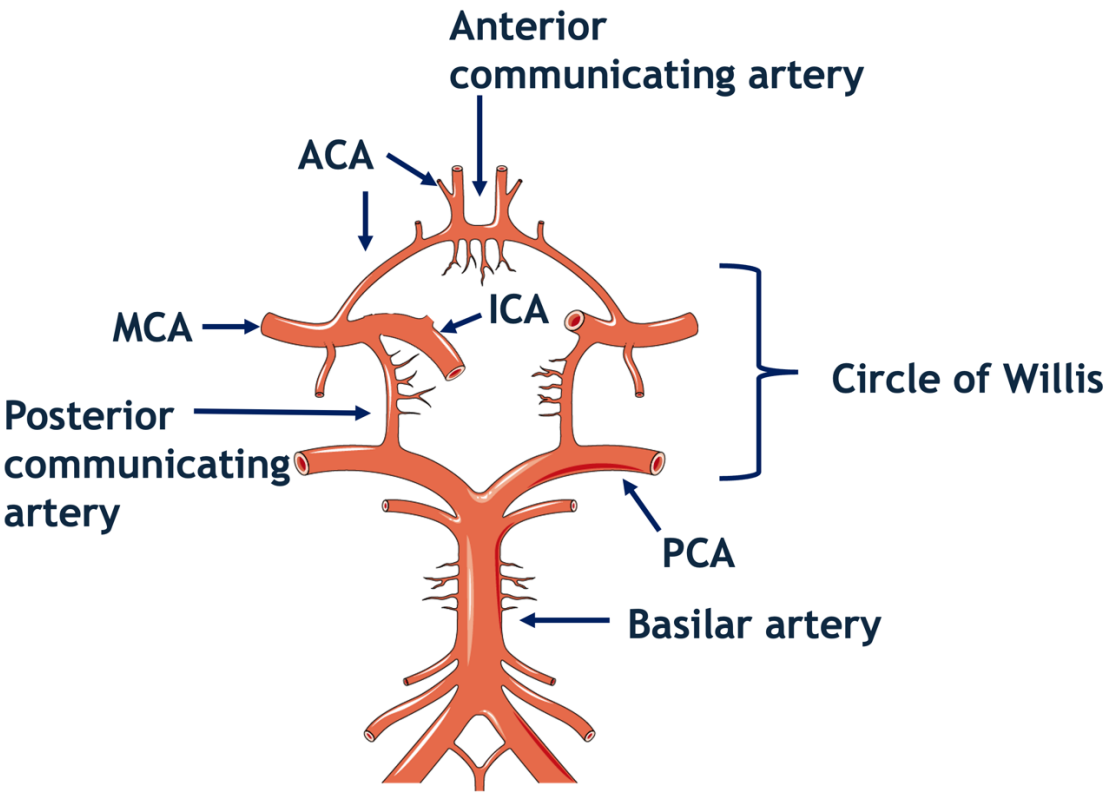

Figure 1-1. Intra-cranial arterial system. The internal carotid arteries (ICA) and basilar arteries supply oxygenated blood to the Circle of Willis, comprising of the anterior and posterior communicating arteries. Blood then travels further to the cortex and midbrain through the anterior (ACA), middle (MCA) and posterior (PCA) cerebral arteries. Image created with elements freely available on Smart Servier Medical Art.

1.2 Stroke

1.2.1 Aetiology and epidemiology of stroke

Stroke is the disruption of blood supply to an area in the brain. Ischaemic stroke is the most common type of stroke and is typically caused by occlusion of a large cerebral artery, with at least every second clinical case affecting the MCA (Figure **1-1**) and its branches (Bogousslavsky et al., 1988, Chung et al., 2014). Intracranial atherosclerotic stenosis is recognised clinically as one of the most common causes of ischaemic stroke (Holmstedt et al., 2013). It is caused by a blood clot formed either at a site of arterial stenosis (thrombus), or elsewhere in the body (embolus) and carried to the stenosed artery. Blood clots are formed by a coagulation cascade of thrombus formation, activation of Factor X, conversion of prothrombin to thrombin and fibrinogen to fibrin monomers and polymers (Flores et al., 2014). Haemorrhagic stroke is caused by an intracerebral haemorrhage – a rupture of an intracerebral artery, while subarachnoid haemorrhage is typically caused by brain trauma resulting in bleeding inside the subarachnoid space between the dural and pial meningeal layers. Rarer stroke subtypes include anterior and posterior circulation strokes, occlusions of deeper penetrating arterioles that cause multiple small lacunar infarcts, basilar artery occlusion, and the latter accounts for only 1% of all strokes (Alemseged et al., 2023).

The World Stroke Organization (WSO) estimates that every fourth person will have a stroke in their lifetime and more than 12 million people have a stroke each year, with 6.6 million deaths per annum caused as a result (http://world-stroke.org). Globally 63% of incident strokes per annum are ischaemic, 28% occur due to intracerebral haemorrhage and 9% are derived from subarachnoid haemorrhage (Hering et al., 2024). By 2019 about 77 million people were documented to have survived a stroke (Feigin et al., 2022), resulting in stroke being the leading cause of long-term disability (Benjamin et al., 2019, Campbell et al., 2019). In 2022/23 136,641 stroke patients were admitted to hospital in the UK and cerebrovascular diseases caused 34,000 deaths (BHF, 2024). These figures demonstrate that despite advances in the treatment and prevention of stroke, it remains a major global health burden.

1.2.2 Risk factors and co-morbidities for ischaemic stroke

Risk factors for ischaemic stroke can be classified into metabolic (>130 mmHg systolic blood pressure, high body mass index, high fasting plasma glucose, high total cholesterol, and low glomerular filtration rate); behavioural (poor diet, smoking, alcohol consumption and low physical activity); and environmental (air pollution and lead exposure). Overall, the greatest modifiable risk factor is hypertension, which is in turn affected by non-modifiable risk factors, such as age, genetics, ethnicity, pregnancy, and co-morbidities, and by some of the behavioural factors mentioned above (Lauder et al., 2022). A common co-morbidity in hypertensive patients and a risk-factor for stroke patients is atrial fibrillation (Feigin et al., 2022).

1.2.3 Current treatment for ischaemic stroke

The therapeutic objective for acute ischaemic stroke is to restore blood flow to brain areas distal to the occlusion, which contain functionally compromised but viable cells, and to protect brain parenchymal tissue from dying. The first clinically approved pharmacological therapy for ischaemic stroke was intravenous thrombolysis (IVT) with the recombinant tissue plasminogen activator (rt-PA) alteplase. This drug attaches to fibrin on the clot surface, activates fibrin-bound plasminogen, which cleaves and activates plasmin. The activated plasmin then breaks up the molecules of fibrin to dissolve the clot (Reed et al., 2025). Alteplase was initially approved for use within 3 hours after stroke onset (NINDS, 1995), and later extended to 4.5 hours (Hacke et al., 1998), which is in the current European Stroke Association's guidelines (Berge et al., 2021). Past this timepoint, there is an increased risk for symptomatic intracranial haemorrhage (ICH), which is a rare but a severe treatment complication (Jickling et al., 2014, Emberson et al., 2014, Yaghi et al., 2017). Evidence from earlier trials suggested that rt-PA is safe and effective 4.5-6 hours after onset of symptoms (Wang et al., 2015), in patients waking up with stroke and carefully selected through imaging (Wang et al., 2015, Thomalla et al., 2018).

1.2.4 Recent advances in treatment

For over three decades, intravenous alteplase has been the primary thrombolytic agent for treating acute ischaemic stroke. However, recent clinical trials over the past two years have shown that a genetically modified variant of alteplase – tenecteplase, is non-inferior to alteplase for acute ischaemic stroke. The TASTE trial (Tenecteplase versus Alteplase for Stroke Thrombolysis Evaluation with Perfusion Imaging Selection within 4.5 hours of Onset) only included patients with a proven tissue target for reperfusion treatment, identified through modern brain imaging techniques measuring salvageable tissue ('target mismatch'), significantly supports this shift (Parsons et al., 2024).

The advances in medical engineering in the late 2010s have revolutionised treatment for patients with large vessel stroke who received IVT but were not showing significant improvement (Bracard et al., 2016). Endovascular thrombectomy (EVT), which involves mechanical removal of the blood clot, was approved in the US for use up to 6 hours from time last known well (as opposed to symptoms onset, which could be missed) (Powers et al., 2018). EVT was reported safe up to 24 hours post stroke in the DAWN clinical trial (Nogueira et al., 2018) and effective at 6-16 hours in the DEFUSE trial in patients selected by perfusion imagining (Albers et al., 2018). More recently it was proposed that EVT is effective even after 24 hours from last known well in patients carefully selected by perfusion imaging (Shaban et al., 2023). While these extended therapeutic windows are yet to be approved, there is evidence that up to a third of patients in the US received thrombectomy past the 6 hour cut-off, however this resulted in higher in-hospital mortality, poorer ambulation at discharge and less frequent discharge to home compared to patients receiving it within 6 hours (Zachrison et al., 2021). Recent studies comparing direct EVT with IVT followed by EVT have shown non-inferiority for IVT followed by EVT (Campbell et al., 2018, Campbell et al., 2020, Fischer et al., 2022). In these trials, alteplase was the most used thrombolytic drug (Fischer et al., 2022), while tenecteplase was used in fewer patients (Campbell et al., 2018). While recanalisation therapy is widely used, preclinical efforts to develop neuroprotective strategies have not resulted in available drugs.

1.2.5 Recent advances in prevention

Anti-inflammatory treatments such as canakinumab or colchicine have been shown to be effective in the secondary prevention of cardiovascular disease (CVD), including ischaemic stroke in several trials such as CANTOS (Ridker et al., 2017), COLCOT (Bouabdallaoui et al., 2020), and LoDoCo2 (Nidorf et al., 2019) trials, leading to the approval of colchicine for CVD prevention by both the US Food and Drug Administration (FDA) and the European Medicines Agency (EMA). While a future for these treatments in intervention rather than in prevention is uncertain, therapeutic effects of canakinumab and cochicine have been shown in experimental stroke (Liberale et al., 2018, Meyer-Lindemann et al., 2022).

1.3 Mechanisms of ischaemic infarct development

The vascular occlusion renders the distal vascular territory ischaemic, with a dramatic reduction in oxygen and glucose content. The infarct core is severely ischaemic, and the cerebral blood flow (CBF) is reduced to 8-10 mL/100 g/min, or <10% baseline. The zone around the core, known as the penumbra or peri-infarct, maintains CBF of 11-35 mL/100 g/min, while areas adjacent to the penumbra where CBF is closer to normal are experiencing oligaemia with 36-50 mL/100 g/min. Normal CBF is 50-60 ml/100g/min (Bandera et al., 2006, Lewis, 2014, Velly et al., 2018) (Figure 1-2).

Figure 1-2. The sliding scale of cerebral blood flow (CBF) after ischaemic stroke in humans.

If the brain does not undergo reperfusion, the penumbra may remain viable for days or weeks due to the recruitment and opening of collateral blood vessels (Ramos-Cabrer et al., 2011). Higher density of collateral vessels is associated with reduced infarct volume and enhanced functional outcome after stroke (Ravindran et al., 2021). Prolonged ischaemia increases the propensity of the penumbra to subsume into the infarct core, and infarct size positively correlates with neurological severity (Tan et al., 2009). If reperfusion occurs, the penumbra can be salvaged but is also subjected to reperfusion injury due to the reoxygenation and oxidative stress (Eltzschig and Eckle, 2011, Zhang et al., 2022).

Oxygen and glucose deficiency disrupts oxidative phosphorylation (OXPHOS), which is followed by adenosine triphosphate (ATP) depletion and ionic imbalance, and results in cellular membrane depolarisation, influx of calcium (Ca^{2+}) and other positively charged ions, and extracellular accumulation of the excitatory amino acid glutamate. A series of events are governed by intra- and inter-cellular biochemical and signalling pathways known as the ischaemic cascade (Moskowitz et al., 2010, Xing et al., 2012) and lead to neuronal cell death and trigger neuroinflammation.

1.3.1 Excitotoxicity

The earliest mechanism in the ischaemic cascade is excitotoxity, which begins with uncontrolled release of excitatory neurotransmitter glutamate due to anoxic depolarisation in dying neurons and glial cells (Lai et al., 2014, Belov Kirdajova et al., 2020). It was first described in the hypothalamus of infant mice over half a century ago (Olney, 1971) and is a common mechanism to neurological disorders, including traumatic brain injury (Yi and Hazell, 2006), Alzheimer's disease (Rudi et al., 2004), Parkinson's disease (Verma et al., 2018) and Huntington's chorea (Fan and Raymond, 2007). It is underpinned by overstimulation of the ionotropic N-methyl-D-aspartate receptor (NMDAR) through excessive agonistic action of glutamate, and acts to increase intracellular calcium in neurons (Hazell, 2007). The ensuing influx of Ca^{2+} leads to the activation of various intracellular complexes, which are partly responsible for excitotoxicity. Excess calcium binds to calmodulin to activate neuronal nitric oxide synthase (nNOS), which facilitates bringing NMDAR and nNOS in close proximity by the scaffolding protein postsynaptic density 95 (PSD95) (Dawson et al., 1993), thereby initiating nitric oxide inhibition of mitochondrial cytochrome oxidase and cell death (Brown and Cooper, 1994). Another mechanism for neuronal and glial cell death is through the death-associated protein kinase (DAPK)-p53 complex, which is a downstream effector of the apoptotic and necrotic pathways (Pei et al., 2014). Ionic imbalances contribute to water accumulation in the extracellular spaces and the development of oedema (brain swelling). These early events occur in the minutes after stroke and contribute the greatest to the core injury.

1.3.2 Oxidative stress

The brain is highly vulnerable to energy failure arising from lack of oxygen and glucose. Despite making up only about 2% of body weight, the brain receives around a fifth of the body's total oxygen (Clarke and Sokoloff, 1999). Furthermore, the brain has low glycogen storage capacity and high metabolic demand for glucose (Dienel, 2019). This is primarily handled by mitochondrial OXPHOS to produce ATP by reducing molecular oxygen to water using the electron transport chain. After ischaemic stroke the deficits in O_2 and glucose, along with excitotoxicity and calcium overload, contribute to deficiency in the mitochondrial respiratory chain and its functional switch from production of ATP to production of reactive oxygen species (ROS) such as superoxide O_2^- (Rodrigo et al., 2013). In endothelial cells excess Ca^{2+} activates other ROS producing enzymes, which may in turn lead to endothelial NOS uncoupling from production of NO to production of ROS (Montezano and Touyz, 2012). The reaction of superoxide with nitric oxide generates downstream products such as peroxynitrite $ONOO^-$ (Jurcau and Ardelean, 2022). The resultant oxidative stress affects cells in ischaemic and penumbral sites, and typically begins in the first hours after stroke (Allen and Bayraktutan, 2009). During the chronic phases of stroke, inflammatory cells make a large contribution to the generation of ROS (Alexandrova and Bochev, 2005).

1.4 Cell death

Cellular death after ischaemic injury is primarily due to necrosis and apoptosis (Unal-Cevik et al., 2004), while other mechanisms of cell demise have also been characterised in the context of ischaemic stroke (Zhang et al., 2022). Morphological and biochemical features of both apoptosis and necrosis are often concomitantly present in dying ischaemic cells, and can be induced by multiple triggers, such as Ca^{2+} overload or oxidative stress (Sekerdag et al., 2018).

1.4.1 Necrosis

Necrosis involves disruption in cellular organelles, the intracellular release of proteolytic enzymes and phospholipases from lysozymes and the subsequent degradation of nucleic acids and proteins (Hajibabaie et al., 2023). Na^{2+} concentrations increase in the cell due to failure of the Na/K ATPase pump and

water influx then occurs due to diffusion. Subsequently plasma membranes burst and the released cellular debris into the extracellular environment attract inflammatory cells. During ischaemia increased intracellular calcium causes endoplasmic reticulum (ER) stress, and promotes the catalytic activity of proteases, nucleases, and lipases, causing the degradation of key proteins, nucleic acids, and the plasma membrane and irreversibly damages the cell.

1.4.2 Apoptosis

Apoptosis is a form of programmed cell death, characterised by shrinking of the cells, which are then tagged for elimination by phagocytic cells (Nagata, 2018). In contrast to necrosis, plasma membranes retain cellular contents, which acts to prevent cytotoxic signals to be released. Apoptosis is mediated through mitochondria-dependent pathways and by tumour necrosis factor alpha (TNFα) cell signalling pathways (Mao et al., 2006). They both converge on the activation of the effector caspase 3, which initiates DNA fragmentation, protein misfolding and cytoskeletal breakdown. Excess calcium accumulation within mitochondria (Pivovarova and Andrews, 2010, Gouriou et al., 2011), and pro-apoptotic factors, such as the Bcl-2 family of proteins such as Bax, permeabilise the mitochondrion's outer membrane and cause the cytosolic release of cytochrome C (Arnoult et al., 2002) (Hüttemann et al., 2012),, which is the primary inducer of caspase-dependent apoptosis. Cytochrome C activates caspase 9 that subsequently activates caspase 3 (Pan et al., 2001). Additionally, apoptosis-inducing factor (AIF) is released from the inner membrane of mitochondria and translocates to the nucleus to promote a caspase-independent apoptosis (Tuo et al., 2022).

1.4.1 Brain repair mechanisms

Neuronal repair is facilitated by cells within the neurovascular unit, which includes endothelial cells, pericytes, neurons, astrocytes, microglia, and oligodendrocytes (Iadecola and Anrather, 2011, Schaeffer and Iadecola, 2021). These cells produce and secrete crucial molecules to clear cell debris and repress inflammation. In endothelial cells hypoxia induces the expression of vascular endothelial growth factor (VEGF), which contributes to angiogenesis (Marti et al., 2000). Neurotrophic factors such as brain-derived growth factor (BDNF) and basic fibroblast growth factor are released from astrocytes and oligodendrocytes. BDNF

has been described as potential predictive biomarker for functional recovery after stroke (Luo et al., 2019) and upregulation of BDNF is correlated with enhanced rehabilitation (Sun et al., 2014). Transforming growth factor beta (TGF-β) is a strong anti-inflammatory cytokine (see below section 1.5.1) produced and released from astrocytes and microglia (Doyle et al., 2010). Evidence suggests that TGF-β signalling is sufficient to reduce infarct volume, reduce neuronal apoptosis and promote neurogenesis (Ma et al., 2008).

Astrocytic end-feet form a glial scar around the necrotic tissue through a process called gliosis, which helps to contain the excitotoxic spread of depolarisation and maintain ionic homeostasis, as well as acting as a physical barrier to spreading inflammation into the penumbra (O'Shea et al., 2024). Conversely, the glial scar contributes to prevention of axonal regeneration, possibly in conjunction with perineuronal nets, a specialised extracellular matrix structure, which acts as an inhibitor of neural plasticity (Campbell et al., 2019). White matter loss (Rosenzweig and Carmichael, 2013), demyelination and Wallerian degeneration, which is an active process of axon self-destruction (Xie et al., 2011), are also observed after stroke and are facilitated by excitotoxicity in oligodendrocytes. Remyelination failure has been attributed to the activation of Nogo receptors of oligodendrocyte progenitors and their blockade in aged mice enhances functional outcomes (Sozmen et al., 2016).

Dying neurons and glial cells release the nucleotides UTP and ATP, which activate microglia (cf. section 1.5.2.3) through $P2Y_2$ receptors to produce pro-inflammatory mediators (Krieglstein et al., 2002). The immunomodulatory effects of microglia include phagocytosis of cell debris from apoptotic cells via several signalling pathways. Nucleotides acting on $P2Y_6$ receptors activate phagocytosis in microglia (Koizumi et al., 2007) and phosphatidylserine-binding proteins expressed on apoptotic cells are recognised by mucin domain-containing molecule 4 (Tim4) receptors on microglia (Miyanishi et al., 2007). Inhibition of $P2Y_6$ receptors has been reported as deleterious in ischaemic stroke due to reduced microglial phagocytosis (Wen et al., 2020), strongly supporting a role for microglia in the brain repair process.

1.5 Immune system

The immune system is responsible for protecting the body from harm by patrolling and identifying pathogens, tumour cells and cellular debris. It is composed of primary immunogenic organs such as the thymus and the bone marrow for lymphocytes maturation, and secondary immune organs that contain mature T and B cells such as the spleen, lymph nodes, tonsils, and Peyer's patches. Cells of the immune system are collectively known as leukocytes or white blood cells and are primarily derived from adult hematopoietic stem cells (HSC) in the bone marrow (Kandarakov et al., 2022), while some niche macrophages arise from the yolk sac (Sheng et al., 2015, Gomez Perdiguero et al., 2015) and will be discussed further below.

1.5.1 Cytokines

Immune cells communicate with each other and other cell types through the production and release of small molecular weight proteins known as cytokines. Cytokines have important regulatory and intercellular mediatory roles in health and disease (Liu et al., 2021a). There are several large families of cytokines, which include interleukins, chemokines, interferons, and tumour necrosis factors. Each cytokine acts as a ligand for a coordinate receptor and activates a signal transduction pathway that is broadly classified as either pro-inflammatory or anti-inflammatory. Examples of pro-inflammatory cytokines include interleukin 1 beta (IL-1β), chemokine (C-C motif) ligand 2 (CCL2), tumour necrosis factors alpha (TNFα) and interferon gamma (INFγ), while TGF-β, IL-4, IL-10, and IL-13 are classically anti-inflammatory. CCL2, also known as monocyte chemoattractant protein-1 (MCP-1), is a critical inflammatory cytokine secreted by immune cells, which regulates leukocyte recruitment during inflammatory responses (Boring et al., 1997).

1.5.2 Innate immunity

The innate immune system constitutes monocytes, macrophages, polymorphonuclear cells (granulocytes), dendritic cells, mast cells and natural killer cells. These cells are first responders to a pathogenic attack or a localised tissue disruption. Their main aim is to contain the injury to a specific site and

attract cells from the adaptive immune branch to neutralise the attack. A common mechanism by which innate immune cells uptake and neutralise foreign particles and cellular particulates within their plasma-membrane envelope is phagocytosis. In addition, the complement system is the humoral branch of the innate immunity, comprised of soluble proteins, which are triggered by foreign entities such as pathogens, antibodies, extracellular vesicles, and some nanomedicines, and by the serial help of several convertases form a protein complex SC5b-9, which permeabilises and neutralises the target.

1.5.2.1 Monocytes and macrophages

Monocytes and macrophages are a family of mononuclear myeloid leukocytes and professional phagocytic innate immune cells present in all tissues. They originate from erythromyeloid progenitors in the embryonic yolk sac (Gomez Perdiguero et al., 2015, Sheng et al., 2015) that give rise to HSCs, which migrate to the foetal liver (Ciriza et al., 2013). After post-natal bone formation, HSCs develop into bone marrow derived monocytes (BMDM) (Winkler et al., 2010) and monocytes in primary immunogenic organs such as the spleen and thymus. Some of these monocytes circulate in the blood, while others migrate into tissues and give rise to adult tissue-resident macrophages through definitive haematopoiesis and adopt a functional phenotype suited to that tissue in health and disease (Epelman et al., 2014, Wynn and Vannella, 2016). Tissue specific factors serve to maintain the committed macrophages through self-proliferation and determine the expression of niche genes (T'Jonck et al., 2018).

Macrophages actively surveille their environment, neutralise pathogens and maintain overall homeostasis by phagocytosing cellular debris. Macrophages also act as antigen presenting cells by processing and presenting antigens on the major histocompatibility complex II to T-cells, consequently activating the adaptive immune system (Guerriero, 2019). Additionally, macrophages can physically ligate two damaged ends of a damaged endothelial cell by using mechanical traction (Liu et al., 2016).

1.5.2.2 Monocytes polarisation

Monocytes-derived macrophages exert their actions by polarising from *M0* macrophages into classically activated (pro-inflammatory) M1 macrophages, or alternative (anti-inflammatory) M2 phenotypes (Figure 1-3). M1 phenotypes arise from several cellular and molecular factors, such as activation of transcription factors nuclear factor kappa-light-chain-enhancer of activated B cells (NF-κB) and signal transducer and activator of transcription 1 (STAT1) (Lyu et al., 2021). Lipopolysaccharide (LPS), IFN-γ, TNFα and Granulocyte-macrophage colony-stimulating factor (GM-CSF) activate pattern recognition receptors (PRRs) like Toll-like receptors (TLRs) on macrophages and drive M1 polarisation (Koncz et al., 2023). M1 macrophages are typically identified by secretion of pro-inflammatory cytokines such as TNF-α, IL-6, IL-1β and hypoxia promotes hypoxia-inducible factor-1 alpha (HIF-1α) (Zis et al., 2015). M1 macrophages express cell surface markers such as CD16, CD32, CD86, and major histocompatibility complex class II (MHCII) (Figure 1-3).

Upon stimulation of *M0* macrophages with TGF-β, IL- 10, colony stimulating factor 1 (CSF1) and IL-33 (Gadani et al., 2015), the transcription factors peroxisome proliferator-activated receptor-γ (PPARγ), nuclear factor erythroid 2-related factor 2 (Nrf2) and STAT6 get activated and *M0* polarise into anti-inflammatory M2-like phenotypes (Cai et al., 2019) (Figure 1-3). M2-like macrophages secrete anti-inflammatory mediators such as TGF-β, IL- 10 or IL-4, IL-13, arginase-1 (*Arg-1*), and chitinase-like 3 (Benakis et al., 2015) and express the pathogen pattern recognition receptor CD206 (also known as mannose receptor C type 1 [*Mrc1*]). PPARγ can be activated by fatty acids and eicosanoid metabolites, and acidic environments and neuron-derived exosomes carrying miRNAs can skew toward M2-like phenotypes.

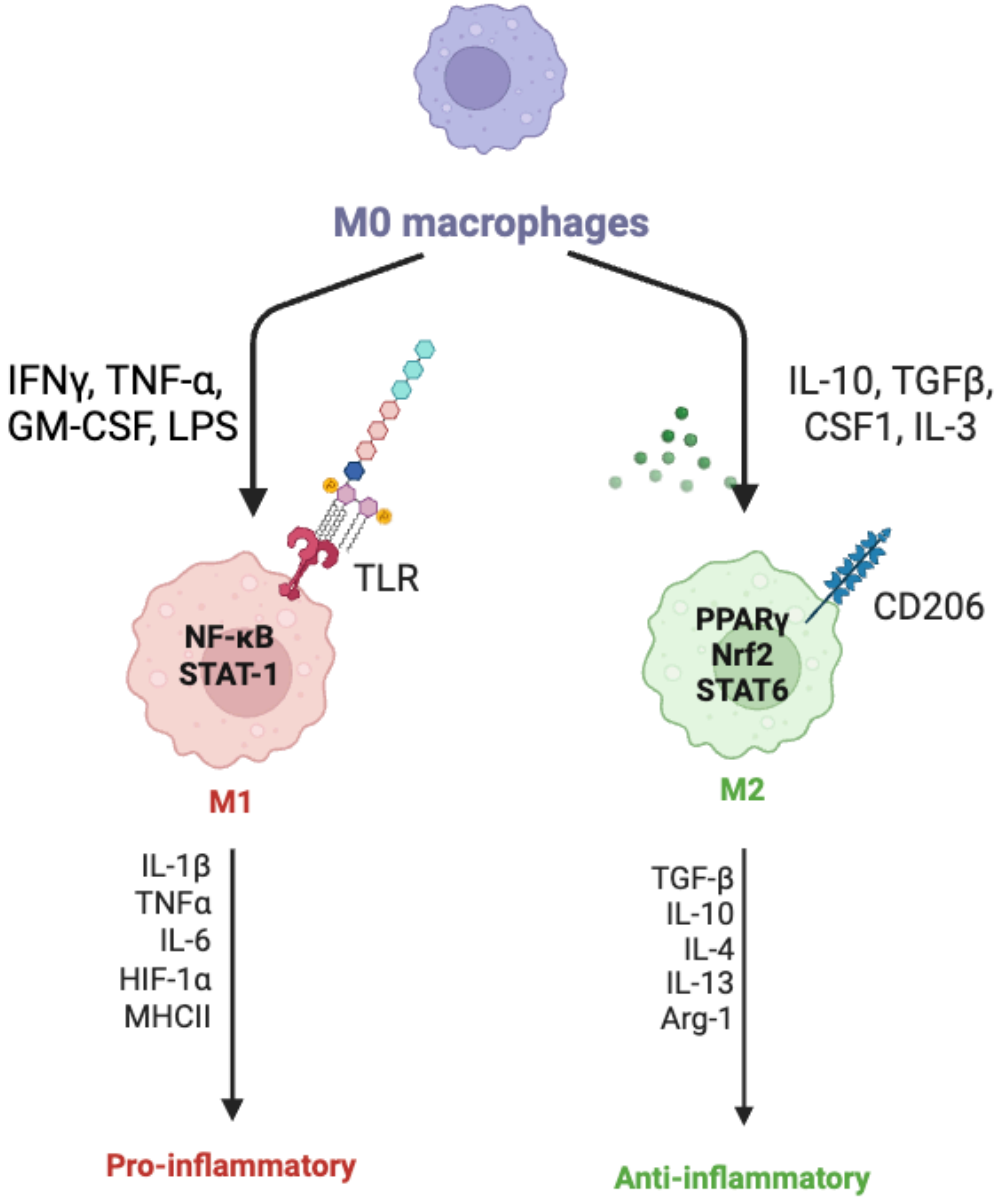

Figure 1-3. Polarisation of *M0* macrophages into pro-inflammatory M1 and anti-inflammatory M2-like macrophages. M1 phenotypes arise from stimulation with LPS, IFN-γ, TNFα and GM-CSF, which activate transcription factors NF-κB and STAT1. M1 macrophages, which produce and release IL-1β, TNF-α, IL-6, HIF-1α, and MHCII. *M0* macrophages stimulated by IL-10, TGF-β, CSF1 and IL-33 activate transcription factors PPARγ, Nrf2 and STAT6, which promote polarisation towards M2 phenotypes. M2 macrophages produce and secrete TGF-β, IL-10, IL-4, IL-13, Arg-1 and express the CD206 mannose receptor. LPS: lipopolysaccharide, INFγ: interferon gamma, GM-CSF: granulocyte-macrophage colony-stimulating factor, IL: interleukin, TNF-α: tumour necrosis factor alpha, TGF-β: transforming growth factor beta, NF-κB: nuclear factor kappa-light-chain-enhancer of activated B cells, STAT: signal transducer and activator of transcription, CSF1: colony stimulating factor 1, PPARγ: peroxisome proliferator-activated receptor-γ, CD206: mannose receptor 1, Arg-1: arginase 1. Figure created on Biorender.

In mice, monocytes highly expressing the antigen complex Ly6C and the C-C chemokine receptor type 2 (CCR2) are regarded as pro-inflammatory ($Ly6C^{+hi}CCR2^{+}$), whereas monocytes positive for the CX3C motif chemokine receptor 1 (CX3CR1) but expressing low Ly6C are known as patrolling or anti-inflammatory ($Ly6C^{lo}CX3CR1^{+}$) (Geissmann et al., 2003). Additionally, macrophage polarisation is closely tied to their metabolic programming and M1 and M2 macrophages have distinct metabolic profiles (Pérez and Rius-Pérez, 2022). Oxidative and nitrosative stress sustain the M1 phenotype by activating glycolysis and lipid biosynthesis, and by inhibiting tricarboxylic acid cycle (TCA) and OXPHOS. The truncated TCA cycle in M1 macrophages facilitates accumulation of intermediates like succinate, which stabilizes HIF-1α and promotes IL-1ß production (Tannahill et al., 2013). Pentose phosphate pathway (PPP) upregulation causes increased nicotinamide adenine dinucleotide hydroxylase (NADPH) and ROS production. In M2 macrophages oxidative phosphorylation (OXPHOS) and fatty acid oxidation (FAO) are dominant (Kelly and O'neill, 2015), and the TCA cycle is intact and PPARγ activation promotes lipid metabolism. IL-4/IL-13 activate STAT6, which further activates peroxisome proliferator-activated receptor-gamma coactivator-1α (PGC-1α) and causes mitochondrial biogenesis (Chen et al., 2023).

It is noteworthy that cells of myeloid lineage display great plasticity and functional heterogeneity, as they are able to switch phenotypes along the M1-M2 spectrum. Therefore, the above classification is now recognised as a sliding dichotomy of a plethora of phenotypes macrophages adopt in health and disease (Mantovani et al., 2005, Andreou et al., 2017, Shapouri-Moghaddam et al., 2018, Yang et al., 2021). An early example for plasticity along the M1-M2 axis was characterised in that pro-inflammatory genes that become induced during macrophage differentiation and activation can be negatively regulated by PPARγ signalling (Ricote et al., 1999). Therefore, throughout this thesis macrophages are referred to as M1-like and M2-like.

Macrophages express pattern recognition receptors (PRR) such as Toll-like receptors and the class B scavenger receptor CD36 to recognise apoptotic cells and phagocytose them (Abe et al., 2010). CD36 is activated by high mobility group box 1 (HMGB1), heat shock proteins (HSPs) and histone H3 (Baranova et al., 2024).

CCR2 was found critical for differentiation of Ly6C^{hi+} monocytes into anti-inflammatory Ly6C^{lo}F4/80^{+} macrophages after stroke and monocyte-derived macrophages were essential in preventing haemorrhagic transformations (Gliem et al., 2012, Chu et al., 2015), suggesting that macrophages act to maintain the integrity of the neurovascular unit (cf. section 1.4.1). Mice lacking CCR2 in macrophages showed decreased brain injury acutely after ischaemic stroke, however these mice fared worse on neurological outcomes a month following stroke (Fang et al., 2018). These studies suggest that CCR2 is required for anti-inflammatory processes in the long term after stroke.

1.5.2.3 Microglia

Microglia are the largest brain resident immune cell population and are derived from early yolk sac precursors that seed the brain parenchyma during embryonic development (Ginhoux et al., 2010). Resting microglia display a ramified morphology in homeostasis and contribute to dendritic pruning, phagocytosis and efferocytosis (Cai et al., 2019). Homeostatic microglia are positive for allograft inflammatory factor 1 (Iba1), CX3CR1, P2Y$_6$R, P2Y$_{12}$R, T-cell membrane protein 4 (Tim4), Triggering receptor expressed on myeloid cells 2 (TREM2), and proto-oncogene tyrosine-protein kinase MER (MERTK) (Masuda et al., 2020, Prinz et al., 2019). Under pathological conditions microglia become activated and assume amoeboid morphology (Ransohoff and Cardona, 2010). Microglia have a lower antigen presenting efficiency compared to dendritic cells and macrophages.

Microglia were recently reported to proliferate and accumulate in the ischaemic core 2 weeks after stroke (Garcia-Bonilla et al., 2023). Nucleotides (ATP/UDP) and adenosine are released from dying cells and activate purinergic P2X and P2Y6 receptors on microglia to induce phagocytosis, as well as production and release of pro-inflammatory cytokines (Li et al., 2013). Like macrophages, microglia display a biphasic polarisation after ischaemic stroke by firstly adopting M2-like phenotypes and subsequently M1-like phenotypes 2 weeks following stroke (Huang et al., 2006, Gulyás et al., 2012, Hu et al., 2012, Ritzel et al., 2015, Xiong et al., 2016, Ma et al., 2017, Anttila et al., 2017, Lyu et al., 2021). Genetic deletion of P2Y$_6$ on microglia prevented neuronal cell loss in the peri-infarct area, assigning a negative role for microglial phagocytosis (Milde and Brown, 2022).

1.5.3 Adaptive immunity

The adaptive branch of the immune system includes the activation of lymphocytes such as T cells and B cells upon binding major histocompatibility complex II (MHC II) molecules on antigen presenting cells such as macrophages and dendritic cells (Iwasaki and Medzhitov, 2015). This system requires clonal expansion, so it generates a slower but long-lasting response and is accompanied by memory formation against the specific inflammation-evoking stimulus (Cooper and Alder, 2006).

1.5.3.1 Lymphocytes

CD4 helper T cells and CD8 cytotoxic T cells infiltrate the brain tissue early after ischaemic stroke (Xie et al., 2019a). These cells exacerbate damage via release of pro-inflammatory cytokines (e.g., IFN-γ, TNF-α), induction of neuronal apoptosis and microvascular injury, disruption of the blood-brain barrier (BBB), and cytotoxic activity by CD8 T cells against neurons and glial cells (Brait et al., 2012). Additionally, it has been established that CD4 T cells enhance delayed B cell responses in the ischaemic brain up to after experimental stroke, as depletion of CD4 cells fails to mount an appropriate expansion of CD19 B cells (Weitbrecht et al., 2021). Several subtypes of T helper cells have been recognised and microglia have been shown to induce Th1 and Th17 but not Th2 (Wlodarczyk et al., 2014). Early contributors to ischaemic injury are also γδ T Cells (Wang et al., 2022), which secrete IL-17 to promote neutrophil recruitment and to exacerbate tissue damage (Dong et al., 2022). Certain B cells produce pro-inflammatory cytokines (e.g., IL-6, TNF-α), and can contribute to neuroinflammation, worsening damage and may act as antigen-presenting cells to activate T cells. B cells can produce autoantibodies following stroke, potentially leading to delayed autoimmune responses, chronic inflammation and cognitive impairment (Doyle et al., 2015).

Regulatory T cells (Tregs) play a protective role in stroke recovery by suppressing excessive inflammation via IL-10 and TGF-ß production and limiting the activation of microglia (Wang et al., 2016). Treg depletion has been associated with worsened stroke outcomes in animal models (Lee et al., 2024). Similarly, regulatory B cells (Bregs) also have a neuroprotective function. They produce IL-

10, which suppresses T cell-mediated inflammation and supports tissue repair and limits secondary injury (Bodhankar et al., 2013).

1.6 Inflammation

1.6.1 The blood-brain barrier

The blood-brain barrier (BBB) is formed of a layer of specialised vascular endothelial cells, which lack fenestrations and are connected by tight junctions such as claudin 5 and occludin, which tightly control the passage of cells and molecules between the blood and the CNS (Lippmann et al., 2012). The BBB serves to protect the brain parenchyma, which is composed of delicate neuronal tissue of limited self-healing capabilities, from the peripheral immune system. Capillary endothelial cells are wrapped in basement membrane, a component of the extracellular matrix (ECM). Individual endothelial cells are encircled by a pericyte at the capillary level and at arteriole level are surrounded by smooth muscle cells, which are also sheathed in basal lamina. These cells are functionally connected with neurons, microglia, and astrocytes to form the neurovascular unit to maintain homeostatic brain functions (Schaeffer and Iadecola, 2021).

1.6.2 Infiltration of immune cells after ischaemic stroke

Dying and injured parenchymal neurons release ROS, pro-inflammatory cytokines TNFα, IL-1β, IL-6 and IL-18, and damage-associated molecular patterns (DAMPs) such as nuclear HMGB1 and S100A8/A9 (Xie et al., 2019b, Jin et al., 2023, Schulze et al., 2013, Schuhmann et al., 2021b), and advanced glycation end-products (AGE), to trigger a disruption in the BBB by degrading tight junction proteins. Additionally, endothelial cells rupture due to stagnant blood flow and abnormal shear stress (Jayaraj et al., 2019, Planas, 2018). This allows local immune cells in the skull bone marrow, which acts as a reservoir of myeloid progenitor cells (Cugurra et al., 2021), to rapidly migrate into the parenchyma via direct vascular channels (Herisson et al., 2018).

CNS antigens such as DAMPs are released into the circulation through the cerebrospinal fluid (CSF) outflow routes, facilitated by lymphatic vessels in the meninges and ventricles. Antigens circulating in the blood can then activate immunogenic peripheral organs to enhance the migration of immune cells to the

injured brain parenchyma (Urra et al., 2014) (Liesz et al., 2015b). The importance of this process on stroke outcome is demonstrated by reversal of the inflammatory response and reduced stroke severity in experimental splenectomy (Ajmo Jr. et al., 2008). CCL2 binds to its cognate receptor CCR2, commonly expressed in monocytes, macrophages, and neutrophils, for the induction of chemotactic activity. Monocyte-derived macrophages are dependent on the CCR2-CCL2 axis for monocytes mobilisation from the bone marrow and for infiltration to inflamed sites (Tsou et al., 2007).

Recruitment of circulating leukocytes to the sites of vascular injury is mediated by their rolling and adhesion to the endothelium. This is facilitated by upregulation in expression of cell adhesion molecules such as integrins: intercellular adhesion molecule-1 (ICAM-1), vascular adhesion molecules (VCAMs), Mac-1, β2 integrin (Martin et al., 2017b), CD11b lymphocyte function-associated antigen 1 (LFA-1) and selectins: P-selectin, E-selectin, on endothelial cells, leukocytes and platelets (Aktan, 2004, Yilmaz and Granger, 2008, Fann et al., 2013). Leukocytes then adhere to the vascular endothelium in cerebral arterioles, venules and capillaries (Sienel et al., 2022). Tissue plasminogen activator upregulates matrix metalloproteases (MMPs) on infiltrating immune cells) which are molecular activators of tissue reorganisation and repair, and act to further break down tight junctions (Lakhan et al., 2013).

Inflammation begins in the hours after stroke and persists for at least a week afterwards in experimental models of ischaemic stroke in rodents (Figure 1-4). Additionally to the localised inflammatory process, a global brain neuroinflammation is also observed, as microglia respond by proliferation in both hemispheres (Shi et al., 2019). Peripherally derived macrophages and neutrophils accumulate in great numbers in the first week of neuroinflammation, while dendritic cells and lymphocytes accumulate to smaller numbers (Gelderblom et al., 2009, Planas, 2018). In experimental stroke the extent of peripheral immune cells infiltration is also determined by the presence or absence of reperfusion, with reports that permanent ischaemic stroke results in twice as many infiltrating leukocytes compared to transient alternatives (Chu et al., 2014).

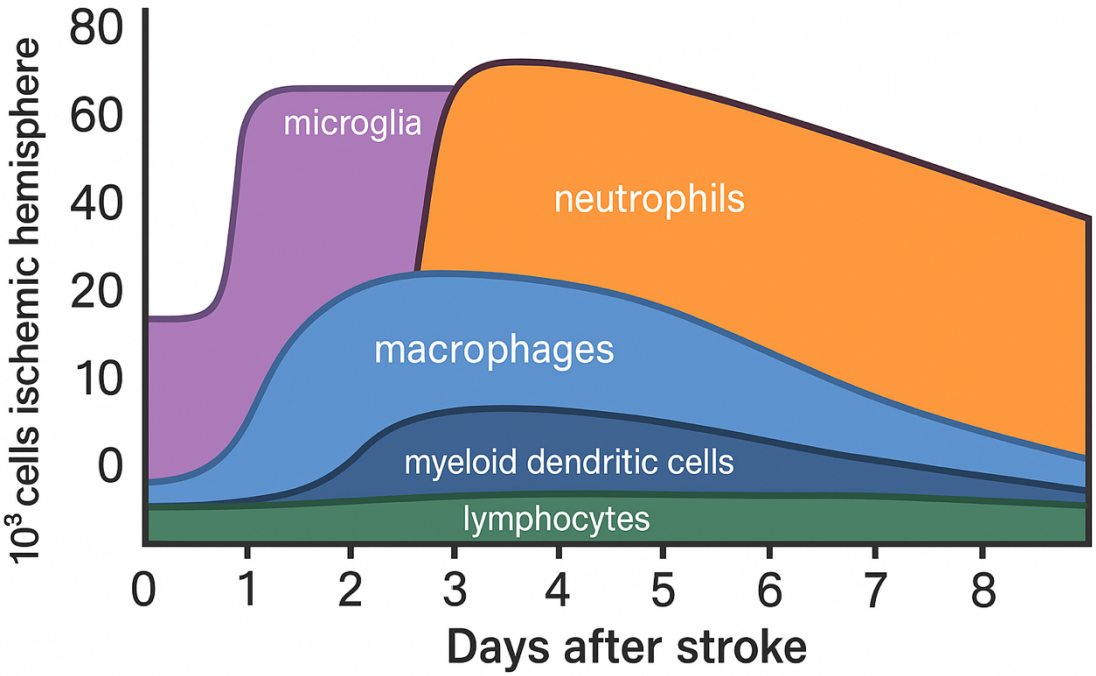

Figure 1-4. Temporal profile of post stroke immune cell accumulation over a period of 1 week. Adapted from (Gelderblom et al., 2009).

1.6.3 Mechanisms of neuroinflammation

DAMPs engage toll-like receptors (TLRs) on resident and peripheral innate immune cells (Kuzan et al., 2024), scavenger receptors, such as CD36, and receptors for advanced glycation endproducts (RAGE). All of these receptors trigger cellular signalling which results in the activation of NFκb-dependent inflammatory signalling (Liesz et al., 2015a, Schuhmann et al., 2021a). In addition, DAMPs activate the NLR family pyrin domain containing 3 (NLRP3) inflammasome in glia (Savage et al., 2012). Neutrophils have been proposed to worsen stroke pathology via several mechanisms, including physical blockade within the microvascular network, contributing to the reduction of cerebral blood reflow (El Amki et al., 2020) and direct entry into the brain parenchyma.

1.7 Phases of neuroinflammation

Inflammation is associated with accumulation of immune cells in the ischaemic brain, with peaks and subsequent decline in cell frequency depending on the cell type. Leukocytes from both the innate and adaptive immune system are involved in the process and have divergent profiles of accumulation and recession from the CNS. Early studies have shown that T lymphocytes localise to the ischaemic penumbra within 24 hours of reperfusion, accumulated further at 72 hours and 1

week after reperfusion and decreased in numbers 2 weeks later (Schroeter et al., 1994). Similarly, T lymphocytes and macrophages were shown to gradually accumulate over several weeks after permanent ischaemic stroke, and the authors observed that after 2 weeks macrophage numbers slightly declined, while T cells continued to accumulate (Vindegaard et al., 2017). Cell accumulation profiles may reflect the functions each cell type performs in the inflammatory process at given timepoints. Macrophages perform functions such as phagocytosis of apoptotic cells and are cleared from the parenchyma through the lymphatics upon completion of their functions (Serhan and Savill, 2005), while T lymphocytes were reportedly secreting anti-inflammatory cytokines 1 month following stroke, suggesting they are involved in a reparative capacity at this later stage (Xie et al., 2019a). These roles may help explain the differential accumulation of the two cell types observed by Vindegaard et al.

To dissect the roles of some of the key cellular players in the neuroinflammatory landscape following cerebral ischaemia, the timeline of inflammation could be divided into phases (Mărgăritescu et al., 2009), while keeping in mind that this process is dynamic and the time scale of each phase in not clear cut. This is illustrated by the fact that for many different immune cell types both salutary and detrimental roles have been described depending on the timepoint after ischaemic stroke chosen by the investigators. A biphasic accumulation pattern has been reported for monocyte-derived macrophages (Garcia-Bonilla et al., 2016, Hu et al., 2012). This could be explained by a polarisation switch, rather than recruitment of fresh monocytes from the periphery (Garcia-Bonilla et al., 2016). Interestingly, while one study reported that macrophages change from M2 to M1 over a 2-week time course (Hu et al., 2012), a later study showed that the biphasic accumulation is due to M1-to-M2 transition (Garcia-Bonilla et al., 2016). Similarly, microglia are initially alternatively activated to promote healing, while after a week they are detected to primarily be involved in pro-inflammatory processes (Kluge et al., 2019), potentially through prolonged accumulation of lipids through phagocytosis and transformation into foam cells (Zbesko et al., 2023).

1.7.1 Acute phase of neuroinflammation

The acute phase characterises the very early events following the initial infarct formation and is typically reported in the literature as early as 6h after stroke

(Price et al., 2004) and acute neuroinflammatory events tends to be reported until 72 hours after. Canonically, T cells are activated by antigen presenting cells such as macrophages and dendritic cells (Eltzschig and Eckle, 2011). However, an early detrimental impact of T cells on ischaemic stroke injury was shown to be independent of antigen presentation in $Rag1^{-/-}$ T-lymphocyte deficient mice (Kleinschnitz et al., 2010). Another early study established that in $Rag1^{-/-}$ mice, or mice deficient in either $CD4^{+}$ or $CD8^{+}$ T lymphocytes, there was reduced leukocyte infiltration and platelet adhesion 24 hours after ischaemic stroke (Yilmaz et al., 2006), indicating that perhaps brain resident T cells are responsible for leukocyte recruitment into the parenchyma.

Despite the evidence for harmful contributions of some leukocytes toward neuroinflammation in the acute phase after stroke, there is also evidence for beneficial contributions from other immune cells. Microglia and infiltrating macrophages rapidly respond to injury by phagocytosing dead cells, myelin debris, and damaged tissue, which prevents further inflammation and supports healing (Zhang et al., 2019). MDM were reported to have a role in limiting infarct size 24 hours after ischaemic stroke in mice (Chu et al., 2015). In this study a pharmacological inhibition of CCR2 resulted in decreased recruitment of $Ly6C^{hi+}$ monocytes to the brain and larger infarct size, and genetic ablation of CCR2 was associated with higher haemorrhagic transformations. Although direct evidence for a role for macrophages in post-stroke angiogenesis and neovascularisation in mice is lacking, RNA sequencing has shown that genes related to these processes such as VEGF, growth/differentiation factor 15, and fibroblast growth factor 1 are upregulated in stroke samples 5 days after permanent stroke (Wang et al., 2020a)

1.7.2 Sub-acute phase

The subacute stage after stroke in mice is an intermediate stage between acute and chronic inflammation and is reported around 1-2 weeks after stroke (Zhang et al., 2019). This phase was reported as a turning point towards resolution of inflammation, and macrophages and microglia switching to M2 phenotypes (Perego et al., 2011, Zhang et al., 2019), accompanied by ongoing phagocytosis of dead cells and debris, and increased vascular remodelling and proliferation (Durán-Laforet et al., 2019). There was a relatively higher protein expression of alternative inflammatory markers such as TGF-ß, nestin, phosphorylated Akt, and

phosphorylated extracellular signal-regulated kinase 1/2 (ERK1/2) in the ischaemic brain hemisphere, which correlated with functional recovery 14 days after stroke in rats (Mostajeran et al., 2022). Ly6C^{lo}F4/80^{+} macrophages have been shown to harness anti-inflammatory properties 6 days after photothrombotic stroke through their secretion of osteopontin to enhance astrocyte extension of the glial scar and resolution of inflammation (Gliem et al., 2015). Macrophages expressing the scavenger receptor CD36 were co-expressing the M2 marker lysosomal acid lipase and were involved in phagocytosis during the resolution of inflammation 7 days after stroke (Woo et al., 2016a). Further, BMDM transplantation through intracerebroventricular injection 2 weeks following ischaemic stroke resulted in improved neurological function, despite not having an impact on infarct volume (Kitamura et al., 2023).

Nonetheless, the sub-acute phase is also accompanied by continued disruption of the BBB (Bernardo-Castro et al., 2020), formation of neutrophil extracellular traps (Kang et al., 2020) and antibody production by B lymphocytes (Doyle et al., 2015), indicating that inflammatory resolution is incomplete after this stage. Chronic inflammation after stroke is associated with accumulation of lipids from myelin breakdown and results in the transformation of macrophages and microglia into lipid-laden foam cells (Chung et al., 2018, Zbesko et al., 2023). Foam cells secrete pro-inflammatory cytokines, which act to increase neurotoxicity and inhibit cell regeneration and remyelination. Administration of lipid chelating agents has shown reduction in lipid droplets in the infarct and reduced transformation of resident macrophages into foam cells (Becktel et al., 2022). One study examined the involvement of B lymphocytes in delayed cognitive decline after ischaemic stroke and determined that antagonising B cells improved long-term potentiation and Y maze deficits 7-12 weeks after stroke in mice (Doyle et al., 2015). Two weeks following stroke the cytotoxic subtype CD8^{+} T cells have been described to accumulate in the mouse brain and their numbers correlate with poorer functional recovery (Selvaraj et al., 2021).

1.7.3 Chronic phase

The chronic phase of neuroinflammation is characterised by the presence of both pro- and anti-inflammatory factors, the fine balance between which dictates termination of inflammation or chronification. For instance, CD4^{+} and CD8^{+} T

lymphocytes express markers of T cell activation such as CD44 and CD25 with a progressive pro-inflammatory phenotype up to a month after rodent stroke, but because these cells accumulate preferentially in the peri-infarct regions, the authors concluded that this phenotype may assist in neural repair (Xie et al., 2019a). The effect of early treatment with the matrix metalloprotease (MMP) inhibitor minocycline following ischaemic stroke was reported to have enhanced blood–brain barrier remodelling 4 weeks after stroke, corresponding with M2 cytokine expression by microglia and macrophages (Yang et al., 2015), suggesting that these cells are typically M1-like in the chronic phase of stroke. Another study showed that microglia and macrophages adopt pro-inflammatory phenotypes 35 days after ischaemic stroke in mice through transforming growth factor beta-activated kinase 1 (TAK1) (Wang et al., 2020b). The authors show improved neurological outcomes at this chronic timepoint upon genetic deficiency or pharmacological inhibition of TAK1, suggesting a deleterious contribution of macrophages and microglia at this later timepoint.

1.8 CNS border-associated macrophages (BAMs)

1.8.1 Sub-types of BAMs

The CNS border-associated macrophages (BAM) are a small cell population located within the perivascular space, the meninges, and the choroid plexus (Figure 1-5), where perivascular (PVMs), meningeal, and choroid plexus macrophages reside, respectively. PVMs are localised to arterioles penetrating the parenchyma (40-50 μm), pial arterioles and veins (200-1000 μm) (Schaeffer and Iadecola, 2021). Arteriole PVMs reside on the abluminal side between the vascular smooth muscle cell basement membrane and the glial limitans formed by astrocyte end feet (Faraco et al., 2016, Yang et al., 2019). Meningeal macrophages are located primarily in the subarachnoid space between the dura and the arachnoid mater (Figure 1-1B) and some reside in the dura mater (Mrdjen et al., 2018). The choroid plexus is the primary site of CFS production, with epithelial cells lining choroid plexus in intracranial ventricles and contains epiplexus and stromal macrophages (Goldmann et al., 2016). Like microglia, BAMs have been shown to derive from embryonic precursors in the yolk sac (Ginhoux et al., 2010, Goldmann et al., 2016, Utz et al., 2020, Dermitzakis et al., 2023) and to form stable, self-renewing populations in adult life. Their maintenance is primarily independent of peripheral

repopulation, while a small fraction of dural and choroid plexus macrophages rely on replenishment from peripheral monocytes (Goldmann et al., 2016, Van Hove et al., 2019).

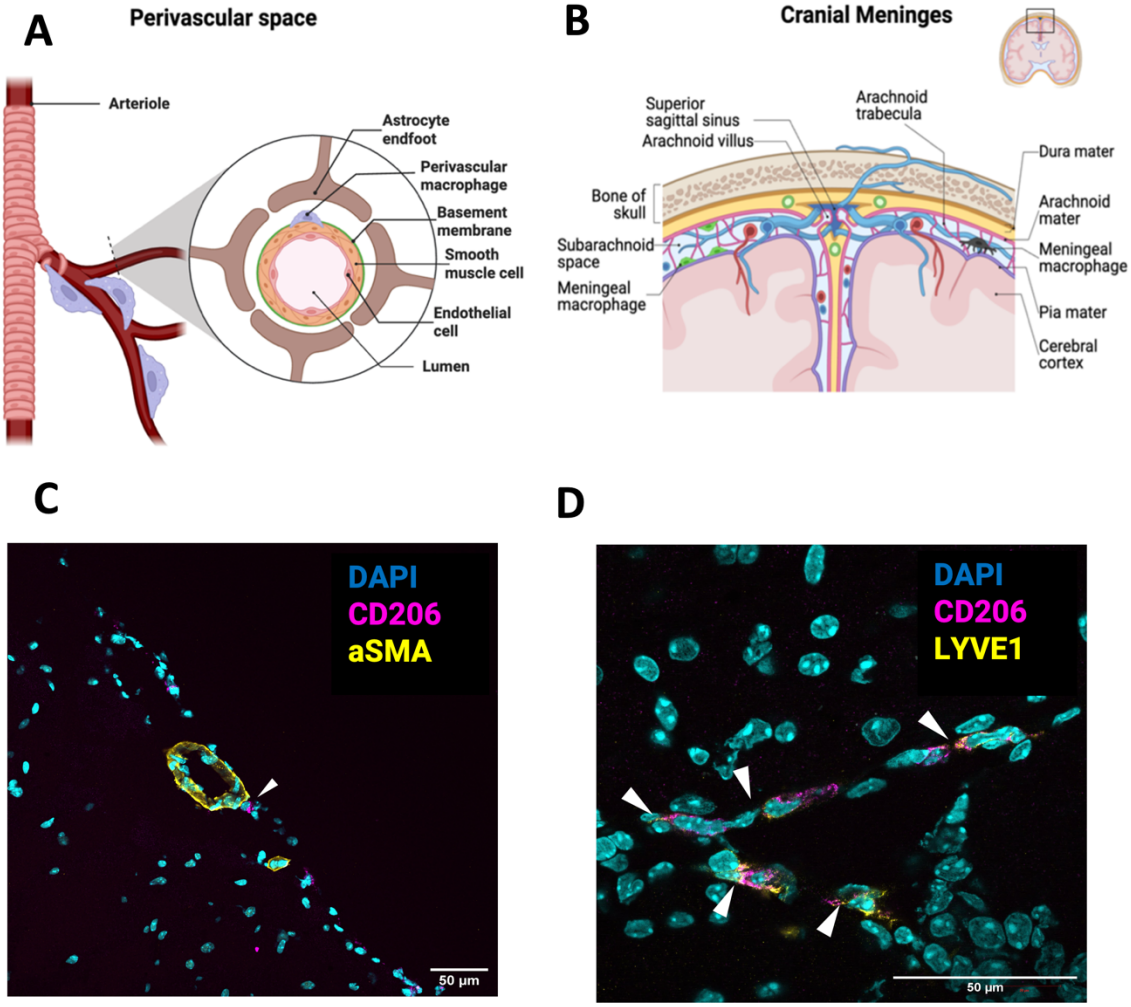

Figure 1-5. Location of CNS border-associated macrophages (BAMs) in the mouse brain. A) A schematic cross section of a cerebral arteriole showing the localisation of perivascular macrophages relative to other vascular structures. B) A schematic anatomy of the cranial meninges indicating meningeal macrophages in the subarachnoid space. C) Perivascular macrophages near a pial arteriole in a mouse coronal section. D) BAMs located near two penetrating arterioles. White arrowheads indicate BAMs. The schematics were based on imaging data published in (Hannocks et al., 2018) and created using elements from BioRender.

1.8.2 Differentiation of BAMs from microglia

Until recently the term '*brain resident macrophage*' has included both BAMs and microglia, owing to similarities in origin, longevity and self-sufficiency compared to peripheral macrophages (Prinz et al., 2017, Prinz et al., 2019). However, while microglia rely on TGF-b signalling for differentiation, BAMs are TGF-b independent

but through interferon regulatory factor 8 (IRF8) signalling differentiate from early 'pre-macrophage' progenitors in the meningeal and cephalic (head) mesenchyme (Utz et al., 2020). Around embryonic developmental stage E14.5 the intronic enhancer for colony stimulating factor 1 receptor (CSF1R) *fms*-intronic regulatory element (FIRE) modulates microglia to switch off BAMs signatures (Munro et al., 2020). There are also notable differences between adult microglia and BAMs such as in morphology (Nayak et al., 2012), transcriptomic signature (Mrdjen et al., 2018) and functions (Bijnen et al., 2024, Dalmau Gasull et al., 2024). Resting microglia have a ramified morphology with multiple protrusions from their cell body, while perivascular macrophages are typically amoeboid (Faraco et al., 2016), or elongated around blood vessels (Goldmann et al., 2016), and meningeal macrophages are spindle-like and have a few thick membrane projections found in proximity to meningeal vessels (Dermitzakis et al., 2023). Healthy perivascular macrophages extend protrusions along the perivascular space, but rarely displace their cell bodies (Goldmann et al., 2016), indicating that they have limited propensity to migrate under physiological conditions. Microglia are quite well known to assume amoeboid and other morphologies in disease (Ransohoff and Cardona, 2010), while not much is known about the shapes BAMs adopt under stress.

1.8.3 Homeostatic roles of BAMs and gene signatures

BAMs represent only about 10% of total leukocytes in the healthy murine brain (Mrdjen et al., 2018). Their functional roles under homeostatic conditions are only beginning to emerge and are understood to include immunosurveillance, phagocytosis, scavenging CNS-derived metabolites and antigens from necrotic neurons (Kida et al., 1993), antigen-presentation (Fabriek et al., 2005), and regulation of vascular permeability through phosphorylation of VE-cadherin (He et al., 2016), production of VEGF and modulating VEGF-regulated glucose uptake by endothelial cells (Jais et al., 2016). Single cell RNA sequencing has revealed that gene signatures differ across BAMs subtypes, revealing these cells as highly heterogeneous in healthy mice (Mrdjen et al., 2018, Van Hove et al., 2019). Homeostatic mouse BAMs express several identification markers, including CD206 - mannose receptor transcribed from *Mrc1* (Galea et al., 2005, Martinez-Pomares, 2012, Mrdjen et al., 2018, Lapenna et al., 2018), LYVE1 - lymphatic vessel endothelial hyaluronan receptor 1 (Zeisel et al., 2015, Mrdjen et al., 2018,

Brezovakova and Jadhav, 2020, Kim et al., 2021a), major histocompatibility complex II (Liu et al., 2005), CD36 (Park et al., 2017), CD169 (Rajan et al., 2020), and CD163, although at levels lower than in rats and humans (Fabriek et al., 2005). Both PVM and meningeal BAMs are double positive for CD206 and Lyve1 (Jordão et al., 2019).

1.8.4 Roles of BAMs in disease

Much like other macrtophages and microglia, BAMs also display phenotypic plasticity along the M1-like and M2-like spectrum. A recent report on the transcriptomic signatures of brain resident and peripheral immune cells after transient ischaemic stroke reported that although BAMs were highly divergent in the acute period after stroke, their transcriptomic profile showed low divergence from sham 2 weeks after stroke (Garcia-Bonilla et al., 2023). This may suggest a decline in a functional role for these cells in the chronic phase of neuroinflammation after stroke, however direct evidence for that is missing. BAMs are often described as having deleterious roles in brain diseases such as Alzheimer's disease (Park et al., 2017), cerebral amyloid angiopathy (Hawkes and McLaurin, 2009), and in hypertension-induced neurovascular and cognitive dysfunction in mice and rats (Faraco et al., 2016, Iyonaga et al., 2020, Kerkhofs et al., 2020, Santisteban et al., 2020). In a mouse model of Alzheimer's disease overexpressing the human apolipoprotein E4 (ApoE4), BAMs were shown to compromise BBB integrity through Nox-derived ROS (Anfray et al., 2024).

However, BAMs were recently described as orchestrating T cell recruitment via antigen presentation through MHC class II, which is beneficial in the context of Parkinson's disease (Schonhoff et al., 2023). In haemorrhagic stroke erythrocytes phagocytosed by BAMs release heme, iron and bilirubin, which increase local inflammation. Depletion of PVM by liposomal clodronate was shown to reduce perivascular inflammation by preventing red blood cells uptake and improved neurological outcome on depletion following subarachnoid haemorrhage, supporting a detrimental function for PVMs in this type of stroke (Wan et al., 2021). Interstitial fluid and solutes drainage along the perivascular spaces was studied by a laser-guided bolus injection and milti-photon imaging of and it was determined that drainage along arterioles and capillaries but not veins was impaired after both ischaemic stroke and in Alzheimer's disease due to reduced

perfusion and amyloid deposition (Arbel-Ornath et al., 2013), suggesting that BAMs may be contributing to oedema and towards long-term cognitive decline through impairment of amyloid beta clearance.

1.8.5 Evidence for deleterious roles of BAMs in ischaemic stroke

After ischaemic stroke BAMs have been reported to have both harmful and beneficial roles (Pedragosa et al., 2018, Rajan et al., 2020, Zheng et al., 2021). In the hyperacute period (16 hours) after stroke better functional recovery was conferred by BAM ablation with liposomal clodronate, which was accompanied by reduced numbers of granulocyte infiltrating the ischaemic cortex, despite no change in thionin-staining assessed infarct size (Pedragosa et al., 2018). Neurological outcome is often thought of as secondary to infarct size, however after focal ischaemic stroke neuroinflammation occurs in both hemispheres (Shi et al., 2019). This might explain why BAMs did not appear to contribute directly to the infarct development, as they might be acting on a whole brain level to worsen the acute outcome of stroke. BAMs underwent changes in their gene expression in this hyperacute phase after stroke, which included increased expression of genes related to leukocyte chemotaxis and vascular leakage. Another study also found no difference in infarct size between ischaemic stroke and sham groups upon BAM depletion, as determined on a T2-weighted MRI, but pointed to BAMs mediating a 'neuroinflammatory priming' on alcohol exposure prior to stroke (Drieu et al., 2020), as prior exposure to alcohol increased BAMs numbers and enlarged infarct volume, while BAM depletion blocked the aggravation. BAMs promoted BBB hyperpermeability by releasing vascular endothelial growth factor (VEGF) (Pedragosa et al., 2018), suggesting that, contrary to the reported role of PVMs in supporting vascular integrity under homeostasis (He et al., 2016), BAMs acquire a damaging phenotype in ischaemic conditions. A more definitive evidence for a harmful role executed by BAMs after ischaemic stroke comes from a recent article, where clodronate depletion was shown to significantly improve infarct volume and reduce neurological burden 24 hours post stroke (Yu et al., 2025). The authors reported a concomitant decreased expression of TNFα in the treated group, suggesting that BAMs perhaps harness M1-like phenotypes in the acute phase after stroke.

1.8.6 Evidence for protective roles of BAMs in ischaemic stroke

On the other hand, BAMs undergo genetic transformations acutely after cerebral ischaemia, indicative of the potential reparative roles of these cells. BAMs upregulate genes related to angiogenesis, extracellular remodelling and proliferation, while genes related to antigen presentation were decreased. Interestingly, the authors identified murine BAMs as $CD169^+$ cells and detected these cells in the parenchyma, raising the possibility that BAMs may leave the CNS borders and migrate into the brain parenchyma after stroke. However, CD169 is also expressed on blood-derived macrophages and comprised almost a third of the detected parenchymal macrophages in another study (Lee et al., 2021). In a recent article depletion of BAMs before stroke in aged mice was associated with increased BBB leakage, a selective increase in the expression of the endothelial adhesion molecule P-selectin, an increase in leukocyte rolling and adhesion, and an increase in infiltration of neutrophils, macrophages and T lymphocytes into the parenchyma 24 hours post stroke (Levard et al., 2024). The authors observed this exacerbated neuroinflammatory response also 5 days after stroke, suggesting an important role for BAMs in controlling the immune response after stroke in the sub-acute stage. In naive aged mice there was no change in BAM number compared to young mice, but a greater proportion expressed human leukocyte antigen (HLA) and CD74, possibly through altering their genetic makeup, which aligns with the authors' transcriptomic data showing an overexpression of genes related to antigen presentation and leukocyte recruitment by BAMs in aged mice. These findings were corroborated in post-mortem human brains from five patients with a mean age of 80, in which $CD206^+$ BAMs highly expressed HLA and CD74 (Levard et al., 2024). Interestingly, expression of CD206 was reported to be confined to the peri-infarct zone (Rajan et al., 2020), suggesting that some BAMs and M2-like polarised macrophages are restricted to areas where salvageable tissue is located.

Upon neuroinflammation following stroke, BAMs may adopt an M1-like phenotype contributing to local inflammation. One of these markers inducible nitric oxide synthase (iNOS, cf. below for more detail in section 1.9.1). Alternatively, BAMs could switch to a M2-like signature at a different timepoint after stroke, which is accompanied by downregulation of iNOS. The expression of this marker within BAMs after stroke has not been yet reported experimentally and would be important to investigate in the context of the functional roles of BAMs in stroke.

1.9 The NO-ADMA-DDAH2 pathway

1.9.1 Synthesis of nitric oxide (NO)

NO is a ubiquitous gaseous cellular messenger and neurotransmitter, which plays a variety of physiological roles, most prominently in vasodilation, neurotransmission, and pathogen elimination (Andrabi et al., 2023). NO is synthesised by a family of enzymes known as nitric oxide synthases (NOS). NOS catalyses the oxidation of L-arginine, requiring molecular oxygen and NADPH as co-substrates, and flavin adenine dinucleotide (FAD), flavin mononucleotide (FMN) and tetrahydrobiopterin (BH4) as cofactors, which bind in the oxygenase domain of NOS (Dao et al., 2021). This results in the production of NO and L - citrulline. Three NOS isoforms have been identified with distinct tissue distribution: endothelial (eNOS, coded by *Nos1*), neuronal (nNOS, *Nos3*) and inducible (iNOS, *Nos2*). Both eNOS and nNOS are constitutively expressed as inactive monomers, which homodimerise at super-physiological concentrations of intracellular calcium, facilitated by binding of the calcium-calmodulin complex to the monomers and activating a homodimer (Ratovitski et al., 1999). The third isoform iNOS was first cloned in 1992 in murine macrophages (Xie et al., 1992). It is coded by the *Nos2* gene and in mice translates into a 1144 amino acid sequence sharing 50% identity to human iNOS (Gross et al., 2014). Unlike eNOS and nNOS, iNOS binds calmodulin at physiologic levels of Ca^{2+} to form an active homodimer but it is not basally expressed (Piazza et al., 2015). Moreover, in contrast with eNOS and nNOS, which rely on co-factors and calcium for maximal action, iNOS is Ca^{2+} and calmodulin independent and predominantly transcriptionally regulated.

1.9.2 Signalling and functions of NO in the CNS

In the neurovascular unit (NVU) glutamatergic neurotransmission regulates neuronal NO production and release, and together with endothelium derived NO, regulate cerebral vascular tone and thereby CBF (Figure 1-6). The eNOS- and n-NOS produced NO diffuses into the smooth muscle cells (SMC) and activates soluble guanylate cyclase (sGC) by binding to a ferrous haem group (Krumenacker et al., 2004, Martin et al., 2005). Soluble GC converts guanosine triphosphate (GTP) to cyclic guanosine monophosphate (cGMP), which in turn activates cGMP-dependent protein kinase G (PKG) to open Ca^{2+} reuptake channels in the endoplasmic

reticulum and result in relaxation (Lourenço et al., 2014). This contributes to a healthy endothelium and dysregulation of this signalling can lead to endothelial dysfunction (Cyr et al., 2020). NO is deactivated by binding to haem in haemoglobin, myoglobin, or cytoglobin (Brown, 2010).

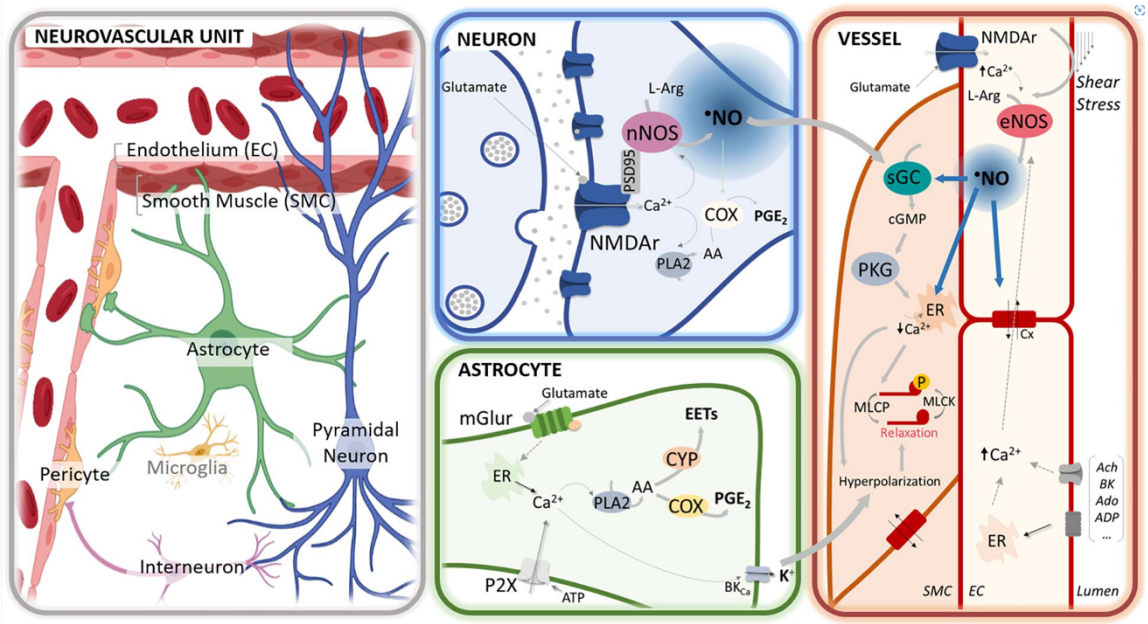

Figure 1-6. Neurovascular coupling between different cells of the neurovascular unit is mediated through nitric oxide (NO) signalling. The NVU is composed of endothelial cells (EC), smooth muscle cells (SMC), pyramidal neurons, astrocytes, interneurons, microglia and pericytes. In neurons the presynaptic terminal releases glutamate in the synapse, which activates N-methyl-D-aspartate receptors (NMDAr) on post-synaptic terminals. The scaffolding protein post-synaptic density protein 95 (PSD95) forms a complex between NMDAr and neuronal nitric oxide synthase (nNOS) and induces the production of nitric oxide (NO). This process requires L-arginine (L-arg) as a substrate and is enhanced by NMDAr mediated calcium (Ca^{2+}) influx. Neuronal NO diffuses into SMC and activates soluble guanylate cyclase (sGC), activating cyclic guanosine monophosphate (GMP) and protein kinase G (PKG) to stimulate calcium reuptake by the endoplasmic reticulum (ER). Reduced Ca^{2+} allows the activation of myosin light chain phosphatase (MLCP) to dephosphorylate myosin light chain and elicit relaxation. Additionally, glutamate activates NMDAr on EC and the resultant Ca^{2+} influx activates endothelial (eNOS) to produce NO. EC-derived NO diffuses into SMC and can activate both sGC and Ca^{2+} sequestration into ER to enhance relaxation. In astrocytes glutamate activates muscarinic glutamate receptors (mGLur), which stimulate the release of calcium from the ER and similar to neurons, activate phospholipase 2 (PLA2). Calcium activates BK_{Ca} receptors, which export potassium K^+ from astrocytes. The diffusion of K+ into SMC causes their hyperpolarisation and causes relaxation through by inhibition of myosin light chain kinase (MLCK). Figure from (Lourenço and Laranjinha, 2021).

1.9.3 Signalling and functions of NO in host defence

Exposure to inflammatory cytokines such as lipopolysaccharide (LPS) and tumour necrosis factor alpha (TNFa), which activate TLRs and CD14 and subsequently activate the transcription factor NFκB (Aktan, 2004), upregulate iNOS. This signalling pathway constitutes the primary mechanism for host defence against bacterial infections in a variety of innate immune cells, such as macrophages (Salim et al., 2016), dendritic cells (Serbina et al., 2003), and microglia (Possel et al., 2000). In sterile inflammation interferon gamma (IFN-γ) induces iNOS via the Jak-STAT signalling pathway (Aktan, 2004). Moreover, macrophage specific knockout of *Nos2* in mice has been shown to provide enhanced macrophage OXPHOS (Palmieri et al., 2020), suggesting that iNOS-derived NO controls macrophage polarisation towards M1-like-phenotypes through a metabolic switch (cf. section 1.5.2.2).

1.9.3.1 NO in cell death

NO can induce apoptosis by oxidating and activating p53, p38 mitogen-activated protein kinase (MAPK) pathway or endoplasmic reticulum stress. Low levels of NO [0.2–2.0] nM can block cell death via cGMP-mediated vasodilation, Akt activation or block of mitochondrial permeability transition. High NO [20–200] nM may protect by killing pathogens, activating NF-κB or S-nitrosylation of caspases and the NMDA receptor, thereby blocking apoptosis and glutamate neurotoxicity.

1.9.4 NO roles in ischaemic stroke

The role of NO after ischaemic brain reperfusion injury depends on the stage of evolution of the ischaemic cascade, the cellular source, NOS isoform and quantity released (Iadecola, 1997, Chen et al., 2017).

1.9.4.1 eNOS and nNOS

In the early stages after ischaemic brain injury, NO generated by eNOS is protective (Asahi et al., 2005, Nan et al., 2018). It has been known for decades that neuronal cell death is mediated through excessive nNOS (Dawson et al., 1996), and at the turn of the century this was shown to be linked to cytotoxic glutamatergic neurotransmission through the NMDAr-PSD95-nNOS complex (Aarts

et al., 2002). A small molecule inhibitor (ZL006) of the interaction between the scaffolding protein PSD-95 and nNOS (Figure 1-6) has been shown to improve ischaemic infarct size after experimental ischaemic stroke (Zhou et al., 2010).

1.9.4.2 iNOS in ischaemic stroke

Excessive iNOS-derived NO production from reactive microglia, astrocytes and infiltrating myeloid and lymphoid cells is neurotoxic after ischaemic stroke (Wierońska et al., 2021, Iadecola, 1997). For instance, *Nos2* knockout mice were shown to reduce ischaemic infarct size and this was reversed by a bone marrow transplant of *Nos2*$^{+/+}$ neutrophils into *Nos2*$^{-/-}$ mice (Garcia-Bonilla et al., 2014). In a rat model of cerebral ischaemia-reperfusion injury excess iNOS-derived NO increased infarct size and cerebral vascular injury by downregulation of tight junction proteins (Mohammadi, 2016) and activation of iNOS induced apoptosis (Zheng et al., 2016). NO modulators such as S – nitrosoglutathione, and small molecule inhibitors of iNOS such as S – methylisothiourea sulfate and aminoguanidine, have demonstrated neuroprotection and reduced infarct size by over 75% after rodent stroke (Khan et al., 2005, ArunaDevi et al., 2010, Danielisova et al., 2011). Depletion of iNOS positive immune cells using $GdCl_3$ or inhibition by the iNOS selective inhibitor 1400W conferred protection and reduction of inflammation in a mouse model of ischaemic stroke (Li et al., 2022).

Following cerebral ischaemia iNOS mRNA and protein were both significantly elevated in mouse ischaemic brains (Kawabori and Yenari, 2015, Bi et al., 2021). The expression levels of iNOS peak 3 days after stroke and decrease to normal a week following stroke (Iadecola et al., 1995, Woo et al., 2016b). NO derived from iNOS in the ischaemic environment readily reacts with superoxide to form peroxynitrite and cause protein nitration of matrix metalloproteases (Suofu et al., 2010), lipid oxidation and DNA damage, and to promote neuroinflammation (Naito et al., 2020). Additionally, iNOS-derived NO has been shown to inhibit microglia proliferation in neonatal mice via PKG action on the proliferation markers Ki67 and pH3 (Maksoud et al., 2020), suggesting that iNOS mediates its negative effects in ischaemic stroke through inhibiting proliferation by microglia. While these findings have not been corroborated in adult mice and no investigation has been reported on the role of iNOS on BAMs proliferation, it is plausible that this mechanims is focal in directing these immune cells functions after stroke.

1.9.5 Endogenous inhibitors of NO synthesis

NO production is regulated by many factors described above such as calcium, which regulates the activity of the constitutive isoforms. Methylarginines such as N^G-monomethyl-L-arginine (L-NMMA), symmetric dimethylarginine (SDMA) and asymmetric dimethylarginine (ADMA) are derived by methylation of protein arginine residues by a family of enzymes known as protein arginine methyltransferases (PRMTs) (Clarke, 1993, Leiper et al., 1999). ADMA and L-NMMA are key regulators of NO synthesis, as they competitively inhibit the binding of L-arginine for the active site of NOS enzymes (Vallance et al., 1992)(Caplin and Leiper, 2012).

ADMA is primarily eliminated by metabolism by the dimethylarginine dimethylaminohydrolases (DDAH) enzymes to L-citrulline and dimethylarginine (Achan et al., 2003, Tran et al., 2003). About a fifth of ADMA is transported into the plasma by cationic amino acid transporters (CATs) (Strobel et al., 2013) and cleared by the kidneys. Two isoforms of CATs are known to act as bidirectional transporters, which can both import and export methylarginines into the cells in exchange of L-arginine and some cationic amino acids (Teerlink et al., 2009). Normal circulating concentrations of ADMA are approximately 5 μmol/L, while in a variety of conditions plasma ADMA is significantly elevated and associated with poor outcomes, including metabolic disorder (Garcia et al., 2007) and sepsis (Nijveldt et al., 2003). Studies have shown that there is a causal relationship between elevated ADMA and cardiovascular disease (De Gennaro Colonna et al., 2009, Szuba and Podgórski, 2006, Liu et al., 2018). There is an association between elevated ADMA and cerebrovascular disease, and it has been suggested as a weak independent marker for stroke but strong marker for transient ischaemic attack (TIA), however causal evidence for its involvement in the pathogenesis is lacking (Wanby et al., 2006). Experimental NOS inhibition with ADMA has been shown to increase vasoconstriction, increase blood pressure (Cooke, 2005), and inhibit macrophage motility (Ahmetaj-Shala, 2013).

1.9.6 Dimethylarginine dimethylaminohydrolase

Dimethylarginine dimethylaminohydrolase (DDAH) was first purified and characterised to intracellularly hydrolyse ADMA and N^G-mono-methylated-L-

arginine (L-NMMA) to L-citrulline and dimethylamine or monomethylamine, respectively (Ogawa et al., 1989). A few years later DDAH and NOS enzymes were histologically detected within the same regions in the rat kidney, which prompted investigation into whether to DDAH acts as a regulator of NOS through regulation of ADMA metabolism (Tojo et al., 1997). The observations that low DDAH protein levels were detected in dissonance with high DDAH activity in certain tissues, led to the hypothesis that more than one isoform exist. In 1999 a seminal article described a second human isoform, thereafter known as dimethylarginine dimethylaminohydrolase 2 (DDAH2) (Leiper et al., 1999), which was found to be a functional homologue of the first enzyme, now known as DDAH1.

The two isoforms have distinct mouse tissue distribution. Early experiments using Northern blot analyses showed that *Ddah1* expression was strongest in kidney and moderate in brain, liver, and pancreatic tissue, while *Ddah2* expression was shown to be highest in the heart, kidney, lung and placenta, and almost absent from the brain (Leiper et al., 1999). This tissue distribution pattern was confirmed using PCR (Dayal et al., 2008) (Figure 1-7). More recently, protein expression of both isoforms has been reported in mouse retinal endothelium (Lange et al., 2016), kidney (Wetzel et al., 2020), lung (Ragavan et al., 2023), and, interestingly, in cerebral neurons (Kozlova et al., 2021) and the whole brain (Ragavan et al., 2023, Gao et al., 2024), while DDAH1 was more abundant in the liver with negligible hepatic expression of DDAH2 (Ragavan et al., 2023).

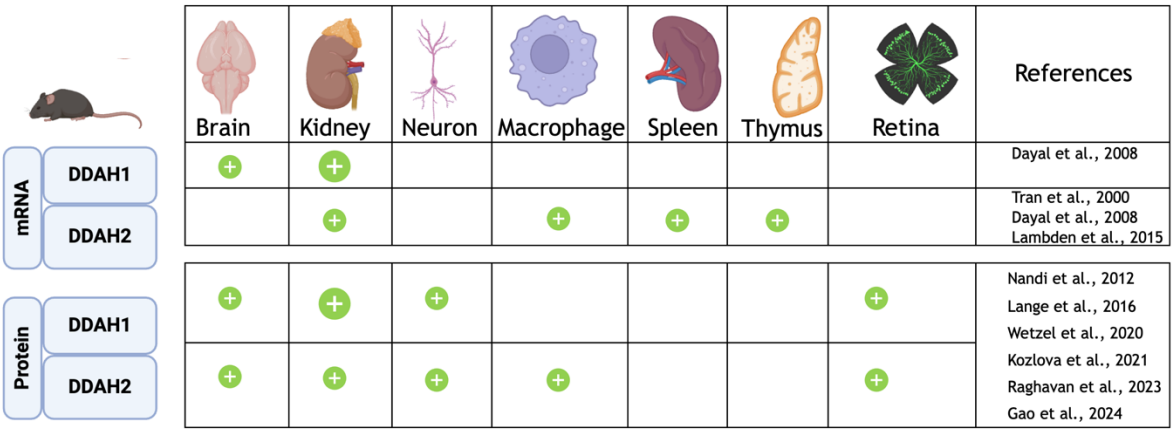

Figure 1-7. Expression of *Ddah1* and *Ddah2* mRNA and DDAH1 and DDAH2 protein levels in different mouse tissues. Larger plus signs indicate stronger expression.

1.9.6.1 Roles of DDAH2 in disease

Preclinical studies have illustrated functional roles for DDAH2 in disease models. DDAH2 was shown to improve diabetic endothelial dysfunction (Lu et al., 2010) and conferred protection in polymicrobial sepsis (Lambden et al., 2015). In dilated cardiomyopathy DDAH2 reduced fibrosis and improved cardiac function (Zhu et al., 2019), and was later shown to stabilise atherosclerotic plaques (Shoeibi et al., 2021). Most recently DDAH2 enhanced pancreatic insulin secretion through Sirt-1 mediated transcriptional up-regulation of secretagogin, an insulin vesicle docking protein (Hasegawa et al., 2013). A functional variant of DDAH2 (rs9267551 C) has been associated with myocardial infarction in patients with type 2 diabetes (T2D) (Mannino et al., 2019).

1.9.6.2 DDAH2 hydrolysis of ADMA

In animals deficient in DDAH2, ADMA levels increased in myocardium and kidney (Lambden et al., 2015) and the retina (Lange et al., 2016), suggesting that DDAH2 hydrolyses ADMA in these tissues. Importantly, DDAH2 is the only isoform expressed in macrophages and primary immunogenic organs such as the spleen and thymus (Tran et al., 2000)(Figure 1-7), suggesting it plays a central role in regulating NO through metabolism of ADMA in those tissues. Rodents deficient in DDAH2, either globally or within monocytes/macrophages, display significant impairment of iNOS-NO-mediated immune function by inadequate mounting of an immune response to septic challenge (Lange et al., 2016, Lambden et al., 2015). Indeed, increased ADMA and decreased nitrate/nitrite concentration was demonstrated in DDAH2-deficient hypoxic peritoneal macrophages (Lambden et al., 2016). The location of the gene encoding *Ddah2* on chromosome 6p21.3 in the gene cluster region of major histocompatibility complex III (MHC III), which is important for immune reactions (Deakin et al., 2006), has led to the investigation of this gene in relation to viral infections (Huang et al., 2021) and inflammation (Lambden et al., 2015), while its role in neuroinflammation is completely unexplored.

1.9.7 ADMA in ischaemic stroke

Evidence from several small clinical studies has implicated ADMA in stroke. ADMA levels were significantly increased in the CSF and plasma of ischaemic stroke

patients, which correlated with stroke severity (Brouns et al., 2009). Another study showed increased plasma ADMA and its analogue SDMA within the first 3 days after ischaemic stroke, which predicted worse clinical outcomes (Worthmann et al., 2011). Higher plasma ADMA and SDMA were highly correlated with inflammatory markers such as monocyte chemotactic protein-1 (MCP-1), matrix metalloproteinase-9 (MMP-9), interleukin-6 (IL-6) and C-reactive protein (CRP) up to a week after ischaemic stroke (Chen et al., 2012). In stroke patients with lower severity scores the ratio of L-arginine/ADMA was higher compared with those with higher severity scores (Lindgren et al., 2014), which indicates that plasma ADMA scales with disease activity and could be a good biomarker to stratify patients.

In a trial in patients with subarachnoid haemorrhage, who developed delayed ischaemic injury and had worse functional outcome, high levels of plasma methylarginines were reported (Appel et al., 2018). Additionally, ADMA was proposed as a potential biomarker for subclinical vascular brain injury (Pikula et al., 2009), as increased ADMA increased the odds ratio of developing white matter hyperintensities and silent brain infarcts in the stroke-free Framingham offspring cohort (Pikula et al., 2009). Collectively these studies demonstrate that ADMA is an important molecular target in ischaemic stroke and cerebral vascular disease.

1.9.8 The NO-ADMA-DDAH2 pathway in ischaemic stroke

The mechanisms for increased ADMA after ischaemic stroke are increased proteolysis and/or disruption in the enzymatic machinery regulating ADMA. Elevated ADMA within endothelial cells is associated with endothelial dysfunction, while enhanced levels of ADMA via decreased DDAH2 activity within macrophages could be potentially beneficial in regulating the excess production of NO through iNOS (Dowsett et al., 2020). In the vasculature, cytokine-stimulated expression of iNOS and DDAH1 in vascular smooth muscle cells increased NO and decreased ADMA (Ueda et al., 2003). The NO-ADMA-DDAH2 pathway (Figure 1-8) in macrophages is still relatively unreported. Indirect evidence for the existence of this pathway in macrophages is derived from a study, in which elevated ADMA downregulated the expression of ATP-binding cassette (ABC) transporters ABCA1 and ABCG1, which are responsible for cholesterol efflux (Chen et al., 2019). This impaired cholesterol efflux from macrophages and led to lipid accumulation and foam cell formation. DDAH2 overexpression in these cells normalised cholesterol

efflux, functionally linking excess ADMA and DDAH2 expression in macrophages for the first time, while the impact of DDAH2 on NO was not directly investigated.

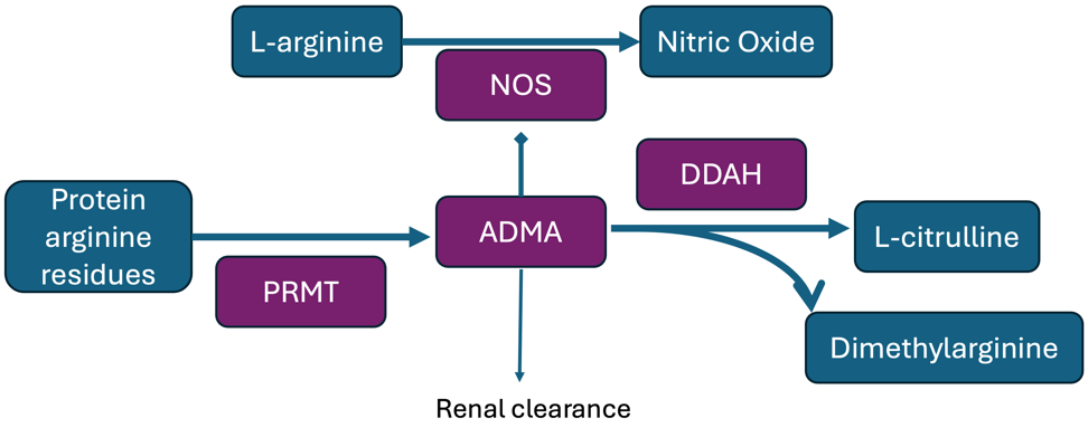

Figure 1-8. The nitric oxide (NO), asymmetric dimethylarginine (ADMA), dimethylarginine dimethylaminohydrolase (DDAH) pathway. Protein arginine methyltransferases (PRMTs).

The role of DDAH2 in mouse peritoneal macrophage function was studied by generating a mouse strain of global and monocytes/macrophage specific DDAH2 knockout (Lambden, 2016). In macrophages lacking DDAH2 challenged with pro-inflammatory stimuli, phagocytosis and motility were disrupted, along with an increased intracellular ADMA (Ahmetaj-Shala, 2013). In the same study this was replicated in macrophages isolated from mice lacking DDAH2 specifically within monocytes/macrophages, and while these was only a modest increase in ADMA in those macrophages, they showed decrease in NO production. A hypoxic challenge in isolated primary murine macrophages induced a 4-fold increase in iNOS over control, an increase in DDAH2, reduced ADMA, and increased NO (Lambden et al., 2016). This was replicated in macrophages from macrophage specific DDAH2 knockout mice in the same study, which showed a decrease in NO production and a modest increase in ADMA. These studies indicate that perhaps in models of cerebral ischaemia upregulation of DDAH2 may be responsible for the above-described deleterious effects of iNOS after stroke.

1.10 Thesis hypothesis and aims

Macrophages and microglia are key cellular contributors to neuroinflammation after ischaemic stroke. A specialised population of macrophages known as BAMs is located in the CNS borders and is likely to respond to the ischaemic insult by

proliferating and/or migrating into the ischaemic parenchyma. It was hypothesised that ischaemia-reperfusion causes a proliferation-driven accumulation in the number of BAMs and differential migration to the ischaemic infarct and peri-infarct areas.

During hypoxia, iNOS expression is upregulated and ADMA concentration is decreased in macrophages, resulting in excess nitric oxide production and release and resultant nitrosative stress, neuronal apoptosis, and infiltration of leukocytes. This process may be enhanced by a potential upregulation or increased activity of DDAH2. In macrophages, where DDAH2 is genetically knocked out (DDAH2 KO), the excess production of NO could be decreased by increased concentration of ADMA in the absence of its regulator. Thus, it was hypothesised that ischaemia upregulates the expression of DDAH2 in macrophages and that lack of DDAH2 in macrophages leads to altered macrophage phenotype. It was also hypothesised that DDAH2 plays a role in potentiating the negative effects of iNOS-derived NO and that stroke outcomes would improve by knocking out *Ddah2* from monocytes. To address these hypotheses, the main aims of this thesis were:

Aim 1: To characterise the effect of ischaemia-reperfusion on the number and localisation of BAMs in the acute, sub-acute and chronic stages of ischaemic stroke (Chapter 3).

Aim 2: To determine *Ddah2* mRNA expression in hypoxic conditions in macrophages *in vitro* and to investigate the effect of cerebral ischaemia-reperfusion on DDAH2 expression in the brain(Chapter 4).

Aim 3: To determine the effect of monocyte/macrophage DDAH2 deletion on acute brain injury, functional outcomes, and neuronal apoptosis after ischaemia-reperfusion (Chapter 5).

2 Chapter 2: General Methodology

2.1 Animals

2.1.1 Home Office licences

All experiments were performed under a UK Home Office Project Licences (P486284C3 and PP1054605) and Personal Licences (Gabriela Gerganova: I50040854, Dr Alyson Miller: IAC7C2F3D) in accordance with the Animals (Scientific Procedures) Act 1986 and approved by the University of Glasgow's Animal Welfare and Ethics Review Board (AWERB). These experiments were also covered by Glasgow Experimental Request Form (GERFs) numbers 005, 082, 109, 110, 156.

2.1.2 Compliance with the ARRIVE guidelines

The ARRIVE guidelines for reporting of animal research (Kilkenny et al., 2010, Percie du Sert et al., 2020) were not strictly adhered to.Deviations include lack of randomisation, lack of blinding during data collection, and omitting female mice from the stroke studies design.

2.1.3 C57BL/6J mice

Male C57BL/6 mice were purchased from Envigo (Blackthorn, UK) at 6-7 weeks of age and acclimatised for at least one week before study. Mice were housed with same-sex littermates in controlled humidity, temperature (22°C) and 12 h/12 h light/dark cycle environment and had access to water and standard chow *ad libitum*.

2.1.4 DDAH2 LysM-Cre mice

The DDAH2 LysM-Cre mice were generated by a deletion targeting a locus of all 7 exons of the DDAH2 gene on a mixed 129/SvEvBrd x C57BL6/J background, with *LoxP* sites flanking exon 2 and exon 5. The addition of a neomycin cassette prior to the *LoxP* 3' end allows deletion of the *LoxP* flanked sequence upon Cre-recombinase (Cre) activity in the murine M lysozyme locus, only expressed in mature monocytes (Cross et al., 1988, Clausen et al., 1999) (Figure 2-1A) (Lambden et al., 2015). These mice were generated over 10 years ago at a different facility and had to be re-derived for this project. DDAH2 floxed mice were generated by Genoway for Professor Leiper's and Dr Dowsett's lab group.

LysM-Cre mice were purchased from the Jackson Laboratory (B6.129P2-Lyz2tm1(cre)Ifo/J). The two strains were crossed (Figure 2-1B) at the Beatson Institute and imported into the SCMH facility by Dr Zaniah Gonzalez. To expand the colony and to minimise genetic drift, mice were bred in with C57BL6/J background. This resulted in offspring that were either heterozygous for a DDAH2 wildtype and a floxed allele, or homozygous carrying two floxed alleles. The presence of bands for both a wildtype (495 bp) and a floxed (552 bp) PCR product on the agarose gel (detailed below) was used to identify a pup as heterozygous for DDAH2, while absence of a wildtype band and presence of a floxed band indicated the pup was homozygous for the floxed DDAH2 allele. Sires positive for Cre were mated with dams negative for Cre (Figure 2-1B) to avoid germline transmission and to maintain Cre carriers in the colony. Heterozygous pups were eventually bred out and subsequently monocyte/macrophage specific excision of DDAH2 was ascertained via Cre expression, demonstrated by the presence of 720 bp PCR product. Throughout this thesis the experimental knockout mice are referred to as DDAH2$^{Mo-/-}$ and their littermate 'floxed' controls as DDAH2$^{fl/fl}$.

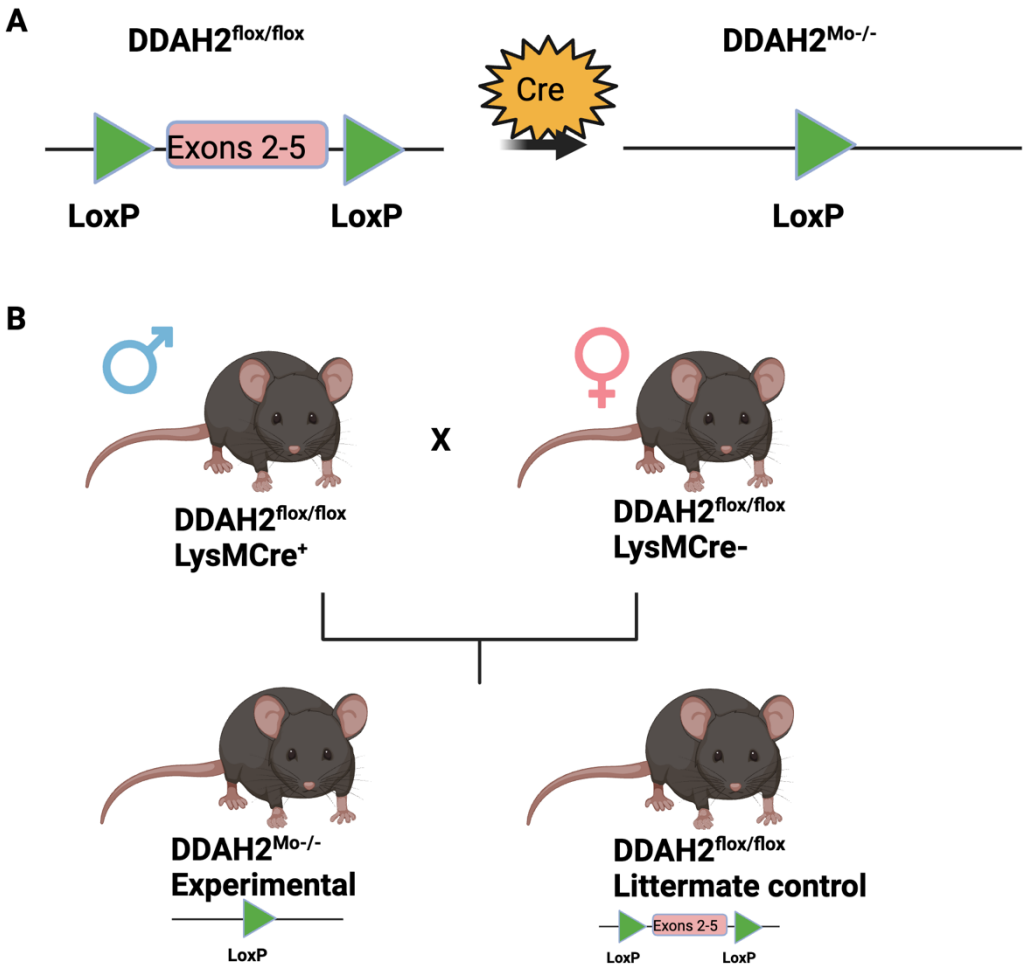

Figure 2-1. Schematic representation of the breeding strategy to obtain DDAH2$^{Mo-/-}$ and DDAH$^{fl/fl}$ mice. Expression of Cre recombinase in the M lysosome locus triggers the excision of exons 2-5 from the *Ddah2* gene. In the absence of Cre, floxed controls are generated. In the presence of Cre, knockout mice are generated, which are the experimental animals. B Breeding strategy for generation of experimental and control mice by crossing a sire positive for Cre recombinase with a dam negative for Cre recombinase. Both breeders are homozygous for the floxed DDAH2 allele. Figure created using elements from Biorender.

Mice were at least 8 weeks of age before mating. Each breeding pair remained active up to five offspring before being terminated. Only male mice were used for experiments that generated data presented in this thesis, while females were used for optimisation work.

Ear notches taken from 3-week-old male and female DDAH2$^{Mo-/-}$ and DDAH$^{fl/fl}$ mice were digested in 100 µl alkalising buffer (containing 25 mN NaOH, 0.2 mM EDTA) for 1 hour at 98 °C, followed by the addition of 100 µl neutralising buffer (40 mM Tris HCl, pH 5.5), vortexed and store at -20 °C until use. End-point polymerase chain reaction (PCR) was performed using undiluted DNA (3 µl), DreamTaq™ Hot

Start Green DNA Polymerase (Thermo EP1712, 10 µl), 1 µl forward primer, 1 µl reverse primer (Table 2-1) and 5 µl nuclease-free water on PCRMAx Alpha Cycler 4 (PCRmax) with PCR running parameters described in Table 2-2.

Table 2-1 Primers used for genotyping the DDAH2 LysM-Cre colony.
F: forward, R: reverse.

GENE	PRIMER SEQUENCES (5'-3')	SOURCE
DDAH2	F GGGCAGGGCTATGGTGAAGG R ACCTCCTGGCTGTTGGGCAG	Sigma, custom oligos
CRE	F GCCTGCATTACCGGTCGATGCAACGA R GTGGCAGATGGCGCGGCAACACCATT	Sigma, custom oligos

Table 2-2. PCR running parameters.

	STAGES	INITIAL DENATURATION	MAIN REACTION		FINAL EXTENSION	
	Steps		Denaturation	Annealing	Extension	
DDAH2	Temperature	95°C	95°C	57°C	72°C	72°C
	Duration	3 min	20 sec	40 sec	1 min	10 min
	Thermal Cycles	1		40		1
CRE	Temperature	95°C	94°C	60°C	72°C	72°C
	Duration	5 min	30 sec	30 sec	1 min	10 min
	Thermal Cycles	1		34		1

To confirm the presence of wildtype or floxed alleles for DDAH2, and the presence or absence of a Cre allele, bands were distinguished on a 1.5% agarose gel. Gels contained 3X Gel Red nucleic acid stain (10,000x, water, Merck, SCT123), were loaded with GeneRuler 100bp DNA ladder (3 µl, Thermo Fisher SM0234) and were visualised on a ChemiDoc XRS+ Molecular Imager (Bio-Rad Laboratories Ltd, UK) to confirm the presence of bands; DDAH2 wildtype: 495 bp, DDAH2 floxed: 552 bp, Cre recombinase: 720 bp.

2.2 *In vivo* procedures

2.2.1 Transient middle cerebral artery occlusion (tMCAo)

Focal cerebral ischaemia-reperfusion injury was induced by tMCAo using the intraluminal filament method (Rousselet et al., 2012, Liu and McCullough, 2014). This model mimics the clinical pathology of acute ischaemic stroke by allowing

reperfusion, which is the therapeutic objective of all currently approved treatments for ischaemic stroke. The Koizumi method of tMCAo was first published in 1986 and involves intraluminal filament insertion through the common carotid artery (CCA) and relies on contralateral reperfusion through the Circle of Willis (Koizumi, 1986). A refined Zea Longa method published in 1989 involves filament insertion via the ECA and therefore allows for bilateral CCA reperfusion (Longa et al., 1989) and typically results in final infarct development at 72 hours post-surgery. This study used the Zea Longa method for findings presented in Chapter 3 and Chapter 5.

Mice were anaesthetised with isoflurane using an inhalation mask; 3% for induction, 2% for maintenance in 1.5 L/min 30% O_2/70% N_20 mix (Zoetis, UK). Body temperature was maintained at 37±0.5° C with a heat lamp (ExoTerra, US) and heat pads laid adjacent to the animal throughout the procedure, and monitored using a rectal probe (Testronics, Australia) every 5 minutes during surgery. Pain relief and hydration prior to surgery were provided as follows; 4 mg/kg bupivacaine (Naropin), by a subcutaneous injection at the two sites of incision – neck and head, and two subcutaneous injections of 0.5 ml of pre-warmed saline into each side of the back of the mouse. An approximately 1 cm-long incision into the skin was made in a sterilised area between the right ear and right eye to expose the skull. To monitor regional cerebral blood flow (rCBF) (PF5010 LDPM Unit, Perimed, Sweden) a laser-doppler flowmetry probe was glued to the skull using superglue in the cortical territory supplied by the MCA (approximately 1 mm posterior and 5 mm lateral to bregma, Figure 2-3).

A nylon monofilament with silicone-coated tip of two sizes was chosen prior to surgery depending on the animal's weight; 602112PK10 if ≤25 g, and 602312PK10 if ≥25 g (Doccol, US), and three marks were scored with a blade at 11±1 mm away from the silicone-coated tip to guide correct positioning. An approximately 1 cm-long incision into the skin was made in a sterilised area along the midline of the neck. A stump was created along the ECA, a suture was passed under the internal carotid artery and an arterial clamp was placed on the common carotid artery (CCA) at the proximal end of the ECA to temporarily cease circulation (for ≤5 minutes) to allow filament insertion, using the Zea Longa method (Li et al., 2023, Longa et al., 1989). The filament was introduced into the ECA stump and advanced

11±1 mm, occluding the MCA at its origin. Laser doppler was used to measure rCBF during filament insertion and removal to verify successful tMCAo as per the set criteria; a reduction in rCBF greater than 70% confirmed correct placement of the filament (Figure 2-2).

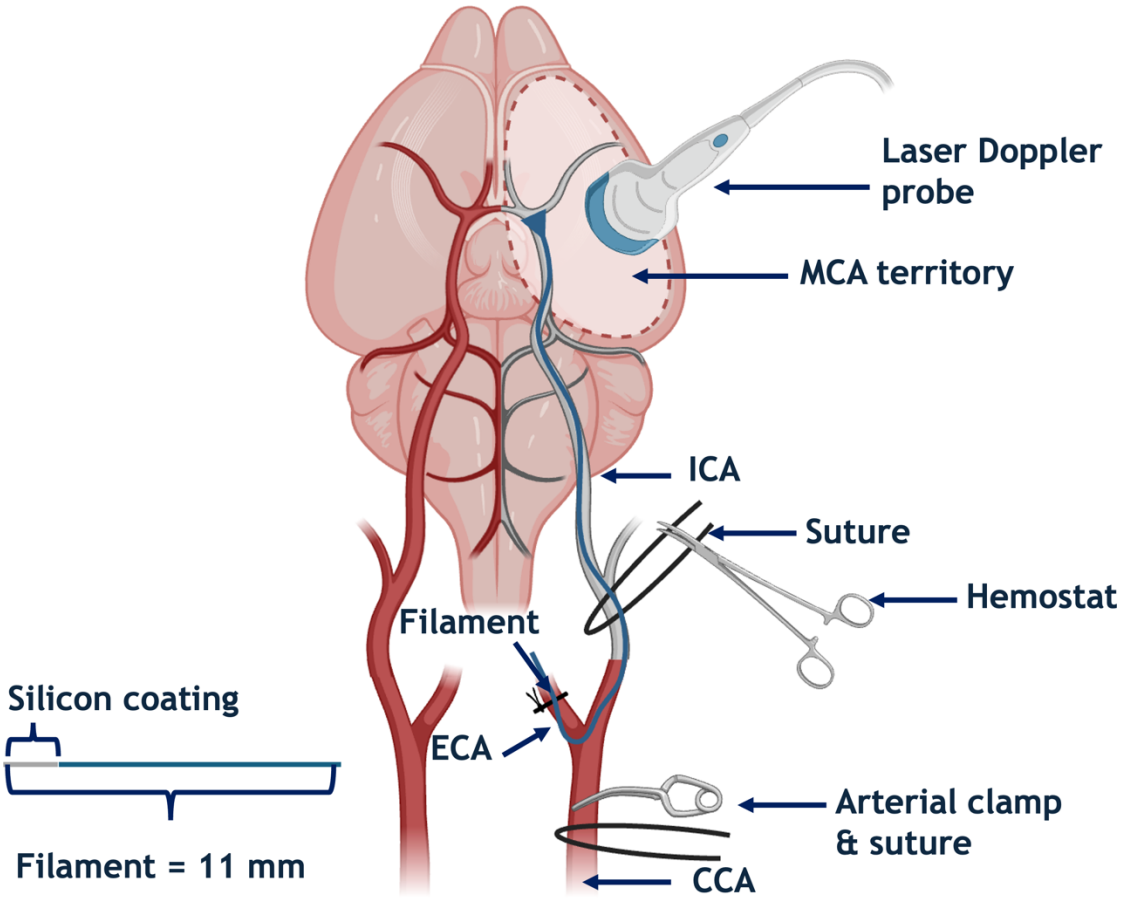

Figure 2-2. Surgical procedures for middle cerebral artery occlusion (MCAO) and monitoring of cerebral blood flow (CBF) using a Laser Doppler probe. CCA – common carotid artery, ECA – external carotid artery, ICA – internal carotid artery, MCA – middle cerebral artery. Figure created using elements from Biorender.

CBF was recorded prior to ischaemia, every 5 minutes for the duration of the ischaemic period and up to 10 minutes of reperfusion. Half an hour before the end of the surgery 0.05 mg/kg buprenorphine (Vetergesic) was injected subcutaneously. At the end of the ischaemic period the monofilament was retracted to allow reperfusion and restoration of >80% of baseline rCBF within 10 minutes of filament withdrawal confirmed successful reperfusion. The probe was detached from the skull and both surgical incisions were sutured with a VICRYL undyed silk suture size 5/0 (Nu-care). For sham-operated animals all experimental procedures were performed except for the insertion and withdrawal of the

filament. Sham and tMCAO mice were terminated on either day 1, day 3, day 7, day 14, or 1 month.

2.2.2 Analgesia and perioperative care

A dose of 0.05 mg/kg buprenorphine (Vetergesic), subcutaneous injection, was administered at 24 hours and 48 hours after tMCAo. Post-surgery animals were returned to their home cages or were housed individually to avoid would exacerbation by cage mate aggressive behaviour, and lined with a vet bedding and recovered in a warm incubation chamber (26±0.5° C) for the initial 4 hours after surgery. Thereafter, the cages were transferred to a designated recovery room on either electrically heated mats heated to 37±0.5° C or in an incubation chamber (26±0.5° C) and mice were allowed to recover overnight. Recovering animals were provided with soft food – freshly prepared mash, baby food and hydration gel, standard chow pellets and water *ad libitum*. Body weight was recorded at baseline, and every day after surgery until the scientific endpoint. Appetite, urine, and faeces output were examined daily, and sutures were checked for infection. Animals were monitored using a clinical severity scoring sheet for physical, clinical, and behavioural symptoms for at least 4 hours following surgery and at least once daily thereafter until the study endpoint. Each of these criteria is assigned a score and a total score calculated (Table 2-3). The total score was interpreted as follows: 0-5 the mouse was monitored once a day; 6–9 the mouse was monitored several times a day and euthanasia considered. In consultation with the Named Animal Care and Welfare Officer and/or the Named Veterinary Surgeon, ≥10 or a score of 4 for a single criterion led to immediate euthanasia.

Table 2-3. Post tMCAo monitoring sheet based on appearance, bodyweight loss, provoked behaviour, and clinical signs. Scores are indicated against each descriptor.

APPEARANCE		**CLINICAL SIGNS**	
Normal	0	Intermittent abnormal breathing	1
Slightly unkempt	1	Diarrhoea	2
Staring coat	2	Dull, pale eyes	2
Slightly hunched	3	Semi-closed eyes	2
Markedly hunched	4	Less inquisitive than normal	2
		Laboured respiration	3
		Barrel-rolling	4
BODYWEIGHT LOSS			
Normal <5%	0	**PROVOKED BEHAVIOUR**	
Mild 5-10%	1	Normal	0
Moderate 10-15%	2	Minor depression/exaggeration	1
High 15-19%	3	Moderate change	2
Severe ≥20%	4	**Reacts violently or very little**	**4**

2.3 Histological methods

2.3.1 Cryopreservation and sectioning of brain tissue for immunofluorescence analyses

Brains were frozen slowly over liquid nitrogen and then stored at -80° C prior to sectioning for histological analyses. Brains were embedded in Tissue-Tek® O.C.T. Compound (Sakura) and mounted on a Cryostat (CryoStar NX50, Epredia) set at -12° C. Coronal sections (10 µm thickness) were obtained by thaw-mounting onto poly-L-lysine coated glass slides. Sections covering three regions of the brain (region 1: +2.8 to +0.76 mm; region 2: +0.25 to -1.79 mm; region 3: -2.3 to -4.34 mm, relative to bregma) were collected in replicates of nine and stored at -80°C. Replicates 1-4 were used for infarct and oedema volume analyses and replicates 5-9 were used for immunofluorescent analyses.

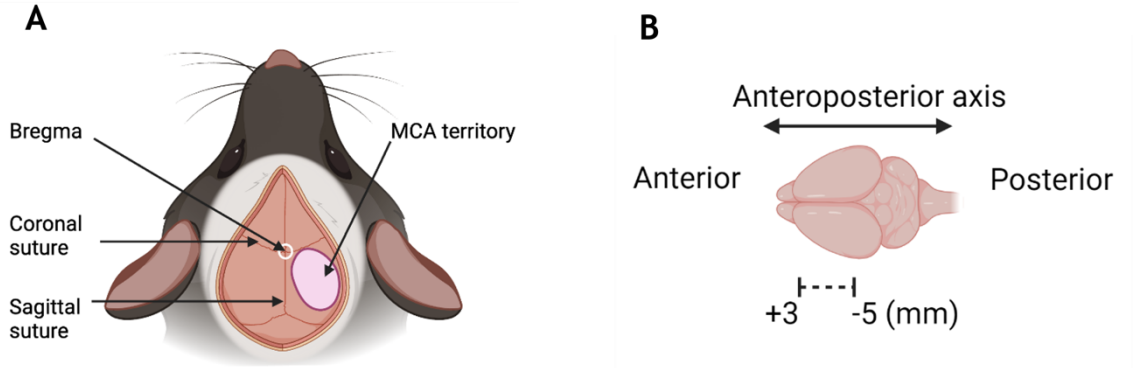

Figure 2-3. Gross anatomy of the mouse cranial sutures. The bregma is the anatomical point on the skull, at which the coronal suture is intersected perpendicularly by the sagittal suture. A) The middle cerebral artery (MCA) territory is depicted in pink, with its core at approximately 1 mm posterior and 5 mm lateral to bregma (Riva et al., 2012). B) Mouse brain dimensions and axis of coronal sections produced on the cryotome.

2.4 Immunophenotyping with flow cytometry

2.4.1 Dissociation of mouse brain tissue

Freshly isolated naïve, stroke and sham mouse brains were dissected into cerebral hemispheres, the cerebellum and olfactory bulb were removed. Brain tissue was then enzymatically digested for 30 min by incubation at 37 °C in digestion buffer containing collagenase XI (0.106 mg/ml), hyaluronidase (0.030 mg/ml), collagenase I-S (1.80 mg/ml) with mechanical agitation every 10 minutes (Reichard and Asosingh, 2019).

Following digestion, the tissue was passed through a sterile 70 µm filter (EASYstrainer, Greiner, 542070) to remove undigested tissue/debris, washed with 25 ml of flow cytometry buffer containing 0.5% bovine serum albumin (in PBS, w/v) and 0.04% sodium azide (in PBS, w/v) and centrifuged at 1500 rpm for 5 min at RT. To remove myelin, the cell pellet was resuspended in 30% (in PBS, v/v) Percoll density medium, pH 8.5-9.5 (Merck, P1644) in a Falcon tube and layered over a 70% (in PBS, v/v) for gradient centrifugation at 2700 rpm for 20 minutes at RT with the brakes of the centrifuge turned off (Martin et al., 2017a). The centrifugation allowed myelin and tissue debris to separate on top of the supernatant and this fraction was removed using vacuum suction. Cells, which separated in the border between the 30% and 70% Percoll gradients, were pipetted out and washed in excess with 2% foetal bovine serum (FBS) (in PBS, v/v) and centrifuged at 1500 rpm for 5 minutes. The cells were then resuspended in 0.5 mL

of ice-cold flow cytometry buffer ready for staining. Where a thin red layer near the bottom of the Falcon tube was observed after this step, indicative of incomplete transcardial perfusion, red blood cells (RBC) lysis was performed prior to washing. Cells were resuspended in 5 mL of 10% RBC lysis buffer (Biolegend, 420301), and incubated on ice for 5 minutes. Cell counting was performed manually using a Burker chamber and 0.4% trypan blue staining. Typically, ~250,000 cells/hemisphere were retrieved per isolation.

2.4.2 Cell staining with fluorescent antibodies.

Cells in flow cytometry buffer (unstained control cells) or flow cytometry buffer, containing antibody cocktails detailed in the relevant results chapters and containing antibodies listed in Table 2-4 were incubated at 4 °C in the dark for 25 min. Cells were then washed in flow cytometry buffer, centrifuged at 1500 rpm for 5 min and re-suspended in flow cytometry buffer.

Table 2-4. Antibodies used for flow cytometry.

ANTIGEN	FLUOROPHORE	HOST, ISOTYPE	CLONE	SUPPLIER	CATALOGUE NUMBER
CD45	PE	Rat, Ig2b, κ	30-F11	Biolegend	103106
CD11B	APC/Cy7	Rat, Ig2b, κ	M1/70	Biolegend	101225
CD206	FITC	Rat, Ig2a, κ	C068C2	Biolegend	141703
LYVE1	APC	Rat, Ig2a	223322	R&D Systems	FAB2125A
CD45.2	FITC	Mouse, IgG2a, κ	104	eBioscience	11-0454
CD3	PE	Armenian Hamster, IgG	145-2C11	Biolegend	100307
CD19	PE-Cy7	Rat IgG2a, κ	6D5	Biolegend	115519
LY-6G	PerCP (Cy5.5)	Rat IgG2a, κ	1A8	BD Biosciences	560602
LY-6C	APC-Cy7	Rat IgM, κ	AL-21	BD Biosciences	560596
CD11B	V500	Rat, IgG2b, κ	M1/70	BD Biosciences	562128
F4/80	PerCP/Cy 5.5	Rat Ig2a, κ	BM8	Biolegend	123128

2.4.3 Compensation

Multi-colour flow cytometry panels require calibration of voltages of the photomultiplier tube and the lasers associated with each fluorophore to allow

spectral separation of the data collection scatter plots. Software automated compensation was conducted on BD FACS Diva prior to each experiment (Manohar et al., 2021). Compensation samples were prepared for each fluorophore used in a panel. A drop of compensation beads (UltraComp eBeads™ Plus Compensation Beads, Invitrogen, 01-3333-42) was mixed with 0.25ml of each antibody (Table 2-4), vortexed and incubated on ice for 15 min in the dark. The beads were then washed with flow cytometry buffer, centrifuged (1500 rpm, 5 min, 4°C) and resuspended in 250ml flow cytometry buffer for acquisition. In instances where spectral separation was difficult for a particular pair of fluorophores, additional controls known as fluorescence minus one (FMO) were used. An FMO contains a mixture of all antibodies in the panel with omission of a particular antibody of interest.

2.4.4 Data acquisition and analysis

Viability was assessed by adding 1μL of 7-aminoactinomycin d (7-AAD), which is a fluorescent dye that binds to guanine and allows for intercalation between single stranded DNA (Adan et al., 2017). The 7-AAD Viability Staining Solution (Biologened, 420403) immediately before data acquisition. Acquisition (50,000-100,000 events) was conducted on BD FACS Canto II (BD Biosciences) coupled with BD FACS Diva software. Analysis was performed on FlowJo 10.8 (BD Biosciences) software. Quantification of absolute numbers of cells per hemisphere was assisted by AccuCheck counting beads (AccuCheck Counting Beads, Invitrogen) using the formula below and by using the specific number of beads per LOT provided by the manufacturer.

$$Absolute\ Count\ \left(\frac{cells}{\mu l}\right) = \frac{Number\ of\ cells\ counted}{Total\ number\ of\ beads\ counted\ Beads}\ x\ Number\ of\ AccuCheck\ Counting\ Beads\ per\ \mu l$$

2.5 Statistics

All datasets were analysed with GraphPad Prism Software 8 and $P<0.05$ was considered statistically significant. Numbers of biological replicates (n), statistical tests and power calculations, where applicable, were described in the methods section of relevant results chapters and figure legends. Continuous data was expressed as mean ± standard error of the mean (SEM). Descriptive statistics were used to determine variance and to inform the choice of statistical test. For data

sets where the variance between groups was not equal, Welch correction was applied. Data sets with 2 groups were analysed using a paired or an unpaired t-test. For datasets with >2 groups, normality tests (Kolmogorov-Smirnov or Shapiro-Wilk test for $n \geq 8$ and D'Agostino & Pearson test for $n < 8$) were performed to inform subsequent statistical analyses. Data that was normally distributed and had equal variance between groups was analysed using ordinary one-way ANOVA with Sidak's multiple comparisons tests. Data that was normally distributed but had unequal variance was analysed by ordinary ANOVA or Brown-Forsythe and Welch ANOVA with Tamhane's T3 multiple comparisons test. For datasets that did not pass any normality test, non-parametric Kruskal-Wallis with Dunn's selected multiple comparisons tests were performed instead. Scored data from nest building activity and the modified neurological severity score was expressed as median and analysed with non-parametric tests: Wilcoxon paired and Mann Whitney unpaired tests.

3 Chapter 3: Effect of cerebral ischaemia-reperfusion on the number and localisation of CNS border-associated macrophages.

3.1 Introduction

The CNS border-associated macrophages (BAM) are a small immune cell population, located in the perivascular space, the meninges and choroid plexus. The perivascular space is a compartment around blood vessels, delimited by the astrocyte end-feet (glia limitans) and basement membrane of the blood vessel. Perivascular macrophages reside within the perivascular space, adhering to the abluminal side of the basement membrane (Yang et al., 2019). They are found around penetrating and parenchymal cerebral arteries and arterioles, around pial and subpial vessels, and venules in the peri-venule space. Meningeal BAMs are located primarily in the subarachnoid space in the recently characterised subarachnoid lymphatic-like membrane, proposed to be the fourth meningeal layer (Møllgård et al., 2023). They are morphologically diverse, with meningeal BAMs being mostly round shaped, while perivascular BAMs show elongated morphology (Nayak et al., 2012, Goldmann et al., 2016). Similar to microglia, and in contrast to peripheral monocytes, BAMs have been shown to derive from embryonic precursors in the yolk sac (Goldmann et al., 2016, Dermitzakis et al., 2023, Utz et al., 2020) and form a stable, self-renewing population in adult life.

Murine BAMs differentially express several identification markers, which have been revealed through cell surface phenotyping and immunohistochemical approaches, and more recently by single cell sequencing. Canonical markers include CD206, which is a pattern recognition mannose receptor transcribed from *Mrc1* (Galea et al., 2005, Martinez-Pomares, 2012, Mrdjen et al., 2018, Lapenna et al., 2018), LYVE1 - lymphatic vessel endothelial hyaluronan receptor 1 (Zeisel et al., 2015, Mrdjen et al., 2018, Brezovakova and Jadhav, 2020, Kim et al., 2021a), major histocompatibility complex II (Liu et al., 2005), CD36 (Park et al., 2017), CD169 (Rajan et al., 2020), and CD163, albeit expressed at lower levels that in rats and humans (Fabriek et al., 2005). BAMs are frequently identified either single positively for CD206 (Rajan et al., 2020), or along with the pan-leukocytic CD45 and pan-myeloid CD11b markers as $CD45^{+}CD11b^{+}CD206^{+}$ cells (Levard et al., 2024). However, CD206 is recognised since the 1990s as a canonical marker of M2-like polarisation in macrophages and is expressed on M2-like resident or peripheral macrophages (Orecchioni et al., 2019) and on some microglia (Franco and Fernández-Suárez, 2015, Zhang et al., 2023). Arginase-1, another anti-inflammatory marker, was upregulated in BAMs isolated from rat brains after

acute ischaemic stroke (Pedragosa et al., 2018), suggesting that post-ischaemic BAMs may adopt a M2-like macrophage phenotype. Therefore, in the present study, $CD206^+$ cells were termed M2-like macrophages that contain some BAMs and other macrophages.

Two large subpopulations of BAMs are now recognised to also express Lyve1 or MHCII (Mrdjen et al., 2018, Drieu et al., 2022). $Lyve1^+$ BAMs regulate arterial motion that drives CSF flow (Drieu et al., 2022), while MHCII expressing BAMs are involved in antigen presentation (Mrdjen et al., 2018). Both CD206 and Lyve1 are expressed under homeostasis and under systemic inflammation in mice (Møllgård et al., 2023). Importantly, acutely after ischaemic stroke this core BAMs gene signature is largely unchanged (Zheng et al., 2021). To obtain the greatest specificity of detection of the largest population of BAMs, BAMs were identified by a $CD45^+CD11b^+CD206^+Lyve1^+$ immunophenotype in this study, which examined the effect of cerebral ischaemic on the number of BAMs.

BAMs represent a small immune cell population, constituting only a tenth of total leukocytes in the healthy murine brain (Mrdjen et al., 2018) but have been described to play various roles in brain diseases and neuroinflammation. In Alzheimer's disease and cerebral amyloid angiopathy BAMs were described as having deleterious roles (Hawkes and McLaurin, 2009, Park et al., 2017), and were found to contribute to hypertension-induced neurovascular and cognitive dysfunction in mice and rats through interaction with endothelial cells (Faraco et al., 2016, Iyonaga et al., 2020, Kerkhofs et al., 2020, Santisteban et al., 2020). Conversely, in a model of mild traumatic brain injury, meningeal macrophages were proliferating and accumulating near the perimeter of the lesion supporting wound healing (Russo et al., 2018). After subarachnoid haemorrhage (SAH) BAMs facilitate the uptake of erythrocytes from the perivascular and meningeal spaces, which improves the outcome of (SAH) (Wan et al., 2021). However, BAMs depletion ameliorated neurological deficit after MCAo (Pedragosa et al., 2018, Rajan et al., 2020, Zheng et al., 2021), suggesting their deleterious roles in ischaemic stroke.

Ontologically, immature macrophages and A2 progenitors migrate to colonise the perivascular and meningeal spaces (Stremmel et al., 2018, Dalmau Gasull et al., 2024). Mature BAMs display less motility and therefore limited capacity to migrate. During inflammation, perivascular macrophages have been demonstrated

to extend processes along the perivascular space (Dermitzakis et al., 2023, Barkauskas et al., 2013).

After acute ischaemic stroke the number of $CD163^+$ perivascular macrophages increased in the ischaemic parenchyma of rodents and humans compared to healthy controls (Pedragosa et al., 2018, Rajan et al., 2020). Alongside this discovery, the authors of these studies revealed that several genes related to cell proliferation were increased (Pedragosa et al., 2018). $CD163^+$ cells specifically accumulated around cerebral blood vessels in tissue from ischaemic patients (Holfelder et al., 2011). In this study, BAMs characterisation was realised through a multi-parameter signature: $CD45^+CD11b^+CD206^+Lyve1^+$ and it was hypothesised that the numbers of these cells in the mouse ischaemic hemispheres would increase compared to sham and non-affected brain hemispheres.

Despite the evidence from the above described studies, BAMs have not been characterised in the sub-acute and chronic phases of experimental stroke yet. The acute phase after tMCAo in rodents is typically considered to be up to 3 days after experimental stroke. Mean infarct volume reportedly peaks on a sliding scale between 24 hours (Turner et al., 2016), 72 hours (Pei et al., 2003, McCabe et al., 2018), or 1 week after tMCAo and lesion size reduces thereafter (Kim et al., 2021b). Concomitantly with infarct development, inflammation develops and resolves in phases too (Mărgăritescu et al., 2009). This is partially manifested by the varying numbers of leukocytes in the ischaemic milieu. After tMCAo immune cell numbers increase and peak between 24 hours (Kleinschnitz et al., 2010, Yilmaz and Granger, 2010) and 1 month after stroke (Selvaraj et al., 2021). To study the different stages of the neuroinflammatory response, some researchers describe an intermediate, sub-acute phase that usually occurs 1-2 weeks following tMCAo and is characterised by increased vascular remodelling and proliferation (Durán-Laforet et al., 2019). Thereafter, a chronic inflammation phase begins, typically characterised by resolution of inflammation, with accumulation of regulatory T lymphocytes up to a 1 month after MCAo (Stubbe et al., 2013, Kim et al., 2021c), while an increased release of adipokines is also reported to persist 60 days after tMCAo (Haley et al., 2020), indicative of chronic inflammation. One study in the sub-acute and chronic stages descibed a progressive accumulation of $CD163^+$ cells in the meninges proximal to the ischaemic tissue in post-mortem brain

tissue from patients 6 days to 5 months after stroke onset (Rajan et al., 2020), suggesting that an increase in BAMs numbers might persist into the chronic phase after stroke in mice too.

3.1.1 Chapter hypothesis and aims

The main hypothesis for this chapter was that ischaemia-reperfusion causes a proliferation-driven accumulation in the number of BAMs and differential migration to the ischaemic infarct and peri-infarct areas.

The aims of this study were to determine if tMCAo causes a change in BAMs numbers in the acute, sub-acute and chronic stages post ischaemia-reperfusion and to characterise the localisation of BAMs after tMCAo with respect to the ischaemic infarct.

3.2 Methods

3.2.1 Animals

In this chapter a total of 71 male C57BL6/J mice 8-12 weeks of age were used for the tMCAo (Figure 3-4) and subsequent analyses with a mean body weight on the day of surgery 24.7 ± 2 g. For experiments assessing the effect of ischaemia-reperfusion on the number of BAMs, a total of 11 naive (non-stroke) mice, 29 tMCAo mice, and 36 sham mice were used. We measured the number of BAMs at five different time points day 1, day 3, day 7, day 14 and 1 month after surgery. For day 1, day 3, and day 7, mice were exposed to 50 min MCAo followed by reperfusion, as described in Section 2.2.1 of General Methods, whereas for day 14 and 1 month the occlusion period was reduced to 40 min to ensure animals did not exceed severity limits (in particular body weight loss >20%) prior to reaching the scientific endpoint. For experiments examining the effect of ischaemia-reperfusion on the localisation of BAMs, tMCAo mice were exposed to 60 min MCAo followed by reperfusion and culled on day 3 following surgeries. Dr Alyson Miller performed 52 surgeries with anaesthetic assistance from me and has supported 90% of the rest. Sham operated mice were subjected to the same surgical procedures as tMCAo mice, except for the introduction of a filament, therefore blinding the surgeon was not possible.

3.2.2 Animal sacrifice and tissue collection

At the scientific endpoint for flow cytometric analyses mice were sacrificed by terminal anaesthesia with 5% isoflurane and transcardial perfusion with 0.9% saline, , brains were harvested and placed in ice cold PBS and the tissue was immediately used. For experiments examining the effect of ischaemia-reperfusion on the localisation of BAMs animals were sacrificed by a rising concentration of CO_2 (Schedule 1 of the Act) followed by decapitation, brains were harvested and slow frozen over liquid nitrogen.

3.2.3 Immunofluorescence

To study the localisation of BAMs the expression of the mannose receptor marker CD206, the hyaluronan receptor 1 (LYVE1), and alpha smooth muscle actin (αSMA) were investigated in naïve C57BL6/J mice and at 72 hours after 60 minutes of tMCAo in C57BL6/J mice (Figure 3-4). Six frozen mouse brain coronal sections on a glass slide spanning region 2 (+0.25 to -1.79 mm relative to bregma, cf. section 2.3.1) were chosen for analysis. The sections were equilibrated at room temperature (RT) and a contour was drawn around them using a hydrophobic pen. The sections were then fixed with 4% paraformaldehyde (PFA) for 3 minutes at RT. Slides were then washed with PBS (3 x 10 minutes) followed by permeabilisation for 30 minutes at RT in blocking solution comprising of phosphate buffered saline (PBS) supplemented with 5% goat serum and 0.1% Triton X-100. Double-labelled immunofluorescence was then performed for CD206 and αSMA or CD206 and LYVE1 with primary antibodies at 4˚C overnight in staining solution (PBS supplemented with 5% goat serum and 0.1% Triton X-100) using a rat monoclonal anti-CD206 (1:200), a rabbit polyclonal anti-Lyve1 (1:200) and a rabbit polyclonal anti-αSMA (1:100) (Table 3-1). Stroke surgeries for this work have been performed by Dr Alyson Miller and Dr Arun Flynn. Cryo-sectioning has been conducted by Dr Arun Flynn.

Table 3-1. Primary antibodies for immunofluorescence

Antigen	Host, Isotype	Concentration (µg/ml)	Clone	Supplier
CD206	Rat, IgG2a	0.025	MR5D3	Bio-Rad
Lyve1	Rabbit, IgG	0.025	Polyclonal	Abcam
αSMA	Rabbit, IgG	0.02	Polyclonal	Abcam

After washing with PBS (3x 10 minutes), samples were incubated for 1.5 hours at RT with the secondary antibodies (Table 3-2): goat anti-rabbit Alexa Fluor 594 (1:200) or goat anti-rat Alexa Fluor 488 (1:200) in blocking solution.

Table 3-2. Secondary antibodies for immunofluorescence

Antigen	Host	Concentration (µg/ml)	Conjugation	Supplier
Rabbit	Goat	0.05	Alexa Fluor 488	Thermo Fisher
Rat	Goat	0.05	Alexa Fluor 594	Thermo Fisher
Rabbit	Donkey	0.05	Alexa Fluor 546	Thermo Fisher
Rat	Donkey	0.05	Alexa Fluor 647	Thermo Fisher

Washing was repeated and sections were mounted onto coverslips using Vectashield mounting medium with 4′,6-diamidino-2-phenylindole (DAPI) for nuclear staining (2BScientific) and allowed to dry overnight prior to sealing with nail varnish. Images of fluorescence-labelled sections were obtained using the preset filters green, red, and blue filters on three different microscopic setups: 20x air lens on an upright AxioImager M1 fluorescent microscope (Zeiss); 10x air, 20x water, 40x water and 63x oil lenses on an inverted laser scanning microscope LSM 800 (Zeiss) or 25x water lens on an inverted laser scanning microscope (LSM 900, Zeiss). A thionin stained brightfield image was used as a guide to identify the infarct core on the immunofluorescent images. Images (638.9 μm^2) were taken from the infarct and 4 peri-infarct regions of the ischaemic hemisphere and an infarct-corresponding region in the contralateral hemisphere (Figure 3-1). Co-expression of two antigens on a single cell as guided by DAPI nuclear staining was used to identify double positive $CD206^+aSMA^+$ or $CD206^+Lyve1^+$ cells. Quantification was performed using manual cell counting and normalising to the area of the image on Fiji software.

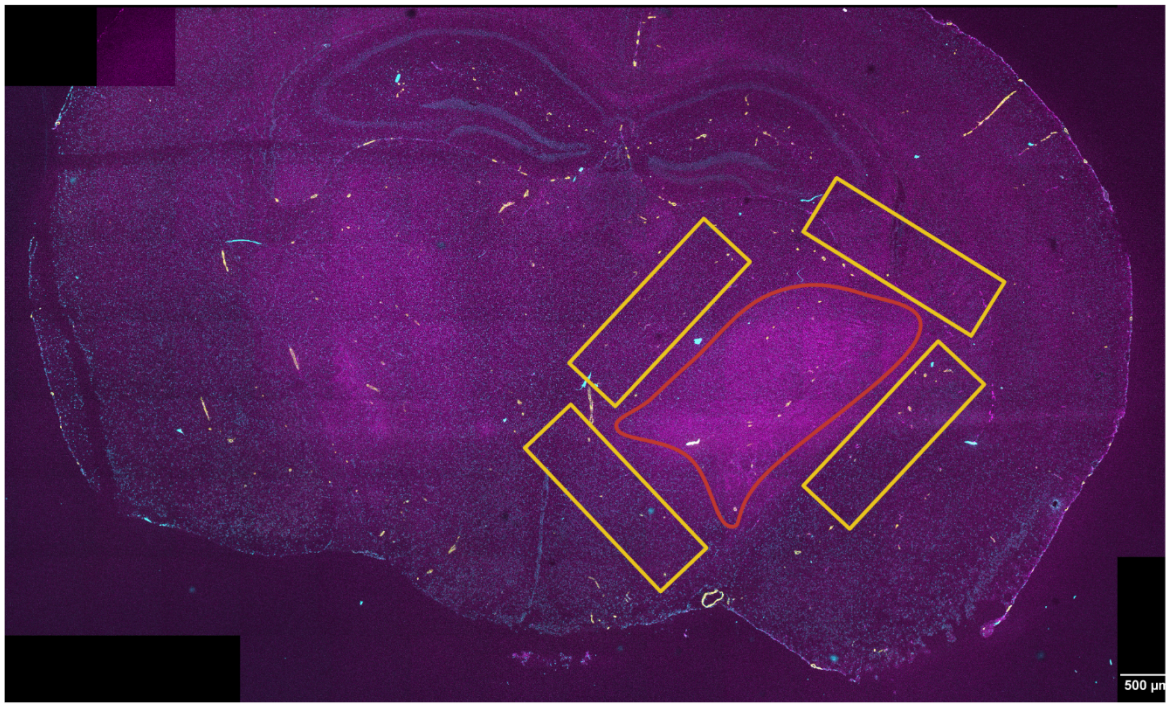

Figure 3-1. Location of the infarct core and peri-infarct regions on a tiled immunofluorescent coronal section of a C57BL6/J mouse brain. The infarct (red delineation) is determined by altered tissue morphology resulting in relatively higher autofluorescence. Yellow rectangles delineate the four areas adjacent to the infarct determined as peri-infarct. DAPI - cyan, nuclei; αSMA – yellow, CD206 - magenta. Scale bar = 500μm, 10x magnification on Zeiss LSM 800.

3.2.4 Immunophenotyping with flow cytometry

Sample preparation, sample acquisition and analyses for flow cytometry were performed as described in Section 1.4.6 of General Methods for several timepoints after tMCAo (Figure 3-4). Myeloid cells were identified as $CD45^{+high}CD11b^{+}$ and microglia were identified as $CD45^{+int}CD11b^{+}$ (Martin et al., 2017a). M2-like macrophages were identified by $CD45^{+high}CD11b^{+}CD206^{+}$. The population of greatest interest was BAMs, immunophenotyped for $CD45^{+high}CD11b^{+}CD206^{+}LYVE1^{+}$ expression. The gating strategy for detecting BAMs, myeloid cells, M2-like macrophages, and microglia (Figure 3-2) was developed by Dr Arun Flynn, Dr Ashton Bernard and Dr Francisco Rios, whose help is gratefully acknowledged. Quantification of the numbers of individual cell populations across timepoints was conducted and presented as ipsilateral cells as a percentage of total ipsilateral leukocytes ($CD45^{+}$).

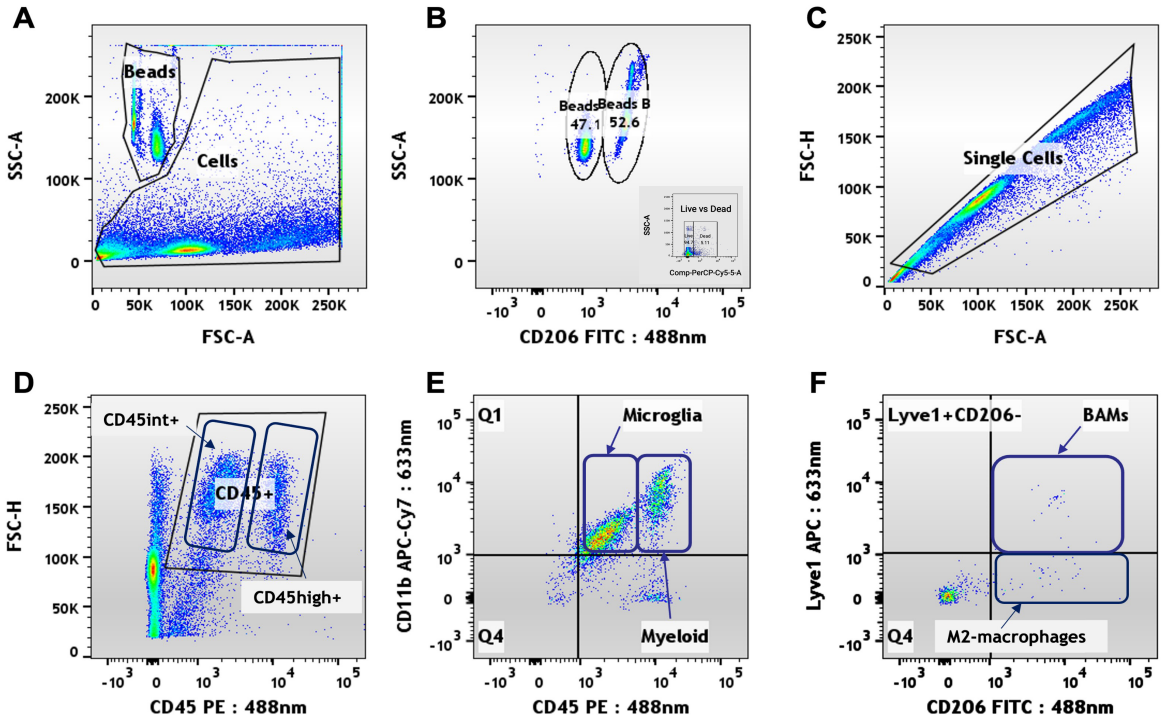

Figure 3-2. Gating strategy for flow cytometric analysis of myeloid cell populations from freshly isolated C57BL6/J mouse brains using counting beads. A) Cells were identified as events on the forward scatter (FSC) versus side scatter (SSC) plot and counting beads by low FSC <100K and high SSC >100K. B) Counting beads formed two populations that were split into 50±3% beads A and 50±3% beads B, used as a double internal standard for sample volume calculation and were identified by plotting SSC against blue laser scatter. Inset represents the viability staining with 7-AAD as detected on the PerCP-Cy5.5 channel. C) Single cells were gated by plotting events on FSC area versus height. D) $CD45^+$ cells were gated from single cells. E) Myeloid cells were identified as $CD45^{+high}CD11b^+$ and microglia were identified as $CD45^{+int}CD11b^+$. F) M2-like macrophages were identified by $CD45^{+high}CD11b^+CD206^+$. CNS border-associated macrophages (BAMs) identified by $CD45^{+high}CD11b^+CD206^+LYVE1^+$ expression.

The antibodies used are listed in Table 3-3 and instrument configuration is detailed in Table 3-4, respectively. Brighter fluorophores based on their stain index, such as FITC and APC, were chosen for conjugation with CD206 and Lyve1, as their relative abundance was expected to be much lower than that of pan-leukocytic markers such as CD45 and CD11b, which were conjugated to PE and APC-Cy7, respectively. The emission spectra for the flow cytometric panel are presented in Figure 3-3.

Table 3-3. Antibodies used for flow cytometry.

Antigen	*Fluorophore*	*Host Isotype*	*Clone*	*Concentration (µg/ml)*	*Supplier*
CD45	PE	Rat Ig2b, κ	30-F11	0.5	Biolegend
CD11b	APC/Cy7	Rat Ig2b, κ	M1/70	1	Biolegend
CD206	FITC	Rat Ig2a, κ	C068C2	6.25	Biolegend
LYVE1	APC	Rat Ig2a	223322	2	R&D Systems

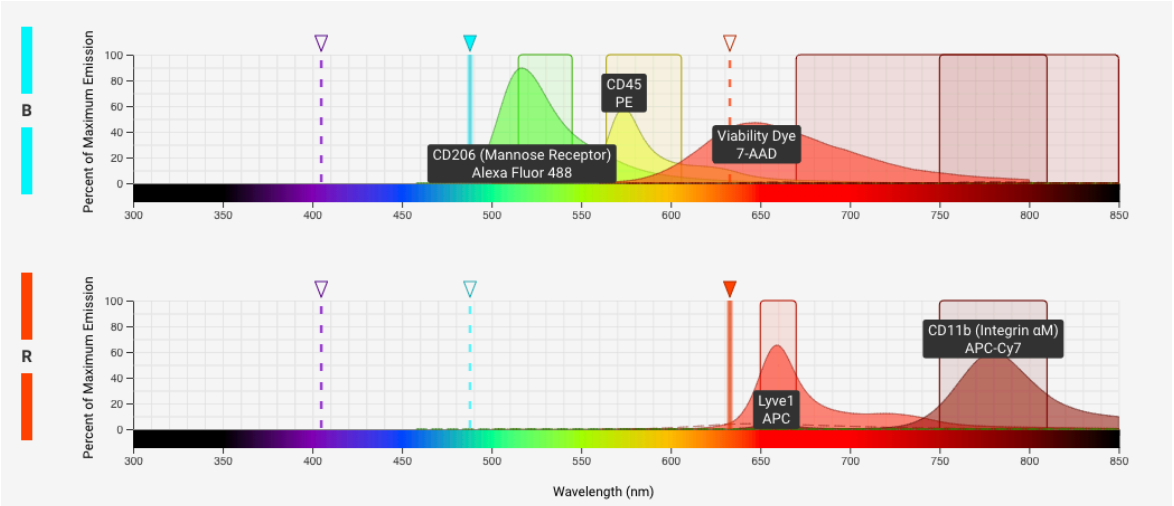

Figure 3-3. Emission ranges of the fluorophores used the CNS border-associated macrophages immunophenotyping panel. The blue laser excited Alexa Fluor 488, PE and the viability dye 7-ADD. The red laser excited APC and APC-Cy7. Figure created on BD Research Cloud.

Table 3-4. BD FACS Canto II cytometer configuration for immunophenotyping.

ANTIGEN	**FLUOROPHORE**	**LASER**	**FILTER**	**MIRROR**
CD45	PE	**Blue Octagon 488 20mW**	585	586LP
CD206	FITC	**Blue Octagon 488 20mW**	530/30	502LP
VIABILITY	PerCP-Cy5.5	**Blue Octagon 488 20mW**	670LLP	655LP
CD11B	APC-Cy7	**Red Trigon 633 17mW**	780/60	735LP
LYVE1	APC	**Red Trigon 633 17mW**	660/20	None

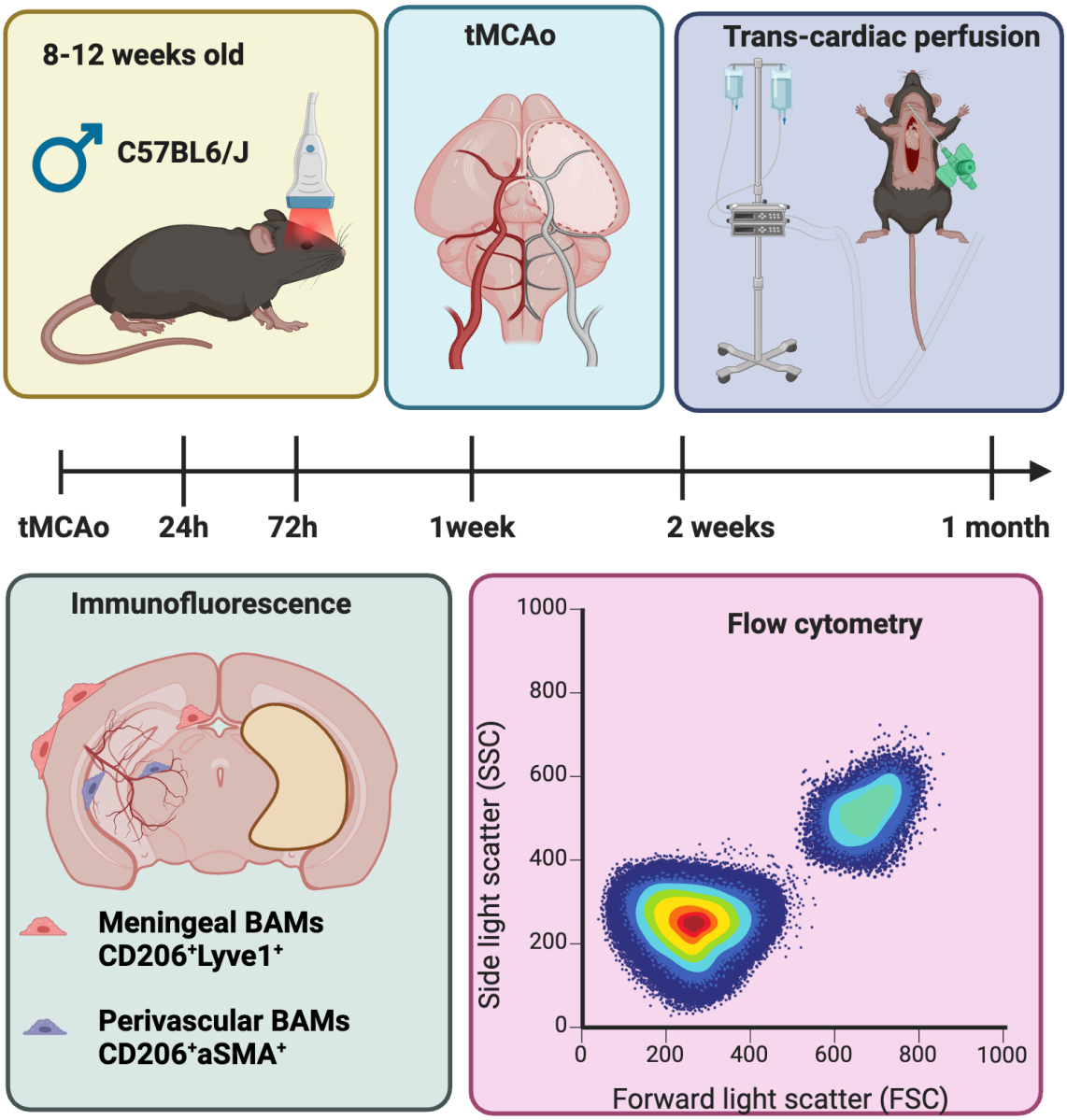

Figure 3-4. Study design to quantify CNS border-associated macrophages (BAMs $CD45^{+high}CD11b^{+}CD206^{+}Lyve1^{+}$) at 5 timepoints following right transient middle cerebral artery occlusion (tMCAo) in C57BL6/J 8 - 12-week-old male mice. Prior to flow cytometric immunophenotyping mice were transcardially perfused with saline under terminal anaesthesia to remove cerebral red blood cells. Cryopreserved coronal brain sections from a separate cohort of animals following 72h tMCAo was used for immunofluorescence analyses of meningeal ($CD206^{+}Lyve1^{+}$) and perivascular ($CD206^{+}aSMA^{+}$) BAMs. Figure created on Biorender.

3.2.5 Statistics and power calculations

Immunofluorescence data were grouped into ipsilateral and contralateral hemispheres that came from the same brain and were analysed by paired t tests. Immunophenotyping data were grouped into three groups – sham, ipsilateral and contralateral hemispheres that were treated as unmatched. Normally distributed data as tested by Kolmogorov-Smirnov or Shapiro-Wilk tests, were analysed with

ordinary one-way ANOVA with Sidak's multiple comparisons test of selected comparisons – ipsilateral vs sham, ipsilateral vs contralateral. Non-normally distributed data were analysed with Kruskal-Wallis with Dunn's multiple comparisons test of selected comparisons - ipsilateral vs sham, ipsilateral vs contralateral.

To determine sample sizes for experiments examining the effect of ischaemia on the number of BAMs, data collected from a pilot study measuring BAM numbers at 24 hours was used. This initial data showed that the number of BAMs was significantly increased approximately 3-fold relative to contralateral hemisphere.

Table 3-5. Data from 24 hours post tMCAo used for power calculations for timepoint examination of BAMs and other myeloid cells in the post-ischaemic mouse brain.

Group name	*Group Mean*	*Group size*	*Group SD*
Sham	293	6	306
Ipsilateral	561	6	561
Contralateral	188	6	193

The effect size (Cohen's *f*) based on grand mean (351) and pooled SD (385.85) for this data was =0.697. To detect differences between three groups using a one-way ANOVA with 2 multiple comparisons tests, it was estimated that the minimum animals required per group were n=10 (α = 0.05, power = 0.8 [β = 0.2], ANOVA: fixed effects, omnibus, one-way).

3.2.6 Mortality and exclusions

There were no mortalities. However, across all time points, 5 sham and 6 stroke mice had to be euthanised prior to the scientific end point due to them reaching the severity limits of the Project Licence (e.g., ≥ 20% body weight loss post-surgery). Therefore, the occlusion period was reduced to 40 min to improve the chances of the mice surviving to the endpoint in the 1-month and 2-week groups. Exclusions were as follows:

- 24-hour time point - for one mouse, flow cytometry data was not acquired correctly for one the contralateral hemispheres. As a result, data for both hemispheres for this mouse was excluded.

- 72-hour time point - 2 mice were excluded from the analyses, as they did not achieve the required ≥70% reduction in rCBF following filament insertion; and 1 additional mouse was excluded as the CCA clamp time was greater than 5 minutes.

- 1-week time point - 1 mouse was excluded as it did not achieve the ≥70% reduction in rCBF.

- 2-week time point - 2 mice were excluded as they did not achieve the ≥70% reduction in rCBF.

- 1-month time point - 2 mice were excluded as they did not achieve the ≥70% reduction in rCBF; and data from 1 additional mouse was excluded due to incorrect acquisition of flow cytometry data.

3.3 Results

3.3.1 Quantification of BAMs and other immune cell populations in the naïve mouse brain using flow cytometry

The number of immune cells in naïve C57BL6/J mouse brain was investigated using flow cytometric analysis. The viability of cells within each sample was consistently above 90%. There were about 8000 leukocytes ($CD45^+$) per hemisphere, the majority of which were microglia ($CD45^{+int}CD11b^+$), almost a quarter were myeloid cells ($CD45^{+high}CD11b^+$), 7.3% were M2-like macrophages ($CD45^{+high}CD11b^+CD206^+$) and BAMs ($CD45^{+high}CD11b^+CD206^+LYVE1^+$) represented 4.2% of the total leukocyte population (Figure 1-9).

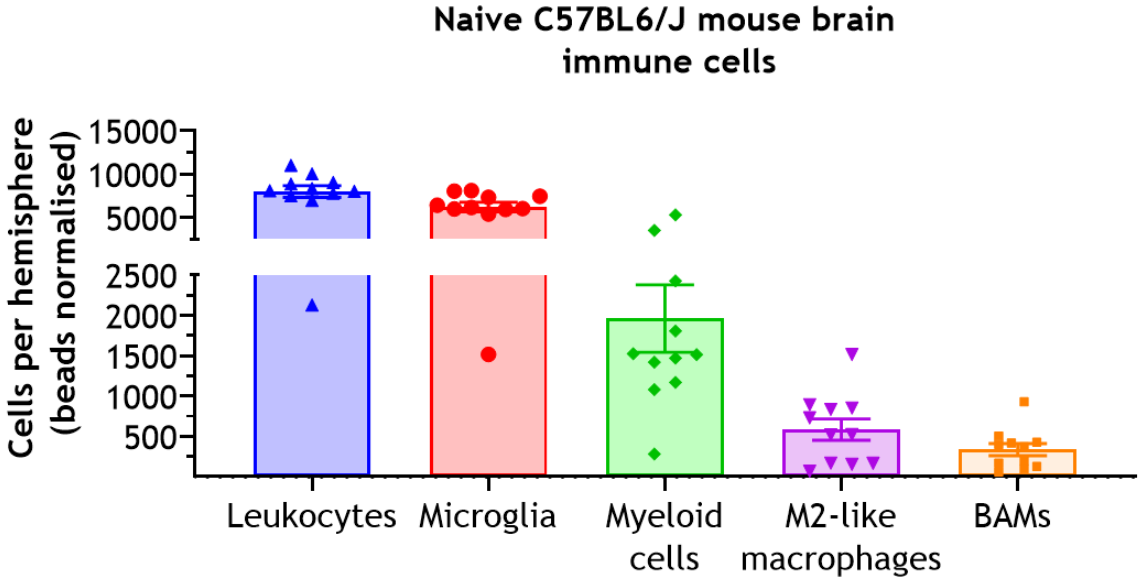

Figure 3-5. Quantification of CNS border-associated macrophages (BAMs) and other immune cell populations per hemisphere in the naive mouse brain. Leukocytes ($CD45^+$), microglia ($CD45^{+int}CD11b^+$), myeloid cells ($CD45^{+high}CD11b^+$), M2-like macrophages ($CD45^{+high}CD11b^+CD206^+$), and CNS border-associated macrophages (BAMs, $CD45^{+high}CD11b^+CD206^+LYVE1^+$). Data is presented as mean ± SEM, n=11. No statistical comparisons were made between cell types.

3.3.2 Accumulation of BAMs and other macrophages in the acute stage after tMCAo

In the acute period after tMCAo there was a significant increase in the number of all investigated cell populations in the ipsilateral hemisphere compared to both the sham and contralateral hemispheres. Total leukocytes ($CD45^+$) were 8-fold higher in the ischaemic hemisphere compared to sham. The numbers of microglia ($CD45^{int+}CD11b^+$) in the ipsilateral hemisphere were about 9100, which was over two-fold higher than those in the contralateral hemisphere at day 1 (Figure 3-6). At day 3 the detected number of microglia were ~6-fold higher than at day 1 in the stroke affected hemispheres, and over 8 times higher compared to sham (Figure 3-6).

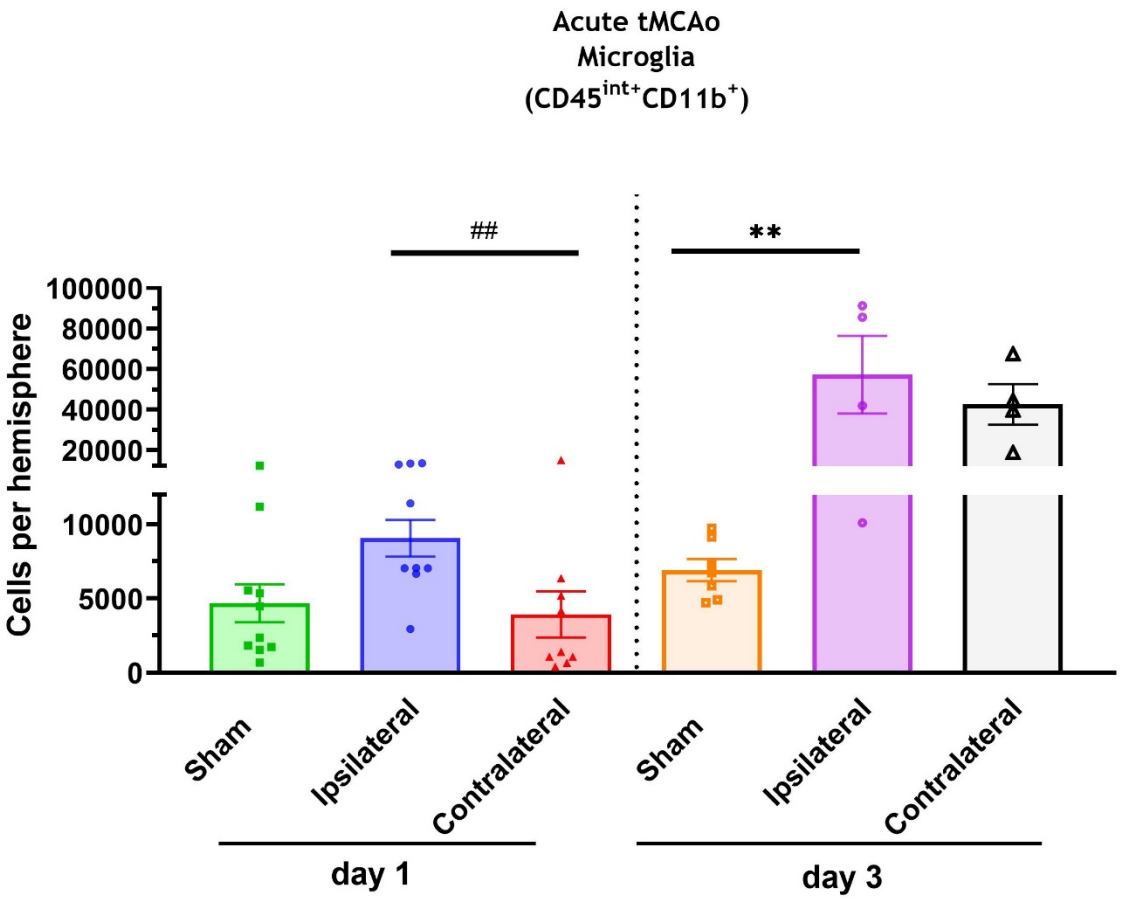

Figure 3-6. Quantification of microglia ($CD45^{+int}CD11b^{+}$) per hemisphere during the acute period of infarct development following transient middle cerebral artery occlusion (tMCAo) using flow cytometry. Data is presented as mean ± SEM, n=9-10 (day 1), n=4-7 (day 3). Data was non-normally distributed and analysed by Kruskal-Wallis with Dunn's multiple comparisons test of selected comparisons (ipsilateral vs sham, **P<0.01, ipsilateral vs contralateral, ##P<0.01). No statistical comparisons were made between timepoints.

Infiltrating M2-like macrophages ($CD45^{+high}CD11b^{+}CD206^{+}$) accumulated in the ipsilateral hemispheres 3.25-fold and 5-fold over sham and contralateral hemispheres, respectively, on day 1 after tMCAo (Figure 3-7). Further, on day 3 their numbers increased 7-fold over the detected 1370 on day 1 and were 60 times higher than sham controls.

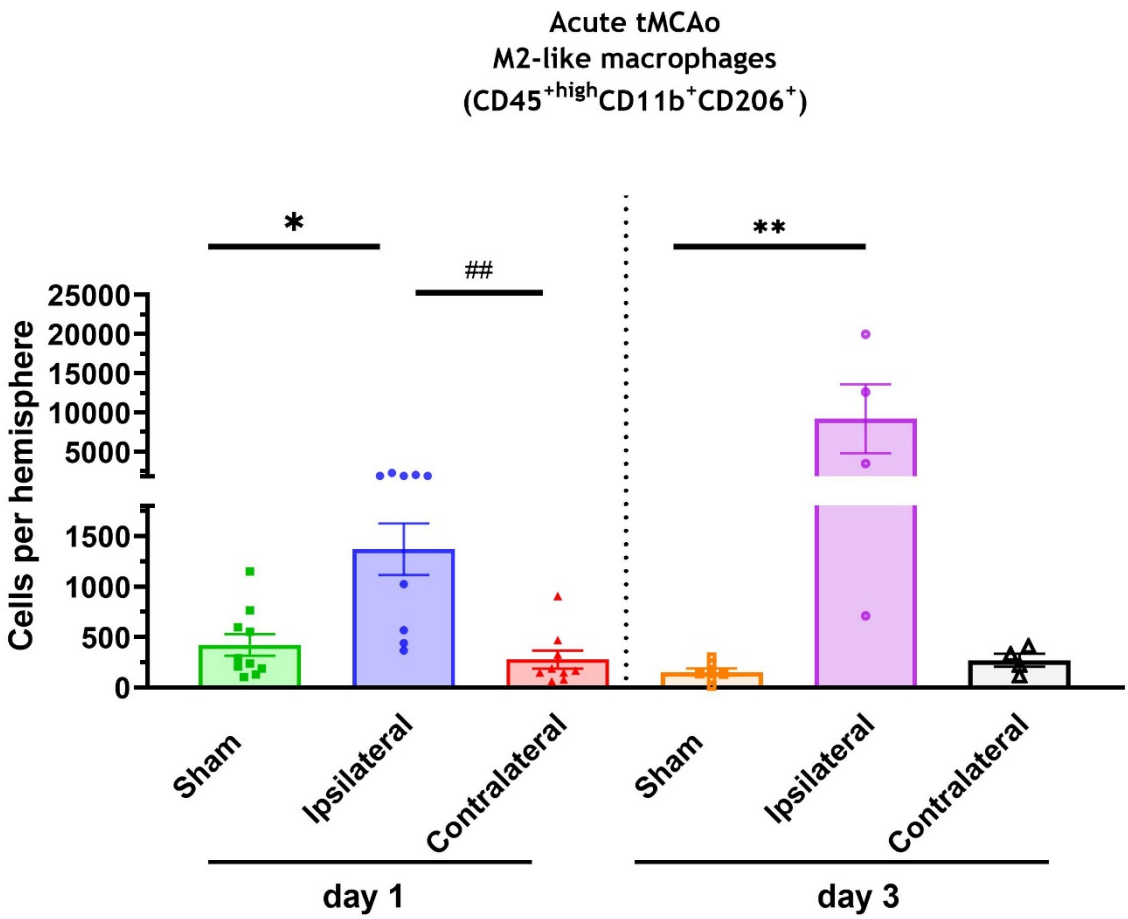

Figure 3-7. Quantification of M2-like macrophages ($CD45^{+high}CD11b^{+}CD206^{+}$) per hemisphere during the acute period of infarct development following transient middle cerebral artery occlusion (tMCAo) using flow cytometry. Data is presented as mean ± SEM, n=9-10 (day 1), n=4-7 (day 3). Data was non-normally distributed and analysed by Kruskal-Wallis with Dunn's multiple comparisons test of selected comparisons (ipsilateral vs sham, *P<0.05, **P<0.01, ipsilateral vs contralateral, ##P<0.01). No statistical comparisons were made between timepoints.

Similar to their brain resident and infiltrating counterparts at this timepoint, CNS border-associated macrophages (BAMs, $CD45^{+high}CD11b^{+}CD206^{+}LYVE1^{+}$) were detected 4.4-fold higher in the ipsilateral hemispheres versus sham and 3-times higher than in contralateral hemispheres on day 1 after tMCAo. The difference in fluorescence intensity between the groups was evident on flow cytometric plots (Figure 3-8). Their numbers further increased to just over 2500 in the ipsilateral hemispheres 3 days after tMCAo, which was almost 40 times higher than both the sham and contralateral hemispheres (Figure 3-9).

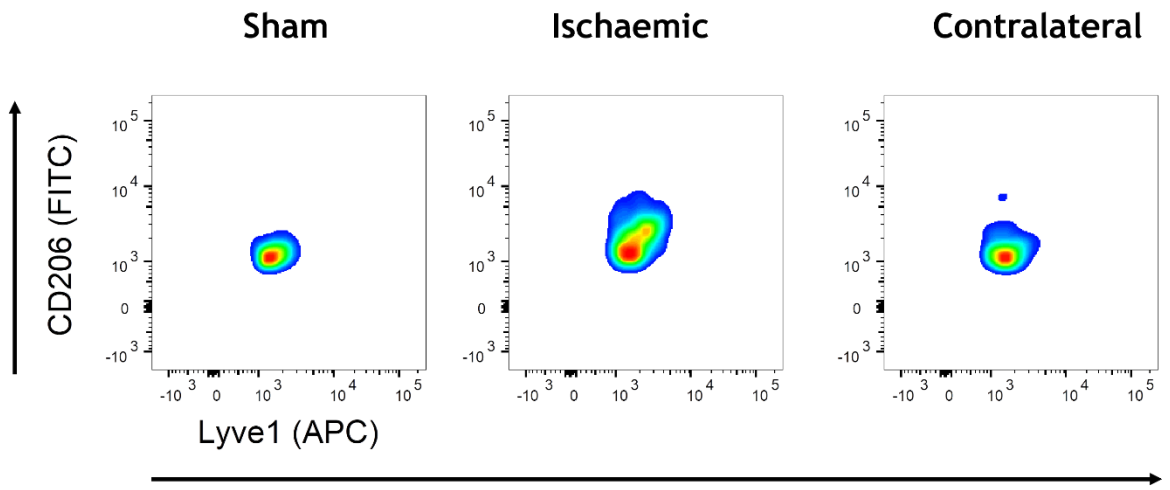

Figure 3-8. Representative flow cytometric smoothed pseudocolour scatter plots of CNS border-associated macrophages (BAMs, CD45^{+high}CD11b^{+}CD206^{+}LYVE1^{+}) 24 hours following transient middle cerebral artery occlusion (tMCAo) in ischaemic (ipsilateral), contralateral, and sham-operated hemispheres from C57BL6/J mice.

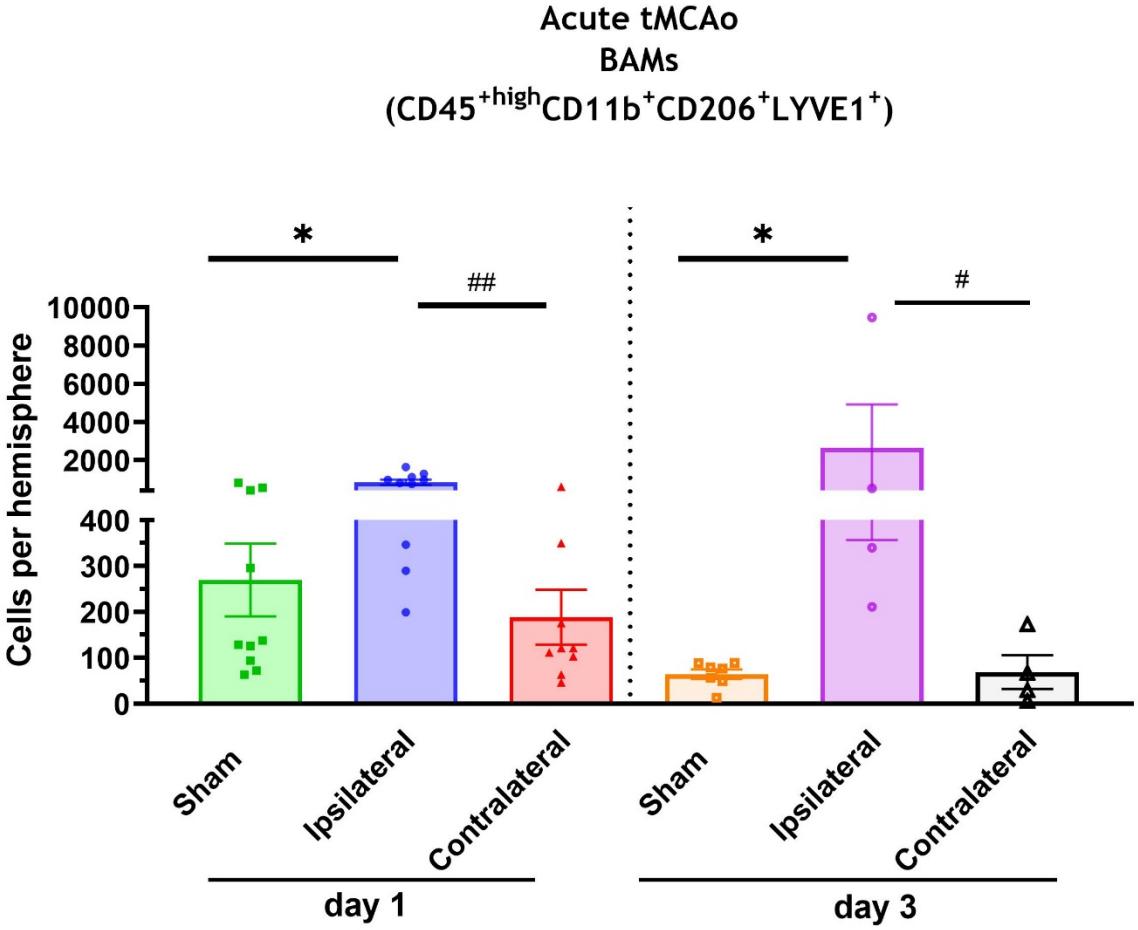

Figure 3-9. Quantification of CNS border-associated macrophages (BAMs, CD45^{+high}CD11b^{+}CD206^{+}LYVE1^{+}) per hemisphere during the acute period of infarct development following transient middle cerebral artery occlusion (tMCAo) using flow cytometry. Data is presented as mean ± SEM, n=9-10 (day 1), n=4-7 (day 3). Data was non-normally distributed and analysed by Kruskal-Wallis with Dunn's multiple comparisons test of selected comparisons (ipsilateral vs sham, *P<0.05, ipsilateral vs contralateral, #P<0.05, ##P<0.01). No statistical comparisons were made between timepoints.

3.3.3 BAMs and other macrophages continue to accumulate in the sub-acute stages of tMCAo

Since the inflammatory response after stroke continues beyond the period of infarct development, the numbers of brain resident and infiltrating macrophages were investigated further in the sub-acute phase on day 7 and day 14 after tMCAo. Elevated numbers of leukocytes, microglia and macrophages persisted in the ipsilateral hemisphere compared to sham controls at these later timepoints.

Microglia ($CD45^{int+}CD11b^{+}$) numbers rose to over 55,000 on day 7 post tMCAo, which was almost 9-fold higher than in sham controls and trended higher than in contralateral hemispheres. By day 14 after tMCAo microglia numbers remained higher in the stroke affected hemisphere and comparable to the results obtained on day 7 (Figure 3-10).

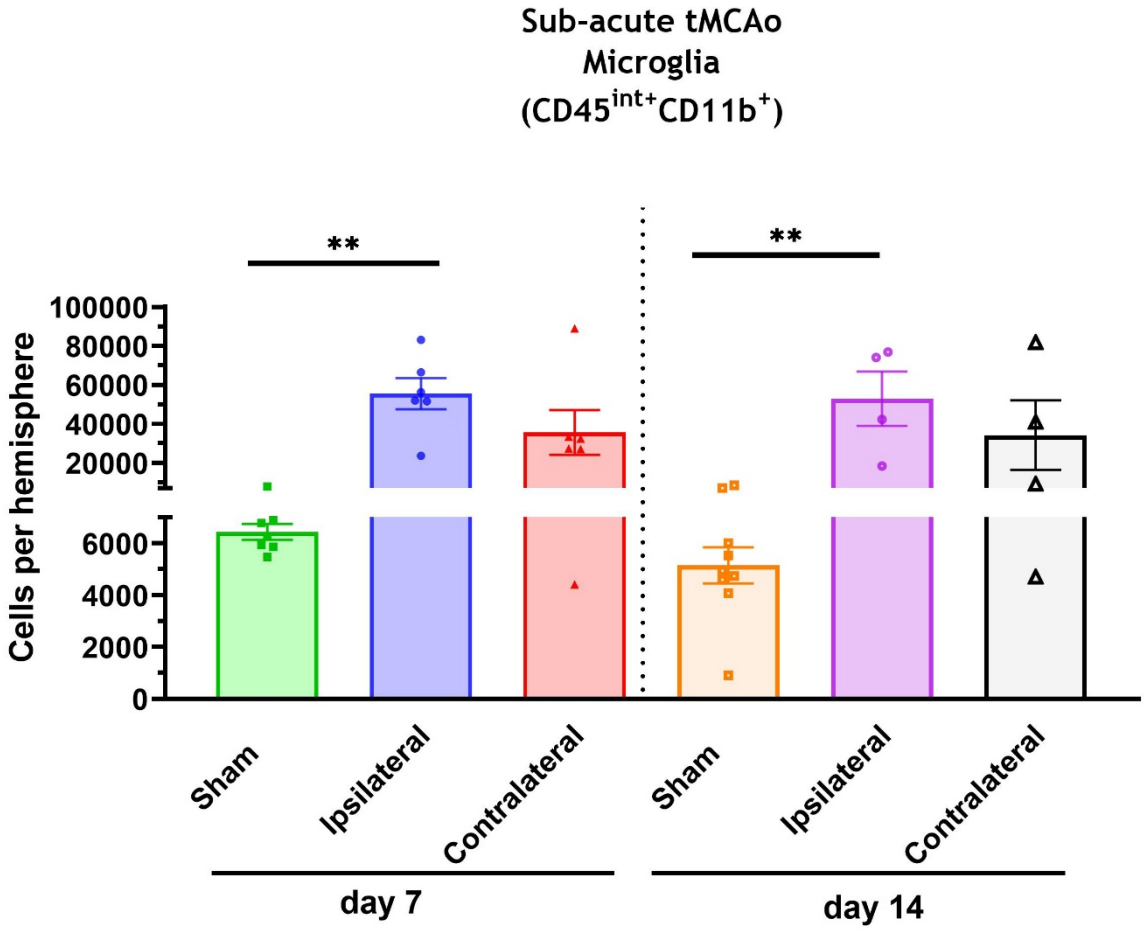

Figure 3-10. Quantification of microglia ($CD45^{+int}CD11b^{+}$) per hemisphere during the sub-acute period of infarct development following transient middle cerebral artery occlusion (tMCAo) using flow cytometry. Data is presented as mean ± SEM, n=6-7 (day 7), n=4-9 (day 14). Data was non-normally distributed and analysed by Kruskal-Wallis with Dunn's multiple comparisons test of selected comparisons (ipsilateral vs sham, **P<0.01, ipsilateral vs contralateral, P>0.05). No statistical comparisons were made between timepoints.

Peripheral M2-like macrophages ($CD45^{+high}CD11b^{+}CD206^{+}$) had risen to a mean of 7200 cells per ipsilateral hemisphere on day 7, which was 24-fold over sham and on average about 14 times higher than in contralateral hemispheres. On day 14 M2-like macrophages in the ipsilateral hemisphere there were 5-fold higher than in sham hemispheres (Figure 3-11), indicative of a continuous infiltration of macrophages.

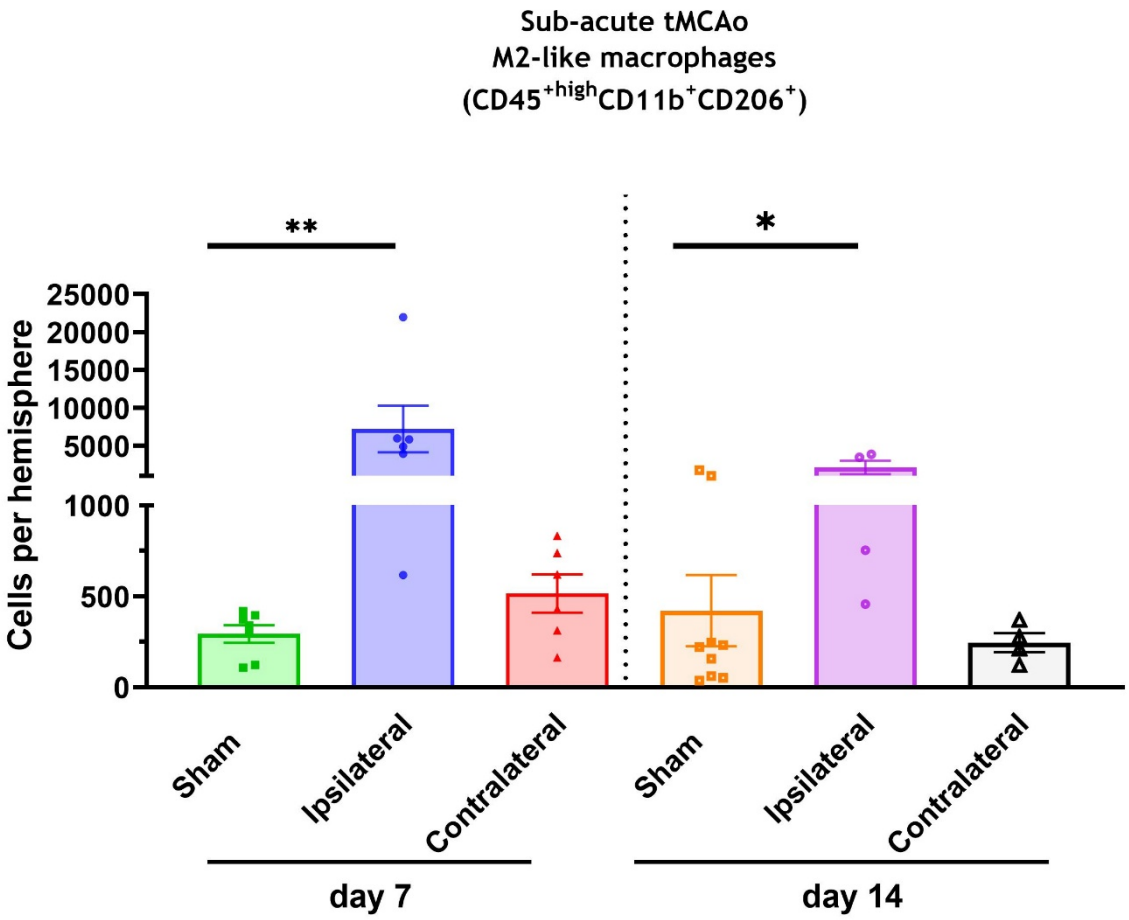

Figure 3-11. Quantification of M2-like macrophages ($CD45^{+high}CD11b^{+}CD206^{+}$) per hemisphere during the sub-acute period of infarct development following transient middle cerebral artery occlusion (tMCAo) using flow cytometry. Data is presented as mean ± SEM, n=6-7 (day 7), n=4-9 (day 14). Data was non-normally distributed and analysed by Kruskal-Wallis with Dunn's multiple comparisons test of selected comparisons (ipsilateral vs sham, *P<0.05, **P<0.01, ipsilateral vs contralateral, P>0.05). No statistical comparisons were made between timepoints.

CNS border-associated macrophages (BAMs, $CD45^{+high}CD11b^{+}CD206^{+}LYVE1^{+}$) were 28-fold higher in the ipsilateral hemispheres versus sham and 18-times higher than in contralateral hemispheres at day 7 (Figure 3-12). Two weeks following tMCAo there was still a strong, 5-fold trend for higher numbers of BAMs in the ipsilateral hemisphere versus sham, which did not reach statistical significance. As detailed in section 3.2.5, an *a priori* power analysis based on preliminary data determined that a sample size of 10 per group was required to properly power the analysis to 80% and there were only 4 tMCAo mice included in this analysis. A post-hoc calculation revealed an effect size (*f*) of 0.88 and achieved power was 63%, meaning that a larger sample size was required to properly power the analysis to 80%.

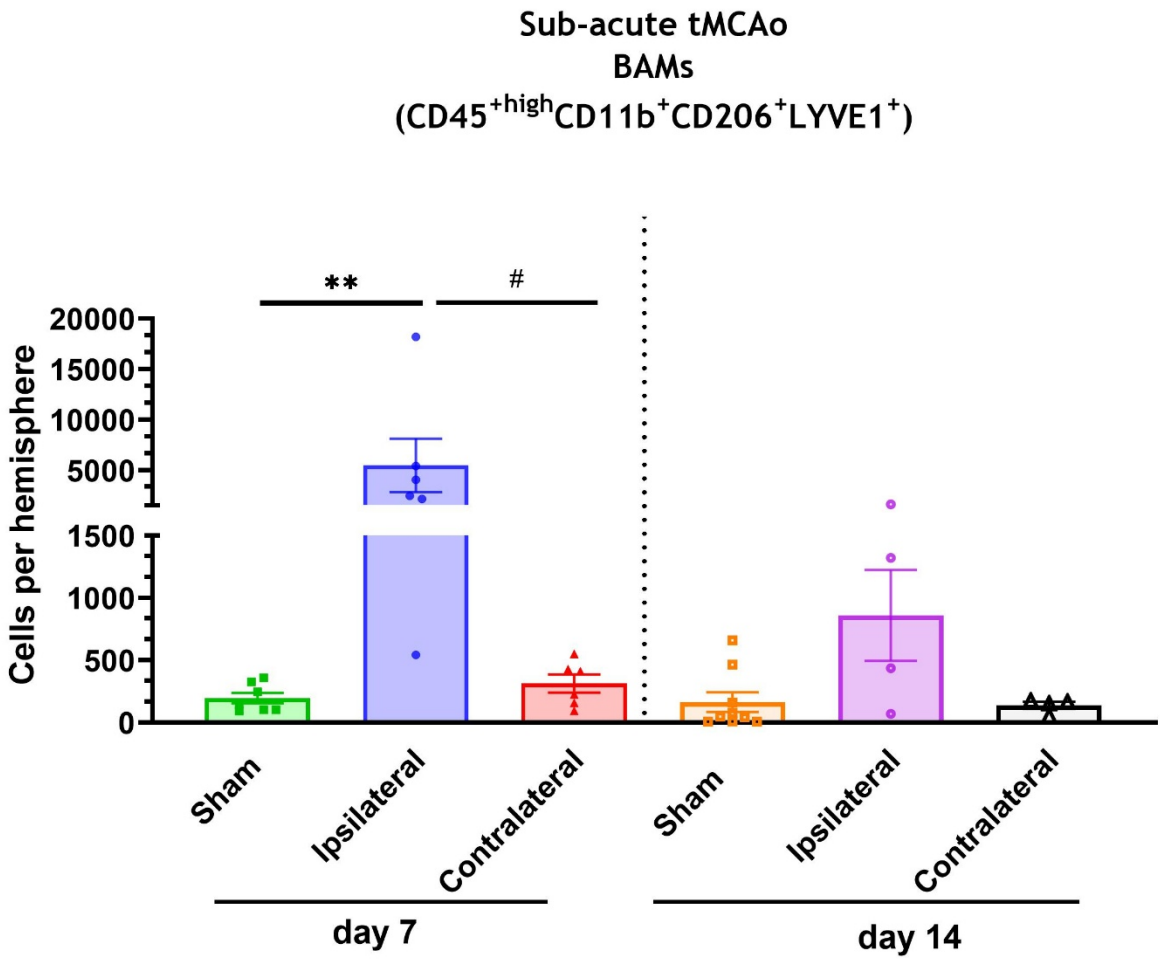

Figure 3-12. Quantification of CNS border-associated macrophages (BAMs, $CD45^{+high}CD11b^{+}CD206^{+}LYVE1^{+}$) per hemisphere during the sub-acute period of infarct development following transient middle cerebral artery occlusion (tMCAo) using flow cytometry. Data is presented as mean ± SEM, n=6-7 (day 7), n=4-9 (day 14). Data was non-normally distributed and analysed by Kruskal-Wallis with Dunn's multiple comparisons test of selected comparisons (ipsilateral vs sham, **P<0.01, ipsilateral vs contralateral, #P<0.05). No statistical comparisons were made between timepoints.

3.3.4 BAMs and other macrophages cease to accumulate in the chronic stages of tMCAo

The continuous trend for stroke-induced higher numbers of BAMs in the sub-acute phase after tMCAo warranted investigating their numbers into the chronic phase. At one month post tMCAo the number of M2-like macrophages and BAMs were comparable between groups (Figure 3-13A-B), however, as mentioned above, a sample size of 10 per group was required to properly power the analysis. A post-hoc calculation revealed an effect size (*f*) of 0.1 and achieved power was 5.7%, meaning that a significantly larger sample size was required for this analysis. There were significant, 40-fold higher numbers of microglia in the ipsilateral

hemisphere compared to sham hemispheres, and almost 4-fold increase over contralateral controls (Figure 3-13C).

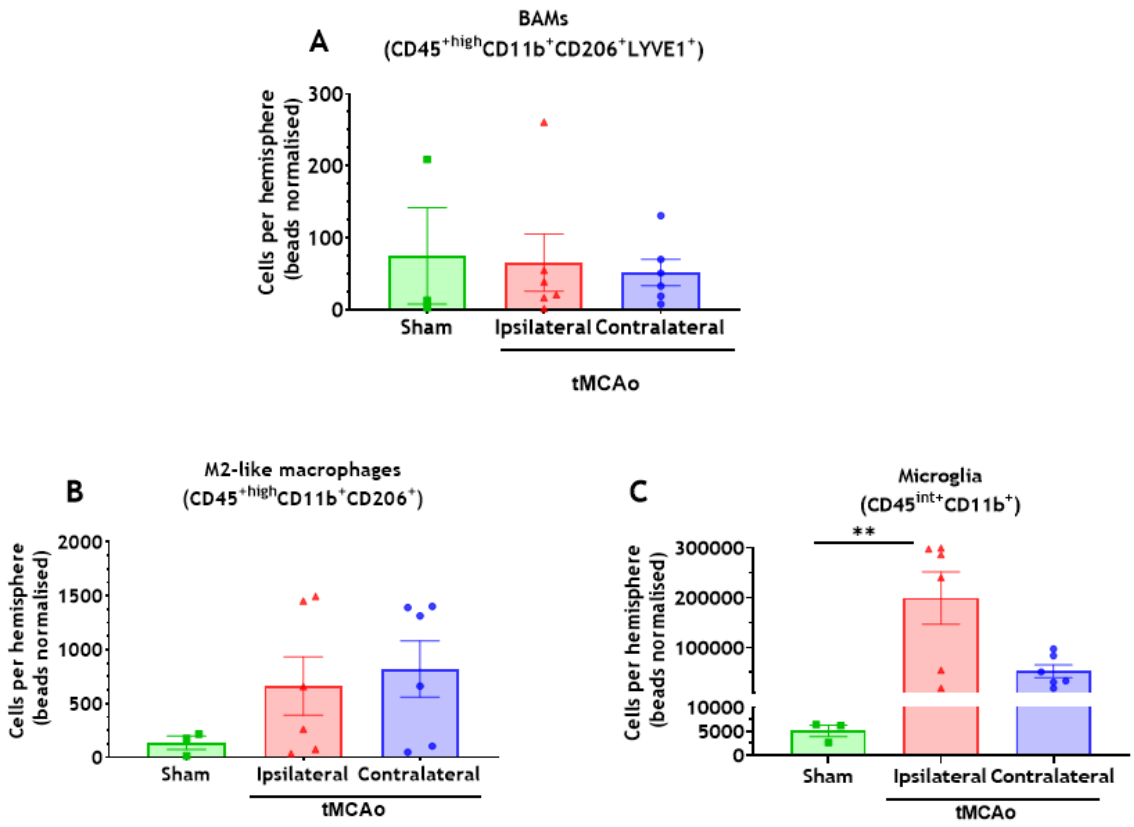

Figure 3-13. Quantification of brain resident and infiltrating macrophages per hemisphere 1 month following transient middle cerebral artery occlusion (tMCAo) using flow cytometry. A) CNS border-associated macrophages (BAMs, $CD45^{+high}CD11b^{+}CD206^{+}LYVE1^{+}$), B) M2-like macrophages ($CD45^{+high}CD11b^{+}CD206^{+}$), C) Microglia ($CD45^{int+}CD11b^{+}$). Data is presented as mean ± SEM, n=3-6. A, C) Data were non-normally distributed, Kruskal-Wallis with Dunn's multiple comparisons test of selected comparisons – ipsilateral vs sham, ipsilateral vs contralateral. B) Data were normally distributed (D'Agostino & Pearson test), and analysed by an ordinary one-way ANOVA with Holm-Sidak's multiple comparisons test of selected comparisons – ipsilateral vs sham, ipsilateral vs contralateral, *P<0.05, **P<0.01, ***P<0.001.

3.3.5 Timescale of the effect of cerebral ischaemia-reperfusion on the number of BAMs and other macrophages after tMCAo

Since this study quantified numbers of cells across several phases after tMCAo, to appreciate the overall trends, the quantification for each population of interest is also presented as a percentage of the total number of leukocytes ($CD45^{+}$ cells) in the ipsilateral hemisphere across the timepoints described above. Neither cell type demonstrated higher frequencies compared to those obtained in sham hemispheres on day 1 after tMCAo. BAMs were consistently around 5% of all

detected leukocytes across the acute and sub-acute phases and their proportions dropped to below 0.1% in the chronic stages (Figure 3-14).

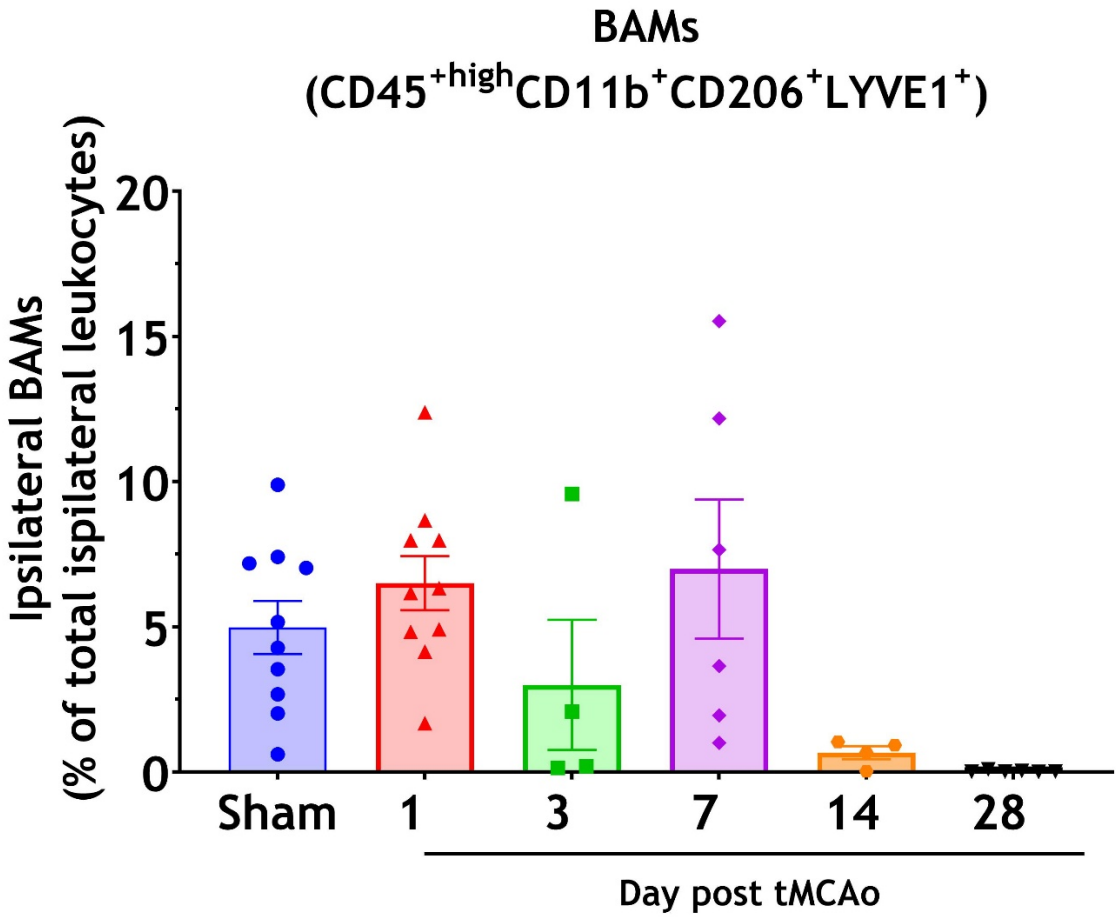

Figure 3-14. Ipsilateral BAMs ($CD45^{+high}CD11b^{+}CD206^{+}LYVE1^{+}$) as a percentage of total ipsilateral leukocytes over all investigated timepoints and compared to sham at 24 hours following transient middle cerebral artery occlusion (tMCAo). Data is presented as mean ± SEM, n=6-12. No statistical comparisons were made between timepoints.

Likewise, the frequency of M2-like macrophages was 8-11% of all immune cells up to day 7 and dropped to a mere 1% by day 28 (Figure 3-15).

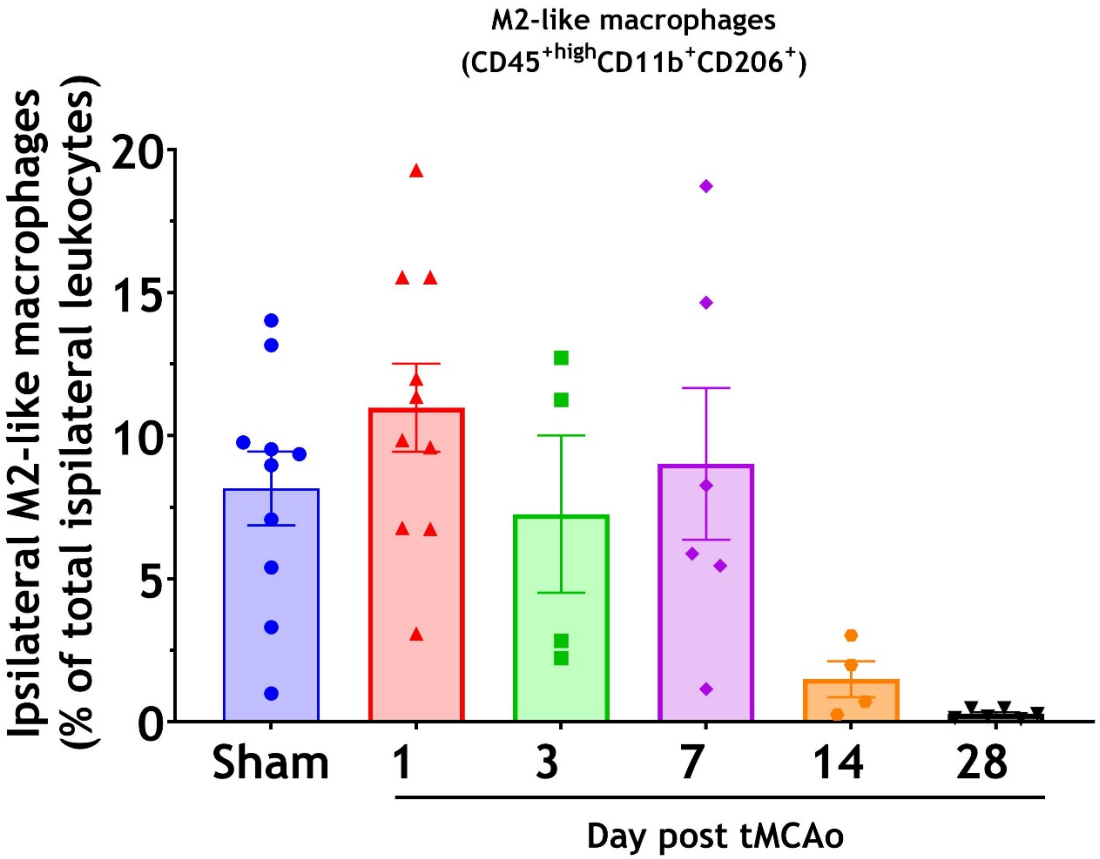

Figure 3-15. Ipsilateral M2-like macrophages ($CD45^{+high}CD11b^{+}CD206^{+}$) as a percentage of total ipsilateral leukocytes over all investigated timepoints and compared to sham at 24 hours following transient middle cerebral artery occlusion (tMCAo). Data is presented as mean ± SEM, n=6-12. No statistical comparisons were made between timepoints.

Interestingly, the frequency of microglia decreased on day 3 and day 14 to below 50%, but increased again in the chronic phases to above 75% of all detectable immune cells (Figure 3-16).

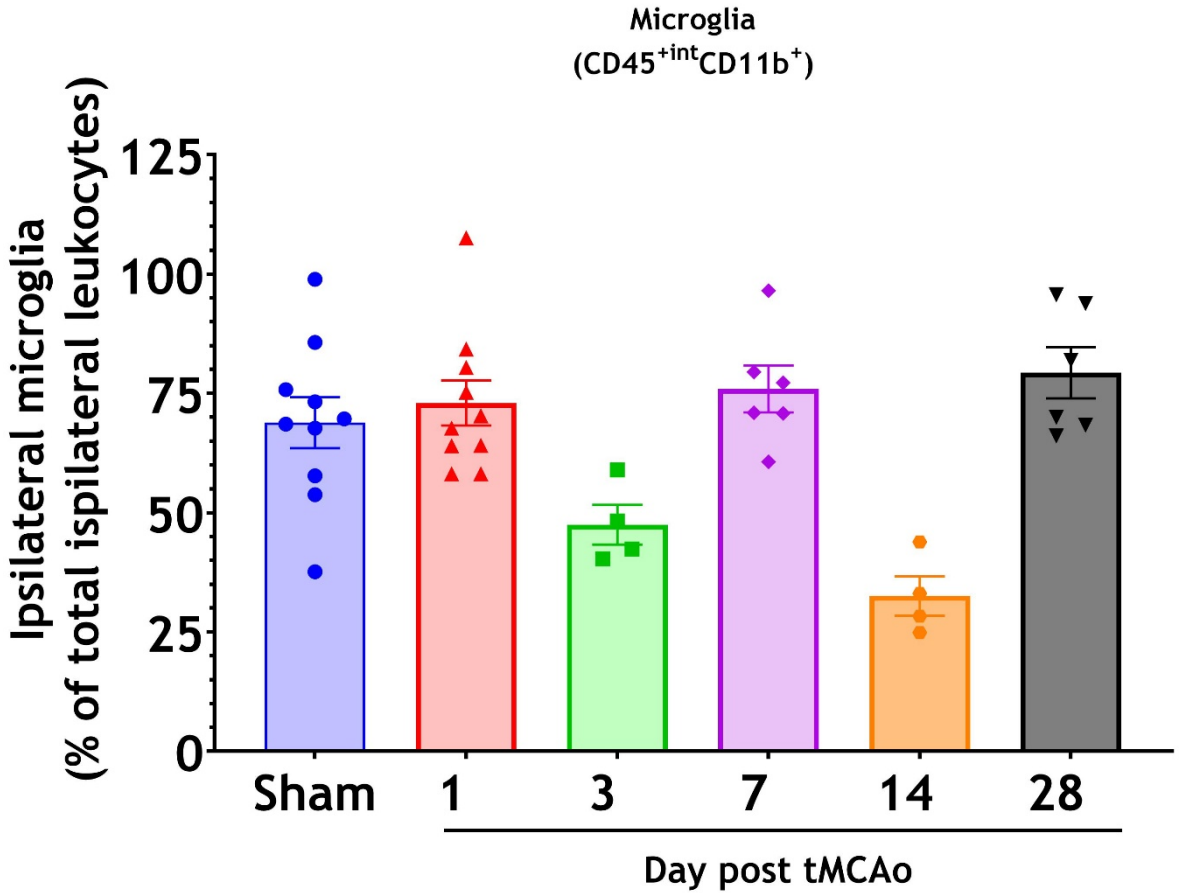

Figure 3-16. Microglia ($CD45^{+int}CD11b^{+}$) as a percentage of total ipsilateral leukocytes over all investigated timepoints and compared to sham at 24 hours following transient middle cerebral artery occlusion (tMCAo). Data is presented as mean ± SEM, n=6-12. No statistical comparisons were made between timepoints.

3.3.6 Identification of BAMs in the naïve mouse brain by double-label immunofluorescence

The most well-established markers to identify BAMs in the naive mouse brain are CD206, transcribed from mannose receptor 1 (*Mrc1)* (Galea et al., 2005, Martinez-Pomares, 2012, Mrdjen et al., 2018, Lapenna et al., 2018) and LYVE1 - lymphatic vessel endothelial hyaluronan receptor 1 (Zeisel et al., 2015, Mrdjen et al., 2018, Brezovakova and Jadhav, 2020, Kim et al., 2021a). Meningeal BAMs were identified as cells expressing both CD206 and Lyve1, localised to the meningeal space (Figure 3-17A). Perivascular BAMs were identified as cells expressing CD206 closely associated with the abluminal side of penetrating arterioles or pial vessels, as identified by positive staining for alpha-smooth muscle actin (aSMA) (Figure 3-17B).

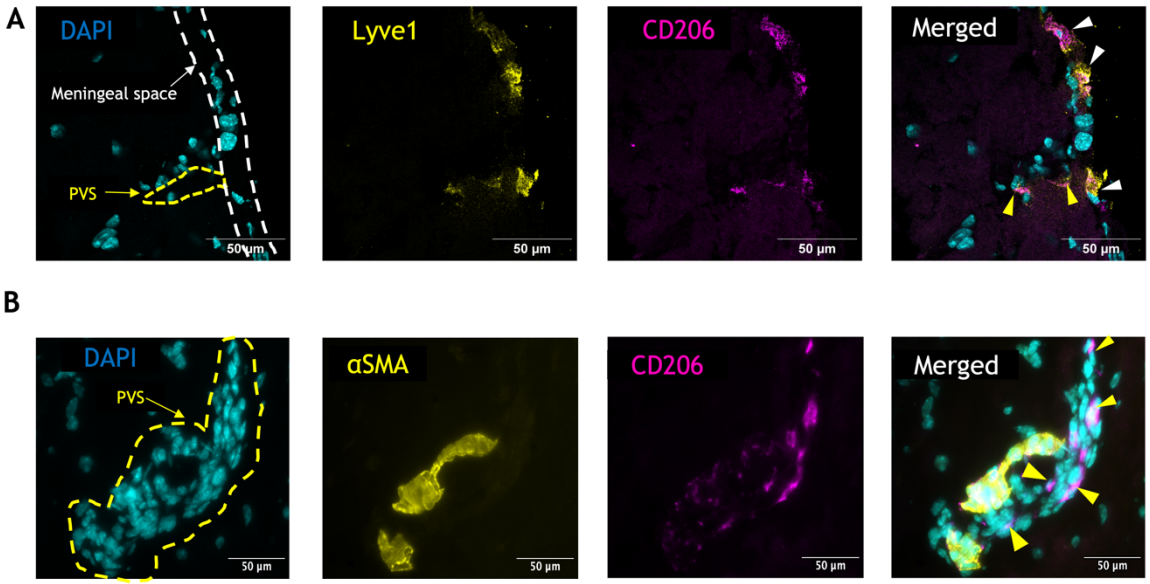

Figure 3-17. CNS border-associated macrophages (BAMs) in C57BL6/J naïve mouse brain. A) CD206$^+$Lyve1$^+$ cells in the perivascular space (PVS, yellow dashed line) of a penetrating arteriole (yellow arrowheads) and in the meningeal space (white dashed line) denoted by white arrowheads. B) CD206$^+$ cells in the perivascular space (PVS, yellow dashed line) of αSMA$^+$ arterioles depicted by yellow arrowheads. DAPI - cell nuclei (cyan), αSMA – alpha smooth muscle actin (yellow) or Lyve1 – lymphatic vessel endothelial hyaluronan receptor 1 (yellow), CD206 – the mannose receptor (magenta). Scale bar = 50µm, at 40x magnification.

3.3.7 Effect of cerebral-ischaemia-reperfusion on the localisation of BAMs

To corroborate the quantification obtained by flow cytometric immunophenotyping, BAMs were identified and quantitated using an immunofluorescent approach. Cerebral arteries, larger arterioles and veins express αSMA and are encased within the perivascular space (PVS), while the PVS gradually disappears with decreasing vessel diameter, meaning that smaller arterioles, postcapillary venules and capillaries do not express αSMA (Schaeffer and Iadecola, 2021). CD206$^+$ cells were identified by immunofluorescent imaging after tMCAo in the PVS of αSMA$^+$ arterioles (Figure 3-18A). CD206+ cells were also identified in the ischaemic parenchyma and sometimes along smaller arterioles or postcapillary venules negative for αSMA, identified by DAPI staining. CD206$^+$ cells, which were not associated with αSMA$^+$ vessels, were excluded from the semi-quantification, as these cells could be infiltrating CD206$^+$ M2-like macrophages (Figure 3-18A). CD206$^+$Lyve1$^+$ cells were identified in the meningeal space (Figure 3-18B) and in the PVS (Figure 3-20). IgG controls for the specificity of the detection of secondary antibodies for the species against which the primaries were raised

was determined experimentally during the first experiment using IgG antibodies at the same concentration as the primary antibodies (cf. Appendix Figure 7-1).

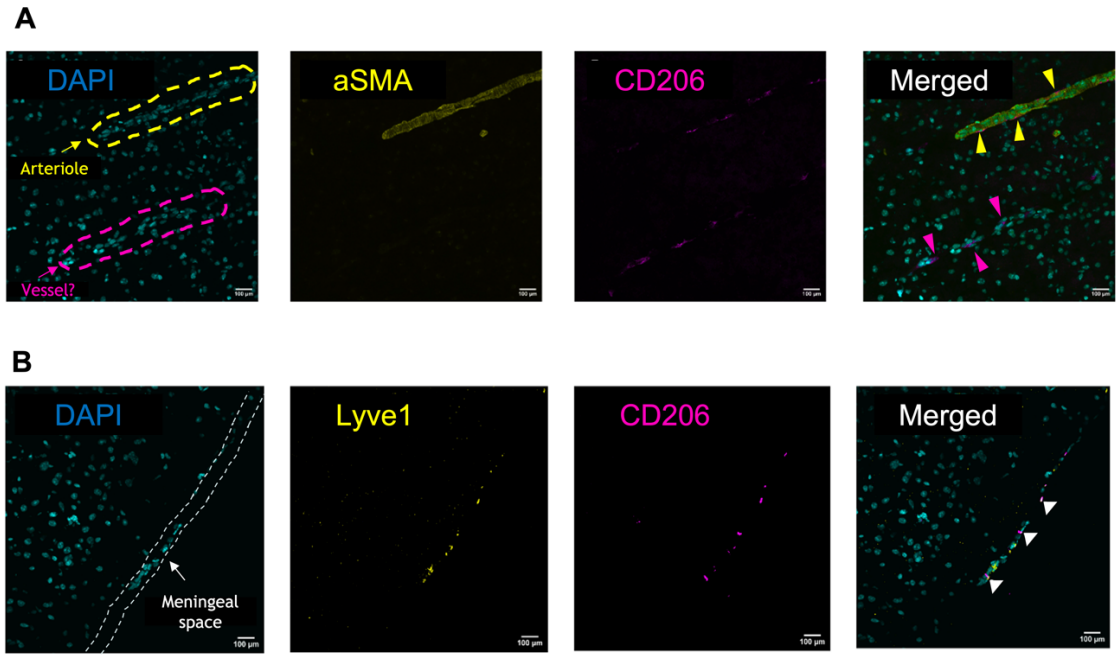

Figure 3-18. CNS border-associated macrophages (BAMs) in C57BL6/J mouse brain following transient middle cerebral artery occlusion (tMCAo). A) $CD206^{+}aSMA^{+}$ cells in the perivascular space (PVS, yellow dashed line) of an αSMA^{+} arteriole depicted by yellow arrowheads. $CD206^{+}$ cells were also detected near what appears to be a vessel in the parenchyma, which does not express $aSMA^{+}$ and are indicated with magenta arrowheads. B) $CD206^{+}Lyve1^{+}$ cells in the meningeal space (white dashed line) denoted by white arrowheads. DAPI - cell nuclei (cyan), αSMA – alpha smooth muscle actin (yellow) or Lyve1 – lymphatic vessel endothelial hyaluronan receptor 1 (yellow), CD206 – the mannose receptor (magenta). Scale bar = 100μm, 40x magnification.

Multiple $CD206^{+}aSMA^{+}$ were often identified along a single arteriole in both the ipsilateral (Figure 3-19 A) and contralateral (Figure 3-19 B) hemispheres. Likewise, the PVS was populated with several $CD206^{+}Lyve1^{+}$ cells in the ipsilateral (Figure 3-20 A) and contralateral hemispheres (Figure 3-20 B). On the whole, the numbers of $CD206^{+}aSMA^{+}$ cells were ~50 cells/mm^2 and were comparable between hemispheres (Figure 3-21A). $CD206^{+}Lyve1^{+}$ cell numbers detected in the PVS and the meningeal spaces trended higher in the ipsilateral 40.5 cells/mm^2 compared to the contralateral hemisphere 35.3 cells/mm^2 but was not significantly different (Figure 3-21B).

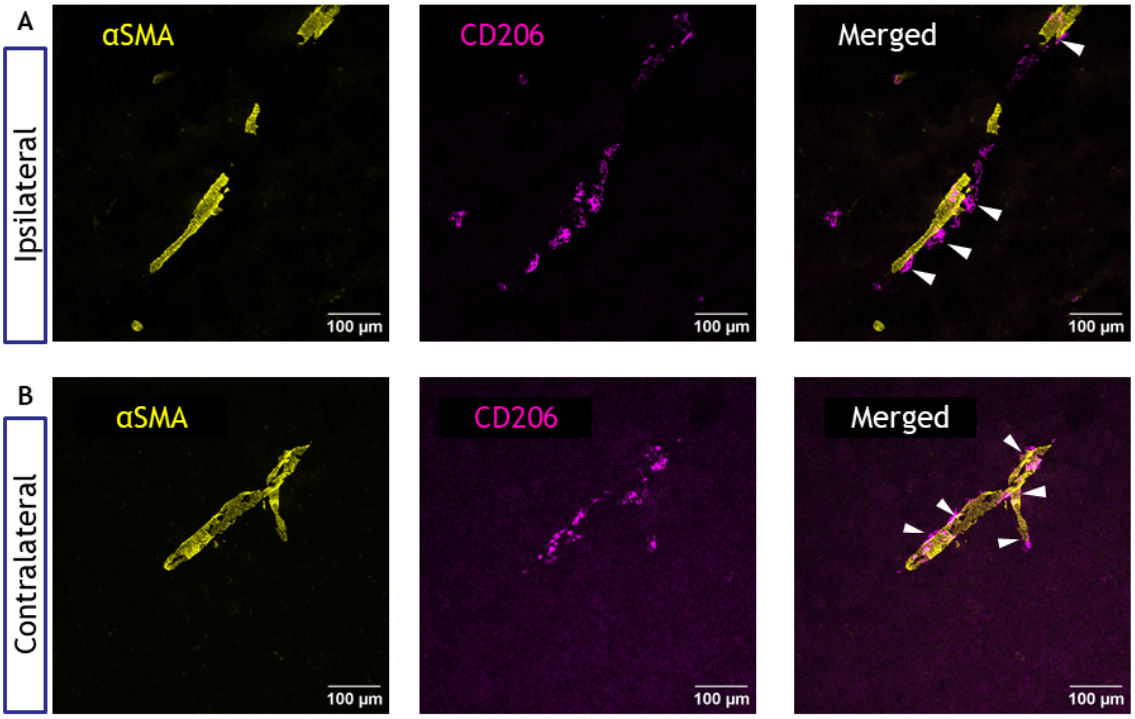

Figure 3-19. $CD206^{+}aSMA^{+}$ cells (white arrowheads) were detected near cerebral arterioles in the ipsilateral (A) and contralateral (B) hemispheres following transient middle cerebral artery occlusion (tMCAo) in C57BL6/J mice. αSMA – alpha smooth muscle actin (yellow), CD206 – the mannose receptor (magenta). White arrows represent co-localisation of independent antigens on identical cells. Representative images at 40x magnification were selected from 6 independent experiments in 6 mice. Scale bar = 100µm.

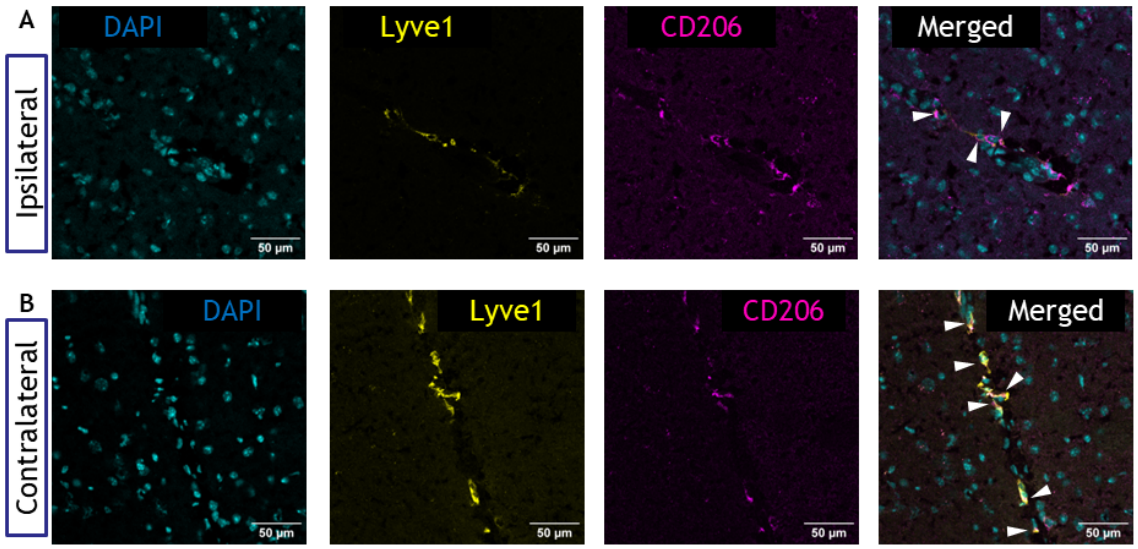

Figure 3-20. CD206⁺Lyve1⁺ cells (white arrowheads) were detected in the ipsilateral (A) and contralateral (B) hemispheres following transient middle cerebral artery occlusion (tMCAo) in C57BL6/J mice. DAPI - cell nuclei (cyan), Lyve1 – lymphatic vessel endothelial hyaluronan receptor 1 (yellow), CD206 – the mannose receptor (magenta). Representative images at 40x magnification were selected from 6 independent experiments in 6 mice. Scale bar = 50µm.

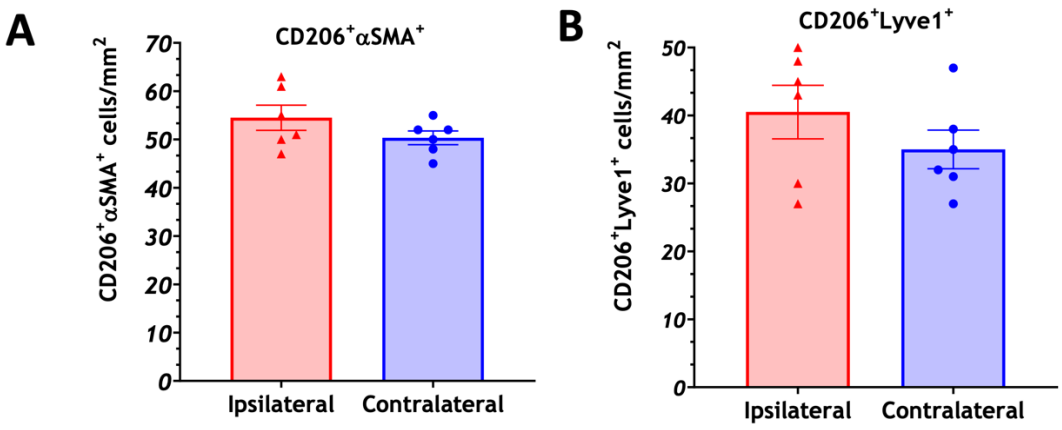

Figure 3-21. Quantification of CD206⁺aSMA⁺ (A) and CD206⁺Lyve1⁺ (B) cells in the ipsilateral and contralateral hemispheres 72 hours following transient middle cerebral artery occlusion (tMCAo). Data is presented as mean ± SEM, n=6, paired t-test, P>0.05.

To further delineate the localisation of BAMs with respect to the ischaemic injury, the numbers of perivascular BAMs were quantified in the peri-infarct and infarct regions. Similar numbers of CD206⁺aSMA⁺ cells were identified in the infarct (26 cells/mm^2) and peri-infarct regions (29 cells/mm^2) (Figure 3-1A, C). Likewise, CD206⁺Lyve1⁺ cells were comparable between the infarct and peri-infarct regions, if relatively fewer (~20 cells/mm^2) than CD206⁺aSMA⁺ cells (Figure 3-1B, D).

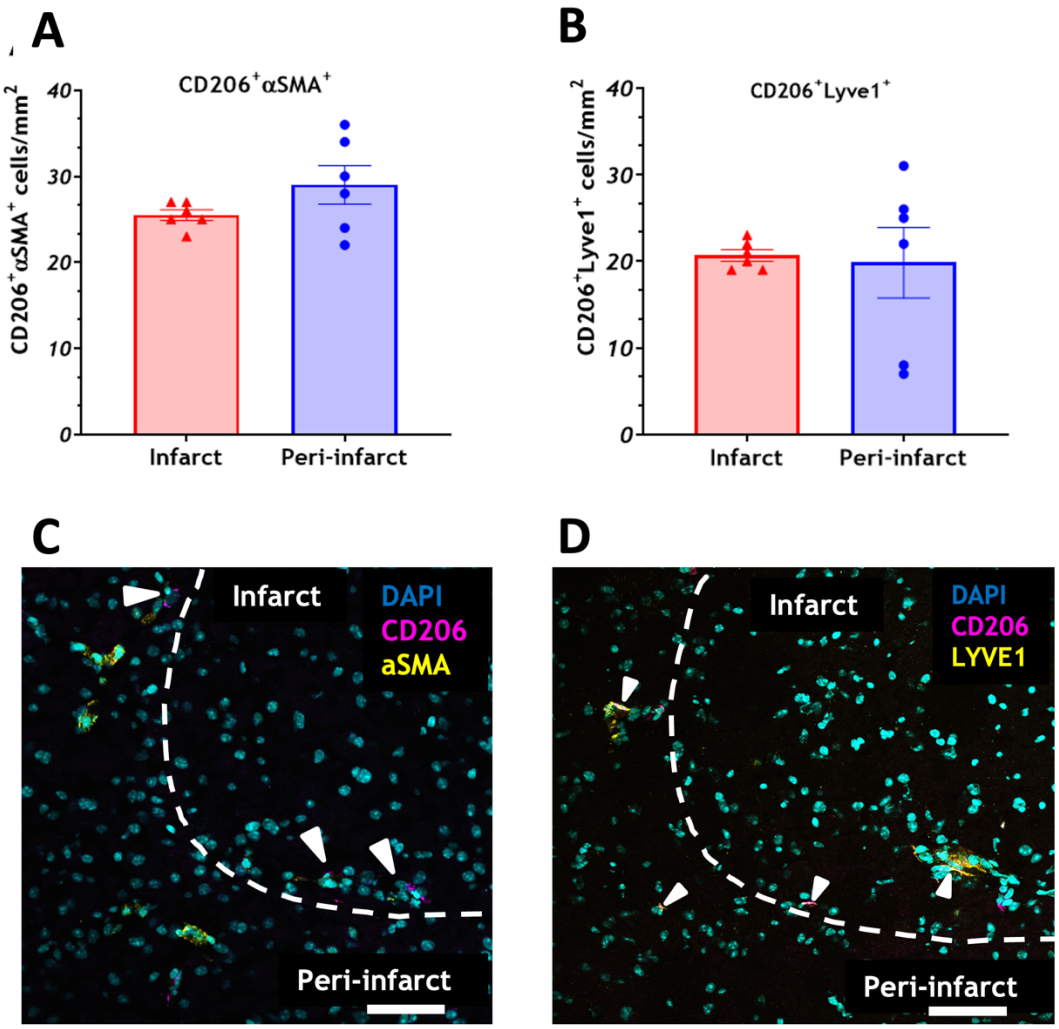

Figure 3-22. Quantification and representative immunofluorescent images of CD206⁺aSMA⁺ (A) and CD206⁺Lyve1⁺ (B) cells in the infarct and peri-infarct following transient middle cerebral artery occlusion (tMCAo) in C57BL6/J mice. Data is presented as mean ± SEM, n=6, paired t-test, P>0.05. Representative images at 20x magnification were selected from 6 independent experiments in 6 mice of CD206⁺aSMA⁺ (C) and CD206⁺Lyve1⁺ (D) cells. White dashed line depicts the border between the infarct and the peri-infarct. Scale bar = 50μm.

The proliferative status of CD206⁺ and Lyve1⁺ cells was investigated by double labelling for CD206⁺Ki67⁺ cells and Lyve1⁺Ki67⁺ cells in the ipsilateral hemispheres of C57BL6/J mice 72 hours after 60 min tMCAo. Although staining for the individual markers was demonstrated and antigen Kiel 67 (Ki-67) expression was determined in the infarct core (cf. Appendix Figure 7-2), co-expression of Ki67 with either BAMs marker was not established (Figure 3-23).

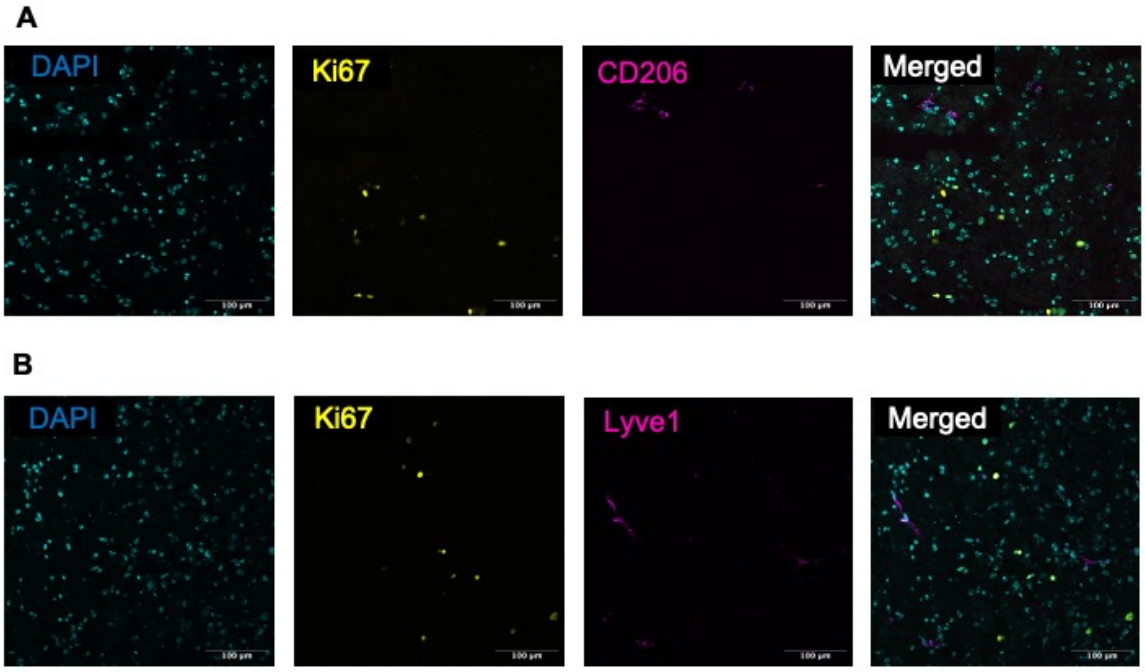

Figure 3-23. Proliferation of CNS border-associated macrophages in C57BL6/J mice following transient middle cerebral artery occlusion (tMCAo). A) Proliferation marker Ki67 (yellow) and CD206^{+} cells (magenta). B) Ki67 (yellow) and Lyve1 (magenta). Also presented are DAPI (cyan) cell nuclei and merged images. Scale bar= 100μm, 10x maginification.

3.4 Discussion

3.4.1 Summary of findings

The aim of this study was to determine if tMCAo is accompanied by a change in BAMs numbers in the acute, sub-acute and chronic stages post ischaemia-reperfusion and to characterise the localisation of BAMs after tMCAo. Whilst BAM numbers have been assessed after stroke before (Pedragosa et al., 2018, Rajan et al., 2020), they have not been assessed over time. Data presented in this chapter demonstrates that BAMs numbers increase in the ipsilateral hemisphere in the acute and sub-acute stages (on days 1 and 3 and 7) after tMCAo, while their numbers were comparable between sham, ipsilateral and contralateral hemispheres in the chronic phase (on day 14 and 1 month) after experimental stroke. The immunofluorescence semi-quantification was not able to demonstrate an effect of ischaemia-reperfusion injury on the numbers of BAMs or discriminate BAMs between the infarct and peri-infarct zones, or migration from their CNS borders to the ischaemic parenchyma.

In this study BAMs ($CD45^+CD11b^+CD206^+Lyve1^+$) were found to be a rare population in the naive brain (4.2%, Figure 3-5), whilst others reported they make up to 10% of leukocytes (Mrdjen et al., 2018). Microglia were detected around $6x10^3$ cells per hemisphere or about 80% of all leukocytes in the naïve mouse brain (Figure 3-5).

3.4.2 BAMs, microglia, and M2-like macrophages in the acute phase after tMCAO

BAMs numbers markedly increased in the acute phase after tMCAo **(**Figure 3-9**)** in similar magnitude to those of infiltrating myeloid cells. In contrast, in a rat model of ischaemic stroke $CD163^+$ BAMs were comparable between hemispheres 16 hours post tMCAo and there was a trend for numbers to increase at 24 hours, which was not significant (Pedragosa et al., 2018). The same group later published results that show that CD163 cells increased a significant 5-fold in the ischaemic brain compared to controls three days post tMCAo (Rajan et al., 2020). This is in line with the findings of this study at day 3 (Figure 3-9).

In this study M2-like macrophages increased on day 3 after tMCAo (Figure 3-7**),** however others have been reported lower numbers of peripherally-derived M2-like macrophages relative to proinflammatory macrophages 72 hours after ischaemic stroke (Wattananit et al., 2016). While the here observed increase might be in part explained by proliferation by some resident $CD206^+$ BAMs, they are mostly peripheral M2-like macrophages infiltrating the brain and acquiring BAM-like phenotypes, as discussed in more detail below.

Early studies in bone marrow chimeric mice have established that microglia activate early after tMCAo, preceding the accumulation of peripheral leukocytes (Schilling et al., 2003). On comparing their frequency in the ipsilateral hemisphere across tMCAo phases, it appeared that there was actually a decrease on day 3 and day 14 (Figure 3-16). Others have reported that on day 3 day after 90 min tMCAo microglia numbers decreased in the stroke compared to sham hemispheres (Ritzel et al., 2015) and attributed this to cell death as the infarct has fully developed at this point.

3.4.3 BAMs, microglia, and M2-like macrophages in the sub-acute and chronic phase after tMCAo

The numbers or functions of BAMs in the reparative phase after tMCAo have not previously been reported. Microglia have both protective and deleterious roles (Ma et al., 2017), a feature which could be extended to BAMs during different phases of post stroke neuroinflammation. This study presents for the first time a significant increase in the number of BAMs up to a week following tMCAo in the ischaemic hemisphere compared to the sham and contralateral hemispheres (Figure 3-12). Two weeks after tMCAo the elevated immune cell numbers persisted across most cell types, although the trend for increased BAMs in the ipsilateral hemisphere does not reach statistical significance (Figure 3-12).

Anti-inflammatory macrophages were reported at higher frequencies over pro-inflammatory macrophages 7 days to 21 days after stroke (Wattananit et al., 2016). Here we observed elevated numbers of M2-like cells up to 2 weeks after tMCAo (Figure 3-11). This indicated that the beginning of resolution of inflammation may not start until after this timepoint in our model, highlighting the need to investigate cell numbers at a more chronic phase after tMCAo. Although one month post ischaemia microglia numbers were still elevated in the ischaemic brain compared to sham (Figure 3-13, Figure 3-16), the numbers of BAMs and M2-like macrophages did not differ significantly between stroke and sham during this chronic phase (Figure 3-13). BAMs remained about 5% of all detected leukocytes in the ipsilateral hemisphere (Figure 3-13) at all timepoints, apart from in the chronic phase, potentially because of a decrease in the expression of CD206 and Lyve1 at this timepoint, or because their self-renewal happens over a longer timescale compared to that of microglia.

Microglial numbers, activation and phenotypes can be detected during the sub-acute, and chronic phases of ischaemicstroke (Gulyás et al., 2012, Morrison and Filosa, 2013, Yan et al., 2015). Peak microglia accumulation was observed in the subventricular zone of rat brains 6 weeks after 2h tMCAo, indicative of the long-term involvement of microglia in the resolution of neuroinflammation (Thored et al., 2009). Microglia numbers were consistently elevated in the ischaemic hemisphere into the chronic phase after tMCAo (Figure 3-6, Figure 3-10, Figure 3-13).

3.4.4 Limitations

The ARRIVE guidelines stipulate allocating animals to experimental groups by randomisation, blinding experimental procedures and using both female and male animals (Kilkenny et al., 2010, Percie du Sert et al., 2020). Randomisation to sham or stroke were omitted from the study design, which may have introduced observer bias and allocation bias. While all animals were handled and assessed using standardised procedures to minimise variability, this is a clear limitation of the study. Future studies must also incorporate random allocation to surgery to strengthen internal validity. Outcome measures were based on objective, quantifiable data, reducing subjective interpretation, but in future work, blinding data collection by concealing tissue identity prior to processing samples for flow cytometric analysis would be necessary. Infarct analysis was blinded by changing data file names and keeping a key to decode the original names must be incorporated to reduce bias. This can be incorporated for flow cytometric and immunofluorescent analyses in future. Additionally, female mice were excluded from the study design, which limits the generalisability of the findings across sexes and must be addressed in future experiments.

3.4.4.1 Flow cytometric analysis limitations

Brain atrophy is synonymous with chronic infarcts in clinical stroke (Lee et al., 2010). It was recently reported that 1 month after tMCAo ipsilateral volume is 6% smaller than contralateral (Morais et al., 2024), with hippocampal atrophy becoming significant at this timepoint (Brait et al., 2021). Therefore, the amount of tissue analysed at 1 month after tMCAo in the presented study must also have been considerably less in the ipsilateral hemisphere than in the contralateral and sham hemispheres, which might explain the lack of increase in numbers at this timepoint (Figure 3-13, Figure 3-14). Another potential limitation of the study pertains to the gating strategy. A recent paper has described a $CD45^{-}Lyve1^{+}$ population of perivascular macrophages (Siret, 2021), indicating that some BAMs were potentially not quantified by the flow cytometric analysis, potentially resulting in underestimating the total numbers of BAMs detected. However, given that lymphatic endothelial cells also express Lyve1, it is undoubtedly difficult to distinguish BAMs from these cells without narrowing down the phenotype to expression of a pan-immune cell marker and may have been obtainable in this

study by post-hoc gating for $CD45^{-}CD11b^{+}Lyve1^{+}$ cells to reveal the frequency of these cells.

3.4.4.2 Semi-quantification of $CD206^{+}aSMA^{+}$ and $CD206^{+}Lyve1^{+}$ cells on day 3 after tMCAo

Since the flow cytometric analyses differentiate cells based on marker expression without regard for anatomical location, an immunofluorescence method was used to recognise cells co-expressing $CD206^{+}aSMA^{+}$ in proximity to arterioles. This approach allowed the exclusion of $CD206^{+}$ cells, which were identified out width the perivascular space (Figure 3-18). The semi-quantification of $CD206^{+}aSMA^{+}$ cell numbers found no significant differences in the stroke versus contralateral hemispheres on day 3 (Figure 3-21), despite the flow cytometric quantification identifying about a 50-fold increase in $CD45^{+high}CD11b^{+}CD206^{+}$ cells in the ipsilateral versus contralateral hemispheres, that was however not statistically significant (Figure 3-7). $CD206^{+}Lyve1^{+}$ cells were detected to a similar degree in both hemispheres on immunofluorescent images, while there were 40 times more $CD45^{+high}CD11b^{+}CD206^{+}Lyve1^{+}$ cells in the ischaemic hemispheres compared to their contralateral counterparts at day 3 (Figure 3-9). This is likely due to the semi-quantitative nature of the immunofluorescence cell counting analysis, which detects cells in a small volume of space from 10 μm sections. Analysing cell counts across a greater number of sections across the same brain region would have increased the accuracy of the quantification, allowing for volumetric cell number comparisons. Additionally, investigating localisation across different timepoints, with concomitant labelling of the glia limitans or markers of remodelling, would have allowed the study of potential BAMs migration during the different stages of stroke.

It is also possible that there is a large fraction of $CD206^{+}Lyve1^{+}$ cells in the choroid plexus, which is more challenging to study on coronal sections and might be better investigated in sagittal sections (Goldmann et al., 2016). The fraction of BAMs in the choroid plexus receives partial replenishment from the periphery (Goldmann et al., 2016) and the higher numbers of $CD206^{+}Lyve1^{+}$ detected in the ischaemic hemisphere by flow cytometry could contain cells, which have just undergone repopulation in this anatomical region.

Another limitation to this study is that the brain excavation method used inadvertently destroys the dural meninges, so dural BAMs subtypes were omitted in these analyses. A refinement method that preserves the dural meninges such as the whole-mount meninges would be needed to investigate the contribution of dural BAMs towards the total BAMs count (Derecki et al., 2015)(Louveau et al., 2018).

3.4.4.3 BAMs in the infarct versus peri-infarct

To understand if BAMs have direct roles in infarct development and/or resolution of inflammation, their localisation with respect to the infarct and peri-infarct was explored. In this study there were no differences in the frequency of BAMs observed in those regions (Figure 3-22). Previously a preferential accumulation of PVMs was reported in the perivascular spaces of the peri-infarct versus the infarct (Rajan et al., 2020), suggesting that BAMs may be mobilised along the perivascular spaces towards areas with salvageable tissue. It is perhaps possible that the observed upregulation of CD206 and CD169 in the periphery of infarction by Rajan and colleagues' is due to cell death of BAMs in the infarct core. BAMs are recognised as a very heterogeneous population (Mrdjen et al., 2018, Jordão et al., 2019, Van Hove et al., 2019), so some subsets may preferentially mobilise to the peri-infarct areas in a reparative capacity, while others execute more deleterious roles in the infarct, resulting in the equal numbers detected across these two regions. Therefore, additional markers such as CD36 or Arg-1 would be needed in these analyses that can resolve BAMs' potential sub-functions after ischaemic stroke.

A limitation to this immunofluorescent analysis is that the peri-infarct zone was estimated in four areas around the infarct (Figure 3-1). Images with higher magnification (10x, 25x and 40x) were chosen in this study and are often presented in articles, which have investigated differential expression of genes between the infarct and peri-infarct regions immunofluorescently (Shimada et al., 2010, Pedragosa et al., 2020, Jiang et al., 2017). This offers better visualisation of anatomical structures such as arterioles, but compromises depiction of the whole hemisphere and therefore accurate presentation of the core and peri-infarct regions within a single image. Guiding the identification of the infarct core using a thionin-stained brightfield image is not ideal, highlighting the need for a more

reproducible method for distinguishing the regions of the peri-infarct from infarct core. A method commonly reported in the literature involves approximation of the peri-infarct as 500 µm laterally and medially to the edge of the infarct core (Ohab et al., 2006, Jiang et al., 2017), which is flawed by determination of the edge in the first instance. Researchers with access to imaging equipment with motorised stages and long hours of use have the ability to record dozens of images per section and use a stitching algorithm to generate high-volume, high-quality data. It has been reported that this allows to determine infarct size by cresyl violet staining and overlaying a mask onto an immunofluorescent image (Garcia-Bonilla et al., 2016). Additionally, to investigate if any preferential localisation of BAMs in the peri-infarct compared to the infarct core occurs independently from of proliferation, but due to region-specific higher or lower viability, adding a method that identifies DNA breakage such as TUNEL may be advantageous in the future.

3.4.4.4 Proliferation of BAMs

Proliferative bursts are known to occur after acute inflammation in tissue macrophages (Davies et al., 2011), driven by signals released from the infarct such as cytokines, which can activate a family of Janus kinases (Jaks) to cause proliferation or the Akt/PKB signalling pathway. The flow cytometric analyses presented here showed elevated numbers of BAMs up to a week after tMCAo (Figure 3-12), suggesting that BAMs are proliferating in response to the ischaemic insult. RNA sequencing data from another study has shown that $CD163^+$ BAMs upregulate genes for transcription factors implicated in proliferation such as Csf1, Ki-67, cyclin-dependent kinases (Cdk) and protein regulator of cytokinesis 1 (Pcr1) (Rajan et al., 2020). These authors showed that 72 hours post tMCAo $CD163^+$ cells co-localised with Ki67, along with expression of genes connected to cell cycle phase transition and mitotic nuclear division compared to sham controls, supporting a proliferative profile for BAMs during the period of infarct development. An antibody against Ki67 had previously been optimised in our lab for immunofluorescent analyses (cf. Appendix Figure 7-2) and since this marker is upregulated during the active phases of the cell cycle (G2 and M), it was chosen to investigate BAMs proliferation. However, in this study CD206 and Lyve1 failed to colocalise with Ki67 (Figure 3-23), potentially as the majority of BAMs were not in the active phase of the cell cycle at the point of investigation. While the likely mechanism behind the observed increase in BAMs numbers remains proliferation,

a definitive confirmation needs more work. Alternative methods to investigate cell proliferation include assays based on rate of deoxyribonucleic acid synthesis using radioactively labelling with ^{3}H-thymine, flow cytometric analysis of 5-bromo-2'deoxyuridine (BrdU), or by measuring the metabolic activity where the reduction potential of cells for tetrazolium or resazurin salts is investigated in a colorimetric assay (Vega-Avila and Pugsley, 2011). Further, a bioluminescence-based assay using luciferase and its substrate luciferin measures the intracellular concentration of ATP could be deployed.

3.4.4.5 Replacement of BAMs by peripheral monocytes

Since proliferation was not conclusively determined, an alternative hypothesis is that BAMs are either solely replaced by peripheral monocytes, or this process occurs concomitantly with proliferation. BAMs attract granulocytes through expression of CCL2 to infiltrate into the ischaemic brain (Pedragosa et al., 2018) and recent evidence indicates that depletion of PVMs and meningeal BAMs in disease states results in their replacement by peripheral monocytes through the CCL2-CCR2 axis (Wang et al., 2024). Therefore, any BAMs that have undergone apoptosis or necrosis in the affected MCA territory are potentially replaced by infiltrating CCR2^{+} monocytes, which may adopt a BAM-like phenotype (Dalmau Gasull et al., 2024). In chimeric mice with bone marrow transplants from CX3CR1^{GFP}CCR2^{GFP} mice, about 30% of CD169^{+} cells post ischaemic stroke originated from CX3CR1^{+}CCR2^{+} patrolling monocytes (Rajan et al., 2020), suggesting that while a significant fraction of cells is replenished through a peripheral mechanism, accumulation through proliferation is still plausible. This mechanism of recruitment of BM-derived monocytes to the CNS is similar in a mouse model of Alzheimer's disease, where circulating monocytes are recruited to cerebral vessels in a CCR2-dependent manner, contributing to the perivascular BAMs pool (Mildner et al., 2011). In experimental autoimmune encephalomyelitis, BAM proliferation occurs alongside continuous monocyte infiltration until peak disease severity (Jordão et al., 2019). In an endotoxemia model, TNFα/angiopoietin 2-dependent pathways promote monocyte adhesion to brain capillary endothelium (Audoy-Rémus et al., 2008). This was followed by transmigration across the BBB, proliferation, and adoption of a BAM phenotype; expression of CD11b, CD163, and stabilin-1 and elongated morphology. CD206^{+} cells derived from the circulation would highly express *Ccl2*, while BAMs are known

to upregulate *Ccl5* in disease states (Jordão et al., 2019), perhaps providing an avenue to differentiate these cells in future investigations. It will ultimately be particularly important to investigate whether infiltrating monocytes, which have converted into BAMs, also acquire some of the previously reported *bona fide* functions of BAMs after tMCAo, such as enhancing granulocyte chemotaxis, secretion of VEGF and increasing BBB permeability (Pedragosa et al., 2018), antigen presentation (Rajan et al., 2020), discussed further below.

3.4.5 Ability of BAMs to migrate from the borders to the parenchyma

In mice, $CD206^+$ and $CD163^+$ cells were found in the brain parenchyma after MCAo, suggesting migration of BAMs from the CNS borders into the ischaemic parenchyma (Rajan et al., 2020). In rats 4 days post tMCAo it was reported that $CD169^+$ cells but not $CD206^+$ cells accumulate in the parenchyma (Rajan et al., 2020), and the authors made a similar observation that it was not possible to conclusively identify these cells as either migrated BAMs or microglia overexpressing CD169. During homeostasis both perivascular and meningeal macrophages have relatively fewer projections and display less motility as described by *in vivo* imaging (Nayak et al., 2012). However, it is plausible that under ischaemic conditions cell behaviours may be altered and may become more akin to juxtavascular microglia, which are a subset of microglia known to make direct contact with the glia limitans and have been documented responding to injury by moving along brain microvessels (Grossmann et al., 2002). A putative mechanism for BAMs migration could involve upregulating matrix metalloproteinases (Rajan et al., 2020) to break down extracellular matrix. In this study some $CD206^+$ cells were found remotely from the perivascular space, however to investigate transmigration of BAMs from the CNS borders across the glia limitans, an additional marker such as glial fibrillary acidic protein (GFAP*)* or markers for extracellular remodelling (Mmps, collagens) would be needed.

3.4.6 Functional roles of BAMs

As discussed above, although we are gaining understanding on the functions of BAMs in the acute phase of stroke, no investigation to date has covered their long-term roles after stroke. BAMs may exert effects on brain repair through promoting

angiogenesis and glial remodelling, since they upregulate VEGF expression in endothelial cells (Pedragosa et al., 2018). However, since this process may be limited by the rate of sprouting, which typically occurs after day 3 and day 7 after MCAO (Kanazawa et al., 2017a), BAMs may only begin to support repair in the subacute phase. Additionally, Pedragosa et al. noted that the increased VEGF production by BAMs caused pial and cortical vessels permeability (Pedragosa et al., 2018), and BAM depletion was able to reverse vascular permeability in another study (Drieu et al., 2022).

The functional importance of BAMs has been extensively investigated using a pharmacological ablation with liposomal clodronate (Polfliet et al., 2001, Galea et al., 2005, Hawkes and McLaurin, 2009, Serrats et al., 2010, Park et al., 2017, Santisteban et al., 2020, Pedragosa et al., 2018, Drieu et al., 2020). BAMs phagocytose the liposomal particles, facilitating the release of a toxin to trigger apoptosis (Galea et al., 2005). BAM ablation in rats by intracerebroventricular (i.c.v) injection of clodronate 4 days prior to stroke did not affect lesion size after tMCAo on a thionin-stained histological assessment (Pedragosa et al., 2018) but it conferred reduced numbers of infiltrating granulocytes to the ischaemic cortex and a better functional recovery in the hyperacute period (16 hours) after stroke (Pedragosa et al., 2018). Another study also refuted a role for BAMs on impacting infarct volume in mice, demonstrating a lack of infarct size reduction on a T2-weighted MRI by BAMs ablation 5 days prior to tMCAo (Drieu et al., 2020). Interestingly, in the same study they demonstrated that alcohol exposure in clodronate treated animals reduced infarct volume, indicative of specific roles of BAMs in neuroinflammatory priming associated with alcohol consumption in stroke, while a mechanism for this is currently unreported. A more recent article reported that clodronate depletion 1.5 days prior to tMCAo reduced infarct volume by 50% and improved neurological burden 24 hours post stroke (Yu et al., 2025). It remains unclear how BAMs may have such a profound effect on infarct size from their anatomical locations, and strengthens the hypothesis that they exert these roles through migration to the infarct and peri-infarct areas.

3.4.7 Future work

BAMs depletion using i.c.v. injection of clodronate was originally going to be employed to study BAM functions after tMCAo by deploying laser speckle contrast

imaging (LSCI) to investigate *in vivo* CBF following stroke but was not feasible due to the time restrains for this project. This approach would allow examining the impact of BAMs on brain function in a longitudinal study at different timepoints. Performing the investigation in the same cohort of mice would not only reduce the number of animals needed but also allow to robustly investigate the neuroinflammatory profile exerted by these cells over time. Most importantly, invaluable insights about ischaemic brain function could be gleaned by BAM depletion, which would be more laborious to investigate through different experimental approaches. However, the clodronate depletion method has disadvantages too. It requires drug delivery using a stereotactic frame, which requires an elaborate procedure, and it was reported to also deplete $Iba1^{+}$ resting microglia (Cunningham et al., 2013), and only lasts about 2 weeks before BAMs replenish from niche-specific stem cell progenitors (Goldmann et al., 2016), rendering this unsuitable for the study of chronic changes after tMCAo.

Over the last 5 years there has been an expansion in the arsenal of genetic tools available to study the functions of BAMs in homeostasis and disease. Reporter mice using Cre recombinase-mediated mutagenesis such as and BAMs were demonstrated to control CSF influx in the meninges using a similar $Lyve1^{Cre}$ reporter mouse (Drieu et al., 2022). More recently a novel $Mrc1^{CreER}$ reporter mouse has been generated to study the roles of BAMs in glioblastoma (Petrova, 2024) and $Mrc1^{CreERT2}$ reporter mouse was used to reveal the roles of BAMs in interacting with meningeal T lymphocytes in hypertension-induced cognitive impairment (Santisteban et al., 2024). Another novel tool to discern embryonically derived microglia and BAMs from peripheral monocytes uses the microglia specific gene *Crybb1 (Brioschi et al., 2023)*, and will be of utility in distinguishing post stoke contributions of microglia from BAMs and peripheral monocytes. Moreover, since single promoter Cre models may report on the activity of multiple cell types containing that promoter, recent advances involve creating a binary Cre recombinase, consisting of two complementary fragments, which recognise the N-terminus of one promoter and the C-terminus of another, and allowed for the generation of $Lyve1^{ncre}$: $Cx3cr1^{ccre}$ mouse to study BAMs and $Sall1^{ncre}$: $Cx3cr1^{ccre}$ to investigate microglia (Kim et al., 2021a). Studies using a reporter mouse can investigate the mechanisms of recruitment of granulocytes by BAMs and their

potential migration into the parenchyma using advanced methods such as two-photon imaging (Wang et al., 2024).

CSF1 is a cytokine which controls the production, differentiation, and function of macrophages. The colony stimulating factor 1 receptor gene (*Csf1r*) is expressed in both macrophages and microglia (Rojo et al., 2019). It was recently reported that deletion of *Csfr1* in cells, which differentially express *Lyve1,* confers BAM depletion and allows to investigate their functions in the glymphatics (Drieu et al., 2022). Since the effect of clodronate on BAMs depletion is reasonably short-lived (as discussed above), to investigate the impact of BAMs depletion in the chronic phase after stroke, an *Lyve1*^{eGFP}- *Csf1r*$^{fl/fl}$ BAMs depletion mouse could be utilised. One of the strains has a targeted insertion of a *Lyve1* allele, and the *Lyve1* promoter drives the expression of Cre recombinase with enhanced green fluorescent protein (EGFP). The other stain is *Csf1r*$^{fl/fl}$ mice, which possesses *loxP* sites flanking exon 5 of *Csf1r* gene to excise Csf1r in tissues expressing a promoter of interest. These two strains were obtained from the Jackson laboratory for this project and the *Lyve1*^{eGFP} strain was going to be crossed with *Csf1r*$^{fl/fl}$ mice to study the role of Lyve1 expressing BAMs in the context of stroke. It was intended to study differences in CBF after stroke by LSCI resulting from BAM depletion, alongside with neurological scoring and infarct size. However, due to breeding issues and time constrains, this was not feasible within this project but would be interesting to investigate further. An alternative depletion approach would be to cross another one of the above-described Cre reporter mice to the *Csf1r*$^{fl/fl}$ mice.

4 Chapter 4: Effect of ischaemia on DDAH2 expression and the role of DDAH2 in regulating macrophage phenotype

4.1 Introduction

In response to infection or inflammation macrophages upregulate genes that generate high amounts of reactive oxygen and nitrogen species such as NO (Boscá et al., 2005). NO can in turn increase the expression and release of pro-inflammatory cytokines such as TNFα and IL-1β from macrophages (Wu et al., 2003). The inducible isoform (iNOS) generates sustained and large amounts NO to support the cytotoxic functions of macrophages in tumours (Kashfi et al., 2021). However, iNOS expression in myeloid cells suppresses the M2-like phenotype (Lu et al., 2015). NO influences macrophage metabolism by interacting with components of the electron transport chain and so iNOS-derived NO controls macrophage mitochondrial function (Palmieri et al., 2020).

DDAH2 is the only isoform expressed in macrophages (Figure 1-7) that modulates NO biosynthesis by metabolising NOS inhibitors such as the methylarginines ADMA and mono methylarginine (L-NMMA) (Leiper and Nandi, 2011). Genetic deletion of DDAH2 in macrophages results in impaired macrophage motility, phagocytosis and cytokine production (Ahmetaj-Shala, 2013). RNA sequencing data from Professor Leiper's laboratory has demonstrated that DDAH2 regulates processes atherosclerotic processes in M1-like macrophages, as genes associated with apoptosis, cell adhesion, lipid binding, and monocyte differentiation were found to be differentially expressed in peritoneal macrophages (Alanazi et al., 2022).

Both ADMA and L-NMMA downregulate NO production in RAW 264.7 macrophage cell line, and ADMA (25 mM) or L-NMMA (50 mM) decrease iNOS expression in these cells (Pekarova et al., 2013), while the mechanism by which this occurs has not been confirmed. Protein levels of DDAH2 are detected in many cell types and organs, including macrophages (Lambden et al., 2015), neurons (Kozlova et al., 2021), and the whole brain (Gao et al., 2024, Ragavan et al., 2023). In mice DDAH2 regulates iNOS-NO mediated macrophage function and immune responses (Lambden et al., 2015, Lange et al., 2016, Huang et al., 2021). Absence of DDAH2 reduces phagocytosis and motility in peritoneal macrophages, along with increased intracellular ADMA (Ahmetaj-Shala, 2013), demonstrating that DDAH2 regulates nitric oxide (NO) mediated functions in macrophages along the DDAH2-ADMA-iNOS signalling pathway. However, global DDAH2 deletion in healthy mice reduced vascular responsiveness through modulation of methylarginines such as

ADMA and monomethyl arginine (L-NMMA), acutely raised circulatory ADMA, which increased blood pressure, and reduced survival rate in a model of polymicrobial sepsis (Lambden et al., 2015). Therefore, selective deletion of DDAH2 in macrophages has been developed and the role of DDAH2 in mouse peritoneal macrophage function was reported (Lambden, 2016). Despite the evidence for a role of each of the components of the DDAH2-ADMA-iNOS pathway in macrophage function, implications of disruptions along this signalling pathway in primary cerebral macrophages in the context of ischaemia is completely unreported.

In vitro models of brain ischaemia typically involve metabolic inhibition induced through application of chemicals such as a dual treatment with 2-deoxyglucose and antimycin (Sundaram et al., 2016) or sodium azide (Marino et al., 2007) and/or glucose deprivation to neuronal cultures (Carpanese et al., 2014). These methods allow the study of specific mechanisms and pathways, which would otherwise be masked by the complex inputs from numerous interconnected systems *in vivo*. Intermittent hypoxia for 4 hours has been shown to increase the expression of iNOS in cultured RAW264.7 macrophages (Baumgardner and Otto, 2003). A hypoxic challenge in isolated primary murine macrophages induced a 4-fold increase in iNOS over control, an increase in DDAH2, reduced ADMA, and increased NO (Lambden et al., 2016). This was replicated in macrophages from macrophage specific DDAH2 knockout mice in the same study, which showed a decrease in NO production and a modest increase in ADMA. In the hereby presented work macrophage culture was subjected to the most frequently used model of *in vitro* cerebral ischaemia - oxygen and glucose deprivation (OGD).

Isolation of brain resident macrophages such as microglia offers the opportunity to examine their transcriptome in healthy and stroke mouse brains and offers the possibility to validate genes found to be dysregulated in ischaemia stroke from previous studies or databases such as the Gene Expression Omnibus database. Magnetic activated cell sorting (MACS) typically involves passing cells through a column composed of ferromagnetic spheres (0.1-0.5 μm in diameter) by using a magnetic field. The spaces in the column are several times larger than macrophages, which are 20–30 μm in diameter, which allows the capture of up to 10^9 cells. This versatile technology was developed in the 1980s (Miltenyi et al., 1990) and has recently been adapted for isolation of $CD11b^+$ cells such as

monocytes, macrophages and microglia (Bordt et al., 2020)(Schroeter et al., 2021). CD11b is a ß2 integrin important in leukocyte recruitment to sites of inflammation, to mediate adhesion to the immunological synapse of T cells, and to regulate both pro- and anti-inflammatory signalling (Schittenhelm et al., 2017).

Several compounds modify the expression or activity of the DDAH enzymes (Leiper and Nandi, 2011, Murphy et al., 2016). Some of these compounds feature selective inhibition of DDAH1 such as N^G-(2-methoxyethyl)-l-arginine methyl ester (also known as L-257) (Rossiter et al., 2005, Leiper et al., 2007). Additionally, investigating the effects of the DDAH1 enzyme has been enhanced by the availability of pharmacological potentiation of DDAH1 through agonism at the farnesoid receptor X (Liu et al., 2013), DDAH1 knockout mice (Hu et al., 2009), including an endothelial-specific DDAH1 mice (Dowsett et al., 2015) and transgenic overexpression of DDAH1 in mice (Gao et al., 2024). However, selective pharmacological inhibition of DDAH2 is currently unavailable and there is lack of methods for pharmacological potentiation of the activity of DDAH2 other than transient overexpression, which has so far only been reported in studies of the endothelium (Hasegawa et al., 2006). Genetically ablating DDAH2 globally has hypertensive effects (Lambden et al., 2015, Lange et al., 2016) and in the context of stroke, it would be important to distinguish the roles of DDAH2 in macrophages from those in endothelial cells or neurons. Specifically deleting DDAH2 in monocytes (and therefore tissue macrophages) by targeted insertion of *cre* recombinase cDNA into the endogenous M lysozyme locus (LysM), encoded by *Lyz2*, (Clausen et al., 1999), presents a strong investigational tool to unravel the roles of the DDAH2 enzyme in inflammatory conditions such ischaemic stroke. Indeed, a monocyte/macrophage specific DDAH2 mouse ($DDAH2^{Mo-/-}$) has been generated (Lambden et al., 2015).

The mouse M lysozyme is a glycoside hydrolase that functions to protect cells from bacteria as part of the innate immune system. It is constitutively expressed in adulthood and has been identified in seminal work from Cross and colleagues as a myeloid lineage marker (Cross et al., 1988). Albeit microglia are not of myeloid origin, *Lyz2* was previously reported to be functionally expressed in subsets of microglia, with 10% of $CD45^{+int}$ cells, a quarter of hippocampal and cerebellar microglia, and 5% of motor cortex Iba-1^+ cells (Orthgiess et al., 2016). More

recently, using the Lyz2-Cre system has achieved up to 50% target gene recombination in microglia (Sarkar and Lipinski, 2024), suggesting that in the DDAH2$^{Mo-/-}$mouse potentially up to half of the microglia population would be lacking in *Ddah2*. Therefore, if microglia were indeed found to express *Ddah2*, validating a *Ddah2* knockout in at least a proportion of these cell would be expected.

As demonstrated in Chapter 3 microglia constitute most resident macrophages in the naïve and stroke brain, necessitating a confirmation of a potential deletion of DDAH2 in these cell types in addition to macrophages. The expression of *Ddah2* in brain resident macrophages such as microglia is relatively unexplored. RNA sequencing data suggests that *Ddah2* is expressed at 4-fold lower levels in microglia from adult P100 mice, compared to one of the canonical microglial markers *Cx3Cr1* (Figure 4-1). However, a recent report suggested that DDAH2 protein expression was lacking in microglia in adult mice (Kozlova et al., 2021).

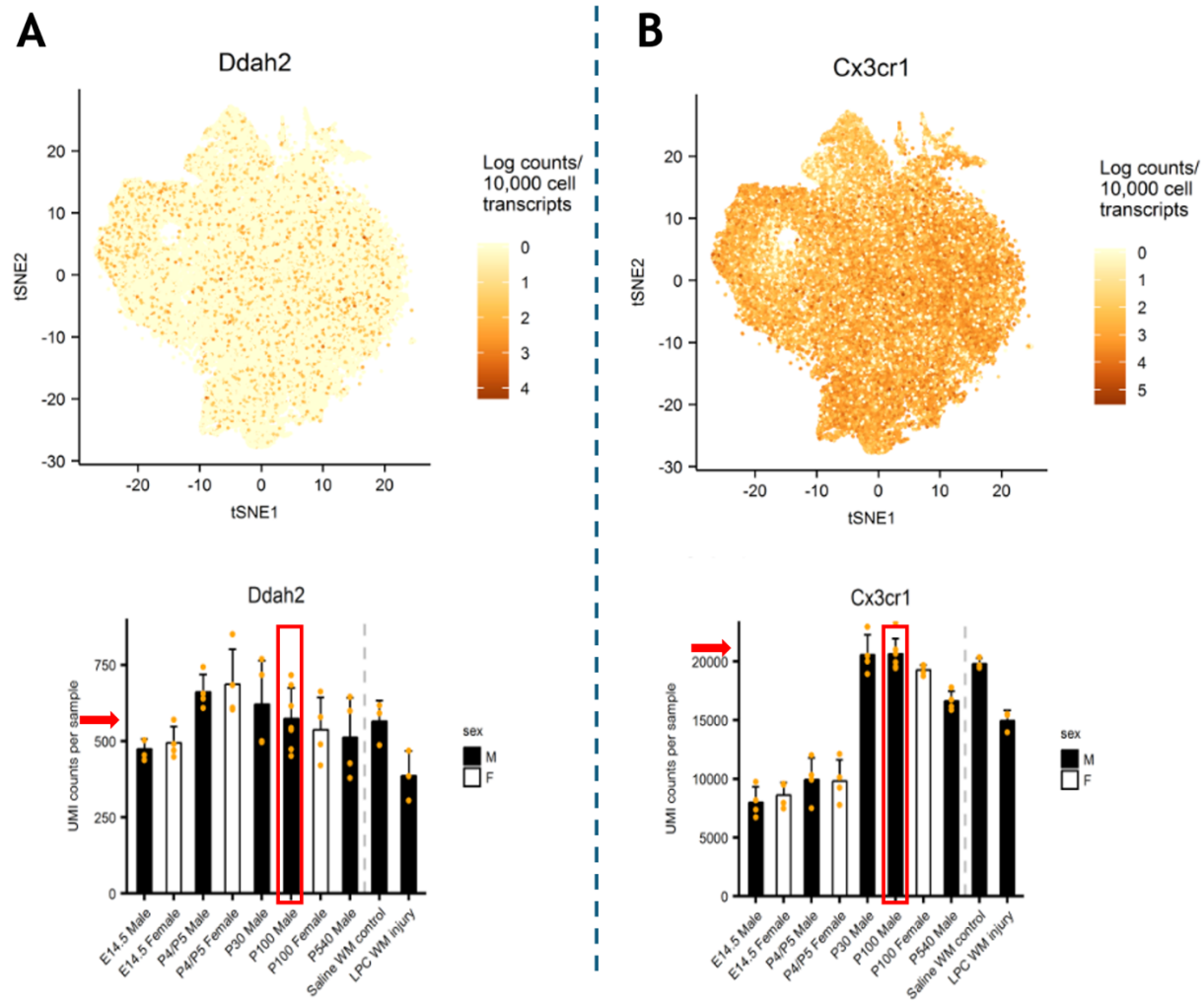

Figure 4-1. Comparison between the expression levels of *Ddah2* and *Cx3cr1* in microglia. A) (top) tSNE plot showing Ddah2 expression is sparse and does not show sub clustering patterns within microglia; (bottom) Ddah2 expression in adult (P100) male mice in unique molecular identifier (UMI) counts. B) (top) tSNE plot showing *Cx3cr1* expression is dense and ubiquitous; (bottom) *Cx3cr1* expression in adult (P100) male mice is around 20,000 UMI. Figure created from an RNA sequencing data set (Hammond et al., 2019) available at https://microgliasinglecell.com

4.1.1 Chapter hypothesis and aims

It was hypothesised that ischaemia upregulates the expression of DDAH2 in macrophages and that lack of DDAH2 in macrophages leads to altered macrophage function.

The first aim was to isolate primary brain macrophages and to validate deletion of DDAH2 in macrophages and microglia.

The second aim of this study was to determine *Ddah2* mRNA expression in hypoxic conditions in macrophages *in vitro* and to investigate the effect of cerebral ischaemia-reperfusion on protein expression of DDAH2 in single hemispheres.

The third aim was to investigate the effect of DDAH2 deletion on the expression of key pro- and anti-inflammatory genes in macrophages as a proxy for macrophage phenotype.

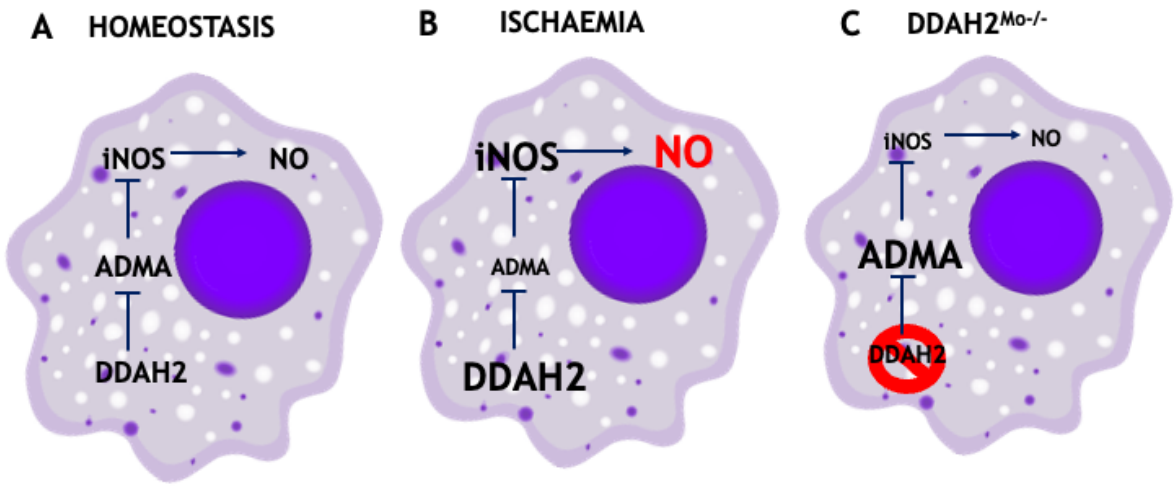

Figure 4-2. The putative mechanism by which DDAH2-ADMA-iNOS pathway controls macrophage phenotype in ischaemia. A) Under homeostatic conditions NO production in monocytes and macrophages is regulated by asymmetric dimethylarginine (ADMA), whose levels are in turn enzymatically controlled by DDAH2. B) During ischaemia, nitric oxide is produced in excess by iNOS, and DDAH2 modulation may be involved in the preservation of this signalling. C) In deleting DDAH2 it was hypothesised that monocyte/macrophage levels of ADMA can be augmented, suppressing the activity of iNOS and reducing NO over-production. Figure created on BioRender.

4.2 Methods

4.2.1 Animals

In this chapter a total of 40 male C57BL6/J mice underwent transient middle cerebral artery occlusion (tMCAo) for Western blot (WB) analyses - 16 mice (8 stroke, 8 sham) for 24 hours and 20 mice (10 stroke, 10 sham) for 72 hours. Twelve male C57BL6/J mice were used for peritoneal macrophage harvest and qRT-PCR optimisation. Ten male C57BL6/J mice were used for monocyte, macrophage, and microglia isolations. Eight female monocyte/macrophage specific ($DDAH2^{Mo-/-}$) mice and 8 female littermate control mice ($DDAH2^{fl/fl}$) were used for monocyte, macrophage, and microglia isolations. Eight male monocyte/macrophage specific

(DDAH2$^{Mo-/-}$) mice and 8 male littermate control mice (DDAH2$^{fl/fl}$) were used for peritoneal macrophage harvest and qRT-PCR analyses. All mice were 8 - 16 weeks of age, and weighed 23 ± 3g. DDAH2$^{Mo-/-}$ and DDAH2$^{fl/fl}$ mice were generated as described in section 1.1.3 in General Methods and breeding pairs were obtained from Professor James Leiper and Dr Laura Dowsett's group.

4.2.2 Animal sacrifice and tissue collection

For peritoneal macrophages harvest and for the stroke and sham mice, animals were sacrificed by a rising concentration of CO_2 (Schedule 1 of the Act) followed by decapitation. For flow cytometric analyses mice were transcardially perfused with 0.9% saline under terminal anaesthesia with 5% isoflurane, brains were harvested and placed in ice cold PBS and the tissue was immediately used.

4.2.3 tMCAo

For protein expression experiments using WB after focal cerebral ischaemia-reperfusion was induced using the intraluminal filament method, as described in General Methodology Section 2.2.1. Briefly, stroke mice and sham matched controls were anaesthetised with isoflurane and a filament was inserted into the internal carotid artery and passed up until it reaches the origin of the middle cerebral artery (MCA) for 60 min. In sham controls all surgical procedures were the same except for the insertion of the filament. For WB analyses brains were harvested at 24 or 72 hours after stroke induction, snap frozen in liquid nitrogen and stored at -80°C until use. The surgeries for these samples had been conducted prior to my research time by Dr Alyson Miller and Dr Arun Flynn.

4.2.4 Dissociation of mouse brains

The cerebral hemispheres from freshly isolated naïve mouse brains (C57BL6/J, DDAH2$^{Mo-/-}$ and DDAH2$^{fl/fl}$) were dissected. Each hemisphere was divided into 3 pieces and incubated in digestion buffer (2 mg/mL collagenase A, 28 U/mL DNase I, Hank's Balanced Salt Solution (HBSS) without calcium/magnesium, 5% FBS,10 µM HEPES (Bordt et al., 2020) and dissociated with mechanical agitation every 10 minutes for 30 minutes at 37 °C on a heat block. Dissociated tissue was then passed through a 70 µm nylon filter and resuspended in HBSS. Cells were then centrifuged for 5 minutes at 300g (4°C). Cell pellets were resuspended in 30%

Percoll, mixed well by pipetting, and overlayed onto 70% Percoll. The cells were centrifuged for 20 minutes at 340 g, with no brake. The myelin sheath disc was aspirated using a vacuum pump, and the cells in the interphase between the 30% and 70% layers were recovered and transferred to a post-Percoll solution (1x HBSS with calcium/magnesium, 5% FBS, 10 µM HEPES). A typical isolation yielded 2 x 10^6 cells/mL as determined by manual counting on a Burker chamber haemocytometer using 0.4% trypan blue solution. To obtain cells for downstream applications such as validation of the monocytes specific DDAH2$^{Mo-/-}$ and expression of key immune cell function genes abrogated in tMCAo, several methods of isolation were employed (Figure 4-3).

4.2.5 Magnetic activated cell sorting (MACS)

Isolation of CD11b$^+$ cells was performed following a recently published methodologies (Bordt et al., 2020)(Schroeter et al., 2021) using a digestive buffer different from that used in Chapter 3.

4.2.5.1 Plate based MACS isolation

MACS was employed to isolate CD11b$^+$ cells in cell suspensions from naïve C57BL6/J mouse brains. Cell suspensions obtained by dissociation of brain hemispheres (section 4.2.4) were counted and a typical isolation yielded 500,000 cells/hemisphere as determined by manual counting on a Burker chamber haemocytometer. Cells were seeded at 5000 cells/mL into round-bottom 96-well plates (Corning, 10520832) placed on a magnetic plate (18102 EasySep Magnet, Stemcell Technologies). A Selection Cocktail (1:1 Component A: Component B) was prepared at 35 µL of cocktail per 1 mL of sample (18970 EasySep Mouse CD11b Pos Slctn Kit II, Stemcell Technologies), incubated for 5 minutes at RT, added to the cells, mixed thoroughly, and incubated for 5 minutes at RT. The cells were then incubated with 80 µL/mL RapidSpheres magnetic beads for positive selection for CD11b$^+$ cells for 5 minutes at RT. Cell suspensions were topped up to 250 µL with MACS buffer consisting of PBS, pH 7.4; 1 mM ethylenediaminetetraacetic acid (EDTA), and 1% BSA, mixed by pipetting and incubated on the magnetic plate for 5 minutes at RT to allow magnetic separation. The supernatant was aspirated, fresh buffer was supplied, and the plate was removed from the magnet. The isolation step was repeated 3 times, and the isolated cells were resuspended in

500 µL of flow cytometry buffer containing 0.5% BSA + 0.4 % sodium azide in PBS. The cells were stained with antibodies against CD11b and the pan-leukocytic marker CD45, which are expressed by myeloid cells and microglia. The stained cells were analysed by immunophenotyping using flow cytometry, to determine if the isolation contained a relatively similar population of $CD45^{+}CD11b^{+}$ microglia and myeloid cells as obtained in Chapter 3.

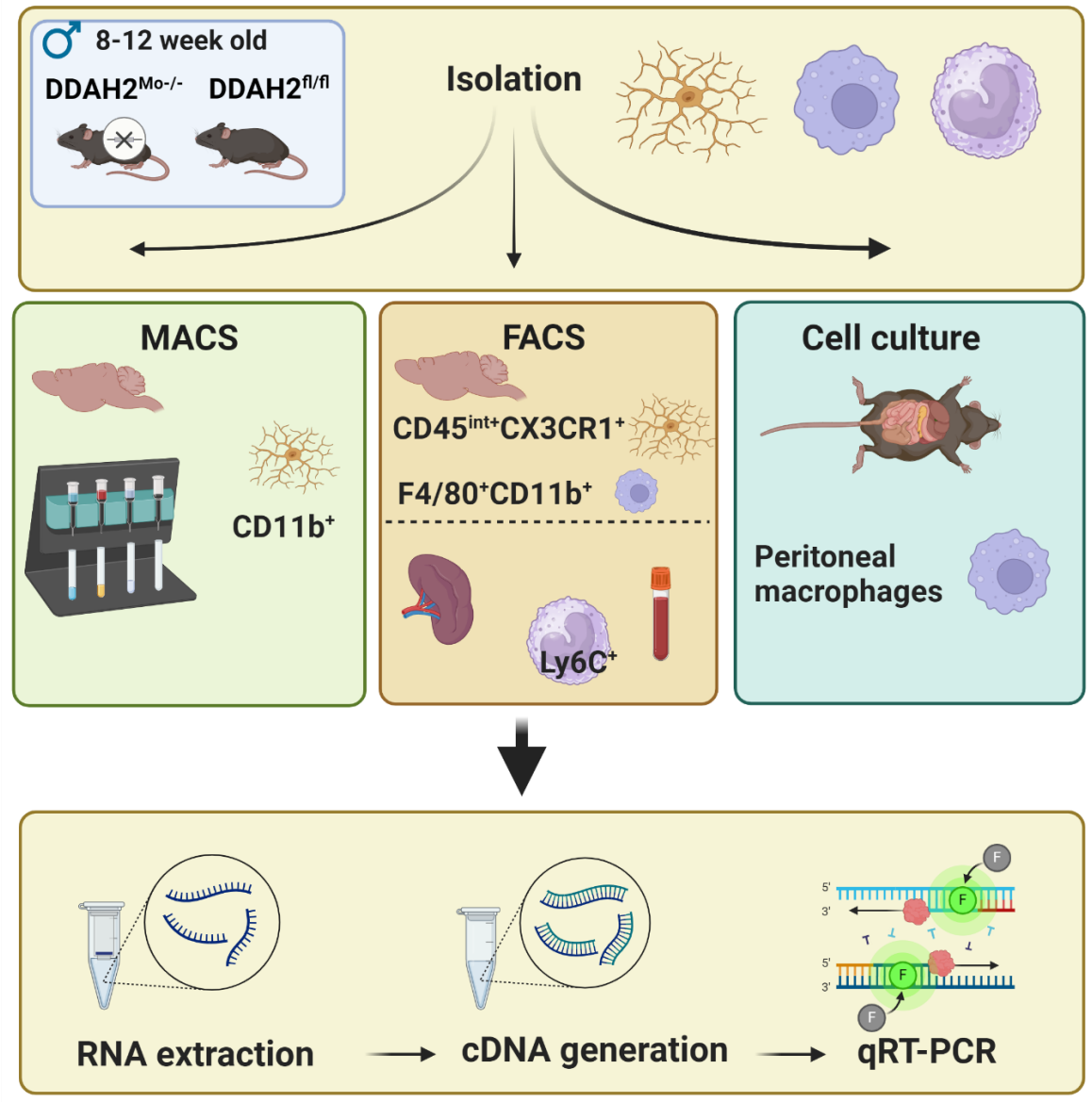

Figure 4-3. Flow diagram of the cell isolation experimental approach. This was used to obtain microglia, macrophages, and monocytes for downstream applications such as validating the monocytes/macrophage-specific knockout $DDAH2^{Mo-/-}$ and differential expression of genes important for macrophage function in homeostatic and ischaemia-reperfusion conditions.

4.2.5.2 Column based MACS isolation

Another MACS approach was also employed to isolate CD11b$^+$ cells. Single cells obtained by dissociation described in Section 4.2.4 were centrifuged for 5 minutes at 300 g, 4°C and pellets re-suspended in 90 µL MACS buffer consisting of PBS, pH 7.4; 1 mM EDTA, and 1% BSA. The cell suspension was then incubated with magnetic microbeads (10 µL/sample), which positively select for CD11b$^+$ cells (Miltenyi Biotec,130-093-634) for 15 minutes, washed with 1 mL of MACS buffer, centrifuged for 5 minutes at 300g (4°C). Magnetic columns (MACS Separation Columns (LS): Miltenyi 130-042-401) were prewashed with 3 mL of MACS buffer, covered with 70 µm filters pre-wetted with HBSS and fitted into a QuadroMACS Separator (Miltenyi 130-090-976) magnetically secured onto a MACS MultiStand (Miltenyi 130-042-303). Cells were then resuspended in 500 µL of MACS buffer and transferred to the columns. The columns were washed 3 times with MACS buffer and CD11b$^-$ cells (negative control) were collected in Falcon tubes. The columns were removed from the magnet, and cells plunged out of the column and eluted in 10 ml of MACS buffer.

4.2.6 Verification of the identity of MACS isolated cells using flow cytometry

To verify the identity and determine the purity of the MACS isolated cells, immunophenotyping was performed by flow cytometry on BD FACS Canto II coupled with BD FACS Diva software as described in Section 1.4.6 in General Methodology. To determine if the MACS isolated cells contained microglia, cells were assessed for intermediate expression levels of CD45 and for expression of CD11b, which should be positively selected by MACS. In view of characterising the identity of these cells after tMCAo, as well as in the naïve mouse brain, cells were also analysed for expression of the fractalkine receptor CX3CR1 on microglia, which assists in phagocytosis of neurons expressing CX3CL1 (fractalkine) (Harrison et al., 1998, Fuhrmann et al., 2010, Olveda et al., 2024). CX3CR1 is upregulated in response to cerebral ischaemia and reperfusion (Tarozzo et al., 2002), as well as in acute and chronic inflammation in the rodent CNS (Hughes et al., 2002). The identity of the isolated cells was determined as CD45^{int+}CD11b$^+$CX3CR1$^+$. The CD11b positive and negative samples were centrifuged for 5 minutes at 300g, 4°C, and stained with a mixture of antibodies CD45-PE, CD11b-APC/Cy7, and CX3CR1-

FITC, as detailed in Table 4-1. The cell suspensions were incubated for 25 minutes at 4°C in the dark, washed in MACS buffer, centrifuged for 5 minutes at 300 g, 4°C, and resuspended in 50 µL MACS buffer.

Table 4-1. Antibodies for immunophenotyping myeloid cells and microglia with flow cytometry and fluorescence activated cell sorting (FACS).

ANTIGEN	FLUOROPHORE	HOST ISOTYPE	CLONE	CONCENTRATION (µG/ML)
CD45	PE	Rat Ig2b, κ	30-F11	0.5
CD11B	APC/Cy7	Rat Ig2b, κ	M1/70	1
CX3CR1	FITC	Mouse IgG2a, κ	SA011F11	1.25
LY-6C	BV785	Rat IgG2c, κ	HK1.4	1
F4/80	PE-Cy7	Rat IgG2a, κ	BM8	2

4.2.7 Fluorescence activated cell sorting (FACS)

4.2.7.1 Microglia and cerebral macrophages

Microglia ($CD45^{int+}CD11b^{+}CX3CR1^{+}$) and cerebral macrophages ($CD45^{hi+}CD11b^{+}F4/80^{+}$) were isolated from freshly harvested brains from $DDAH2^{Mo\,-\,/\,-}$ and $DDAH2^{fl/fl}$ mice by staining with antibodies listed in Table 4-1. FACS was performed on BD FACS Aria IIu or FACS Aria III with a laser, filter and mirror configuration described in Table 4-2. Sorting gates were established on FACSDiva v9.0.1 software and the sort was conducted with 130 µm nozzle size and sheath pressure 10 psi. The numbers of cell populations sorted were recorded and data analysis was performed using FlowJo v10 10.8.1 (FlowJo, LLC, Ashland OR). Sorted cells were collected in RNAse inhibitor containing FACS buffer and stored in - 80 ºC until use.

Table 4-2. FACS ARIA IIu base configuration for sorting.

ANTIGEN	FLUOROPHORE	LASER	FILTER	MIRROR
LY-6C	BV785	Violet Octagon 405	780/60	750LP
CX3CR1	FITC	Blue Trigon 488	530/30	502LP
VIABILITY	PerCP-Cy5.5	Blue Trigon 488	695/40	655LP
CD45	PE	Yellow Green Octagon 561	585/15	None
F4/80	PE-Cy7	Yellow Green Octagon 561	780/60	735LP
CD11B	APC-Cy7	Red Trigon 640	780/60	755LP

4.2.7.2 Peripheral monocytes

Peripheral monocytes (Ly-6C$^+$) were isolated from blood and spleen from DDAH2$^{Mo-/-}$ and DDAH2$^{fl/fl}$ mice by staining with an antibody against Ly-6C (Table 4-1). Blood was obtained by cardiac puncture during terminal anaesthesia with 5% isoflurane. Spleens harvested from the same animals and cells were dissociated by sequentially passing the tissue through a 70 µm and 40 µm filter, followed by washing in PBS and centrifuging for 5 minutes at 500 g (4°C).

4.2.8 RNA extraction

RNA was extracted from RAW264.7 macrophages, primary peritoneal macrophages, peripheral and cerebral monocytes, macrophages, and microglia isolated using MACS or FACS using phenol-free based methods. Peritoneal macrophages and RAW264.7 cells were lysed and homogenised with RNA lysis buffer on ice. The lysis buffer contains guanidine thiocyanate, a salt capable of protecting RNA from endogenous RNases. The lysate is then mixed with ethanol and loaded on a purification column. Guanidine thiocyanate and ethanol cause RNA to bind to the silica membrane while the lysate is spun through the column. Afterwards, washing the column with wash buffers removes impurities from the membrane. Pure RNA was then eluted under low ionic strength conditions with 20-50 µl of nuclease-free water. RNA concentration and purity were determined using NanoDrop ND-3300 Fluorospectrometer (Thermo Fisher). Lysates from RAW264.7 macrophages, primary peritoneal macrophages, and MACS isolated macrophages and microglia were processed with the RNEasy Mini kit (Qiagen; 74104). Lysates obtained from FACS isolated macrophages, microglia and monocytes were processed with the RNEasy Micro kit (Qiagen; 74004) or the GeneJET RNA Purification kit (Thermo Fisher; K0731). For the latter, the lysis buffer was supplemented with 14.3 M ß-mercaptoethanol and Proteinase K solution diluted 60x with TE buffer (10 mM Tris HCl, pH 8.0, 1 mM EDTA). All RNA samples were placed on ice immediately for subsequent use or stored at -80 °C until further use.

4.2.9 Reverse transcription (RT)

RNA was converted by a reverse transcriptase to complementary DNA (cDNA) templates in two steps using reagents from a QuantiTect kit (Qiagen; 205311). First, to digest genomic DNA (gDNA) 2 µl of a gDNA wipeout buffer containing

DNase I was added to 12 µl undiluted RNA, samples were incubated at 42 °C for 2 minutes and placed immediately on ice. Second, a master mix (1 µl of reverse transcriptase, 1 µl reverse transcriptase primer mix and 4 µl RT buffer) was added and mixed in, followed by an incubation at 42 °C for 15 minutes for primer annealing and an incubation at 95 °C for 3 minutes for enzyme inactivation.

For samples obtained from isolation by FACS the RNA quantity and purity were lower, so these samples were reverse transcribed to cDNA using a different kit (Invitrogen™ SuperScript™ IV Reverse Transcriptase, Thermo Fisher; 11756050), with higher sensitivity for degraded or unpurified RNA samples. To digest gDNA, 1 µl ezDNAse enzyme and 1 µl of 10X ezDNAse buffer were added to 8 µl undiluted RNA, mixed and incubated at 37 °C for 2 minutes and placed immediately on ice. Superscript IV VILO Master Mix or Superscript IV VILO No Reverse Transcriptase control (4 µl) was diluted in 6 µl nuclease free water (NFW) and added to the samples. The samples were mixed and incubated in a PCRMAx Alpha Cycler 4 (PCRmax) at 25 °C for 10 minutes to anneal primers, followed by 50 °C for 10 minutes to reverse transcribe RNA and 85 °C for 5 minutes to inactivate the enzyme. All cDNA samples were placed on ice immediately for subsequent use or stored at -20 °C until further use.

4.2.10 Real-time quantitative polymerase chain reaction (RT-qPCR)

Real-time quantitative PCR (RT-qPCR) was performed on cDNA samples for expression of total mRNA using SYBR Green, which is a fluorescent dye that binds to double-stranded DNA (dsDNA). When bound to dsDNA, the dye fluoresces brightly, whereas it has low fluorescence in the presence of single-stranded DNA or in the absence of DNA. PCR amplification leads to increasing amount of dsDNA, which enables more SYBR Green dye to bind, leading to an increase in fluorescence. The fluorescence intensity is measured at the end of each PCR cycle, allowing for the quantification of DNA. The RT-qPCR reaction contained 5 µl SYBR Green (Fast SYBR™ Green Master Mix (Applied Biosystems™, 4385612) or QuantiNova™ SYBR Green RT-PCR Kit (Qiagen, 1076717), 0.5 µl of 10 µM forward primer, 0.5 µl of 10 µM reverse primer (listed in Table 4-3), 2.5 µl NFW and 1.5 µl cDNA (≤5 ng/µl). For the relative quantification of the *Ddah2* transcript, the primer sequence was specific for the portion of the gene between exon 2 and exon

3, which are excised in the monocytes Ddah2 null mice. The qRT-PCR running parameters are described in Table 4-4 and the reaction ran for 40 cycles on a QuantStudio 12K Flex Real-Time PCR System and QuantStudio® 12K Flex Software v1.3. Expression was normalised to the housekeeping gene *R18s or Rpl13*, and quantified using the comparative ΔΔCt method using the following formula: $2^{-\Delta\Delta Ct}$, where Ct is the cycle threshold, ΔCt = Ct (gene of interest) – Ct (housekeeping gene), ΔΔCt = ΔCt (experimental sample) – average ΔCt (control sample) (Schmittgen and Livak, 2008). Relative quantification for each gene of interest was expressed as $2^{-\Delta\Delta Ct}$ values, which are presented as relative to the relevant control sample's average $2^{-\Delta\Delta Ct}$ value.

Table 4-3. Primers used for investigating pro- and anti-inflammatory genes in $DDAH2^{Mo-/-}$ and $DDAH2^{fl/fl}$ mice using RT-qPCR.

GENE SYMBOL	GENE NAME	SEQUENCES
Ddah2	Dimethylarginine dimethylaminohydrolase 2	F- AAGGAGACACGGCCCTAATC; R - GGTGAAGAGGACGTCGGTG
R18s	Ribosomal subunit 18	F - GCTCAGCGTGTGTGCCTACC R - GGCCTCACTAAACCATCCAA
Rpl13	Ribosomal protein L13	F – CTCATCCTGTTCCCCAGGAA; R - TGGGTGGCCAGCTTAAGTTC
Arg1	Arginase 1	F – GGGACCTGGCCTTTGTTGAT; R - TGTCAGTGTGAGCATCCACC
Tgf-β	Transforming growth factor beta	F – CTGCTGACCCCACTGATAC; R - AGCCCTGTATTCCGTCTCCT
Il-6	Interleukin 6	F – CCGGAGAGGAGACTTCACAG; R - TTCTGCAAGTGCATCATCGT
Ccl2	Chemokine (C-C motif) ligand 2	F – CCTGCTGCTACTCATTCACCA; R - ATTCCTTCTTGGGGTCAGCA
Tnf-α	Tumour necrosis factor alpha	F – CTGAGGGGGCTGAGCTCAAAC; R - GGTCTACTTTGGAGTCATTGC
Il-1β	Interleukin 1 beta	F – GCTGCTTCCAAACCTTTGAC; R - TGTCCTCATCCTGGAAGGTC

Table 4-4. Quantitative RT-PCR running parameters on QuantStudio 12K.

STAGES	HOLD STAGE	PCR STAGE		MELT CURVE STAGE		
STEPS		Step 1	Step 2	Step 1	Step 2	Step 3
TEMPERATURE	95°C	95°C	60°C	95°C	60°C	95°C
DURATION	10 min	15 sec	1 min	15 sec	1 min	15 sec

4.2.11 Oxygen-glucose deprivation of immortalised mouse macrophages

Immortalised mouse macrophages (RAW264.7 cells, p=56+3) were cultured in Dulbecco's Modified Eagle Medium (DMEM) supplemented with 10% FBS and 1% penicillin-streptomycin in T75 flasks (Corning) maintained at 37 ± 0.5 °C in a humidified 5% CO_2 atmosphere by changing media every 48 hours until reaching 75% confluency. To passage, cells were washed with D-PBS with calcium and magnesium, fresh media was added to the flask and cells were lifted off with a cell scraper.

To mimic ischaemia-like conditions *in vitro*, cells were seeded at 500,000 in T75 flasks and allowed to adhere and grow for 24 hours. Once the cells reached 75% confluency, they were washed twice with D-PBS with calcium and magnesium, and media was replaced with oxygen glucose deprivation (OGD) media, which was composed of FBS-free and glucose-free DMEM. Flasks were then transferred to a humidified hypoxic chamber pre-equilibrated with an OGD gas mixture maintained by a digital oxygen controller (95% N_2, 5% CO_2, 0.2-0.5% O_2, 37 ± 0.5 °C; Biospherix, US) for 24 hours. For each OGD experiment, time-controlled normoxic controls were incubated in the same tissue culture incubator in serum-free but glucose containing DMEM media (5% CO_2, 0.2-0.5% O_2, 37 ± 0.5 °C). After 24 hours, the cells were washed twice with D-PBS and lysed on ice by scraping in RLT lysis buffer (Qiagen, UK). Samples were centrifuged for 20 min at +4°C and stored at -20°C until use.

4.2.12 Protein extraction from mouse brain tissue

Mouse tissues (brain or kidney) were lysed in 1.5X Laemmli buffer (7.5% Glycerol, 3.75% 2-Mercaptoethanol, 0.225% SDS, 75 mM Tris HCl, 0.003% Bromophenol Blue) with metal lysis beads for 2700 shakes in MM300 Retsch TissueLyser (Qiagen, UK). To separate fractions of protein and cellular debris lysates were centrifuged at 13,000 g for 30 minutes. The upper phase of the supernatant (protein) was collected and divided into aliquots. Protein concentration was determined using the RC DC™ protein quantification kit (Bio-Rad Laboratories Ltd, UK) following the manufacturer's instructions. Lysate stocks were diluted to 20, 40, or 60 µg working stocks in 1.5X Laemmli buffer for Western blotting. Stocks and working samples

were stored at -80°C. Brain tissue harvesting and protein extraction had been conducted by Dr Arun Flynn.

4.2.13 Western blotting

4.2.13.1 Acrylamide gels preparation

To investigate the protein levels of the DDAH2 enzyme after stroke Western blotting was performed using protein lysates from mouse hemispheres which had undergone 65 min MCAO and sham matched controls and sacrificed at 24- or 72-hours post-stroke. Glass plates were assembled with spacers, ensuring proper alignment. The 12.5% resolving gel containing 3M Tris base (Roche, 10708976001), Acrylamide/Bis-acrylamide 29:1 (Sigma, A7802), sodium dodecyl sulfate (SDS, Sigma, L3771, 1%), ammonium persulfate (APS, 0.5%, Sigma, A3678-25g), N,N,N',N'-Tetramethyl ethylenediamine (Temed, 0.05%), in distilled water, pH 8.85, was vortexed and poured into the gel cassette and allowed to polymerise. Subsequently, the 4% stacking gel containing 0.5M Tris base (Roche, 10708976001), Acrylamide/Bis-acrylamide 29:1 (Sigma, A7802), SDS (Sigma, L3771, 1%), APS (0.5%), Temed (Millipore, 110732, 0.1%), in distilled water, pH 6.8) was poured on top and a 10-well comb (1.5mm, BioRad, 165-3365) was inserted. The freshly prepared APS solution (10% in distilled water) and Temed solution (Millipore, 110732, 0.1%) were added just prior to pouring the gel to avoid premature polymerisation.

4.2.13.2 SDS-PAGE (sodium dodecyl sulfate-polyacrylamide gel electrophoresis)

Gel cassettes were placed into an electrophoresis tank (Mini-PROTEAN Tetra Cell for hand-cast gels, Bio-Rad, 1658001) and connected to a PowerPac Basic Power Supply, Bio-Rad, 1645050). Working stock protein lysates were denatured at 95 °C for 2 min and equal amount of lysate (20 µg) was loaded into the cassette wells. A molecular weight marker Precision Plus Dual Colour Protein Standard (Bio-Rad, 161-0374) was loaded in the first well of each gel. Electrophoresis was conducted at 60-120 volt at RT until the dye front reached the bottom of the gel. Protein samples were separated by SDS-PAGE at RT at 60 V to initially stack proteins for 20-minutes, followed by 120 V to resolve proteins for 1.5 hour.

4.2.13.3 Semi-dry transfer

Following electrophoresis, gels were immediately soaked in transfer buffer (0.025 M Tris-Base, 20% methanol, in distilled water, pH 10.4). Polyvinylidene fluoride (PVDF) membranes (Immobilon-P, Millipore, IPVH00010) were then pre-cut to gel size and activated in 100% methanol for 5 min. A sandwich assembly (Figure 4-4) comprised of two pieces of blotting paper (Whatman, 580 mm^2, Millipore, GB005) soaked in a discontinuous transfer system using 3 different buffers with differing concentrations of Tris-Base, pH and presence of ß-Alanine. These were layered on the transfer cell in the following order: transfer buffer 1 (0.3 M Tris-Base, 20% methanol, in distilled water, pH 10.4), a blotting paper, a membrane, and a gel soaked in transfer buffer 2 (0.025 M Tris-Base, 20% methanol, in distilled water, pH 10.4), topped with a couple of blotting papers soaked in transfer buffer 3 (0.038M Tris-Base, 0.01M ß-Alanine, 20% methanol, in distilled water, pH 9.4). Proteins were transferred to PVDF membranes by semi-dry electroblotting at 15 V for 1 hour at RT on Trans-Blot SD Semi-Dry Electrophoretic Transfer Cell, Bio-Rad, 1703940.

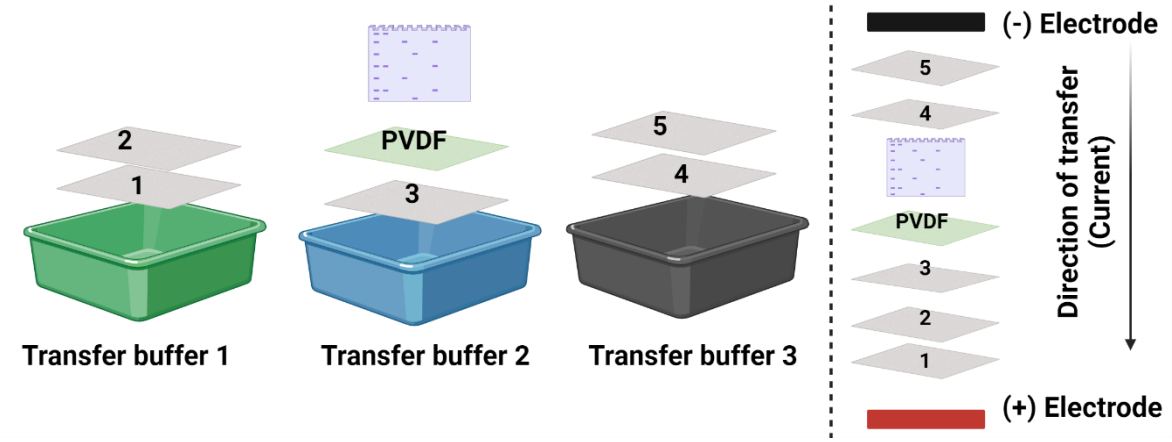

Figure 4-4. Semi-dry transfer setup using transfer buffers with different salt compositions. The assembly order and the direction of protein transfer is illustrated on the right. Figure created on Biorender.

4.2.13.4 Blocking & antibody incubating

Membranes were blocked in 5% Skim Milk Powder (Bio-Rad 1706404) made up in Tris Buffered Saline (TBS) for 30 min at RT followed by incubation with a rabbit anti-DDAH2 primary antibody (1:500, EPR15508(B), Abcam, ab184166) at 4 °C in the dark overnight. Membranes were washed (3 x 5 minutes) in TBS to remove unbound antibodies. The membranes were then incubated with a IRDye 800CW donkey anti-rabbit IgG secondary antibody (1:10000, 926-32213, LiCor) for 1.5

hours at RT. The membranes were visualised on Odyssey® DLx imaging system (Licor). To detect β-tubulin expression as a loading control, membranes were then incubated with a rabbit anti-β tubulin antibody (1:500, Abcam, ab6046), washed and incubated with IRDye 800CW donkey anti-rabbit IgG secondary antibody (1:10000, 926-32213, LiCor) and imaged as above.

4.2.13.5 Image analysis and quantification

Protein bands for DDAH2 were detected at 30 kDa and for ß-tubulin at 50 kDa. The relative intensity of the protein of interest was determined using the rectangular tool of Image Studio Lite software (Odyssey, Licor) and presented as normalised to housekeeper (ß-tubulin). Relative intensities for ischaemic and non-ischaemic hemispheres were then normalised to intensities from sham hemispheres.

4.2.14 Isolation of peritoneal macrophages

Peritoneal macrophages from DDAH2$^{Mo-/-}$ and DDAH2$^{fl/fl}$ male mice were isolated from peritoneal exudates. Mice were culled by a rising concentration of CO_2 and then laid supine onto a dissection board and the skin was wiped with chlorhexidine. A small incision was made in the posterior section of the abdomen to expose the peritoneal wall, which was gently lifted with sterile forceps. A 25-gauge needle was then inserted through the wall into the peritoneal cavity and ice-cold PBS (supplemented with 3% FBS) was injected (6-10 ml) avoiding puncture of the abdominal organs. The mouse was gently rocked side to side, the peritoneal exudate fluid was slowly drawn into a syringe and stored in a 50 ml centrifuge tube on ice. Following isolation, the peritoneal exudate cells were spun at 500g, 4 °C for 10 minutes and the pellet was resuspended in cold DMEM (supplemented with 10% FBS and 1% penicillin-streptomycin mix) by gently tapping the bottom of the tube and pipetting up and down. Cells were counted using a haemocytometer, plated at a density of 300,000 - 500,000/well in a 12-well plate containing DMEM, and allowed to adhere for 1 to 3 hours. Non-adherent cells were removed by gently washing three times with warm D-PBS with calcium and magnesium and replaced with fresh DMEM. Adherent cells were further incubated at 37 ± 0.5 °C in a humidified 5% CO_2 atmosphere for 24 hours to allow for transcriptional quiescence prior to mRNA expression analyses, washed twice with D-PBS and lysed in RLT lysis buffer (Qiagen).

4.2.15 Statistics

Quantitative and graphical analysis was performed on GraphPad Prism 8.0 and flow cytometric plots were created using the Layout editor on FlowJo 10.0.

- Ordinary one-way ANOVA (for equal SD) with Sidak's multiple comparisons test and Brown-Forsythe and Welch ANOVA (for unequal SD) with Tamhane's T2 multiple comparisons test and were used for comparing DDAH2 protein expression in sham, ipsilateral and contralateral hemispheres.

- Paired t-tests were used for comparisons of *Ddah2* mRNA expression in OGD and normoxic RAW267.4 cells.

- Unpaired t-tests with Welch's correction for unequal SD were used for *Ddah2* and inflammatory markers mRNA expression levels in DDAH2$^{Mo\ /-}$ and DDAH2$^{fl/fl}$ mice using qRT-PCR.

4.3 Results

4.3.1 Genomic DNA analysis for DDAH2$^{Mo-/-}$ mice genotyping

A monocyte/macrophage specific DDAH2 mouse (DDAH2$^{Mo-/-}$) has been generated and validated (Lambden et al., 2015). However, the mouse line has since been re-derived in a new facility, necessitating a confirmation of the genetic manipulation. A mouse homozygous for the DDAH2 floxed allele was crossed with a mouse that harboured the LysM cre promotor, which cuts the floxed genes in monocytes and macrophages as detailed in section 2.1.3 in General Methods. Dual end point PCR analyses were performed to determine the presence of either a DDAH2 heterozygous, a DDAH2 wildtype homozygous, or a DDAH2 'floxed' allele, concomitantly with the presence or absence of a Cre recombinase allele (Figure 4-5A). For experiments, only mice carrying a DDAH2 'floxed' allele were selected and the expression of a Cre recombinase allele determined the full knockout (DDAH2$^{Mo-/-}$, Cre positive) and or 'floxed' control (DDAH2$^{fl/fl}$, Cre negative) (Figure 4-5B).

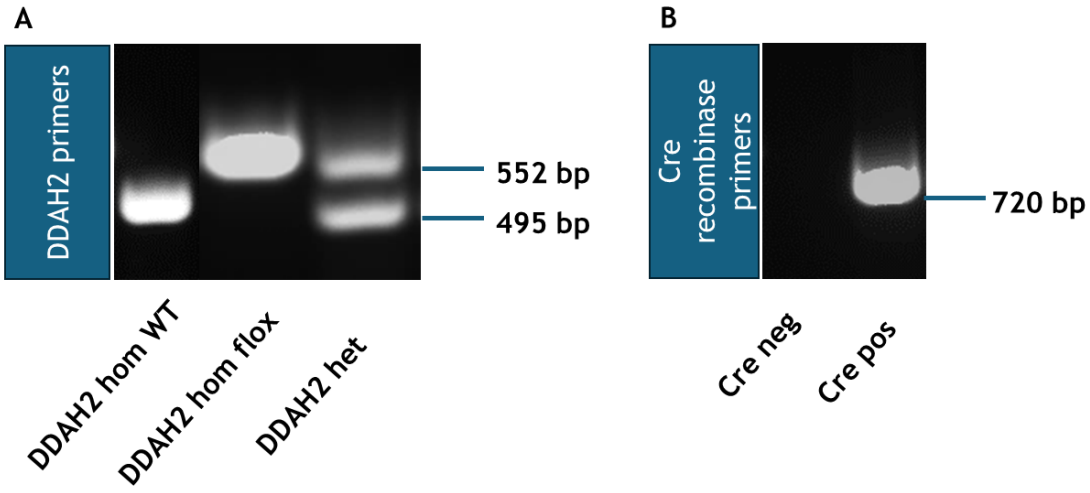

Figure 4-5. Representative genotyping bands obtained from breeding animals. A) Genomic DNA PCR analysis validated expression of homozygous (hom) DDAH2 'floxed' alleles by the appearance of a single band at 552 bp. Homozygous DDAH2 wildtype (wt) alleles appeared at 495 bp. Heterozygous (het) mice carried both the 'floxed' and wt alleles, confirmed by the appearance of two bands at 552 and 495 bp, respectively. B) Genomic DNA PCR demonstrated Cre recombinase expression via the appearance of a single band at 720 bp. The concomitant expression of the DDAH2 'floxed' allele and Cre recombinase (Cre pos) from a single mouse ascertained the DDAH2 knockout.

4.3.2 Isolation of CD11b+ cells

4.3.2.1 Plate based immunomagnetic sorting

Figure 4-6 shows that using a MACS method of isolation >90% of single cells were CD45$^+$ leukocytes, while the detected frequency of CD45$^+$CD11b$^+$ cells was only ~1%. The RNA isolated from the obtained CD45$^+$CD11b$^+$ cells from three separate experiments was <5 ng/ul and no further analyses were conducted using this method.

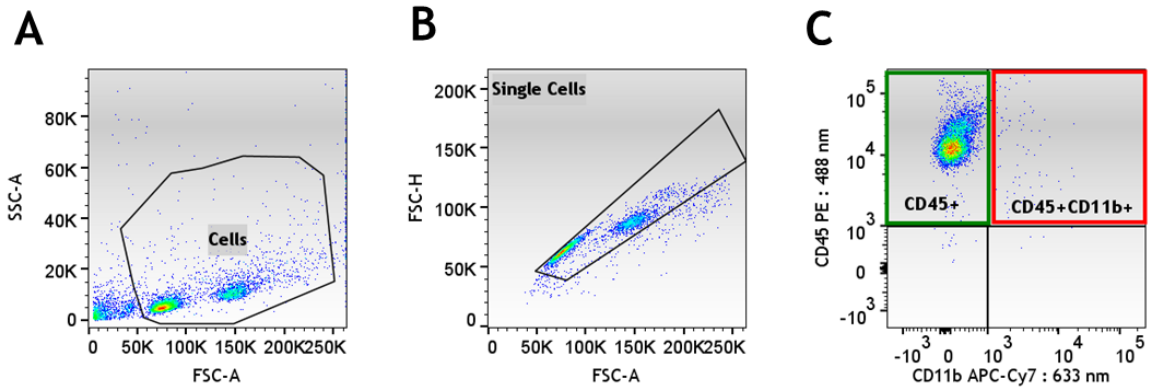

CELLS	SINGLE CELLS	CD45$^+$	CD45$^+$CD11B$^+$
81.3±6.1%	89.7±5.4%	92.3±5.5%	1.2±0.1%

Figure 4-6. Flow cytometric plots of immunomagnetically sorted CD45$^+$CD11b$^+$ cells in a plate-based MACS from WT mice and percentages of cells obtained. A) Cells gated from debris, B) single cells gated from doublets, C) bi-exponential plot showing the observed scatter distribution of CD45$^+$ leukocytes (green) and the absence of double positive CD45$^+$CD11b$^+$ cells (red gate) gated from single cells. Percentage each population provided in the table below. Data presented as mean ± SEM, n=3.

4.3.2.2 Column-based magnetic activated cell sorting

A similar MACS method of cell isolation was next employed. Cells from mouse brain expressing CD11b were positively selected for in a cell suspension using a column-based approach (Bordt et al., 2020, Schroeter et al., 2021). The cells were then stained with anti-CD11b, anti-CD45 and anti-CX3CR1 antibodies, as well as with 7-AAD for viability. Non-MACS isolated cells from naïve C57BL6/J mouse brains were also stained with the same antibodies to demonstrate compatibility of the CD11b antibody with the labelling of the magnetic beads. In control cells 60% of viable cells were positive for CD11b, of which 87% were also positive for CD45, while only 3% of CD45$^+$ cells were double positive for CD45 and CX3CR1 (Figure 4-7 C&D),

indicating that the CX3CR1 antibody was perhaps used at a sub-optimal concentration. However, although there were 85% viable cells upon MACS isolation, 1% were positive for CD11b and 1% were double positive for CD45 and CX3CR1 expression (Figure 4-7). Overall, in a total of 4 experiments, there was a very low frequency of immunomagnetically sorted leukocytes in the column, which was a worse result than that achieved with the plate method.

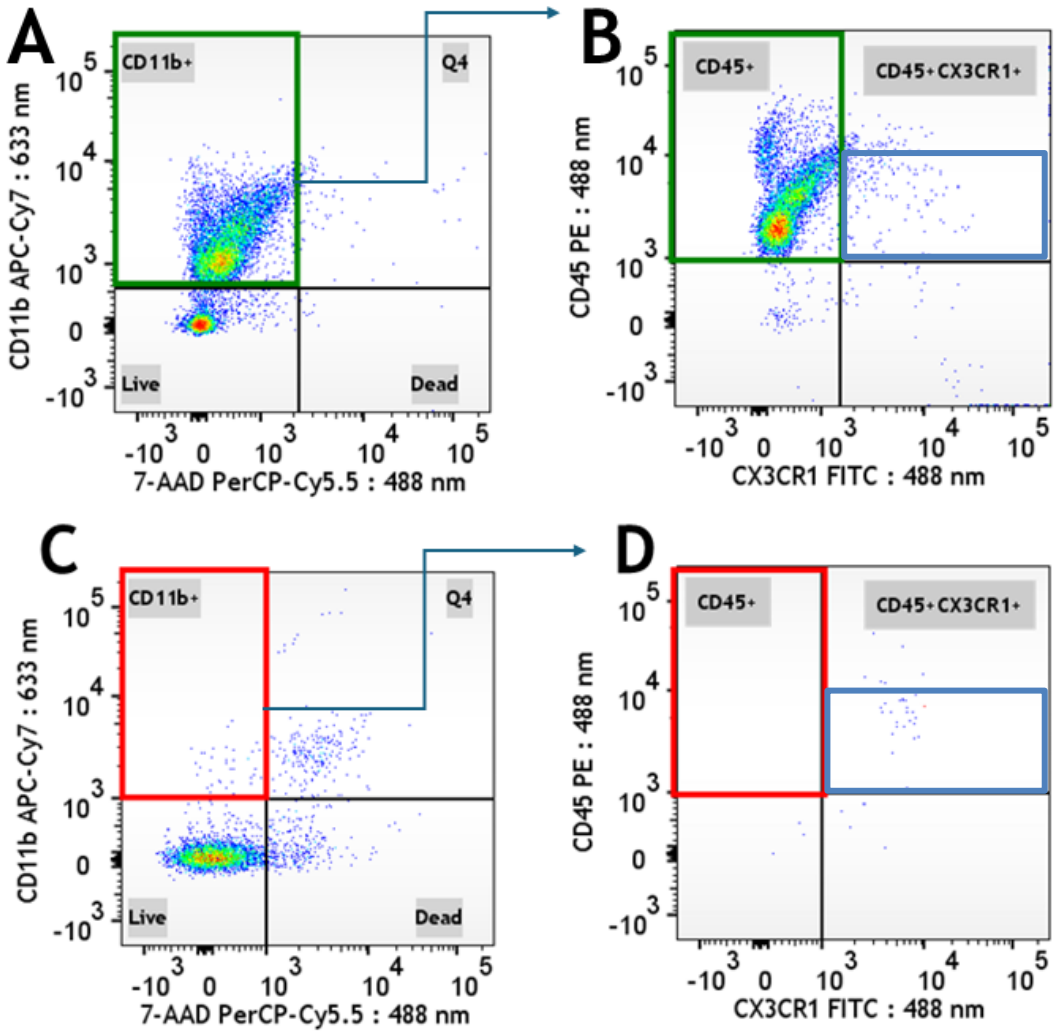

Figure 4-7. Flow cytometric bi-exponential plots of immunomagnetically sorted $CD45^+$ and $CD11b^+$ cells from WT mice in a column-based MACS. Cells were stained for CD11b, CD45, CX3CR1 and 7-AAD for viability. A) Control $CD11b^+$ viable cells were identified and gated further (arrow) in (B) as $CD45^+$ and $CD45^+CX3CR1^+$ cells (blue gate). C) MACS isolated $CD11b^+$ viable cells, which were gated further (arrow) in D) $CD45^+$ and $CD45^+CX3CR1^+$ cells (blue gate). Green rectangles denote the presence of viable leukocytes, while red rectangles demonstrate the absence of these viable leukocytes following MACS.

In summary, two methods of positive selection for $CD11b^+$ cells were investigated: one using a cell culture plate on a rectangular magnet (STEMCell) and another

using a column-based isolation (Miltenyi Biotec). Neither method proved suitable for obtaining a reliable CD11b^{+} cells isolation.

4.3.2.3 FACS for microglia and cerebral macrophages

Following from the unsuccessful isolation of CD11b^{+} cells using MACS, another approach was adopted for the isolation of microglia and brain-derived macrophages. Cerebral macrophages (CD45^{hi+}CD11b^{+}F4/80^{+}) and microglia (CD45^{int+}CX3CR1^{+}) were isolated using FACS from DDAH2$^{fl/fl}$ and DDAH2$^{Mo-/-}$ mice (Figure 4-8).

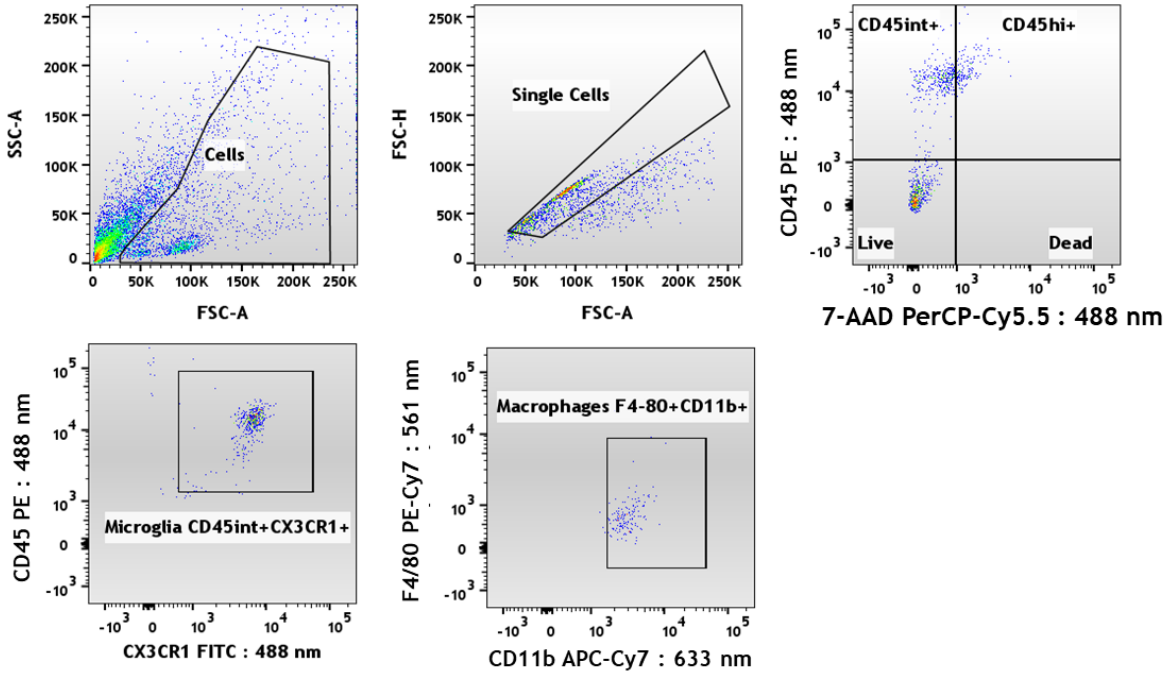

Figure 4-8. Representative plots for microglia and cerebral macrophages FACS isolated from DDAH2$^{fl/fl}$ and DDAH2$^{Mo-/-}$ mice. Cells were gated from debris, single cells were gated away from doublets, quadrangle gates were used for the gating off viable CD45^{int+} cells, which were then subsequently gated for double positive expression of CD45^{int+}CX3CR1^{+} (microglia). CD45^{hi+} cells were further gated for CD11b^{+} F4/80^{+} (macrophages).

Viable cells in the hundreds (macrophages) or thousands (microglia) were obtained using this approach and provided the first opportunity to investigate gene expression in those cells. From a total of 9.5x10^{4} cells isolated by FACS, macrophages (F4/80+CD11b+) were <1% in both genotype groups, while microglia (CD45int+CX3CR1) comprised 84% of all cells in the DDAH2$^{fl/fl}$ mice and 74% in the DDAH2$^{Mo-/-}$ mice. However, there were no significant differences between genotypes in respect to cell number, viability and RNA concentration were comparable (unpaired t test, P>0.05) (Table 4-5).

Table 4-5. Average cell number, viability (%), and RNA concentration (ng/µl) obtained from DDAH2$^{fl/fl}$ and DDAH2$^{Mo-/-}$ mice in fluorescence activated cell sorting (FACS) isolated macrophages (CD45^{+high}CD11b^{+}F4/80^{+}) and microglia (CD45^{+int}CX3CR1^{+}). Data presented as mean ± SEM, n=4.

	Macrophages (CD45^{+high}CD11b^{+}F4/80^{+})			**Microglia (CD45^{+int}CX3CR1^{+})**		
	Cells number	**Viability (%)**	**RNA (ng/µl)**	**Cells number**	**Viability (%)**	**RNA (ng/µl)**
DDAH2$^{fl/fl}$	438±93	90±1	20.5±0.4	$8x10^4$±$5x10^3$	91±2	17.5±0.6
DDAH2$^{Mo-/-}$	643±79	91±2	21.3±0.5	$7x10^4$±$3x10^3$	89±3	16.3±0.3

The DNA contamination check ratio 260/280 equalled 1.61 in RNA isolated from microglia (optimal reference = 2) and the protein contamination ratio 260/230 was 0.5 (optimal reference = 2-2.2). In RNA samples from macrophages 260/280 = 1.52 and 260/230 = 0.52, suggesting sample impurity. The RT-qPCR analysis revealed that for both macrophages and microglia the mean Ct values were above 30 (Table 4-6), suggesting negligible *Ddah2* mRNA expression even in the DDAH2$^{fl/fl}$ mice.

Table 4-6. Mean Ct values for mRNA derived from macrophages and microglia from DDAH2$^{fl/fl}$ and DDAH2$^{Mo-/-}$ mice isolated by FACS. Data presented as mean ± SEM, n=4.

	Macrophages (CD45^{+high}CD11b^{+}F4/80^{+})		**Microglia (CD45^{+int}CX3CR1^{+})**	
	R18S	**DDAH2**	**R18S**	**DDAH2**
DDAH2$^{fl/fl}$	21.57±0.28	35.93±0.25	22.20±0.21	31.82±0.18
DDAH2$^{Mo-/-}$	20.32±0.22	34.47±0.26	21.89±0.21	32.21±0.16

There were no significant differences in relative quantification ($2^{-\Delta\Delta Ct}$) of Ddah2 mRNA between genotypes for either microglia or macrophages (Figure 4-9). Although there was a slight trend for a lower Ddah2 expression in microglia ($P>0.08$), the higher variability in the DDAH2$^{Mo-/-}$ group and the high Ct values for both groups disallow for a conclusive interpretation.

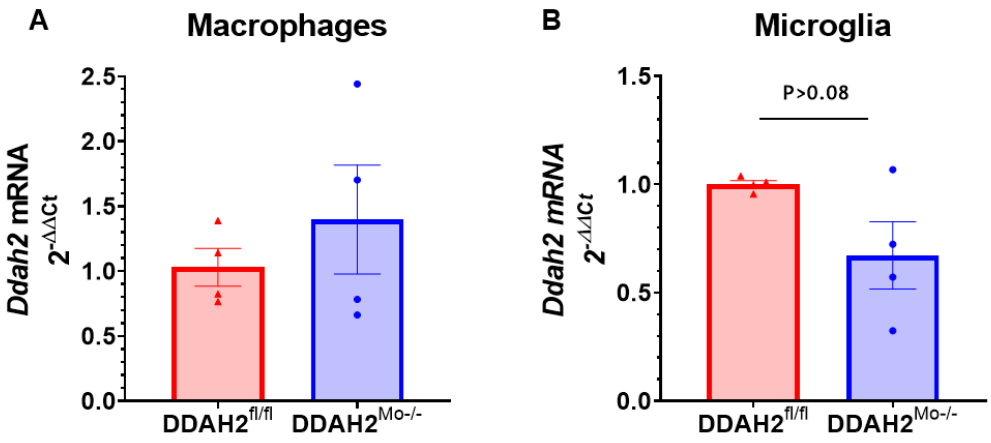

Figure 4-9. Relative quantification ($2^{-\Delta\Delta Ct}$) of *Ddah2* mRNA between DDAH2$^{fl/fl}$ and DDAH2$^{Mo-/-}$ mice in A) macrophages and B) microglia. Data presented as mean ± SEM, n=4, unpaired t test with Welch correction, P>0.05.

4.3.2.4 FACS for peripheral monocytes

The inability to validate *Ddah2* deletion using this method of brain macrophage isolation, raised the possibility that obtaining pure myeloid cells with this method is compromised. It was then decided to pursue isolating monocytes and macrophages from peripheral tissues as an alternative. Viable monocytes from blood and spleen were identified as 7-AAD^{-}Ly6C^{+} cells in DDAH2$^{fl/fl}$ and DDAH2$^{Mo-/-}$ mice (Figure 4-10).

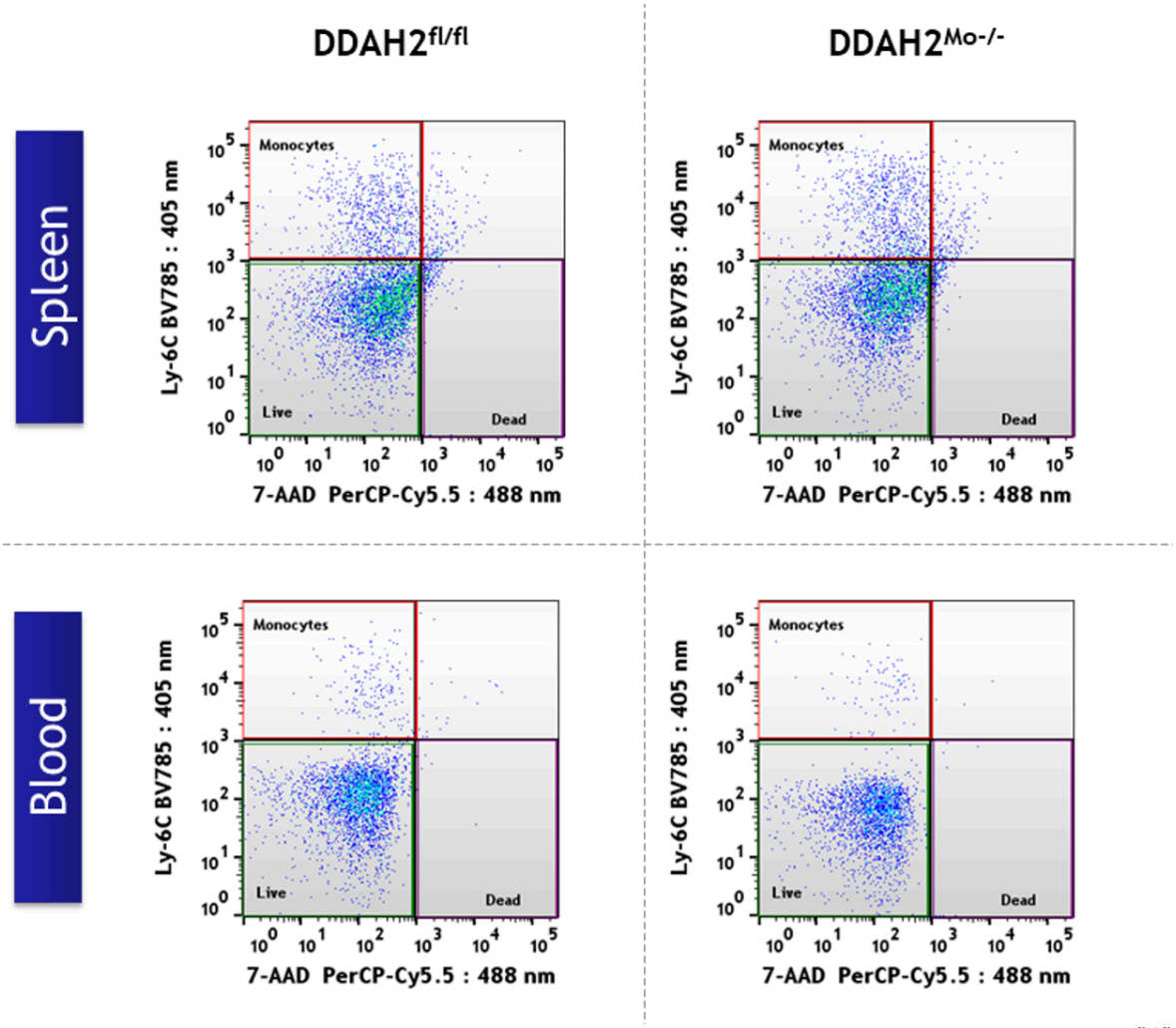

Figure 4-10. Flow cytometric plots of peripheral Ly6C$^+$ monocytes from DDAH2$^{fl/fl}$ and DDAH2$^{Mo-/-}$ mice. Cells were derived from spleen (top panel) or blood (bottom panel).

Cell numbers and viability were comparable between genotypes (Table 4-7). The average number of Ly6C$^+$ monocyte obtained from blood were around 65,000, while the number of splenic monocytes was approximately 2.5-fold higher. The isolations consistently yielded above 85% live cells across genotypes and source of monocytes. However, the RNA yield was consistently low at around 4 ng/µl in monocytes isolated from DDAH2$^{fl/fl}$ and DDAH2$^{Mo-/-}$ mice (Table 4-7).

Table 4-7. Average number of cells, percentage viability, and RNA concentration (ng/µl) from FACS isolated Ly6C$^+$ monocytes obtained from blood or spleen of DDAH2$^{fl/fl}$, and DDAH2$^{Mo-/-}$ mice. Data is presented as mean ± SEM, n=4.

Ly6C+ monocytes	**Blood**			**Spleen**		
	Cells number	**Viability (%)**	**RNA (ng/µl)**	**Cells number**	**Viability (%)**	**RNA (ng/µl)**
DDAH2$^{fl/fl}$	67,810±52	87±1	3.98±0.43	162,50±29	90±2	3.70±0.35
DDAH2$^{Mo-/-}$	60,198±43	85±2	3.87±0.53	175,03±57	87±1	4.83±0.41

Despite the low RNA concentrations gene expression analysis was pursued. The level of *Ddah2* mRNA was determined as negligible in both genotypes, as evidenced by high mean Ct values (>30) (Table 4-8).

Table 4-8. Mean Ct values for mRNA derived from Ly6C$^+$ monocytes obtained from blood or spleen in DDAH2$^{fl/fl}$ and DDAH2$^{Mo-/-}$ mice. Data presented as mean ± SEM, n=4.

Ly6C$^+$ monocytes	**Blood**		**Spleen**	
	R18s	***Ddah2***	***R18s***	***Ddah2***
DDAH2$^{fl/fl}$	21.34±0.21	33.41±0.29	21.14±0.23	32.86±0.22
DDAH2$^{Mo-/-}$	20.92±0.24	33.89±0.25	21.03±0.25	32.43±0.20

4.3.3 Effect of oxygen glucose deprivation on DDAH2 mRNA expression in RAW264 macrophages

To examine the effect of ischaemia on DDAH2 expression in macrophages, a cell line of immortalised macrophages RAW264.7 was subjected to OGD. The housekeeper gene *R18s* was determined to have good stability across samples from both genotypes, with mean Ct value fold change of 0.987 and CV=0.27 (Figure 4-11A). The expression of Ddah2 mRNA was significantly, 2.5-fold higher in the OGD group (Figure 4-11B), indicating that there is an *in vitro* effect of ischaemia on *Ddah2* expression in macrophages.

A

	Ddah2		*R18S*	
	Normoxic	OGD	Normoxic	OGD
Mean Ct	23.43	22.29	11.51	11.66
SEM	0.38	0.12	0.26	0.15

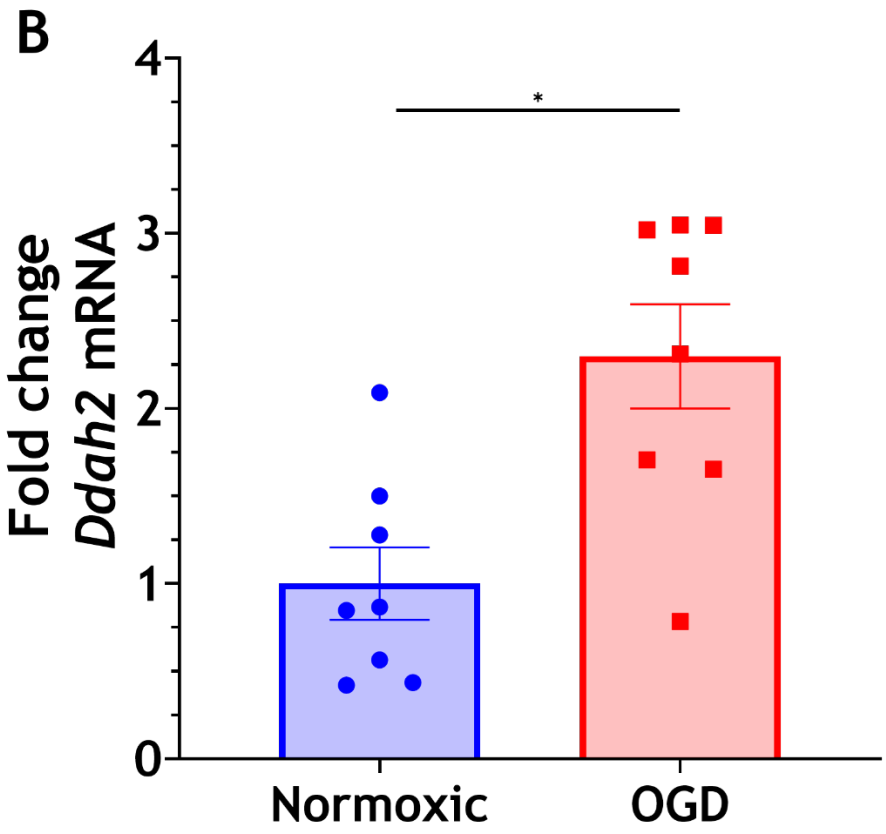

Figure 4-11. Relative quantification ($2^{-\Delta\Delta Ct}$) of *Ddah2* mRNA using qRT-PCR following oxygen-glucose deprivation (OGD) of RAW264.7 macrophages. A) Mean Ct values for *Ddah2* and the housekeeping gene ribosomal 18 subunit (*R18s*). B) Relative quantification ($2^{-\Delta\Delta Ct}$) of mRNA expression levels in normoxic and OGD macrophages. Data presented as mean ± SEM, n=8, paired t-test, *P<0.05.

4.3.4 Effect of cerebral ischaemia-reperfusion on DDAH2 protein expression in C57BL6/J mice post-tMCAo

To characterise the effect of brain ischaemia-reperfusion on the protein level of DDAH2 *in vivo*, lysates from cerebral hemispheres of C57BL6/J mice 24 hours and 72 hours post-tMCAo were probed for DDAH2 expression. At 24 hours post-tMCAo, the relative protein level between groups was comparable (Figure 4-12, A and C). There were also no significant differences in DDAH2 protein levels at 72 hours post tMCAo (Figure 4-12, B and D). Overall, the quantification from this biochemical

approach showed that there were no differences between sham controls, ipsilateral and contralateral hemispheres at either timepoint. This indicates that brain ischaemia-reperfusion has no effect on DDAH2 expression in the whole hemisphere, potentially owing to this tissue mainly consisting of neuronal and glial cells. Full Western blots demonstrating antibody selectivity can be found in Appendix (Figure 7-3).

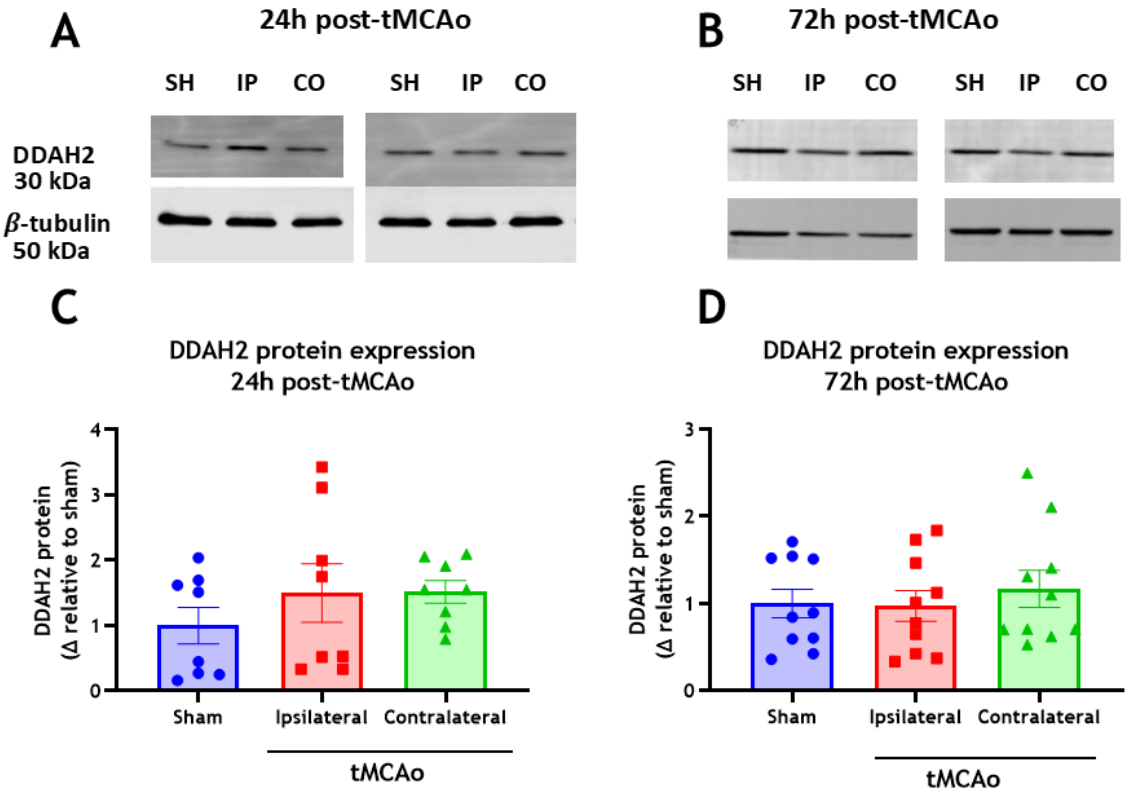

Figure 4-12. Western blot analysis of DDAH2 protein expression in C57BL/6J mice post tMCAo. Representative blots from A) 24 hours and B) 72 hours post-tMCAo with protein bands detected at 30 kDa for DDAH2 and at 50 kDa for ß-tubulin. SH: sham, IP: ipsilateral, CO: contralateral. Quantified protein expression is presented as mean ± SEM and normalised to housekeeper (ß-tubulin) and to sham average at C) 24 hours, Brown-Forsythe and Welch ANOVA with Tamhane's T2 multiple comparisons test, P>0.05, n=8, and D) 72 hours, using ordinary one-way ANOVA with Sidak's multiple comparisons test, P>0.05, n=10.

4.3.4.1 Validation of DDAH2 monocyte/macrophage specific DDAH2$^{Mo-/-}$ in isolated peritoneal macrophages

An approach to isolate microglia, monocytes and macrophages was needed to examine the impact of ischaemia on DDAH2 expression, to validate the KO, and to examine the impact of DDAH2 deletion on macrophage phenotype/polarisation. To address that, primary macrophages from DDAH2$^{fl/fl}$ and DDAH2$^{Mo-/-}$ mice were

recovered from peritoneal exudates, cultured for quiescence, and lysed for molecular analyses. The isolated cells yielded sufficient average RNA of 200 ng/ml and optimal mean Ct value difference between the genotypes (Figure 4-13A). The housekeeper gene *R18s* demonstrated good stability across samples from both genotypes, with mean Ct value fold change of 0.992 and CV<0.25 (Figure 4-13A). The Ct values for DDAH2 in the DDAH2$^{Mo-/-}$ were >35 indicating negligible RNA template, while Ct values of around 29 were found in the DDAH2 $^{fl/fl}$ mice. By using the $2^{-\Delta\Delta Ct}$ method *Ddah2* mRNA was 100-fold higher in DDAH2 $^{fl/fl}$ mice compared with DDAH2$^{Mo-/-}$ (Figure 4-13B).

A

	Ddah2		*R18S*	
	DDAH2$^{fl/fl}$	DDAH2$^{Mo-/-}$	DDAH2$^{fl/fl}$	DDAH2$^{Mo-/-}$
Mean Ct	28.75	35.72	19.28	19.43
SEM	0.07	0.13	0.08	0.12

B

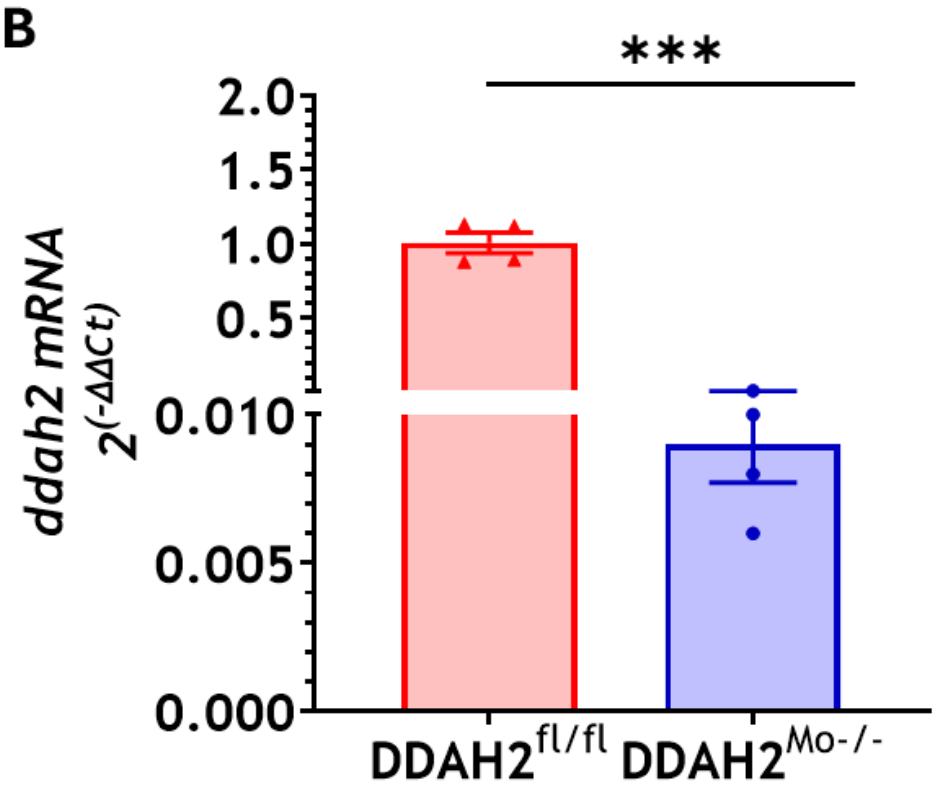

Figure 4-13. Validation of macrophage specific DDAH2 deletion in peritoneal macrophages isolated from DDAH2 $^{Mo-/-}$ and DDAH2 $^{fl/fl}$ mice using quantitative real-time polymerase chain reaction (qRT-PCR). A) Average Ct values for *Ddah2* and *R18S*. B) Relative quantification ($2^{-\Delta\Delta Ct}$) of *Ddah* mRNA. Data presented as mean ± SEM, unpaired t test with Welch's correction for unequal SD, *P<0.05, n=4.

4.3.5 Effect of DDAH2 deletion on the expression of key genes involved in regulating macrophage function.

The housekeeper gene *Rpl13* has been shown to be more stable in primary macrophages and showed good stability across samples from both genotypes, with mean Ct value fold change of 1.007 and CV=0.26 (Table 4-9).

Table 4-9. Average Ct values for *Rpl13* (housekeeper gene) and genes involved in macrophage function as investigated by qRT-PCR.

	Rpl13	*Arg1*	*TgfB*	*Il6*	*Ccl2*	*Tnf-a*	*Il-1B*
	DDAH2$^{fl/fl}$						
MEAN	18.69	25.38	21.29	20.11	20.45	21.21	18.96
SEM	0.21	0.65	0.59	0.86	0.75	0.60	0.92
NUMBERS	8	8	8	8	8	8	8
	DDAH2$^{Mo-/-}$						
MEAN	18.56	25.91	21.75	22.52	22.73	23.52	20.69
SEM	0.17	0.47	0.57	0.63	0.84	0.40	0.41
NUMBERS	7	7	7	7	7	7	7

The relative expression of genes involved in regulating macrophage function were next investigated from lysates obtained from peritoneal macrophages from DDAH2$^{fl/fl}$ and DDAH2$^{Mo-/-}$mice. Arginase-1 (*Arg-1)* is a marker highly expressed in M2-like macrophages. *Arg-1* mRNA was comparable between DDAH2$^{Mo-/-}$ and DDAH2$^{fl/fl}$ peritoneal macrophages (P=0.71) (Figure 4-14 A). *Tgf-B* is a potent anti-inflammatory cytokine and *Tgf-B* mRNA expression was comparable between genotypes (P=0.3) (Figure 4-14 B).

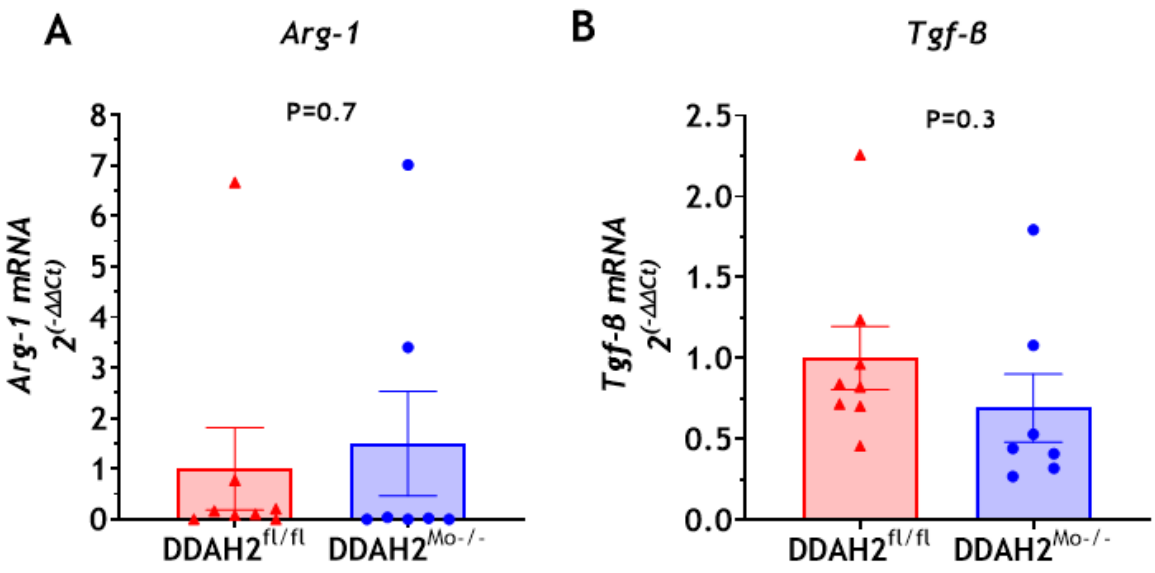

Figure 4-14. Relative quantification ($2^{-\Delta\Delta Ct}$) of mRNA expression for anti-inflammatory genes *Arg-1* and *Tgf-β* in peritoneal macrophages from DDAH2$^{Mo-/-}$ and DDAH2$^{fl/fl}$ mice. Data presented normalised to *Rpl13* housekeeping gene as mean ± SEM, n=7-8, unpaired t test with Welch's correction for unequal SD, P>0.05.

Conversely, the expression of pro-inflammatory cytokines associated with M1-like macrophage phenotypes was significantly decreased in DDAH2$^{Mo-/-}$ mice compared to DDAH2$^{fl/fl}$ mice (Figure 4-15). *Il-6* and *Tnfa* were both 7-fold lower, *Ccl2* was 3-fold lower and *Il-1β* was 4-fold lower in DDAH2$^{Mo-/-}$ versus control mice.

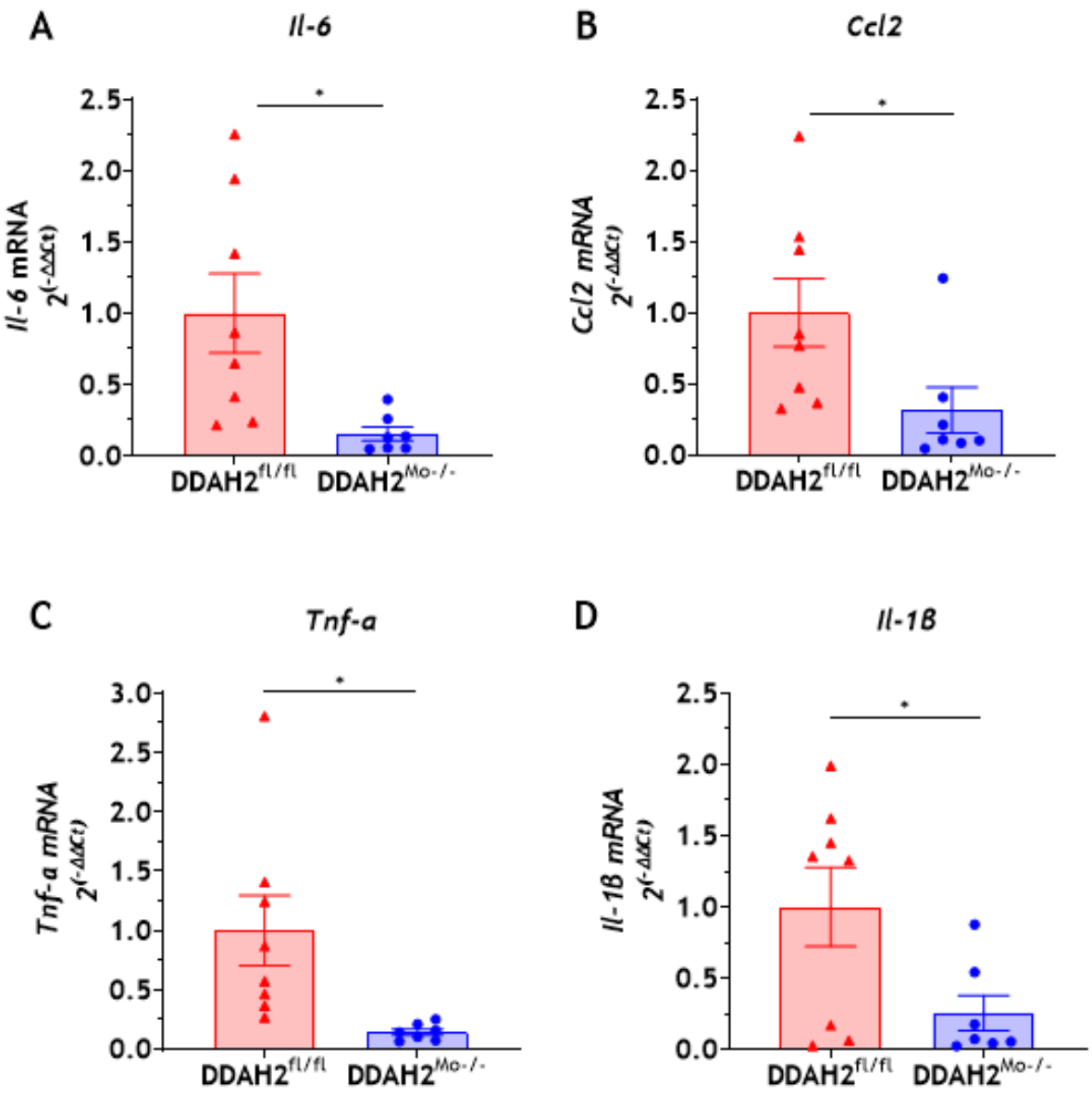

Figure 4-15. Relative quantification ($2^{-\Delta\Delta Ct}$) of mRNA expression for pro-inflammatory genes. A) *Il-6*, B) *Ccl2*, C) *Tnf-a*, D) *Il-1B* in peritoneal macrophages from DDAH2$^{Mo-/-}$ and DDAH2$^{fl/fl}$ mice. Data is presented as normalised to *Rpl13* housekeeping gene, mean ± SEM, n=7-8, unpaired t test with Welch's correction for unequal SD, *P>0.05.

4.4 Discussion

4.4.1 Method optimisation for isolation of brain macrophages

4.4.1.1 MACS

A reliable method for isolation of primary brain macrophages from mice needed to be established to allow investigation of the impact of DDAH2 deletion on macrophage phenotype and to verify the DDAH2 knockout in brain macrophages.

Furthermore, MACS could offer examining the effect of ischaemia on macrophage gene expression by either *in vivo* or *in vitro* approaches. FACS is a frequently used method for isolating single cells (Gross et al., 2015) and has been demonstrated to yield high-quality microglia in numerous publications (Bohlen et al., 2019, Volden et al., 2015). In deliberating the use of the method, important caveats in the context of ischaemic stroke were considered. There is a potential for increased cellular stress due to passage of cells through fluidic channels and laser excitation that may induce gene expression changes, upregulate transcription markers such as factors associated with a pro-inflammatory phenotype, and alter the redox state of the isolated cells (Llufrio et al., 2018, Pan and Wan, 2020). Additionally, the access to a flow cytometric facility and staff-assisted sorting were amounting to a significant cost added to the project. In comparison, MACS requires a benchtop magnet, which costs much less than a cytometer, and is easier to maintain compared to the lasers and detectors used in FACS instruments (Pan and Wan, 2020). MACS consumables include columns or plates, and a variety of commercially available kits (Hu et al., 2015). Immunomagnetic isolations can then be followed up by flow cytometric multiparameter analysis (Volden et al., 2015) for initial verification of the purity of the MACS isolation. Several MACS protocols exist that have demonstrated the successful retrieval of 4.2×10^5 microglia from an adult mouse brain and up to $0.5 - 2 \times 10^5$ microglial cells from mouse bilateral hippocampal slides or single hemispheres (Bordt et al., 2020, Buenaventura et al., 2022).

Therefore, initially the approach involved immunomagnetically isolating brain macrophages and microglia that express CD11b. Monocytes and macrophages highly express CD11b, and microglia express low-to-intermediate levels of this surface marker under homeostatic conditions (Martin et al., 2017b). MACS allows for a significantly gentler passage of cells compared to passing them through narrow fluidic channels at high speeds using the microfluidic systems of flow cytometers, decreasing the possibility that cells become activated or phenotypically altered, which would compromise their utility for measuring gene expression changes. Indeed, high viability of cells was observed using the column-based MACS approach (Figure 4-7). However, with either column- or plate-based technique, only 1% cells of interest were retrieved (Figure 4-6) (Figure 4-7). This resulted in very poor RNA yield, which would have not sufficed to conduct analyses

of multiple genes of interest. Potentially the magnetic beads used to pull down CD11b positive cells may have sterically hindered the binding of the antibody against CD11b in the verification step (Pezzi et al., 2018). Additionally, a major disadvantage to single-bead magnetic isolation is the lack of distinction between immune cell subtypes co-expressing the marker under investigation. As mentioned above, monocytes and macrophages express high levels of CD11b, but the frequency of these cells in a healthy brain is much smaller compared to microglia, which express intermediate to low levels of CD11b but are found in abundance in healthy mouse brain (Chapter 3). Following ischaemic stroke, the frequency of myeloid cells in the brain increases, contributing significantly to the total pool of $CD11b^+$ cells. Therefore, to distinguish $CD11b^+$ microglia from $CD11b^+$ myeloid cells after stroke, additional markers for identification of subtypes were needed. The fractalkine receptor CX3CR1 is highly expressed on microglia (Olveda et al., 2024) and is upregulated in response to cerebral ischaemia-reperfusion (Tarozzo et al., 2002), suggesting that this marker would be reliably expressed in microglia from both naïve and stroke mice. However, the frequency of $CD45^{int+}CD11b^+CX3CR1^+$ cells determined by flow cytometry upon MACS was below <1% (Figure 4-7).

4.4.1.2 FACS

Due to the above-described challenges and consideration for future work following stroke, isolation of brain macrophages was attempted using FACS in the adjacent institute's flow cytometric facility. This method was only performed in naïve mice because of the time constraints for this PhD project but was intended for characterising the identity of different $CD11b^+$ cells after cerebral ischaemia-reperfusion. FACS had an advantage over MACS in that it allows the use of multiple markers for sorting cells, as well as verifying the identity of cells pulled down by a single marker. The FACS results obtained high cell viability (>89%), if modest cell numbers and RNA yield (Table 4-5). The frequency of isolated macrophages ($CD45^{+high}CD11b^+F4/80^+$) was comparable to MACS-obtained CD11b positive cells, while microglia ($CD45^{int+}CX3CR1^+$) were isolated in much greater numbers by FACS (Figure 4-8, Table 4-5). Perhaps unsurprisingly, RNA concentration from macrophages was negligible (<5 ng/ul) and from microglia low but sufficient to investigate gene expression (approximately 20 ng/μl), albeit for only a few genes. This provided an opportunity to at least confirm the deletion of *Ddah2* in the macrophages from $DDAH2^{Mo-/-}$ mice. However, the RT-qPCR analysis was unable

to demonstrate absence of *Ddah2* transcript in macrophages or microglia from knockout mice, potentially due to Ct values of >32 for both $DDAH2^{fl/fl}$ and $DDAH2^{Mo-/-}$ samples (Table 4-6).

Robust evidence for expression of *Ddah2* in microglia is lacking. Therefore, it is plausible that the isolated microglia and brain macrophages do not express *Ddah2* mRNA at basal levels. Alternatively, the sorting contained a high fraction of other cell types with similarly low abundance of *Ddah2*. However, *Ddah2* mRNA expression level was expected to be moderate-to-high in macrophages but demonstration of a knockout was not achieved even in those cells (Figure 4-9B), suggesting that there was a problem either with the isolated cells, which were of low frequency, or the molecular methods thereafter.

Subsequent optimisation steps involved isolating monocytes from peripheral tissues, which would mitigate poor cell dissociation from brain tissue and would theoretically provide higher cell yields. Indeed, it was shown in Table 4-7 that cell numbers upwards from $6x10^4$ for blood derived $Ly6C^+$ monocytes and $1.6x10^5$ splenic monocytes were achieved with very high viability (>85%). However, RNA yield was once again <5 ng/µl across samples (Table 4-7), and Ct values were high (Table 4-8), strengthening the reasoning that a major challenge for this method was in obtaining high quality nucleic acids for molecular analyses.

4.4.1.3 RNA purity

The 260/280 ratio is a measure of sample purity, used to assess the purity of DNA and RNA. Nucleic acids absorb light at 260 nm and proteins absorb at 280 nm, and a ratio of ~2.0 is generally accepted as "pure" for RNA. Salts and other contaminants, such as EDTA, phenol and guanidine hydrochloride absorb light at 230 nm and the 260/230 ratio is used to control for the presence of these contaminants in nucleic acid samples. The expected 260/230 values are commonly in the range of 2.0-2.2. Both RNA purity values (A260/280 and A260/A230) were below the optimal ranges, suggesting protein contamination and/or contaminants, such as the guanidine hydrochloride present in the RNA extraction buffer, could have been carried over into the elution step and impacted the quality of RNA and subsequently cDNA.

It is increasingly more common to use alternative methods of nucleic acid concentration determination such as the fluorescent dye detection RiboGreen from Ambion/Applied Biosystems, especially from samples with low RNA abundance and particularly in the field of neuroinflammation in preparation of samples for high dimensional single cell RNA sequencing (Delbridge et al., 2020). Others have used microfluidic analysis (Pulido-Salgado et al., 2018) or chip based capillary gel electrophoresis (Buenaventura et al., 2022) to quantify RNA from mouse microglia, highlighting that adopting these technologies into the work flow would be important in the future. Another important index for quality control of RNA sequencing is RNA integrity number (RIN), which is obtained by digestion of RNA and determination of 18S and 28S fragments. Fragmented RNA poses problems to the capacity of the reverse transcription enzyme. Others have demonstrated good integrity of RNA isolated from immunomagnetically sorted cells, by showing clear 18S and 28S peaks on electropherograms and expression of these ribosomal units on protein blots (Buenaventura et al., 2022).

4.4.1.4 RNA isolation and reverse transcription

To investigate the possibility that the microglia isolation methodology was robust enough, but the downstream applications were failing due to poor RNA purity or suboptimal reverse transcription, RNA isolations were attempted using a different kit (GeneJET, Thermo Fisher). Comparative RNA isolations using phenol-free methods with reagents from two different kits GeneJET RNA purification kit versus Qiagen RNeasy Micro kit using wildtype mice showed no significant differences between RNA concentration or purity obtained with each kit (data not shown). It was then proceeded to use the GeneJET kit for RNA extraction from blood and spleen monocytes, due to reagent availability. Furthermore, as trace amounts of reagents such as guanidine hydrochloride discussed above used in the RNA isolation procedure can cause problems with the reverse transcription, cDNA for samples obtained by FACS was generated using an alternative kit - Invitrogen™ SuperScript™ IV Reverse Transcriptase. This reverse transcription enzyme purportedly has high capacity for small, contaminated and heavily fragmented amounts of RNA (RIN<3). Since cDNA amounts are not measured prior to RT-qPCR, the result of the change in kit was appraised on the basis of the RT-qPCR analysis. Although the variability between technical replicates seemed to improve, no significant difference in DDAH2 expression was achieved.

4.4.1.5 Housekeeper stability

A limitation to the study is that a dilution curve for identifying optimal concentration for the primers of housekeeping gene *R18s* was not conducted in advance. This would have allowed for the concentration of the primers for the gene of interest *Ddah2* to be matched to this empirically derived concentration. There was a shift in average Ct between the *R18s* housekeeper values of about 1.5 (macrophages: 21.57 vs 20.32, microglia: 22.2 vs 21.89, $DDAH2^{fl/fl}$ vs $DDAH2^{Mo-/-}$) (Table 4-6), indicating that *R18s* was perhaps not very stable in these cells. There was much less mean Ct variability in *R18s* mRNA in samples from both genotypes (21.34 vs 20.92, control vs knockout) in monocytes derived from blood and even more robust stability in splenic monocytes (21.14 vs 21.03, $DDAH2^{fl/fl}$ vs $DDAH2^{Mo-/-}$) (Table 4-8). In peritoneal macrophage samples *R18s* showed good stability between samples (19.28 vs 19.43, $DDAH2^{fl/fl}$ vs $DDAH2^{Mo-/-}$). Upon consulting with Prof Leiper's and Dr Dowsett's lab group, later work was performed using *Rpl13* as a housekeeping gene, which has been shown to be stable in peritoneal macrophages (Alshuwayer, 2024) and showed good stability in this study (18.69 vs 18.56, control vs knockout) (Table 4-9).

4.4.2 The potential consequences of increased DDAH2 in macrophages.

In peritoneal macrophages hypoxia has been demonstrated to upregulate *Ddah2* mRNA 3.6-fold and *iNOS* mRNA 4-fold (Lambden, 2016). The study by Lambden et al. demonstrated that in macrophages isolated from mice with a macrophage specific DDAH2 knockout and challenged with hypoxia, basal nitrite and nitrate (NOx) levels were reduced. In comparison, in the floxed control cells, intracellular NOx species increased, demonstrating that in mice deficient in DDAH2, NO mediated function could be impaired (Lambden et al., 2016). Although direct evidence is missing, it could be inferred that hypoxia causes increase of NOx by upregulating iNOS, which may be mediated by regulation of ADMA by DDAH2.

4.4.3 Ischaemia upregulated *Ddah2* mRNA in cultured macrophages but did not change DDAH2 protein levels in whole brain

An original aim for this study was to investigate the effect of ischaemia on the expression of genes along the DDAH2-ADMA-NOS axis, for which brain macrophages and/or microglia had to be isolated from C57BL6/J and macrophage specific DDAH2 knockout mice following experimental stroke. However, given the challenges described above in obtaining primary mouse brain macrophages from naïve mice, *in vitro* experiments were conducted in the immortalised macrophage cell line RAW264.7. *Ddah2* mRNA was significantly elevated following 24h OGD in these cells (Figure 4-11). Another study has previous reported elevation of iNOS after 1h OGD/reoxygenation in these cells (Li et al., 2016), suggesting that the DDAH2-ADMA-NOS axis is quickly activated in macrophages following a hypoxic challenge. LPS stimulation in RAW264.7 cells was reported to upregulate iNOS as early as 6 hours and be maintained up to 24 hours after stimulation (Alanazi, 2024), suggesting that perhaps the expression of *Ddah2* scales with iNOS mRNA following OGD too. Although LPS stimulation differs from hypoxia in some of the downstream signalling pathways it elicits, both stimuli trigger pro-inflammatory signalling pathways such as NF-κB, MAPK (p38, JNK, ERK) and PI3K/Akt, suggesting that parallels could be drawn between the expression of elements of the DDAH2-ADMA-NOS axis in these different studies.

The increased iNOS expression in macrophages exposed to hypoxic challenge (Lambden et al., 2016) may be secondary to the hereby presented upregulation of DDAH2. However, since both iNOS and DDAH2 are induced by hypoxia, albeit possibly through different mechanisms, it is difficult to discern a transcriptional regulation role for DDAH2 on iNOS and thus DDAH2 is still more likely to control iNOS through inhibition of ADMA. The molecular mechanisms of hypoxia mediated induction of DDAH2 are not yet revealed fully. In endothelial cells nuclear factor E2-related factor 2 (Nrf2), which is induced by hypoxia, transcribes DDAH2 expression to enhance NO biosynthesis by binding to antioxidant response element (ARE)-2 on the promoters for DDAH1 and DDAH2 (Luo et al., 2015). Nrf2 is an important transcriptional regulator of inflammation in macrophages (Kobayashi et al., 2016) and may therefore be mechanistically responsible for upregulating DDAH2. Additionally, HIF-1α and GLUT1 (Glucose Transporter 1) are commonly

upregulated in OGD experiments and might be the drivers of *Ddah2* upregulation. Inducible NOS is transcriptionally activated by the NF-κB and STAT signalling pathways (Aktan, 2004), while it is presently unknown if these canonical transcription factors also regulate DDAH2 expression. Nevertheless, the mechanisms for *Ddah2* regulation *in vivo* are likely to be different than *in vitro*, and investigating other transcriptional regulators that are susceptible to hypoxic challenge in macrophages would be needed.

To fully reveal the impact of ischaemia on the DDAH2-ADMA-iNOS pathway, concomitant measurements of other components of this pathway such as intracellular NO, iNOS and ADMA could have been measured in RAW264.7 cells after OGD to provide an insight into potential functional changes of the increased DDAH2 expression. These measurements could have then be followed by investigation of the DDAH2-ADMA-iNOS pathway in peritoneal macrophages from the DDAH2$^{Mo-/-}$ mice. Additionally, targeted deletion of DDAH2 in RAW264 cells by small interfering RNAs could provide an alternative way to probe the function of DDAH2 in ischaemia. Exploring macrophages function under OGD conditions could provide an insight into the functional consequences of hypoxic *Ddah2* upregulation.

4.4.3.1 Limitations of OGD

The experiments using OGD aimed to complement the investigation of the impact of ischaemia on expression of DDAH2, albeit in a macrophage cell line, instead of in circulating monocytes, brain macrophages and microglia from the DDAH2$^{Mo-/-}$ mice or a co-culture model of NVU cells and macrophages. Therefore, the findings obtained by this reductionist approach do not fully replicate ischaemic stroke pathology. *Ddah2* mRNA was increased under OGD in RAW264.7 cells, but in the intact ischaemic brain these cells may receive signals from adjacent cells that transcriptionally or translationally alter the expression of *Ddah2*.

4.4.3.2 Limitations of Western Blotting

There was a lack of change in expression of DDAH2 in cerebral hemispheres from C57Bl6 mice after 24 hours and 72 hours after tMCAO (Figure 4-12), while increased DDAH1 was recently reported in mouse brain hemispheres 24 hours after

cerebral ischaemia-reperfusion (Gao et al., 2024). It is conceivable that any DDAH2 changes in macrophages would have been too subtle to detect using a whole hemisphere lysate, which primarily contains neurons relative to other cell types and therefore any changes in other cell types would be difficult to detect using this method. Therefore, ischaemia does not have an effect on brain DDAH2 protein levels *in vivo*. However, since cerebral ischaemia reperfusion leads to neuroinflammation, altering macrophage function by deleting the NO-regulating enzyme DDAH2 in these cells may have an effect on the outcomes of stroke.

4.4.4 Validation of macrophage specific *Ddah2* knockout

The data presented in Figure 4-13 confirms that the floxed sequence between exons 2 and 5 in the *Ddah2* gene is deleted by Cre recombinase in peritoneal macrophages, and by extension in monocytes, given that macrophages are derived from monocytes.

4.4.4.1 Advantages in using peritoneal macrophages for validation

LysMCre activity differs substantially across tissue resident macrophages, potentially resulting in differential absence of *Ddah2*. For example, it has been reported that 90–100% of peritoneal macrophages have LysM-Cre activity, whereas only 40% of spleen macrophages are LysM-cre positive (Abram et al., 2014, Shi et al., 2018). This makes peritoneal macrophages a good cell type for verification of the knockout. Whilst peritoneal macrophages are ontologically different from brain macrophages, a principle component analysis of macrophage diversity has reported a correlation coefficient of 0.798 between peritoneal macrophages and microglia (Gautier et al., 2012). Ultimately, however, peritoneal macrophages are quite different to microglia. Regardless, using these cells provided an opportunity to explore the potential importance of DDAH2 for macrophage-immune cell function.

4.4.4.2 Limitations of the validation

The absence of *Ddah2* transcript in knockout animals was only investigated at the mRNA level. A confirmation for that could be obtained by immunofluorescent protein analysis, where morphology and markers typically expressed on macrophages could guide a definitive presence or absence of DDAH2 in these cells.

The original article, where this mouse model was first described has demonstrated that DDAH2 expression was preserved in the kidney, liver, heart, and aortic tissue. However, it would also be beneficial to validate that DDAH2 expression in other brain cell types, such as neurons and microglia, was not affected.

Additionally, a limitation to this validation is that the DDAH2$^{Mo-/-}$ was not confirmed in brain-resident macrophages, which was one of the original aims for this project. Determining a deletion of DDAH2 in microglia and BAMs is of functional consequence in delineating the contribution of brain-resident macrophages versus circulating monocytes and other tissue-resident macrophages on the outcomes of stroke. This may involve the multiplex immunofluorescent staining with antibodies against markers of demonstrated specificity towards microglia such as Cx3cr1, Iba-1 and Trem112, or BAMs such as Lyve1 and CD206, in conjunction with DDAH2.

Furthermore, although in healthy brain neurons lysozyme production is lacking, the LysM promoter is reported to be active in hippocampal neuronal cells (Orthgiess et al., 2016). Since neurons also express DDAH2 (Kozlova et al., 2021), it is conceivable that DDAH2 is deleted in those cells under the LysM promoter too. Therefore, examining the co-expression of DDAH2 with a neuronal marker such as NeuN would need to be investigated in the context of ischaemic stroke.

4.4.4.3 DDAH2 expression in microglia

Recently it was reported that DDAH2 is not expressed by microglia in adult mice (Kozlova et al., 2021). Even though this may be the case in naïve mice, or they may have low expression of the *Ddah2* transcript, an upregulation of *Ddah2* mRNA in microglia following cerebral ischaemia-reperfusion is conceivable, as suggested by the upregulation of *Ddah2* mRNA under OGD in RAW264.7 cells (Figure 4-11). Therefore, despite the presented evidence that DDAH2 is not expressed in microglia at mRNA level, a more robust validation of these results would be needed prior to proceeding with investigating the expression of *Ddah2* following cerebral ischaemia-reperfusion.

4.4.5 Pro-inflammatory genes expression is reduced in monocyte/macrophage *Ddah2* null mice

Since cells obtained with the above methods did not result in reliable transcript expression and peritoneal macrophages provided a stable platform to validate the monocyte/macrophage specific DDAH2 deletion (Figure 4-13), gene expression studies were also performed in lysates from peritoneal macrophages (Figure 4-14, Figure 4-15). It was hypothesised that deletion of DDAH2 will reduce the amount of iNOS-derived NO production and that because NO is involved in macrophage metabolic reprogramming/polarisation there may be altered phenotype/function. The pro-inflammatory cytokines *Il-6*, *Il-1β*, *Tnf-α* and *Ccl2* mRNA were reduced in macrophages from DDAH2$^{Mo-/-}$ mice (Figure 4-15), providing tentative evidence that DDAH2 activity might contribute to M1-like phenotypes. While some evidence suggests that upregulated iNOS is a hallmark of M1-like macrophages (Cho et al., 2014, Villalta et al., 2009), others have demonstrated that iNOS derived from myeloid cells suppresses M2-like polarisation (Lu et al., 2015). What remains more puzzling is the lack of effect of DDAH2 absence on anti-inflammatory genes. Since Arg-1 competes with iNOS for L-arginine in macrophages (Li et al., 2012), in the presence of reduced levels of iNOS in the DDAH2 null macrophages, it is reasonable to expect the activity and/or expression of Arg-1 towards L-arginine to be enhanced. Additionally, iNOS inhibition significantly increased *Tgf-β* mRNA and protein levels in rats (Abd El-Aleem et al., 2020), suggesting that the level of this anti-inflammatory marker would increase in macrophages lacking *Ddah2*. However, no significant changes in mRNA expression of *Arg-1* and *Tgf-β* were found between DDAH2$^{Mo-/-}$ and control mice (Figure 4-14), perhaps indicative of an incomplete inhibition of iNOS by ADMA in cells lacking DDAH2.

Since the DDHA2 knockout seemed to decrease pro-inflammatory genes and this thereby suggests that *Ddah2* null mice may adopt M2-like phenotypes, identification of M2-like macrophages was conducted by double label immunofluorescence for CD206^{+}DDAH2^{+} cells in mouse brain tissue following experimental stroke. This work had the additional aims of substituting for DDAH2 expression in isolated microglia/macrophages from stroke brains and provided an additional avenue to validate the deletion of DDAH2 in these cells. The latter may have been more appropriately conducted by investigating common macrophage and microglia markers, such as F4/80, CD68 and Iba-1. Preliminary work from

three independent experiments using different brain sections from the same mouse identified some $CD206^{+}DDAH2^{+}$ cells but semi-quantification was not attempted, as images were not systematically collected from sequential brain regions.

It is worth noting that although it would be remiss to ignore the established dichotomous macrophage classification into M1-like (pro-inflammatory) and M2-like (anti-inflammatory), which these signalling molecules are grossly assigned to, its utility to discern subtleties in disease-dependent macrophage function is often obsolete and needs to be interpreted with caution (Mills, 2012). Therefore, more work will be needed to fully characterise M1-like and M2-like adjacent phenotypes.

4.4.6 Putative mechanism for regulation of pro-inflammatory gene expression by DDAH2

4.4.6.1 Limitations of the work

DDAH2 deletion in macrophages was hypothesised to potentiate the inhibitory action of ADMA on iNOS and therefore reduce NO production. Lower iNOS activity in $DDAH2^{Mo-/-}$ mice could therefore lead to a reduction in pro-inflammatory genes. Indeed, pro-inflammatory cytokines *Il-6*, *Il-1β*, *Tnf-a* and *Ccl2* mRNA were reduced in macrophages from $DDAH2^{Mo-/-}$ mice (Figure 4-15). However, iNOS expression levels were not investigated to ascertain that this observation pertains to expression alterations of iNOS. The key limitation of this work is that the peritoneal macrophages were allowed to reach quiescence and not stimulated by hypoxic or inflammatory stimuli, therefore all transcripts were investigated under homeostatic conditions. Previous work in our lab has shown that ADMA (100 μM) and SDMA (100 μM) had no effect on nitrite production in unstimulated human macrophages lacking DDAH2 (Ahmetaj-Shala, 2013) and incubation of resting Raw264 cells with ADMA (100 μM) did not result in increased nitrite species (Alshuwayer, 2024).

4.4.6.2 Production of NO by iNOS versus eNOS

Since iNOS is not basally expressed in macrophages, there is a strong possibility that the findings arise from eNOS-generated NO rather than iNOS or are

completely NO-independent. Although iNOS is the primary isoform in macrophages, nNOS and eNOS are also constitutively expressed in macrophages (Huang et al., 2012). The production of NO by macrophages, and by extension their phagocytic function, is conventionally attributed to iNOS. However, in unstimulated macrophages iNOS-independent receptors and enzymes produce low output NO. For example, it has been shown that FcgR -mediated engulfment relies on Ca^{2+} dependent ERKs phosphorylation, which in turn increases nNOS and eNOS, and the produced NO increases phagocytosis in neighbouring macrophages (Huang et al., 2012). The peritoneal macrophages were cultured in media with 0.2g/L $CaCl_2$ concentration, therefore it is conceivable that despite the absence of inflammatory stimulation, these macrophages produced sufficient levels of eNOS-derived NO to affect the pro-inflammatory transcripts. Additionally, eNOS-derived NO concentration is only nanomolar, compared to the low micromolar NO produced by iNOS, but has been reported as necessary for the induction of iNOS by NF-κB (Darra et al., 2010). Furthermore, soluble guanylate cyclase (sGC) is expressed at both mRNA and protein level in murine macrophages, and the effect of eNOS-derived NO in regulating pro-inflammatory gene expression is partly dependent on sGC activation and cyclic GMP production (Connelly et al., 2003). Studying these molecular targets in Ddah2 null macrophages could confirm the observed changes in gene expression as attributable to eNOS-derived NO. Additionally, the observed decrease in pro-inflammatory genes in macrophages from $DDAH2^{Mo-/-}$ mice could be mediated through L-NMMA inhibition of eNOS, rather than ADMA inhibition of iNOS. L-NMMA is slightly more sensitive to regulation by DDAH2 than ADMA in macrophages, as intracellular concentration of L-NMMA in peritoneal macrophages increased to 30 μM in *Ddah2* null peritoneal macrophages compared to 20 μM of ADMA, while ADMA was 5 μM and L-NMMA was undetectable in control cells (Ahmetaj-Shala, 2013).

An additional point of consideration is that the experiments were conducted in a peripheral tissue resident macrophage. Even if microglia or other brain resident macrophages from *Ddah2* null mice were eventually obtained by isolation after tMCAo, they may have different effects on pro-inflammatory cytokines compared to that found in the peritoneal macrophages. After permanent cerebral ischaemia, macrophages were reported to upregulate the expression of pro-inflammatory and

neutrophil recruitment genes, while microglia downregulate these genes (Zarruk et al., 2018).

4.4.7 Future work

Future work would benefit from investigating the functional consequences of the observed inflammatory gene changes. Macrophages phagocytose immune complexes composed of IgG-opsonised pathogens, particles, or proteins through for the Fc portion of IgG (FcgR) (Huang et al., 2012) and this function could be examined in vitro in the peritoneal macrophages to demonstrate a critical role for DDAH2 in the process. Alternatively, the impact of iNOS-derived NO release from macrophages on cytotoxicity of other cells in culture could be examined. Mitochondrial DDAH2 expression has been reported in human chondrocytes (Cillero-Pastor et al., 2012) and DDAH2 has been shown to relocate to the mitochondria upon viral stimulation in mice (Huang et al., 2021). Therefore, mechanistic studies might want to explore the protein expression of mitochondrial targets impacted by NO-toxicity induced apoptosis such as complexes I and IV of the mitochondrial respiratory chain, ribonucleotide reductase, aconitase, and glyceraldehyde-6-phosphate dehydrogenase and through DNA modification (Palmieri et al., 2020). Downregulation of OXPHOS and ATP production directs M1-like macrophages to a glycolytic commitment and in DDAH2 null macrophages this process may potentially be reversed. Since mitochondrial dysfunction has been shown to abolish reversal of polarisation (Van den Bossche et al., 2016), investigating this may be of particular interest in defining the M1-like/M2-like phenotype of *Ddah2* null macrophages and provide a more definitive insight into functional changes.

Abnormal NO signalling in macrophages could impact their antigen presentation to T cells through a reduced major histocompatibility complex II (MHCII) expression (Harari and Liao, 2004, Iwasaki and Medzhitov, 2015), however evidence for a regulatory role of DDAH2 on the ability of macrophages to present antigen is lacking and would warrant investigation in the context of adaptive neuroinflammation following stroke.

4.4.8 Summary and conclusion

In this chapter optimisation work is presented related to the overarching aim of establishing a method for macrophage and microglia isolation from mouse brain tissue and investigating transcriptional changes in genes important for macrophage function in the context of inflammation after stroke. Several techniques for deriving myeloid cells such as monocytes, macrophages, and microglia were presented. RNA isolation methods, cDNA generation and qRT-PCR were also optimised to validate the utility of these methods of cell isolation to study gene expression and to validate the monocyte/macrophage specific DDAH2 knockout in mice. Obstacles were encountered when the obtained cells from naive mice were found to express low or negligible amounts of *Ddah2* and overall low RNA yield and purity. This hindered the progress for investigating the impact of DDAH2 deletion in microglia and macrophages on multiple genes important for macrophage function.

Therefore, alternative ways to investigate the effect of ischaemia on DDAH2 expression were utilised in macrophages from an established cell culture line and mouse brain tissue after experimental stroke. Upregulation of *Ddah2* mRNA expression in oxygen-glucose deprivation was demonstrated, however protein expression of DDAH2 in mouse brain tissue was unchanged following cerebral ischaemia-reperfusion. DDAH2 knockout validation was demonstrated by negligible *Ddah2* mRNA in peritoneal macrophages from DDAH2$^{Mo-/-}$ mice compared to control mice. The ability of DDAH2 to regulate macrophage function was also investigated in peritoneal macrophages. Key pro-inflammatory genes were downregulated in macrophages from DDAH2$^{Mo-/-}$ mice, suggesting these cells may adopt an anti-inflammatory M2-like phenotype. In conclusion, hypoxia upregulates DDAH2 in macrophages and tentative evidence is presented that DDAH2 deletion in macrophages has the potential to modulate iNOS-NO mediated macrophage phenotype through regulating the expression of pro-inflammatory genes. These findings may have important implications for the impact of DDAH2 absence on the outcomes of cerebral ischaemia-reperfusion.

5 Chapter 5: Effect of monocyte/macrophage DDAH2 deletion on acute brain injury, functional outcomes, and apoptosis after cerebral ischaemia-reperfusion

5.1 Introduction

DDAH2 regulates iNOS-NO signalling in inflammatory cells through inhibition of ADMA (Lambden et al., 2015, Lambden et al., 2016, Huang et al., 2021) and depletion of macrophage iNOS after ischaemic stroke in mice improves outcomes (Li et al., 2022). However, the impact of DDAH2 on stroke outcomes has not been directly studied before.

The two main hallmarks of ischaemic stroke are formation of an infarct, as a result of the reduction in perfusion of the vascular territory, and brain oedema, caused by ionic gradients imbalance. The MCA has a superficial division, which supplies cortical regions such as the primary somatosensory cortex and the motor cortex, and lenticulostriate branches, which supply subcortical territories such as the basal ganglia (globus pallidus and striatum) and the genu of the internal capsule (ten Donkelaar et al., 2020). Thus, in the mouse tMCAo model of focal ischaemic stroke the infarct typically affects the striatum, the sensory and motor cortices.

Clinical ischaemic stroke is accompanied with long-term disability, which dictates reduction of neurological and functional deficits following stroke as a key objective in rehabilitation programmes (Langhorne et al., 2009, Shahid et al., 2023). It follows that a major outcome to measure in preclinical stroke research, alongside infarct size, is neurological impairment. Assessment of deficits in cognitive and functional outcomes in rodents is gaining importance in enhancing the translatability of such studies (McFall et al., 2020, Percie du Sert et al., 2020). Healthy mice typically exhibit behaviours with functional symmetry, while unilateral ischaemia in the right hemisphere results in contralateral (left) forelimb impairment (Schaar et al., 2010, Mani et al., 2013). Consequently, numerous tests have been developed to assess upper motor weakness and hemiparesis after mouse tMCAo (Ruan and Yao, 2020). The MCA supplies the lateral surface of the parietal lobe and the superior temporal lobes, which are the location of the upper limb and face on the primary somatosensory cortex. Therefore, a stroke affecting the MCA results in sensory loss in these areas. In mice, this can manifest in deficits in forelimb strength (Crum et al., 2013) and foot placement on the contralateral side (Gibson et al., 2005, Feng et al., 2020). Hemi-spatial neglect is a common clinical feature of stroke and can be assessed by the walking and tail suspension swing tests (Balkaya et al., 2013). A composite neurological score such as the

neurological severity score (NSS), which combines scores from several tests, offers better predictive validity than single tests (Schaar et al., 2010). Additionally, nest building, which is a natural behaviour for rodents to provide shelter, heat conservation, and protection from predators, can also be assessed to determine sensorimotor and cognitive deficits, wellbeing, and depressive-like symptoms (Deacon, 2006a, Gaskill et al., 2013, Jirkof, 2014, Sanz-Moreno et al., 2024).

If CBF is not fully restored following tMCAo, over time cells in the peri-infarct succumb and undergo apoptosis. The peri-infarct is therefore incorporated into the infarct and the infarct enlarges. Excessive macrophage iNOS-derived NO contributes to neuronal apoptosis (Belenichev et al., 2024), therefore reduction in NO in DDAH2$^{Mo-/-}$ mice may counter the apoptotic signalling.

Monocytes and macrophages are first responders to ischaemic brain injury, while their roles in controlling the inflammatory response are a subject of debate. For example, depletion of spleen monocytes/macrophages by liposomal clodronate reduced brain atrophy and improved neurological recovery after 90 min tMCAo (Ma et al., 2016), implying that these cells may have harmful effects after tMCAo. However, another study showed that acutely after tMCAo in CCR2 deficient mice, despite a lack of change in lesion volume, there was reduced angiogenesis within infarcts and impaired neurological outcome, suggesting that monocytes-derived macrophages may be beneficial in resolution of inflammation by driving vasculoprotection and improving cognitive function (Pedragosa et al., 2020). Monocyte-derived macrophages are dependent on the CCR2-CCL2 axis for monocytes mobilisation from the bone marrow and for infiltration to inflamed sites (Tsou et al., 2007), and monocyte chemotaxis is the primary trigger for macrophage accumulation in the injured brain. It has been known since the late 1990s that NO controls monocytes chemotaxis through increased expression of CCL2 (Tsao et al., 1997) and the presence of iNOS inhibitors reduces monocyte chemotaxis (Belenky et al., 1993). In Chapter 4 evidence was presented for a decreased expression of the chemokine *Ccl2* in macrophages from naïve mice lacking monocyte/macrophage DDAH2, suggesting that perhaps circulating monocytes secrete less CCL2 in DDAH2$^{Mo-/-}$ mice, and may therefore affect the recruitment of further myeloid cells after tMCAo in these mice. Additionally, monocyte numbers in the brain are influenced by adhesion to endothelial cells

and resultant transmigration. It was recently demonstrated that S-nitrosylation of integrin β1 in monocytes promotes monocyte–endothelial adhesion in an iNOS-dependent pathway (Yao et al., 2023). A role for iNOS in leukocyte infiltration has been demonstrated in hepatic ischaemia-reperfusion injury, as monocyte iNOS deletion resulted in reduced infiltration of neutrophils into the ischaemic liver (Hamada et al., 2009). However, in mice lacking monocytic iNOS, immune cell infiltration into the ischaemic brain was not affected (Garcia-Bonilla et al., 2014), indicating that DDAH2 is unlikely to affect ischaemic stroke outcome secondary to aberrant leukocyte infiltration, while this has not been previously reported. As discussed in Chapter 4, there is a possibility that additionally to monocytes and macrophages, DDAH2 is deleted in LysMCre expressing microglia in DDAH2$^{Mo-/-}$ mice, therefore the effect of ischaemic stroke on microglia numbers in these mice also deserves investigation.

5.1.1 Chapter hypothesis and aims

The main hypothesis for this chapter was that DDAH2 plays a role in potentiating the negative effects of iNOS-derived NO and that by knocking out *Ddah2* from monocytes, stroke outcomes in DDAH2$^{Mo-/-}$ mice 72 hours after tMCAo would improve. This study aimed to investigate the hallmarks of cerebral ischaemia-reperfusion such as infarct volume, neurological and behavioural deficits, and neuronal apoptosis upon deletion of DDAH2 from monocytes. Additionally, it was hypothesised that DDAH2 manipulation may affect the rate of accumulation of myeloid cells in the brain. To test this hypothesis, the study aimed to quantify the numbers of infiltrating immune cells into the ischaemic brain.

5.2 Methods

5.2.1 Animals

In this chapter a total of 16 monocyte specific DDAH2 knockout (DDAH2$^{Mo-/-}$) mice and 15 littermate control mice (DDAH2$^{fl/fl}$) were used for the tMCAo and subsequent analyses, of which 7 DDAH2$^{Mo-/-}$ and 6 DDAH2$^{fl/fl}$ mice were subjected to 60 min occlusion period, while 9 DDAH2$^{Mo-/-}$ and 9 DDAH2$^{fl/fl}$ mice underwent 40 min tMCAo. DDAH2$^{Mo-/-}$ and DDAH2$^{fl/fl}$ mice were generated as described in section 1.1.3 in General Methods. Dr Alyson Miller performed all surgeries with

anaesthetic assistance from me. The mice used in this study were all male, of good health, and similar age: 13.9±1.7 vs 15.7±1.8 weeks old, $DDAH2^{Mo-/-}$ vs $DDAH2^{fl/fl}$ and weight: 23.7±2 vs 24±1 g, $DDAH2^{Mo-/-}$ vs $DDAH2^{fl/fl}$ on the day of surgery. One $DDAH2^{Mo-/-}$ mouse was excluded from the study as it had to be euthanised prior to the scientific endpoint due to receiving a score of ≥9 on the clinical severity scale (section 1.2.2 of General Methods).

5.2.2 Adherence to ARRIVE guidelines

Two or three surgeries were performed on a single day and the order of genotypes undergoing surgery was unknown to the surgeon. Procedures were performed blinded by concealing the mouse's genotype during pre- and post-surgical neuroscoring, sample handling and data analyses. Video behavioural analysis was blinded by concealment of the animal's genotype.

5.2.3 Stroke surgery

Cerebral ischaemia-reperfusion was induced by the tMCAo model described in detail in Section 2.2.1 in General Methods. In this study (Figure 5-1), mice were subjected to tMCAo for 40 min for the immune cell quantification and for 60 min for infarct analyses, using a monofilament. Neurological and functional deficit testing was conducted prior to surgery in all mice that underwent 60 min occlusion but not in those used for 40 min occlusion. Testing was conducted at 24 hours and 72 hours post tMCAo for all mice. At the scientific endpoint animals were sacrificed by terminal anaesthesia with 5% isoflurane or by a rising concentration of CO_2 (Schedule 1 of the Act) followed by decapitation. For flow cytometric analyses mice were transcardially perfused with 0.9% saline under 5% isoflurane, brains were harvested and placed in ice cold PBS and the tissue was immediately used. For infarct and oedema volume, and terminal deoxynucleotidyl transferase dUTP nick end labelling (TUNEL) analyses, brains were carefully harvested, placed in ice cold PBS, slowly frozen over liquid nitrogen and stored at -80° C. Cryo-sectioning was then performed as described in Section 2.3.1 in General Methods by Dr Alexandra Riddell.

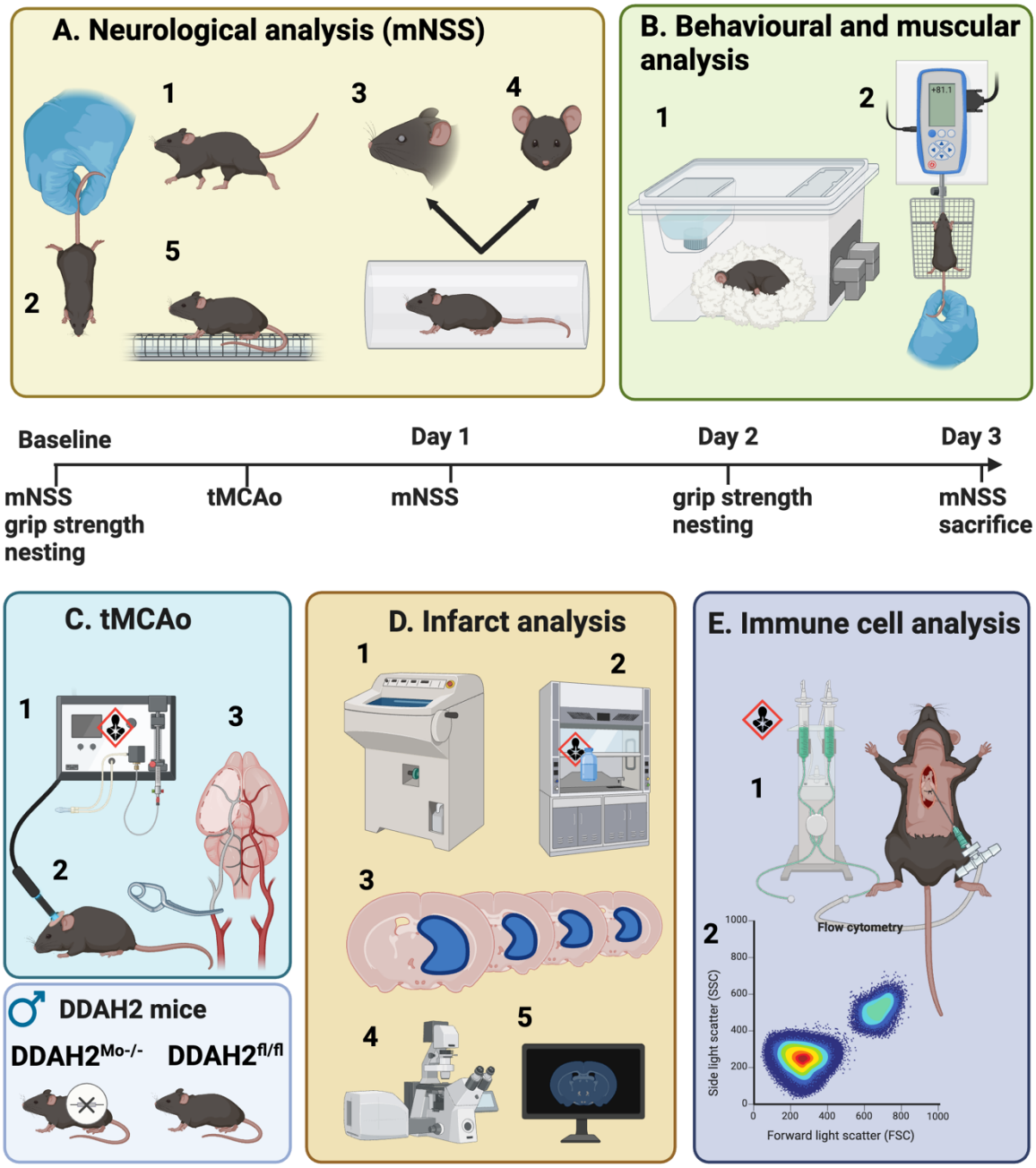

Figure 5-1. Schematic presentation of the experimental procedures used in this chapter. A-1 walking test, A-2 hanging test, A-3 corneal reflex, A-4 pinna reflex, A-5 grid walking test. B-1 nest building test, B-2 grip strength test. C-1 isoflurane anaesthesia, C-2 positioning of the laser Doppler probe, C-3 position of the arterial clamp on the common carotid artery and the affected brain area in the territory of the middle cerebral artery, D-1 cryo-sectioning brain tissue, D-2 thionin staining, D-3 infarct distribution, D-4 confocal laser microscopy used for terminal deoxynucleotidyl transferase dUTP nick end labelling (TUNEL) imaging, D-5 cell count analysis of apoptosis. E-1 terminal transcardial perfusion procedure, E-2 flow cytometric analysis of major immune cell populations. mNSS – modified neurological severity score, $DDAH2^{Mo-/-}$ – monocyte specific DDAH2 knockout, $DDAH2^{fl/fl}$ - littermate controls.

5.2.4 Infarct and oedema volume analysis in mice after tMCAo

Infarct and oedema volumes were determined in 15 cryo-sectioned coronal sections spanning 3 regions of the brain. Sections were stained 0.125% thionin (Sigma, Cat# C-0775), which stains brain matter in blue Nissl and allows for detection of colourless necrotic tissue. Sections were immersed in thionin for 2 minutes at 37°C in the dark followed by two washes in distilled water. Sections were then dehydrated in ethanol (70% followed by 100%) for 1 min, air dried and dipped in xylene substitute. Sections were mounted onto coverslips with DPX mounting medium and allowed to dry overnight. Images were taken with a digital camera (Canon Ixus 160, Japan) using an illuminated platform. Images were pre-processed for enhanced contrast and correct orientation using a Fiji macro. Total cortical, subcortical infarct and oedema volumes were determined by delineating the left hemisphere, right hemisphere, infarct, cortical and subcortical areas (Fiji software; National Institutes of Health) with the assistance of the online Mouse Brain Atlas (Allen Institue for Brain Science, 2004).

Total infarct volume was corrected for oedema using the following formula:

$$CIV = [RIA - (RHA - LHA)]\ x\ [section\ thickness + distance\ between\ sections\ (mm)]$$

CIV is the corrected infarct volume, RIA is right hemisphere infarct area, RHA is right hemisphere area, LHA is left hemisphere area. Total oedema volume (OV) was measured using the following formula:

$$OV = [RHA - LHA]\ x\ [section\ thickness + distance\ between\ sections\ (mm)]$$

Infarct and oedema volumes from each section were summed and expressed as mm^3.

To examine the distribution of the infarct, total, cortical, and subcortical infarct area (mm^2) were also expressed relative to bregma.

For comparison with clinically relevant infarct sizes, total infarct volume was also calculated as a percentage relative to right hemisphere volume (RHV) using the following formula:

$\%\ Infarct\ Volume$ = (CIV/(RHV-OV)) x 100

RHV was calculated by multiplying the RHA by the distance to the previous section (mm) and totalled for all 15 sections (Figure 5-2).

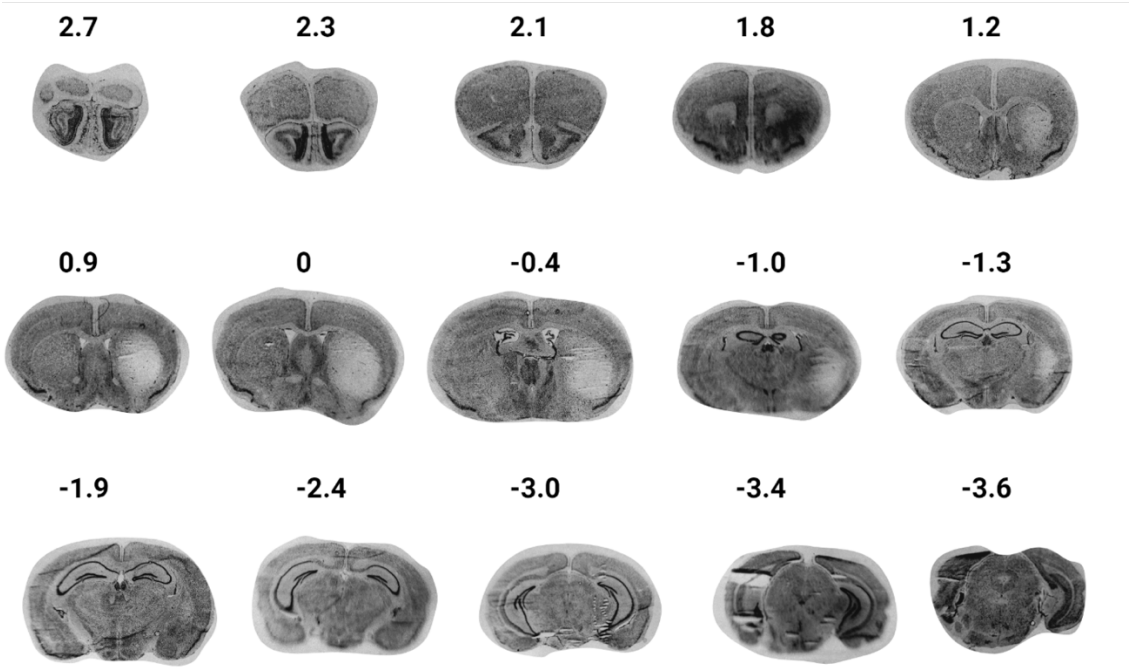

Figure 5-2. Representative coronal sections stained with thionin for infarct and oedema volume analysis, and for infarct distribution in the anteroposterior axis. Hypo-intensities delineate the infarct, which is primarily in the subcortex in most mice with the transient middle cerebral artery occlusion model. Numerical values above each section represent the location along the anteroposterior axis with values expressed relative to bregma.

5.2.5 Neurological and functional assessment in mice after tMCAo

Neurological testing was conducted at baseline (for some experiments), 24 hours and 72 hours post tMCAo in sham- and tMCAo-operated mice.

5.2.5.1 Walking test

The walking and body swing tests assess locomotion and sensorimotor function. For the walking test animals were allowed to explore an open area (30 cm x 15 cm) for 2 minutes and their walking ability was evaluated as detailed in Table 5-1. Healthy mice walk freely in all directions, while mice with a unilateral ischaemic lesion often circle to one direction when walking.

5.2.5.2 Hanging body swing test

For the hanging body swing test, mice were suspended by the tail for approximately 20 seconds. Healthy mice hang straight with forelimbs extended towards the ground and their hindlimbs in rapid locomotion mimicking a run. Mice that swing to either side with no preference show a mild deficit unrelated to the ischaemic lesion. Mice with a unilateral ischaemic lesion present with a swing biased to their left side (contralateral to the lesion). Mice that bend their body by less than 30 degrees are moderately affected by the lesion, while mice that bend by further than 30 degrees are more severely affected. Mice with the highest degree of severity display uncontrollable circling or spasms when suspended from the tail or hang straight with no response. Scores were assigned as described in Table 5-1.

5.2.5.3 Reflexes

Reflexes were also measured to ascertain nerve conduction. Using a sterile cotton bud, the pinna (external part of the ear) of the left ear and cornea of the left eye were gently touched. Normal pinna reflex involves the flattening of the ear along the surface of the head and normal eye reflex involves a blink. Absence of reflex resulted in addition of 1 point to the total mNSS assessment (Table 5-1).

5.2.5.4 Forelimb foot fault test (grid walking)

The forelimb foot fault test assesses deficits of locomotion and sensorimotor coordination by quantifying asymmetrical foot faults. This test is included instead of the commonly used balance beam test for mNSS (Schaar et al., 2010). Animals were allowed to explore an elevated circular frame with a wire grid (1.5 cm^2) by placing their feet on the wire for a maximum of 60 seconds and their movements are being recorded. A foot fault is considered a slip of a fore paw through the wire and is determined on a slowed down video analysis. Normal mice typically display relatively lower number of faults and would make faults with both their forelimbs equally (symmetrically). Mice with a unilateral ischaemic lesion display asymmetric deficits with the left (contralateral) forelimb typically being more affected. Foot fault was calculated as **contralateral forelimb faults/total number of steps*100** (Gibson et al., 2005).

During video analysis mice were observed for their general demeanour during the test and speed of movement. Mice that typically explored the whole area and moved at a fast pace were scored zero. Mild deficit (score = 1/2) was registered when animals showed preference to a small area of the platform or circled around the periphery. Moderate deficit (score = 3/4) was ascribed to mice that moved slower and hesitantly. Animals which moved very little during the test were scored as displaying a severe deficit (score = 5/6). These scores were taken towards the mNSS and are summarised in Table 5-1.

5.2.5.5 Modified neurological severity score (mNSS)

The 14-point modified neurological severity score (mNSS) was a composite of the scores ascribed through the tests described above (Bieber et al., 2019b) and summarised in Table 5-1. Data from a small pilot study has been compiled to illustrate the average contribution of each test towards the total mNSS (Figure 7-5). On day 1 after tMCAo mice scored a median of 7 or 8, and the most points were accrued from the grid walking test. On day 3 in this small cohort mice displayed a lower median score between 4-6 and the pinna reflex test did not contribute to the scores (cf. Appendix Figure 7-5).

Table 5-1. Tests included in the composite 14-score modified neurological severity score (mNSS). The walking test assessed directional bias or circling (0-3, lowest-highest deficit), the hanging body swing test to observe bias towards one side of the body (0-3, lowest-highest deficit), pinna reflex (0-1, lowest-highest deficit), corneal reflex (0-1, lowest-highest deficit), and a wire grid walking tests to measure forelimb foot fault (contralateral as % total steps, 0-6, lowest-highest deficit).

TEST	SCORE RANGE	SCORE ALLOCATION
WALKING	0-3	0 = Normal, no deficit 1 = Slight circling, mild deficit 2 = Clear circling and contralateral leaning, moderate deficit 3 = Minimal movement and contralateral leaning, severe deficit
HANGING BODY SWING	0-3	0 = Straight, normal 1 = Slight swing, mild deficit 2 = Clear swing, moderate deficit 3 = Circling/spasm, severe deficit
PINNA REFLEX	0-1	0 = Reflexes present, normal 1 = ≥1 reflexes absent, clear deficit
CORNEAL REFLEX	0-1	0 = Reflexes present, normal 1 = ≥1 reflexes absent, clear deficit
FORELIMB FOOT FAULT	0-6	0 = normal 1 = mild deficit 2 = mild deficit 3 = moderate deficit 4 = moderate deficit 5 = severe deficit 6 = severe deficit

5.2.5.6 Forelimb grip strength

Forelimb grip strength was investigated prior to, and 48 hours post tMCAo using a BIO-GS3 V3.48 grip strength meter with maximal capacity 3507 mg (BioSeb, UK). Mice were held by the base of the tail in a way which allowed them to grasp onto the T-bar of the strength meter. Once both forelimbs firmly grasped the T-bar, the mouse was gently pulled away until both forelimbs failed to hold onto the bar. The maximal force applied to the T-bar in three repetitions was recorded and the test was conducted in triplicate with sufficient breaks between measurements.

5.2.5.7 Behavioural assessment

Dexterity and motivation were assessed by the ability of the animals to build nests (Deacon, 2006b, Balkaya et al., 2013, Bieber et al., 2019b). Nest building is an innate behaviour, which indicates the animal's general wellbeing, motivation, and cognition, as it requires executive functioning. Single-housed mice were provided with 3 g of compacted square of nesting material (nestlet) and a wooden chip (cf. Appendix **Figure 7-4**) prior to stroke induction and at 48 hours after tMCAo. They were provided with soft food – freshly prepared mash, baby food and hydration gel, standard chow pellets and water *ad libitum*. Nests were assessed the following morning for several criteria and scores assigned by subtracting points for deviation from a perfect nest. For an exemplary nest, a mice would have torn all the material provided, shaped the nest into a crater with >50% of the walls higher than the mouse's height, and incorporated the wooden chip into the nest. If the nestlet was completely untouched, that resulted in a score of 2. If there was a clear attempt to build a nest, half a point was subtracted for each of the following: lack of crater shape, <80% torn nestlet material, <50% of walls being higher than mouse's body, and lack of incorporation of the wooden chip. Representative images from nesting activity are shown in Figure 5-3 for each score attributed in this study. The lowest observed score post-tMCAo in this study was 2 and the highest 5. This scoring system was adapted from (Deacon, 2006a).

Figure 5-3. Representative images of nesting 24 hours after transferring mice into single-housed cages and providing them with nesting material. A score of 2 was the lowest in this study and scores went up in 0.5 increments to a maximal score of 5. **Score 2** represents no attempt to tear the material, the wooden chip is not incorporated into the nest. **Score 2.5** the nest does not have a crater shape, the wooden chip is not incorporated into the nest. **Score 3.5** material has been torn but no crater shape has been formed, whilst an attempt to incorporate the wooden chip into the nest is clearly visible. **Score 4** has clearly tried to shape the nest into a crater, with >50% of the walls higher than the mouse's height, but points are deducted for not incorporating the wooden chip into the nest and some nesting material left untorn. **Score 4.5** has made an excellent effort building a nest, incorporated all the material with >50% of the walls higher than the mouse's height and it's only scoring sub-maximally because the wooden chip is not incorporated into the nest. **Score 5** this is an exemplary nest built prior to tMCAo; all the material provided is torn, the nest is crater shaped, >50% of the walls are higher than the mouse's height, the wooden chip is incorporated into the nest. The identities of individual animals and facility information are concealed in line with Home Office regulations on work with experimental animals.

5.2.6 Neuronal apoptosis

The TUNEL assay (Figure 5-4) is widely used to quantify the number of apoptotic cells in the infarct and peri-infarct areas after ischaemic stroke (Zhao et al., 2021, Liu et al., 2021b). An immunofluorescent TUNEL analysis was performed using In Situ Cell Death Detection Kit, Fluorescein (Roche) (Negoescu et al., 1996).

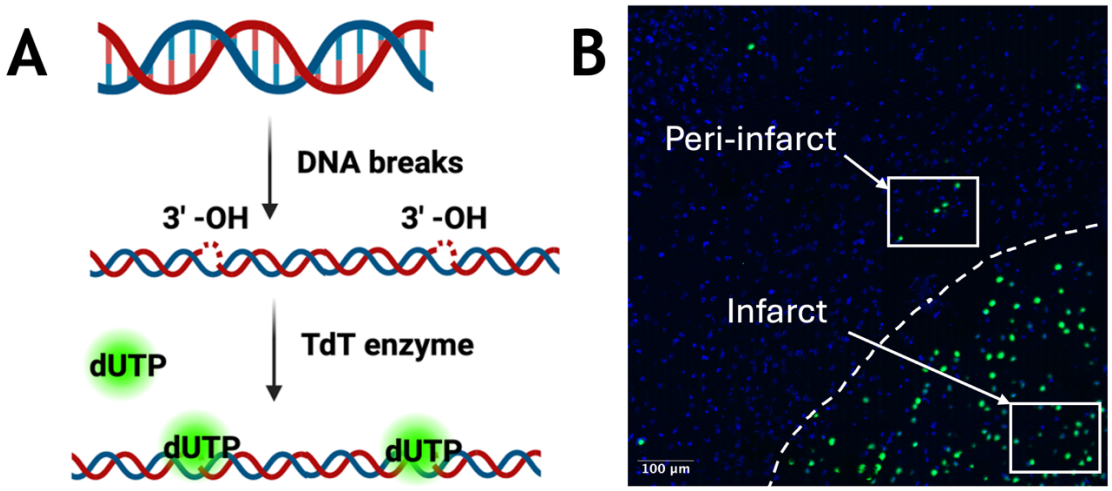

Figure 5-4. Terminal deoxynucleotidyl transferase dUTP nick end labelling (TUNEL) assay for detection of neuronal apoptosis. A) Schematic representation of the principle behind TUNEL. Single strand DNA breaks are detected and the enzyme TdT intercalates FITC-conjugated dUTP at the hydroxy terminal. B) Immunofluorescent image of C57BL6/J mouse ischaemic brain labelled with TUNEL. White dotted line depicts the border between infarct and peri-infarct and white rectangles are regions of interest for quantification of TUNEL positive cells.

Two brain sections per animal were selected for staining from region 2 (+0.25 to -1.79 mm relative to bregma). Sections were air dried for 5-10 minutes and incubated in fixation solution (4% PFA) for 20 minutes at RT. The slides were washed three times with PBS and incubated in permeabilisation solution (0.1% triton X-100 in PBS) for 2 min on ice. The slides were rinsed twice with PBS and individual sections were incubated with TUNEL reaction mixture in a humidified chamber in the dark for 60 min at 37°C. Slides were washed three times with PBS, mounted on glass coverslips (0.17 µm thickness) with Vectashield PLUS antifade mounting medium with DAPI for counterstaining (Vector Laboratories, H-2000) and allowed to dry overnight in the dark. The slides were sealed along the edges the next day with nail polish and stored at 4°C until imaging. Images were taken from 5 locations in the infarct core and 5 locations in the peri-infarct of the ischaemic hemisphere and an image was taken of the contralateral hemisphere using a 25x/0.8 W DICII objective (Zeiss LSM 900). TUNEL positive cells were counted using the Cell counter tool in Fiji imaging software, normalised to image area, and presented as cells/mm^2.

5.2.7 Immunophenotyping with flow cytometry

Immune cell numbers were assessed in DDAH2$^{fl/fl}$ and DDAH2$^{Mo-/-}$ mice from each hemisphere on day 3 following tMCAo by flow cytometric immunophenotyping. Flow cytometric sample preparation, acquisition and analysis were performed as described in section 1.4.6 in General Methods. For each sample 100,000 events were recorded, and event number was normalised to counting bead events to allow for quantification of absolute numbers per hemisphere. An immunophenotyping antibody panel was selected (Table 5-2). As discussed in Chapter 3, CD45 is a pan-leukocytic marker and CD11b is highly expressed on myeloid cells and intermediate-to-low expression is found on microglia. Ly-6G is expressed on polymorphonuclear cells and neutrophils, Ly-6C is highly expressed on monocytes and low expression is typical for macrophages, CD3 is highly expressed on T lymphocytes, and CD19 is a hallmark B cell marker. A gating strategy to assess the main leukocytes in the brain was adapted from (Pösel et al., 2016) (Figure 5-5).

Table 5-2. Antibodies for immunophenotyping myeloid and lymphoid cells.

ANTIGEN	FLUOROPHORE	HOST ISOTYPE	CLONE	CONCENTRATION (µG/ML)
CD45.2	FITC	Mouse, IgG2a, κ	104	0.25
CD11B	V500	Rat, IgG2b, κ	M1/70	5
LY-6G	PerCP (Cy5.5)	Rat IgG2a, κ	1A8	0.2
LY-6C	APC-Cy7	Rat IgM, κ	AL-21	0.2
CD3	PE	Armenian Hamster, IgG	145-2C11	5
CD19	PE-Cy7	Rat IgG2a, κ	6D5	5

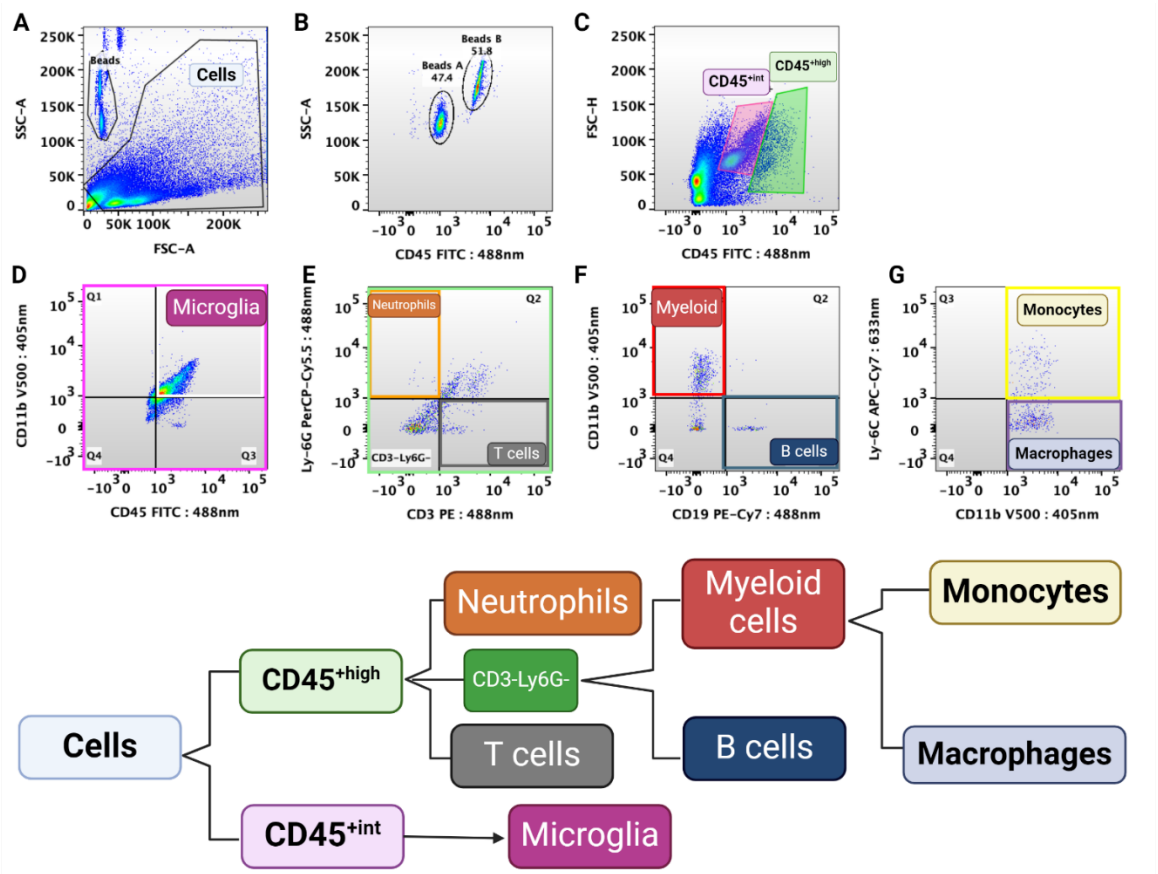

Figure 5-5. Flow cytometric gating strategy for analysis of major leukocyte populations from freshly isolated mouse brains. Counting beads were gated and further separated using the FITC channel into beads A and beads B to ensure the validity of the counting. Single cells were gated for pan-leukocytic marker CD45 and then into $CD45^{+high}$ and $CD45^{+int}$ cells. The following leukocyte populations were then gated from the $CD45^{+high}$ populations: neutrophils ($CD45^{+high}Ly6G^{+}$), T cells ($CD45^{+high}CD3^{+}$), and double-negative cells ($CD3^{-}Ly6C^{-}$), the latter subsequently gated into B cells ($CD45^{+high}CD19^{+}$) and myeloid cells ($CD45^{+high}CD11b^{+}$). Myeloid cells were split into monocytes ($CD45^{+high}CD11b^{+}Ly6C^{+high}$) and macrophages ($CD45^{+high}CD11b^{+}Ly6C^{+low}$). Microglia ($CD45^{+int}CD11b^{+}$) were gated from the intermediate CD45 ($CD45^{+int}$).

All flow cytometric acquisition was performed on BD FACS Canto II with excitation and emission parameters for the antibody panel presented in Figure 5-6 and the cytometer's configuration is presented in Table 5-3.

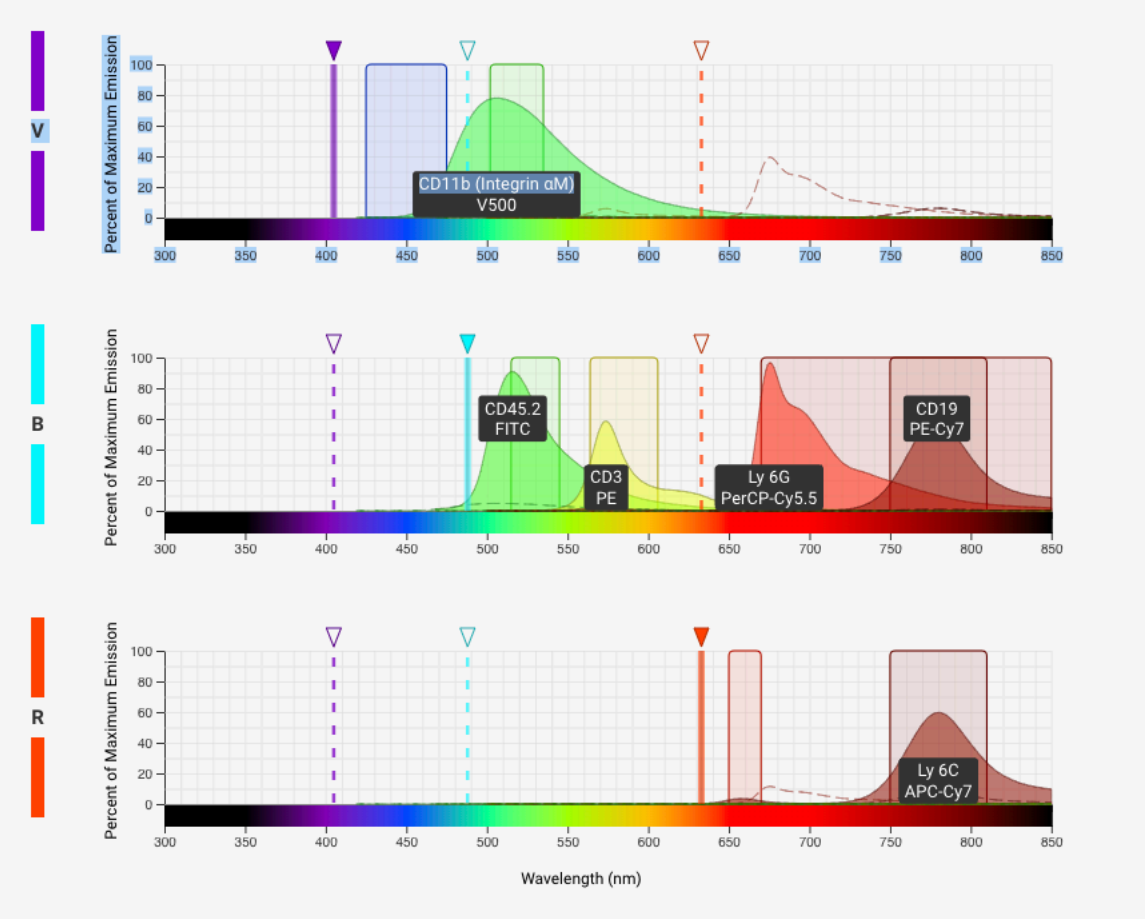

Figure 5-6. Cytometer setup - excitation and emission ranges of the leukocyte panel. The Violet Trigon laser excites V500, the Blue Octagon laser excites FITC, PE, PE-Cy7 and PerCP-Cy5.5. Figure created on BD Research Cloud.

Table 5-3. BD FACS Canto II cytometer configuration for immunophenotyping.

ANTIGEN	FLUOROPHORE	LASER	FILTER	MIRROR
CD11B	V500	**Violet Trigon 405 30mw**	510/50	502LP
CD45.2, CD3	FITC, PE	**Blue Octagon 488 20mW**	585	586LP
CD19	PE-Cy7	**Blue Octagon 488 20mW**	780/60	735LP
LY6G	PerCP-Cy5.5	**Blue Octagon 488 20mW**	670LLP	655LP
LY6C	Apc-Cy7	**Red Trigon 633 17mW**	780/60	735LP

5.2.8 Power calculations and statistical analysis

To estimate the size of groups needed for this pilot study, statistical power was calculated using G* Power calculation software (Heinrich Heine University, Germany). The infarct volume analysis is the most variable outcome measure in

this study, due to the variability of this stroke model, which substantiated its use for sample size calculations (Serdar et al., 2021). It was presumed that the estimated power is also sufficient to test for differences in the neurological and functional data. Using mean and SD infarct volume data from previous data sets from our laboratory, where infarct size was either increased or decreased by a pharmacological agent, it was estimated that n=14 per group were required to detect a minimum difference of 65% infarct size between knockout and control mice (α=0.05, power = 0.8 [β=0.2], effect size=1.14). To calculate the number of animals required per group for the immune cell infiltration analysis, mean and SD values from previously published data were used (Chu et al., 2014). To detect differences between two groups using a two-way ANOVA, it was estimated that the minimum animals required per group were n=10 (α = 0.05, power = 0.8 [β = 0.2], ANOVA: fixed effects, omnibus, one-way).

All data sets were analysed with GraphPad Prism Software 8.0. Group numbers are indicated in the corresponding figure legends and $P<0.05$ was considered statistically significant. Continuous data was expressed as mean ± standard error of the mean (SEM). This includes percentage changes in rCBF and body weight loss after tMCAo, cell numbers obtained with flow cytometric analysis, infarct area, infarct volume, and oedema volume, and neurological (forelimb foot fault test) and motor function (forelimb grip strength, and the semi-quantification of TUNEL-positive cells after tMCAo.

Descriptive statistics were used to determine mean or median, standard deviation (SD) and standard error of the mean (SEM), and to inform the choice of statistical test. Normal data distribution was analysed by Kolmogorov-Smirnov test or Shapiro-Wilk test for n>8 and D'Agostino & Pearson test for n<8. Unpaired t-tests (with Welch's correction for unequal SD) were used for comparisons between genotypes of rCBF drop at the beginning of ischaemia and rCBF reperfusion 10 min after filament withdrawal, % body weight loss pre tMCAo and on day 3, infarct and oedema volumes. A two-way ANOVA with Šídák's multiple comparisons test was used for comparing immune cell numbers between genotypes and hemispheres. A two-way ANOVA with Tukey's multiple comparisons post hoc test was used to compare TUNEL-positive cells in the infarct core and peri-infarct brain regions. For analyses with missing values, mixed effects ANOVA model with Šídák's

multiple comparisons test was used instead of a two-way repeated measures ANOVA. These include comparisons between genotypes of rCBF in the ischaemic period, forelimb grip strength and foot fault asymmetry index.

Scored data from nest building activity and the modified neurological severity score was expressed as median. For comparisons of nest building activity between genotypes pre- and post-tMCAo Mann Whitney U test was used and for comparisons between pre- and post-tMCAo in each genotype a Wilcoxon test was used. A Mann Whitney U test was also used to compare mNSS score between genotypes on day 1 and day 3. A Friedman test with Dunn's multiple comparisons test was used to compare mNSS score between pre-tMCAo, day 1 and day 3 for each genotype.

5.3 Results

5.3.1 Quantification of infiltrating immune cells and microglia in the brain of DDAH2$^{fl/fl}$ and DDAH2$^{Mo-/-}$ mice after tMCAo

To investigate the potential effect of monocyte/macrophage specific DDAH2 deletion on immune cell infiltration into the ischaemic brain, the numbers of infiltrating immune cells and microglia in the brain of DDAH2$^{fl/fl}$ and DDAH2$^{Mo-/-}$ mice after tMCAo were quantified. A relatively short occlusion period of 40 min was chosen, as this was the first stroke study in these genetically modified animals.

5.3.1.1 Extent of cerebral hypoperfusion and weight loss in DDAH2$^{fl/fl}$ and DDAH2$^{Mo-/-}$ mice after 40 min tMCAo

The impact of genetic deletion of DDAH2 in macrophages on surgically induced changes in rCBF were investigated. In our laboratory, successful tMCAo requires a ≥70% reduction of rCBF following insertion of the filament, while reperfusion requires a ≥80% restoration of baseline rCBF within 10 minutes of filament withdrawal. The rCBF drop following insertion of the filament did not reach ≥70% in 4 out of the 8 DDAH2$^{Mo-/-}$ mice. In 3 DDAH2$^{Mo-/-}$ and 2 DDAH2$^{fl/fl}$ mice rCBF did not reach ≥80% of baseline upon filament removal. However, incorrect probe placement over the vascular territory affected by tMCAo could affect the rCBF readings and given that this was the first stroke study using DDAH2 knockout mice, all mice were included in subsequent analyses. There were no statistical

differences between the two genotypes for rCBF at the time of filament insertion (unpaired t test, P>0.05), following filament removal (unpaired t test, P>0.05). Regional CBF was mostly stable throughout the ischaemia period in both genotypes, apart from at 10 minutes after filament insertion, mixed effects analysis with Sidak's multiple comparisons test, P<0.05 (Figure 5-7A).

Acute weight loss is a common feature after tMCAo and some studies have shown that it positively correlates with infarct volume (Cai et al., 2015). There was no difference between the genotypes in terms of baseline body weight: 25.4±0.9 g vs 25.8±1.1 g, DDAH2$^{fl/fl}$ vs DDAH2$^{Mo-/-}$, unpaired t test, P>0.05, mean±SEM, n=8. Body weight decreased in both genotypes to a similar degree on day 3 post 40 min tMCAo: - 10.9±1.4% vs – 9.4±1.4%, DDAH2$^{fl/fl}$ vs DDAH2$^{Mo-/-}$, unpaired t test, P>0.05, mean±SEM, n=8 (Figure 5-7B).

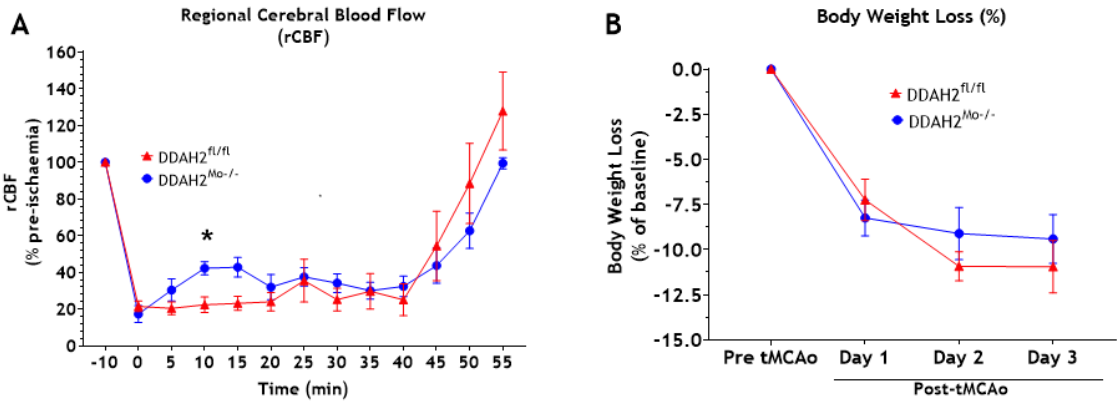

Figure 5-7. Temporal changes in regional cerebral blood flow (rCBF) (A) and body weight loss (B) in DDAH2$^{fl/fl}$ and DDAH2$^{Mo-/-}$ mice following 40 min transient middle cerebral artery occlusion (tMCAo). Data is presented as mean ± SEM, n=8. Statistical analyses for DDAH2$^{fl/fl}$ vs DDAH2$^{Mo-/-}$ included mixed effects analysis with Sidak's multiple comparisons test during ischaemia (P>0.05, *P<0.05 at 10 minutes), unpaired t test at the time of filament insertion (at 0 min, P>0.05), unpaired t test following filament removal (at 60 min, P>0.05), and unpaired t test for weight loss on day 3 post tMCAo, DDAH2$^{fl/fl}$ vs DDAH2$^{Mo-/-}$ (P>0.05).

5.3.1.2 Monocyte/macrophage specific DDAH2 deletion has no impact on total leukocyte and microglia into the ischaemic brain

To confirm that any effect of monocytes/macrophage DDAH2 deletion on stroke outcomes can be attributed to direct actions on the ischaemic brain, rather than occurring secondary to reduced immune cell infiltration, leukocyte frequencies were investigated using flow cytometry. Although it has previously been reported

that iNOS deletion does not affect rates of leukocyte infiltration in the ischaemic brain (Garcia-Bonilla et al., 2014), genetic deletion of DDAH2 in monocytes and macrophages might result in altered infiltration of immune cells into the brain, possibly through releasing an activator of Sp1 transcription factor in endothelial cells and inducing a VEGF-dependent signalling pathway (Hasegawa et al., 2006). The number of single cells was around 700,000 cells per hemisphere and comparable between the ipsilateral and contralateral hemispheres and between genotypes (Figure 5-8A). The numbers of leukocytes ($CD45^{+}$) were about 100,000 per hemisphere and were higher in the ipsilateral compared to contralateral hemispheres in $DDAH2^{Mo-/-}$ mice but there were no statistical differences, and there were comparable numbers of $CD45^{+}$ cells in the $DDAH2^{fl/fl}$ mice (Figure 5-8B). Microglia ($CD45^{int+}CD11b^{+}$) numbers constituted about a half of the detected leukocytes and no statistically significant differences were observed (Figure 5-8C).

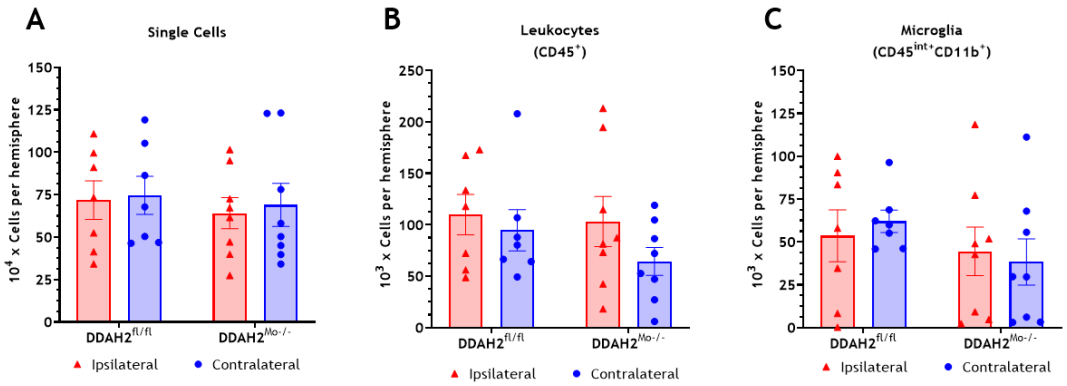

Figure 5-8. The impact of monocyte/macrophage specific DDAH2 deletion on immune cell infiltration following transient middle cerebral artery occlusion (tMCAo) obtained by flow cytometric analysis. Single cells (A), total leukocytes ($CD45^{+}$) (B), and microglia ($CD45^{int+}CD11b^{+}$) (C). Data is presented as mean±SEM, n=7-8, two-way ANOVA with Sidak's multiple comparisons test, P>0.05.

5.3.1.3 Monocyte/macrophage specific DDAH2 deletion does not impact on the number of myeloid sub-populations in the ischaemic brain

No genotype effects were detected within ipsilateral or contralateral hemispheres between $DDAH2^{fl/fl}$ and $DDAH2^{Mo-/-}$ mice after stroke (Figure 5-9). Additionally, the numbers of myeloid cells ($CD45^{+high}CD11b^{+}$) was comparable between the ischaemic and contralateral hemispheres of $DDAH2^{fl/fl}$ and $DDAH2^{Mo-/-}$ mice after stroke (Figure 5-9A). Similarly, the number of monocytes ($CD45^{+high}CD11b^{+}Ly\text{-}6C^{+high}$) remained insignificantly higher in ipsilateral versus contralateral hemispheres (Figure 5-9B). The numbers of macrophages ($CD45^{+high}CD11b^{+}Ly\text{-}$

6C^{+low}) were likewise detected in comparable numbers in the two hemispheres in both genotypes (Figure 5-9C).

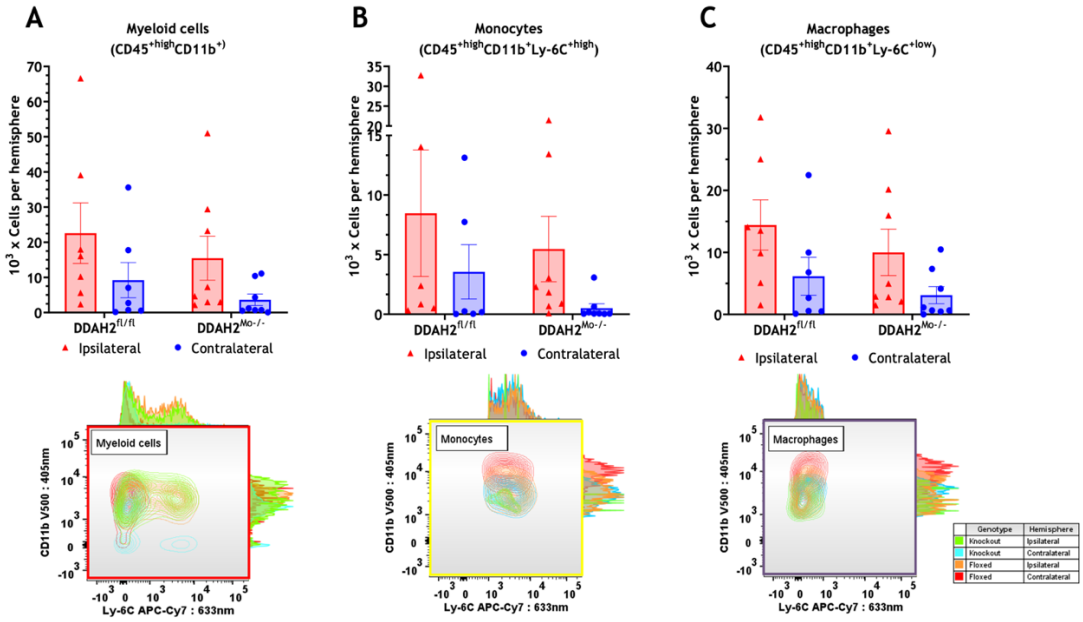

Figure 5-9. Quantification and representative contour flow cytometric plots of myeloid cells (CD45^{hi+}CD11b^{+}), monocytes (CD45^{+hi}CD11b^{+}Ly6C^{+hi}), and macrophages (CD45^{+hi}CD11b^{+}Ly6C^{+low}) in ipsilateral and contralateral hemispheres from DDAH2$^{fl/fl}$ and DDAH2$^{Mo-/-}$mice following transient middle cerebral artery occlusion (tMCAo). Data is presented as mean ± SEM, n=7-8, two-way ANOVA for genotype and stroke effects with Sidak's multiple comparison test, P>0.05.

5.3.1.4 Lack of impact of monocyte/macrophage specific DDAH2 deletion on the number of other immune cell populations infiltrating into the ischaemic brain

The ability of other leukocytic populations to infiltrate into the brain of mice that are lacking DDAH2 in monocytes/macrophages was additionally examined. Similar to the myeloid populations, there was a trend for higher numbers of T lymphocytes (CD45^{+hi}CD3^{+}) and B lymphocytes (CD45^{+hi}CD19^{+}) in the ipsilateral hemispheres, but there were no statistical differences (Figure 5-10A). On average only <100 neutrophils (CD45^{+hi}Ly6G^{+}) and B lymphocytes were detected, and in half of the mice from both genotypes cells from these subpopulations were not detected (Figure 5-10B-C).

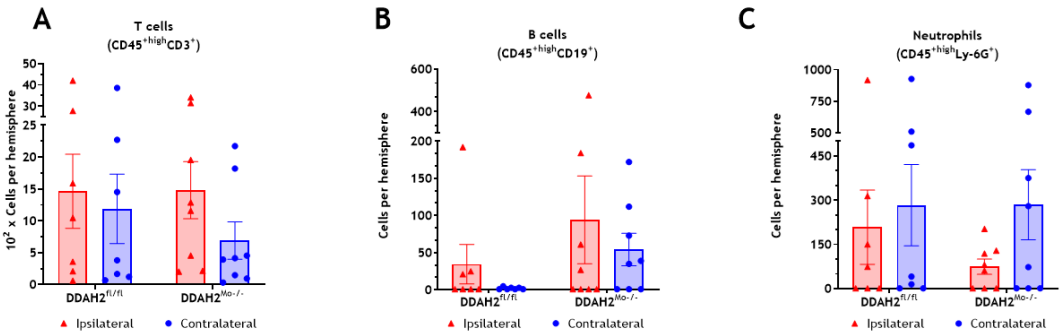

Figure 5-10. Number of neutrophils ($CD45^{+hi}Ly6G^{+}$) (A), T lymphocytes ($CD45^{+hi}CD3^{+}$) (B), B lymphocytes ($CD45^{+hi}CD19^{+}$) (C), in ipsilateral (ischaemic) and contralateral hemispheres of $DDAH2^{fl/fl}$ and $DDAH2^{Mo-/-}$ mice following transient middle cerebral artery occlusion obtained by flow cytometric analysis (tMCAo). Data presented as mean ± SEM, n=7-8, two-way ANOVA for genotype and stroke effects with Sidak multiple comparison's test, P>0.05.

Overall, the data suggests that monocyte/macrophage specific DDAH2 deletion does not affect the number of brain resident microglia or the capacity of myeloid cells to infiltrate into the ischaemic brain.

5.3.2 Effect of monocyte/macrophage-specific DDAH2 deletion on stroke outcomes in $DDAH2^{fl/fl}$ and $DDAH2^{Mo-/-}$ mice after 60 min tMCAo

5.3.2.1 Mortality and exclusions

There were no mortalities, and one mouse was culled due to exceeding severity limits. While CBF values were collected by a laser Doppler probe to confirm the level of hypoperfusion in each mouse, to mitigate for probes becoming loosened during the procedure or for faulty positioning over a vascular territory different from the MCA, the successful placement of the filament was additionally determined by scores on the filament that denote it was inserted to a depth of approximately 10 ± 1 mm (Hata et al., 1998, Ansari et al., 2011). Therefore, as this was a pilot study in these genetically modified mice aiming to assess infarct volume, despite some mice not achieving this ischaemia-reperfusion threshold criteria discussed above in Section 5.3.1.1, they were recovered, assessed to not have surpassed severity limits, culled at the scientific timepoint, and included in all analyses with the following omissions.

- Data for rCBF was not recorded for one $DDAH2^{fl/fl}$, as the laser doppler probe got detached during surgery.

- Pre-tMCAo forelimb grip and foot fault data were collected from all but two mice from the DDAH2$^{fl/fl}$ group.

- Post tMCAo (day 1 and day 3) neurological and forelimb grip tests were not performed on two of the DDAH2$^{fl/fl}$ mice due to them scoring ≥6 on the clinical severity (for reference, scores of 6–9 resulted in the mouse being monitored several times a day and euthanasia considered).

- The quality of coronal sections in one DDAH2$^{fl/fl}$ mouse and in one DDAH2$^{Mo-/-}$ was too poor to allow accurate infarct analysis.

5.3.2.2 Extent of cerebral hypoperfusion and weight loss

The rCBF was compared between the genotypes to ensure both groups have experienced the same degree of ischaemia and reperfusion. Likewise, weight loss was also investigated, and thus any differences in infarct size and neurological outcomes cannot be attributed to one group of mice experiencing a more severe drop/better reperfusion in rCBF or greater weight loss. All DDAH2$^{fl/fl}$ mice and 4 out of the 6 DDAH2$^{Mo-/-}$mice achieved the required ≥70% reduction in CBF following insertion of the filament (Figure 5-11A). Following filament removal, 4 out of the 5 DDAH2$^{fl/fl}$ mice, and 4 out of the 6 DDAH2$^{Mo-/-}$mice achieved the required ≥80% restoration of CBF. Nevertheless, as mentioned, given this is a pilot study, all mice were included in subsequent analyses. Importantly, the extent of hypoperfusion following filament insertion, during ischaemia and upon restoration of perfusion following removal of the filament were comparable between genotypes (Figure 5-11A). There was no difference between the genotypes in terms of baseline body weight: 23.7±2g vs 24±1g, mean±SEM, n=6, unpaired t test, DDAH2$^{fl/fl}$ vs DDAH2$^{Mo-/-}$, $P>0.05$. Body weight decreased in both genotypes to a similar degree on day 3 post 60 min tMCAo: - 10±2% vs - 13±2%, mean±SEM, n=6, unpaired t test, DDAH2$^{Mo-/-}$ vs DDAH2$^{fl/fl,}$, $P>0.05$ (Figure 5-11B).

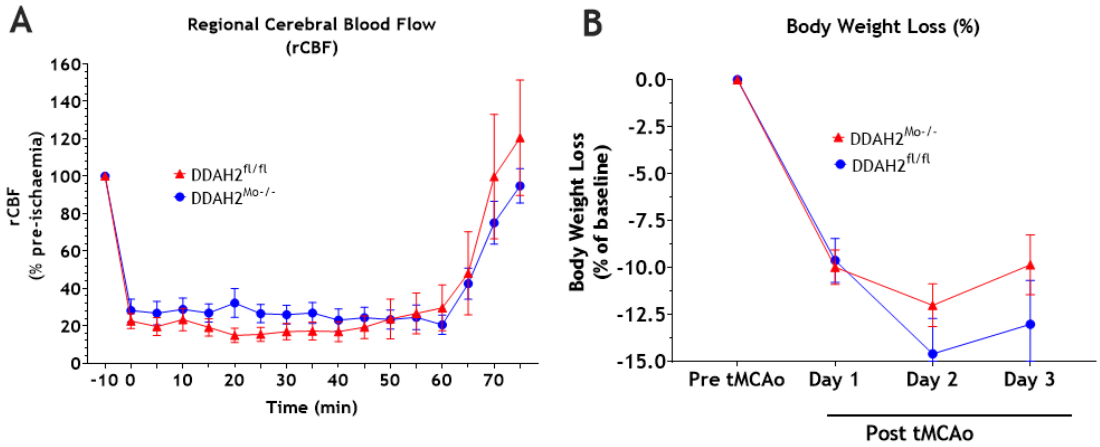

Figure 5-11. Temporal changes in regional cerebral blood flow (rCBF) (A) and body weight loss (B) in DDAH2$^{fl/fl}$ and DDAH2$^{Mo-/-}$ mice following 60 min transient middle cerebral artery occlusion (tMCAo). Data presented as mean ± SEM, n=5-6. Statistical analyses for DDAH2$^{fl/fl}$ vs DDAH2$^{Mo-/-}$ included mixed effects analysis with Sidak's multiple comparisons test during ischaemia (P>0.05), unpaired t test at the time of filament insertion (at 0 min, P>0.05), unpaired t test following filament removal (at 60 min, P>0.05), and unpaired t test for weight loss on day 3 post tMCAo, DDAH2$^{fl/fl}$ vs DDAH2$^{Mo-/-}$ (P>0.05).

In mice hypothermia has been shown to be neuroprotective in stroke models (Zhao et al., 2020). To avoid hypothermia core body temperature was monitored by the use of a rectal probe every 5 minutes during the surgery (a total of 17 readings), both for animal welfare and to mitigate the protective effects of hypothermia on infarct size (Hemmen and Lyden, 2009). The average recorded temperature over the tMCAo period was comparable between genotypes: 36.5 ± 0.2 °C vs 36.7 ± 0.01 °C, mean±SEM, n=6, DDAH2$^{Mo-/-}$ vs DDAH2$^{fl/fl}$, unpaired t test, P>0.05.

5.3.2.3 Lack of effect of monocyte/macrophage-specific DDAH2 deletion on neurological and functional deficits after 60 min tMCAo

To investigate forelimb muscle strength and neuromuscular function, forelimb grip strength was measured (Au et al., 2024). There were no significant differences in grip strength between genotypes (Figure 5-12A). Cognitive deficits in building a nest after tMCAo were also investigated. DDAH2$^{fl/fl}$ mice built poorer nests (median score 2.5) post-tMCAo compared to pre tMCAo (median score 5) (Wilcoxon paired test, *P<0.05). In comparison, DDAH2$^{Mo-/-}$ mice retained a median score of 4.5 post-stroke versus a median of 5 pre-tMCAo (Wilcoxon paired test, P>0.05). Despite the higher scoring in DDAH2$^{Mo-/-}$ mice post-tMCAo, there were no significant genotype differences post-tMCAo (Mann Whitney unpaired test, P>0.05, DDAH2$^{fl/fl}$ vs DDAH2$^{Mo-/-}$) (Figure 5-12B).

Differences in the ability to integrate motor responses, asymmetry, locomotion, and sensorimotor coordination were assessed by the foot fault test. Pre-tMCAo mice displayed functional symmetry in the use of forelimbs, which resulted in <3.5% contralateral faults as a percentage of total steps taken (average of 85 steps/test) (Figure 5-12C). On day 1 following tMCAo both genotypes showed lower total step count to an average of 55 steps/test and higher deficits in neurological function resulted in increased frequency of foot faults in both genotypes, but no differences arose between genotypes (mixed effects ANOVA with Sidak's multiple comparison tests between $DDAH2^{fl/fl}$ vs $DDAH2^{Mo-/-}$, $P>0.05$). While mice from both genotype groups made more faults compared to baseline on day 3 too, differences between genotypes were not significant (mixed effects ANOVA with Sidak's multiple comparison tests between $DDAH2^{fl/fl}$ vs $DDAH2^{Mo-/-}$, $P>0.05$).

Mice that have not experienced tMCAo scored zero on the composite neurological score mNSS (Figure 5-12D). Unsurprisingly, mice in both genotypes scored higher on day 1 post tMCAo. On day 3 following tMCAo, $DDAH2^{Mo-/-}$ mice showed an improvement in mNSS between day 1 and day 3 (Wilcoxon paired tests (day 1 vs day 3, $DDAH2^{Mo-/-}$ #$P<0.05$, $DDAH2^{fl/fl.}$, $P>0.05$). However, there were no differences between $DDAH2^{Mo-/-}$ and $DDAH2^{fl/fl}$ mice at either timepoint (Mann-Whitney unpaired tests $DDAH2^{fl/fl}$ vs $DDAH2^{Mo-/-}$ on day 1, $P>0.05$, on day 3, $P>0.05$). Since this data is very preliminary, it is hard to conclude an effect of DDAH2 on neurological outcomes after tMCAo.

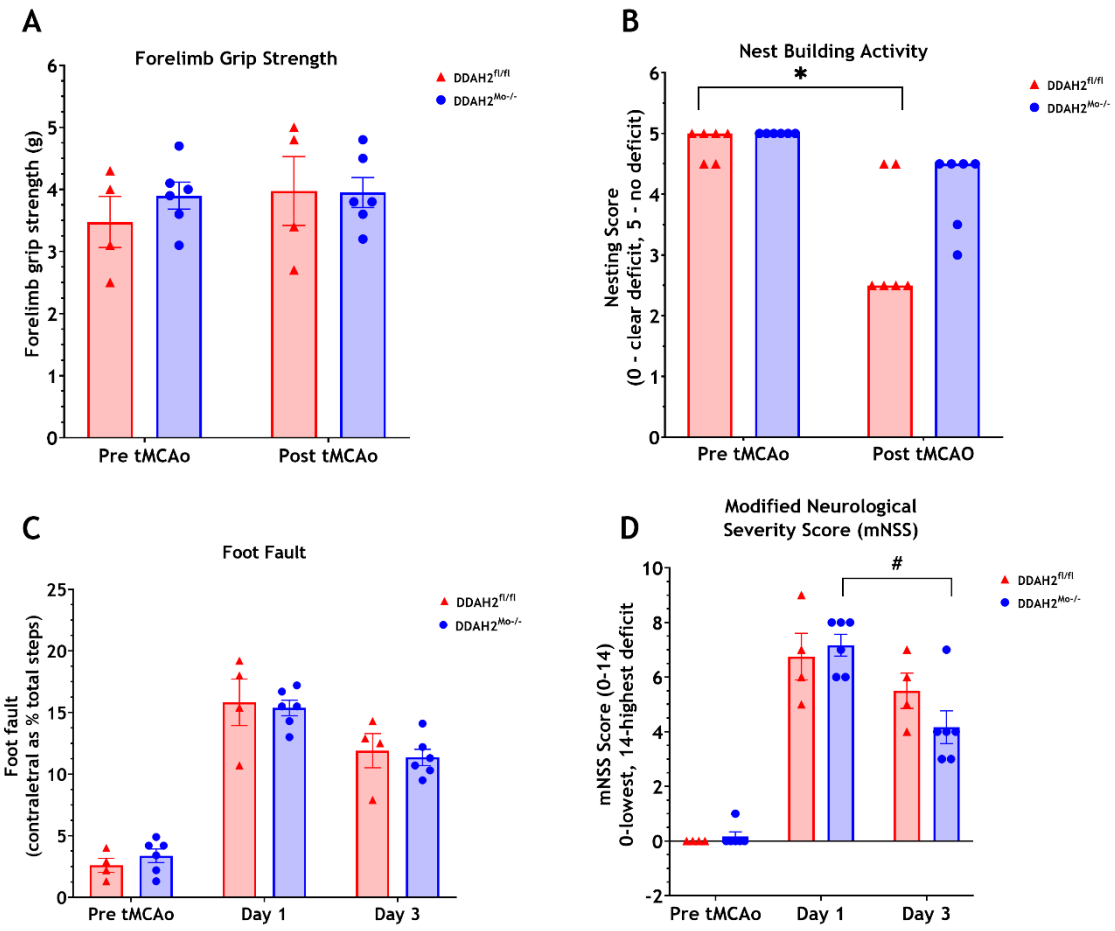

Figure 5-12. Effect of monocyte/macrophage selective DDAH2 deletion on neurological and functional outcomes after 60 minutes transient middle cerebral artery occlusion (tMCAo) in DDAH2$^{fl/fl}$ and DDAH2$^{Mo-/-}$ mice. Functional deficits were investigated pre and on day 2 post tMCAo. A) Forelimb grip strength, data is presented as mean ± SEM, n=4-6, two-way ANOVA with Sidak multiple comparisons test, P>0.05. B) Nest building activity score, data is presented as median, n=6, Mann Whitney test (DDAH2$^{fl/fl}$ vs DDAH2$^{Mo-/-}$, P>0.05) and Wilcoxon matched pairs test (pre vs post tMCAo, DDAH2$^{fl/fl}$ *P<0.05, DDAH2$^{Mo-/-}$, P>0.05). Neurological deficits were investigated pre tMCAo, on day 1 and on day 3 post tMCAo. C) Foot fault is presented as the number of errors made by the contralateral limb as a percentage of the total steps taken, mean ± SEM, n=4-6, mixed model ANOVA with Sidak's multiple comparisons test (DDAH2$^{Mo-/-}$ vs DDAH2$^{fl/fl}$, P>0.05). The modified neurological severity score (mNNS) is presented as median, n=4-6, Wilcoxon paired tests (day 1 vs day 3, DDAH2$^{Mo-/-}$ #P<0.05, DDAH2$^{fl/fl.}$, P>0.05) and Mann-Whitney unpaired tests DDAH2$^{fl/fl}$ vs DDAH2$^{Mo-/-}$ (on day 1, P>0.05, on day 3, P>0.05).

5.3.2.4 Lack of effect of monocyte/macrophage-specific DDAH2 deletion on total infarct and oedema volumes after 60 min tMCAo

A major measurable outcome from the tMCAo model is infarct and oedema volume. In this pilot study the effect of monocyte specific DDAH2 deletion on infarct and oedema volume were examined. There was no statistical difference in infarct volume between the DDAH2$^{Mo-/-}$ and DDAH2$^{fl/fl}$ mice (Figure 5-13A). Oedema volume was comparable between DDAH2$^{fl/fl}$ and DDAH2$^{Mo-/-}$, with a mouse in each

group displaying higher oedemic volume (Figure 5-13B). Representative images of thionin stained coronal sections demonstrate the infarct area was primarily subcortical and only 3 animals displayed cortical infarcts in this study(Figure 5-13C&D).

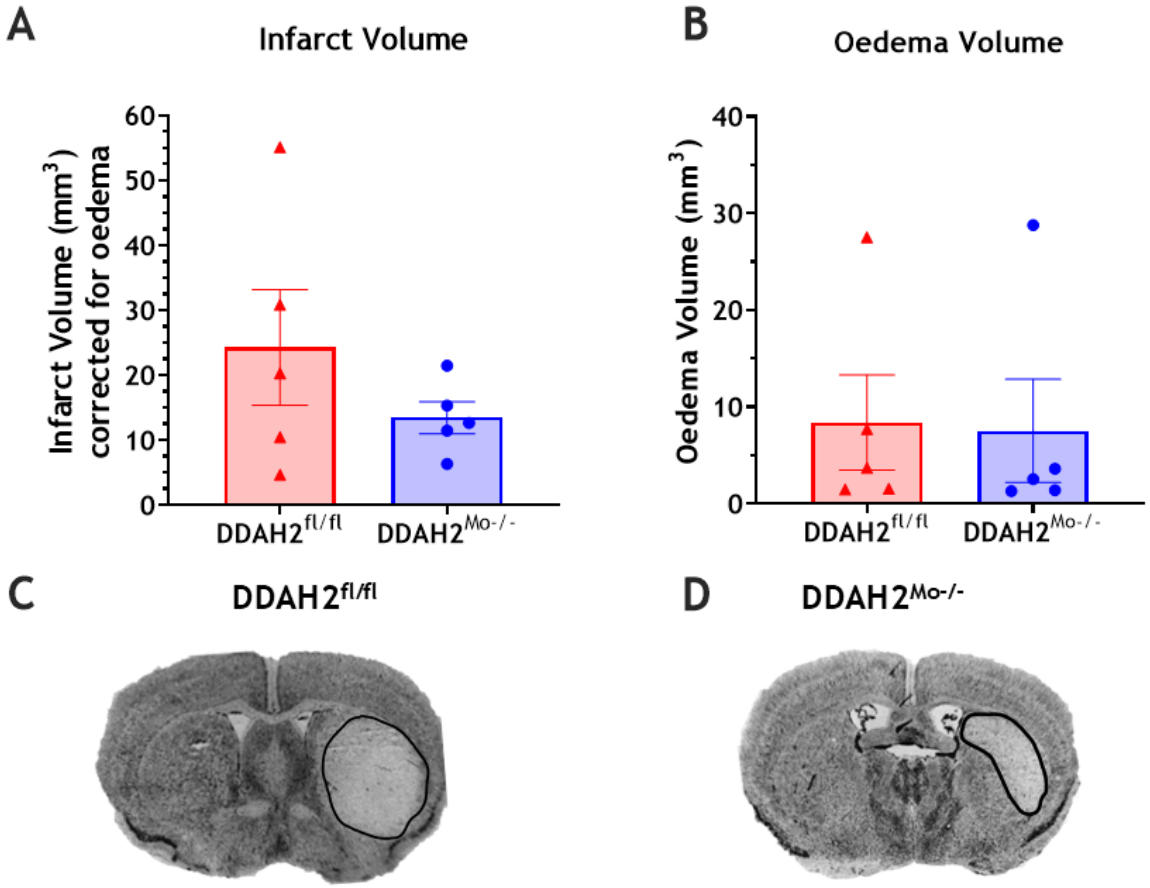

Figure 5-13. Extent of brain injury and oedema following 60 minutes transient middle cerebral artery occlusion (tMCAo) in DDAH2$^{fl/fl}$ and DDAH2$^{Mo-/-}$ mice. Total infarct (A) and oedema volumes (B), mean ± SEM, n=5, Welch t test, P>0.05. Representative thionin stained coronal sections from DDAH2$^{fl/fl}$ (C) and DDAH2$^{Mo-/-}$ (D) mice and infarct area was determined by discoloration and is annotated by a black contour line.

In clinical stroke infarct volume is typically about 4-14% of the hemispheric volume, or about 20 mm^3 in mice (Carmichael, 2005). In this study the volume the infarct occupied in the ipsilateral hemisphere of DDAH2$^{Mo-/-}$ mice was 1.6-fold lower compared to control, but it was not significant, and in both experimental groups the percentage from the ipsilateral hemisphere fell within the reference range (Figure 5-14A). The bulk of the infarct positioned between 2 and -2 mm from bregma in both DDAH2$^{fl/fl}$ and DDAH2$^{Mo-/-}$ mice, and the distribution of

infarct area along the anteroposterior axis had a distinctive peak at 0.5 mm posterior to bregma (Figure 5-14B).

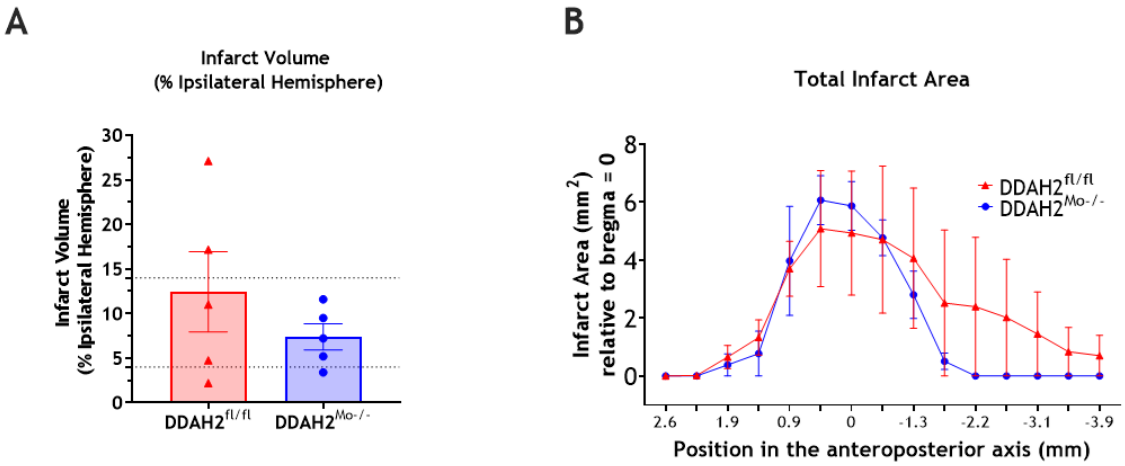

Figure 5-14. Characterisation of infarct volume and distribution in DDAH2$^{fl/fl}$ vs DDAH2$^{Mo-/-}$mice after 60 min transient middle cerebral artery occlusion (tMCAo). A) Infarct volume as a percentage of total ipsilateral hemispheric volume. Dotted lines depict the infarct size range (4-14%) reported in clinical studies (Carmichael, 2005). B) Total infarct area along the anteroposterior brain axis relative to bregma. Data is displayed as mean ± SEM, n=5. Welch t test, DDAH2$^{fl/fl}$ vs DDAH2$^{Mo-/-}$, P>0.05 (A) and two-way ANOVA (B), P>0.05.

5.3.3 Monocyte/macrophage DDAH2 contributes to DNA strand breaks after tMCAo

The number of TUNEL-positive cells in the infarct core and peri-infarct brain regions in DDAH2$^{fl/fl}$ and DDAH2$^{Mo\ -/-}$ mice after 60 minutes tMCAo was investigated using the TUNEL assay. There were 2-fold more TUNEL-positive cells in the DDAH2$^{fl/fl}$ mice compared to DDAH2$^{Mo\ -/-}$ in both the ischaemic core and the peri-infarct (Figure 5-15, Figure 5-16). There were negligible TUNEL-positive cells in the contralateral hemispheres from both genotypes. This data indicates that in the DDAH2$^{Mo\ -/-}$ mice the extent of DNA strand breaks was lower compared with the DDAH2$^{fl/fl}$ mice, indicating that monocyte/macrophage DDAH2 may contribute to apoptosis after tMCAo.

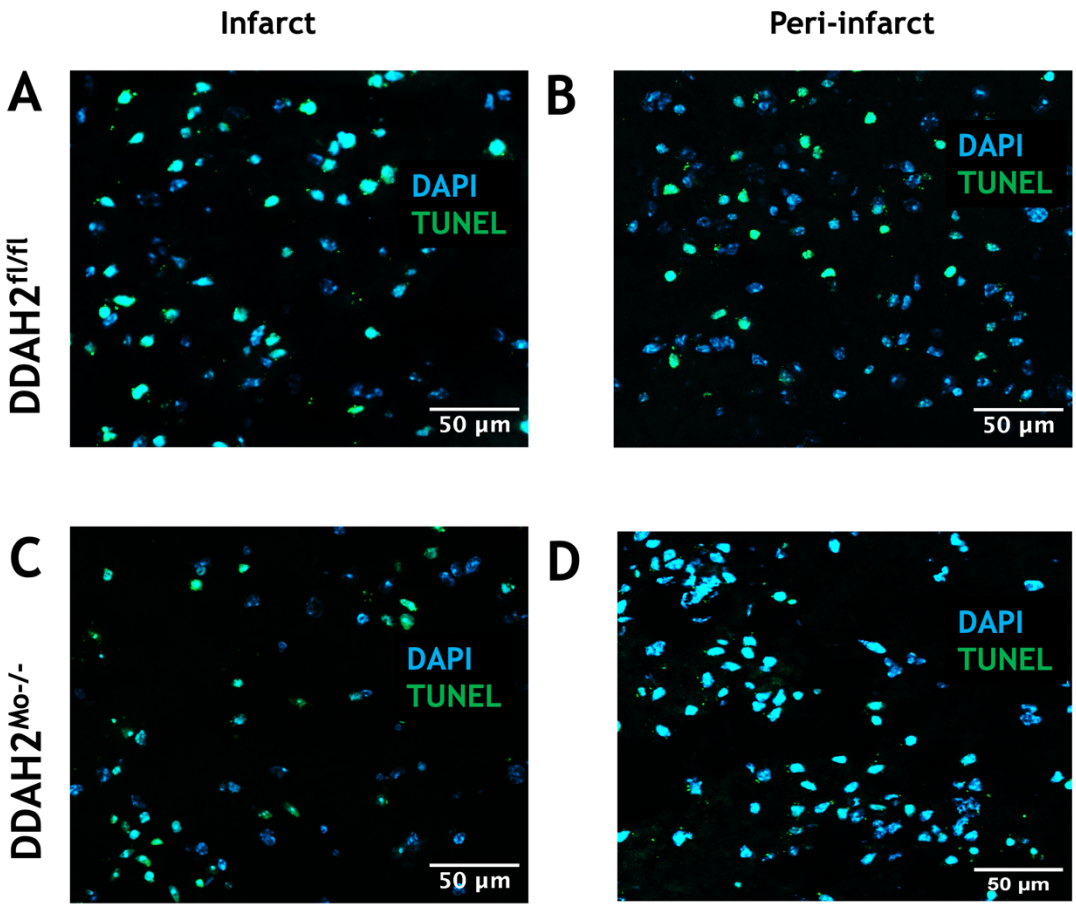

Figure 5-15. Representative confocal images of terminal deoxynucleotidyl transferase dUTP nick end labelling (TUNEL) positive cells in the infarct and peri-infarct areas following transient middle cerebral artery occlusion (tMCAo) in DDAH2$^{fl/fl}$ and DDAH2$^{Mo\ -/-}$ mice. Scale bar = 50 µm, 25x magnification.

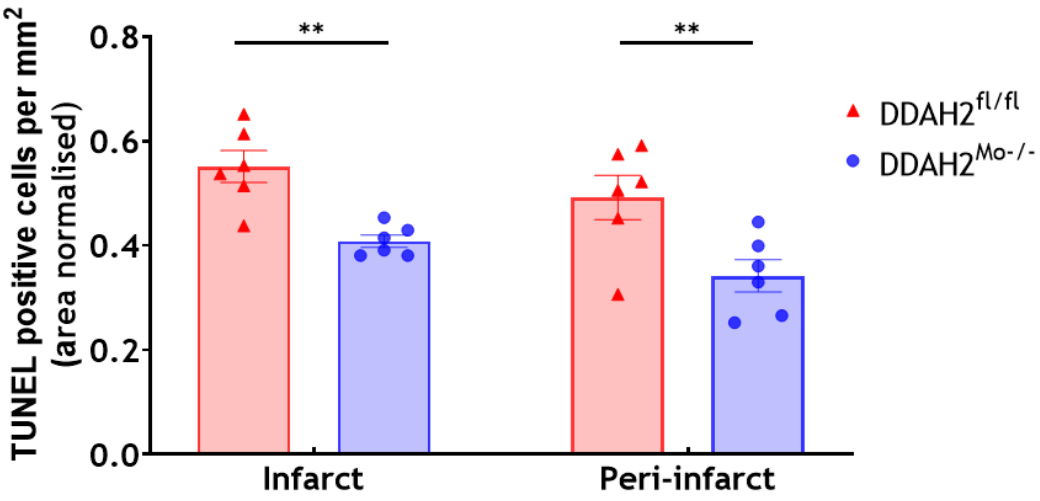

Figure 5-16. Quantification of DNA strand breaks as determined by terminal deoxynucleotidyl transferase dUTP nick end labelling (TUNEL) positive cells per area in the infarct and peri-infarct areas following transient middle cerebral artery occlusion (tMCAo) in DDAH2$^{fl/fl}$ and DDAH2$^{Mo\ -/-}$ mice. Data is presented as mean ± SEM, n=6, two-way ANOVA with Sidak's multiple comparison test (DDAH2$^{fl/fl}$ vs DDAH2$^{Mo\ -/-}$), **P<0.01.

5.4 Discussion

In this chapter it was aimed to establish whether deletion of DDAH2 in monocytes can influence the outcomes of stroke. It was hypothesised that lower levels of iNOS-derived NO in monocytes, owing to decreased degradation of ADMA by DDAH2, may reduce infarct size, improve neurological and behavioural deficits, and reduce neuronal apoptosis. A sub-aim of the project was to evaluate whether DDAH2 may impact stroke outcome via attenuating the infiltration of immune cells into the brain.

5.4.1 Choice of timepoint to study infarct development and infiltration

To address the aims of the project, the peak of infarct development was chosen as a suitable timepoint of investigation, which also matches with the time course of peak immune cell infiltration (Figure 1-4). In C57BL6/J mice using the tMCAo model the infarct is typically fully developed by 24-72 hours, while by day 7 it halves in size and almost fully recovers by 2 weeks (Feng et al., 2017). Many studies commonly assess infarct volume at 24 hours after tMCAo (Chen et al., 2015, Bieber et al., 2019a), and leukocytes are reported to increase as early at 24 hours after tMCAo (Chu et al., 2014, Gelderblom et al., 2009). However, in the rodent ischaemic brain, monocytes are first to cross the BBB, while lymphocytes and neutrophils only accumulate in the ischaemic hemisphere at 72 hours post tMCAo (Gelderblom et al., 2009). Therefore, to capture ischaemia-induced infiltration of innate and adaptive immune cells, the study was conducted 72 hours after tMCAo. The number of myeloid cells, monocytes and macrophages was trending higher in the ipsilateral hemispheres but neither a stroke, nor a genotype effect were observed (Figure 5-9). Ultimately, to definitively establish whether NO is important for monocyte infiltration, it remains to be determined whether this is primarily due to monocytes upregulating iNOS remotely (in the circulation, spleen, thymus, or bone marrow) or if this occurs upon exposure to ischaemic cues in the brain.

Myeloid cells have been shown to increase 3-fold in the ipsilateral versus the contralateral hemisphere in previous studies (Chu et al., 2014). In the present study a 2.5-fold increase was observed but the effect size was not large enough

to determine a significant difference, indicating that the study was underpowered and that an n=10 is required for a large enough effect size.

5.4.2 Monocyte/macrophage DDAH2 deletion had no impact on immune cell infiltration

Myeloid cells ($CD45^{hi+}CD11b^{+}$), monocytes ($CD45^{+hi}CD11b^{+}Ly6C^{+hi}$), and macrophages ($CD45^{+hi}CD11b^{+}Ly6C^{+low}$) infiltration was not only unaffected by DDAH2 deletion, but surprisingly also did not increase significantly in the ipsilateral hemispheres compared to control, despite sharing the phenotypic signature $CD45^{+hi}CD11b^{+}$ with myeloid cells ($CD45^{+hi}CD11b^{+}$) and M2-like macrophages ($CD45^{+hi}CD11b^{+}CD206^{+}$), which were detected in higher numbers in stroke affected hemispheres in Chapter 3 (Figure 3-7). A possible explanation for this discrepancy is that the CD11b antibody was conjugated to a different flurophore in this panel - V500, compared to APC-Cy7 in Chapter 3. Additionally, it is likely that while M2-like macrophages ($CD45^{+hi}CD11b^{+}CD206^{+}$) predominate at this timepoint, monocytes ($CD45^{+hi}CD11b^{+}Ly6C^{+hi}$) differentiate into M1-like macrophages, which dominate at later stages of tMCAo (Kanazawa et al., 2017b). However, macrophages which express $Ly6C^{+low}$ are typically M2-like and would have been expected to increase similarly to the $CD206^{+}$ macrophages in Chapter 3. While the difference may have arisen from differences in the flow cytometric panels, this may also be inherent to the spectrum of phenotypes M1-like and M2-like polarised macrophages represent.

Neutrophils and lymphocytes increase in the ipsilateral hemispheres of rodents after MCAo (Perez-de-Puig et al., 2015, Kang et al., 2020), and neutrophils' tendency to accumulate and block capillaries for prolonged periods of time contributes to the no-reflow phenomenon (El Amki et al., 2020). In this study neither neutrophils nor lymphocytes were detectable in half of the mice or were detected at a very low frequency (Figure 5-10). Paradoxically, these cases were observed in mice that were suspected to have undergone a more severe stroke based on not achieving the threshold values for reperfusion. Immune cell infiltration rate does not appear to scale linearly with the duration of occlusion, as others have reported that increasing the duration of the ischaemic period from 60 min to 2 hours did not yield higher $CD45^{+}$ leukocyte numbers (Chu et al., 2014), indicating that the low numbers of neutrophils and lymphocytes observed here

were unlikely resulting from a shorter duration of tMCAo. Recent evidence suggests that accumulation of neutrophils precedes that of macrophages and monocytes (Planas, 2018), and neutrophil turnover is high (Cai et al., 2020), suggesting that by 72 hours post tMCAo they may have cleared from the brains of some mice. The low frequency of lymphocytes can possibly be explained by the fact that lymphocytes might only be accumulating after 72 hours, as was found in a meta-analysis of 20 human and 188 rodent studies (Beuker et al., 2021).

5.4.3 Monocyte/macrophage DDAH2 deletion had no impact on infarct volume

In this study the mean infarct volume for the control mice was relatively small at 24.3 ± 8.9 mm^3 (Figure 5-13A), which is comparable to lesion volume obtained by others. Chen et al. reported on a mean lesion size of approximately 23 mm^3 using thionin staining at 24 hours after 60 min tMCAO (Chen et al., 2015). Jackman et al. used a shorter occlusion period but achieved a similar infarct volume (Jackman et al., 2009). Additionally, the infarct volume as a percentage of the hemisphere was in line with the 4.5–14% of hemisphere size (Figure 5-14A) that is observed in ischaemic stroke patients (Carmichael, 2005). However, in other experimental studies in mice of the same strain, sex, age, occlusion period, and method of analysis (thionin staining), infarct size was reported to equal 30% of hemispheric volume (Seifert et al., 2017). Another study with a much lower occlusion duration (20 minute) determined infarct volume by magnetic resonance imaging (MRI) as large as 75 mm^3 (Haley et al., 2020), which is almost four-fold larger than the one found in this study. Similar infarct volume was reported in C57BL6/N mice (77.5 mm^3) (Bieber et al., 2019a) using triphenyltetrazolium chloride (TTC) staining. Overall, the differences in infarct volume between this study and the ones discussed above demonstrate that this model results in a wide range of brain injury and that parallelism between studies is difficult to establish.

5.4.4 Effect of monocyte/macrophage DDAH2 deletion on neurological outcome of stroke

There were no detectable differences between grip strength pre- and post-tMCAo (Figure 5-12A). A pitfall in the way this test was conducted is that recordings were taken from both forelimbs, while an important control would be to measure strength in each forelimb separately, and inform on asymmetry similarly to the

foot fault test (Crum et al., 2013). The nest building activity was most robust in detecting differences pre- and post- tMCAo (Figure 5-12B) was significantly impaired in control mice as reported by others after 60-minute tMCAo in wildtype mice (Yuan et al., 2018). While there were no statistically significant genotype differences in the ability of mice to build nests post tMCAo, DDAH2$^{Mo-/-}$ mice scored similarly between baseline and after ischaemia, suggesting that cognition and wellbeing could perhaps be impacted by aberrant NO regulation within macrophages. Asymmetric forelimb foot fault is a hallmark of unilateral brain injury and there were more detectable deficits in the DDAH2$^{fl/fl}$ mice compared to DDAH2$^{Mo-/-}$ mice on both day 1 and day 3 (Figure 5-12C). Similarly, the on composite mNSS test experimental mice scored poorer on day 1 versus day 3 after stroke, but no genotype effect was detected at either timepoint (Figure 5-12D).

Of note, this study was underpowered, and more experiments will be needed to determine possible differences arising from lack of DDAH2. The infarcts in this study were primarily in subcortical striatal regions (Figure 5-13C-D), which is common for this tMCAo model (Rousselet et al., 2012). However, a limitation to this study is that some of the neurological tests are developed to detect deficits arising from cortical injury. While the walking test and the tail suspension swing tests may be able to detect deficit arising solely from a subcortical lesion, correct placement of a foot on a walking grid requires higher executive function. However, a mouse, which only experienced a subcortical lesion, may be able to compensate for deficits by an intact somatosensory cortex. To effectively measure deficits in subcortical regions, alternative tests need to be considered. For example, the skilled reaching test has been used in mice following stroke to assess functional deficits arising from an intra-striatal lesions (Pilipenko et al., 2024). The rotarod test and the adhesive tape removal test are also distinguishing impairments associated with altered striatal function (Gao et al., 2024, Sun et al., 2020).

5.4.5 Evidence that monocyte/macrophage DDAH2 deletion impacts DNA strand breaks

DNA strand breaks are a hallmark of programmed cell death and after stroke this process is mediated in part by iNOS-produced NO in both endothelial cells and neutrophils (Garcia-Bonilla et al., 2014). A recent study demonstrated that

reducing the number of iNOS-positive microglia and astrocytes by intracerebroventribular injection of $GdCl_3$ slows down neuronal degeneration and mitigates cerebral ischaemic damage by dampening the inflammatory response (Li et al., 2022). Work presented in this Chapter demonstrated higher numbers of TUNEL positive cells in the ischaemic core and in the peri-infarct of $DDAH2^{fl/fl}$ mice compared to $DDAH2^{Mo-/-}$ mice (Figure 5-15, Figure 5-16), suggesting that in macrophages DDAH2 exerts control over iNOS-mediated cytotoxicity across both affected regions. In a typical ischaemic hemisphere TUNEL positive cells are found in the infarct core and significantly less in the peri-infarct area (Figure 5-4)(Ku et al., 2016, Jiang et al., 2017). In the present study the number of TUNEL positive cells was comparable between infarct core and peri-infarct in mice from the same genotype. Possibly these differences arose from the method of normalisation to the area of the image instead of normalising to the whole hemisphere, and could also have been a result of misjudging the border between the infarct and peri-infarct during image acquisition. Additionally, it can be further explored whether the detected DNA strand breaks arise solely from neuronal cells or includes other brain cells such as glia, microglia, and even immune cells and can be further strengthened by utilising additional parameters to conclude apoptosis such as aberrant morphology, or expression of caspase-3 or Annexin V (Mirzayans and Murray, 2020).

5.4.6 Limitations

Only male animals were used in this study, which limits the generalisability of the findings across sexes. This decision was made to reduce biological variability in the current proof-of-concept study.The importance of sex as a biological variable will need to be addressed in future experiments to comply with the newest guidelines on preclinical stroke research ARRIVE II (Percie du Sert et al., 2020). The surgeon was blinded to the mouse's genotype and since all mice underwent stroke as a treatment, randomisation was not implemented, but future studies could incorporate a random order generator to fully randomise allocation to surgery. Efforts were made to minimise the impact of bias by investigating outcome measures based on objective, quantifiable data, reducing subjective interpretation, but in future work blinding data analysis must be incorporated.

5.4.7 Summary

In this pilot study monocyte/macrophage DDAH2 deletion had no effect on infarct or oedema volume. Stroke outcome was not affected by the ability of DDAH2 lacking monocytes and other immune cells to infiltrate the ischaemic brain. Neurological deficit remained comparable between $DDAH2^{Mo-/-}$ and $DDAH2^{fl/fl}$ mice, as determined by similar foot fault and mNSS. A reduced level of DNA breakage was observed in the ischaemic hemisphere of $DDAH2^{Mo-/-}$ mice, which may be secondary to infarct volume. These data suggest that DDAH2 does not impact the outcome of ischaemic stroke in mice. However, to fully refute an effect of DDAH2 after tMCAo, a larger sample size is needed.

6 Chapter 6: General Discussion

6.1 Summary of results

The findings presented in this thesis provide a previously under-reported characterisation of a rare and specialised population of immune cells in the CNS borders in the context of ischaemic stroke and reveal the role of the enzyme DDAH2 in regulation of physiological macrophage phenotype and the effect of DDAH2 on stroke outcomes.

6.1.1 CNS border-associated macrophages accumulate in the ischaemic hemisphere after cerebral ischaemia-reperfusion in a time-dependent manner.

In Chapter 3 a temporal quantification of the numbers of a small population of CNS borders-associated macrophages (BAMs) in a mouse model of focal ischaemic stroke was presented. BAMs ($CD45^{+}CD11b^{+high}CD206^{+}Lyve1^{+}$) accumulated in the ipsilateral hemisphere after tMCAo in a time-dependent manner. This response was most pronounced in the acute phase after stroke, peaked at 1 week and subsequently the numbers of BAMs declined in the chronic phase of stroke. The localisation of BAMs in the ipsilateral and contralateral hemispheres after ischaemic stroke was presented and semi-quantified. BAMs were identified in the perivascular spaces as $CD206^{+}\alpha SMA^{+}$ and in the meningeal spaces as $CD206^{+}Lyve1^{+}$.

6.1.2 Oxygen and glucose deprivation in macrophages increased *Ddah2* mRNA expression and macrophage inflammatory profile is regulated by *Ddah2*.

Nitric oxide (NO) is a signalling molecule, which regulates macrophage function such as phagocytosis and motility. Dimethylarginine dimethylaminohydrolase (DDAH2) is an enzyme that belongs to a family of enzymes that regulate NO production and is the only isoform expressed in macrophages. Work described in Chapter 4 demonstrated that *Ddah2* mRNA expression increased following oxygen and glucose deprivation in RAW264 macrophage cell line, however, DDAH2 protein levels in the whole brain remained unchanged in the acute phase after tMCAo in C57BL6/J mice. The expression of the pro-inflammatory genes Il- 1β, *Tnf*α, *Il-6* and *Ccl2* was reduced in peritoneal macrophages from naïve monocytes/macrophages specific *Ddah2* knockout mice, indicating that DDAH2 may regulate the inflammatory phenotype and function of these cells.

6.1.3 Trends for improvement in neurological function and reduced apoptosis in monocyte/macrophage *Ddah2* deficient mice after tMCAo

In Chapter 5 a study exploring the role of monocytes/macrophages DDAH2 in ischaemic stroke outcomes was presented. DDAH2 did not alter immune cell infiltration into the brain after tMCAo, demonstrated by comparable numbers of total leukocytes, myeloid cells, and lymphocytes between $DDAH2^{Mo-/-}$ and $DDAH2^{fl/fl}$ mice. DDAH2 did not appear to have an impact on infarct volume or neurological deficit in $DDAH2^{Mo-/-}$ mice after tMCAo. A reduced level of DNA breakage was observed in immunostaining with TUNEL in $DDAH2^{Mo-/-}$ mice compared to $DDAH2^{fl/fl}$ controls.

6.2 Significance of findings

6.2.1 Accumulations of BAMs following ischaemic stroke by proliferation and/or replenishment by peripheral monocytes

As discussed in the General Introduction, BAMs are a heterogeneous population of cells, but may lose their heterogenicity in the acute phase after stroke and become transcriptionally similar to microglia and BM-derived macrophages. Microglia are composed of diverse clusters of cells in response to permanent stroke in mice (del Águila et al., 2024). Interestingly, one of the microglial clusters defined in the study by Del Águila and colleagues showed upregulation of antigen presentation genes such as of histocompatibility 2 class II antigen A, alpha (*H2-Aa*), beta1 (*H2-Ab1*), and *Cd74*, which are also upregulated in BAMs after experimental autoimmune encephalomyelitis (Jordão et al., 2019), highlighting that subsets of microglia and BAMs share functionality. BM-derived macrophages also undergo phenotypic transformations that camouflage them as BAMs (Croese et al., 2021). While BAMs are long-lived and mainly self-renewing under homeostasis, recent evidence described repopulation of BAMs by CCR2+ peripheral monocytes under conditions of BBB disturbance such as in a brain compression model (Wang et al., 2024). This could mean that the observed numbers of BAMs after tMCAo in Chapter 3 could be derived, at least partially, from peripheral monocytes. Fate mapping can now be combined with single cell RNA sequencing studies or high-dimensional single-cell mass and fluorescence cytometry (Mrdjen

et al., 2018), to study the identity, location, and characteristics of populations across the brain not only in homeostasis but also in pathology.

6.2.2 BAMs as a suitable therapeutic target

The efficacy of BMDMs as cell therapy has been reported in a mouse experimental model of stroke (Kitamura et al., 2023). BMDMs were administered in the intracerebral spaces 2 weeks after stroke and mice showed improved CBF, increased expression of IL-4, decreased expression of TNFα and IL-1β, preserved neurons and improved sensorimotor function on assessment one month after stroke (Kitamura et al., 2023).

Several functional roles for BAMs have been identified after ischaemic stroke, mostly through studies of perivascular subpopulations. Among these is extracellular matrix remodelling (Pedragosa et al., 2018), which has more recently been shown to be a characteristic of meningeal macrophages in the steady state (Drieu et al., 2022). Pedragosa et al., also demonstrated that absence of BAMs reduced granulocytes chemotaxis, which is a role now shown to be preserved in BAMs from aged mice too (Levard et al., 2024).

An important aspect of the evidence presented in this thesis is that it was conducted in young mice, while ischaemic stroke mainly affects aging populations. With age BAMs alter their activation signature (lower LYVE-1 and higher MHC-II expression) and exacerbate amyloid ß (Aß) pathology in transgenic mice (Drieu et al., 2022). Furthermore, it is probable that different subsets would have distinct and perhaps opposing functions, as some may be involved in repair, while others might be drivers of neuroinflammation. For instance, only perivascular and choroid plexus BAMs have been shown to participate in iron uptake through the ferroportin-1 (Dani et al., 2021), and perivascular BAMs are involved in erythrocytes clearance in subarachnoid haemorrhage (Wan et al., 2021). Dural and choroid plexus macrophages are located in the most immunologically exposed CNS borders, and are the only subpopulations to express MHCII and possess antigen presenting capabilities (Mrdjen et al., 2018). However, to study the contributions of subpopulations of BAMs in ischaemic stroke, a sorting pipeline with multiple markers would be required.

BAMs are gatekeepers at the CNS borders; they are more accessible, uniquely positioned, and immunologically active at the brain's interfaces with the body. This makes them prime therapeutic targets compared to microglia, which are harder to reach and more tightly integrated into brain function (Dalmau Gasull et al., 2024, McCullough and Moro, 2021). Strategies to enhance the function of BAMs may involve therapeutic delivery of CSF-1. It has recently been shown that meningeal BAMs can alter extracellular matrix leading to defective cerebrospinal/interstitial fluid flux via the glymphatic system. CSF-1 administration into the murine brain regenerates BAMs, which upregulates LYVE-1, and leads to improved CSF glymphatic flow (Drieu et al., 2022).

More mechanistic investigation into BAMs interactions with cells of the neurovascular unit and the parenchyma, such as microglia, would provide an insight into their relevance for development of cell therapies. Evidence for signalling between perivascular BAMs and endothelial cells is illustrated in hypertension and vascular cognitive impairment (Santisteban et al., 2020). An example of BAMs-microglia crosstalk is found in the secretion of osteopontin by activated perivascular macrophages, which exacerbates microglial activation and excessive neuronal synaptic pruning in Alzheimer's disease (De Schepper et al., 2023).

6.2.3 DDAH2 may be a better target than iNOS for treating ischaemic stroke

There are several iNOS inhibitors which have shown promise in rodent models of ischaemic stroke, but their poor pharmacokinetic profiles make them unlikely therapeutics clinically. Recently, a structural alteration to the chemical structure of 1400W with structural isomers of DL-3-n-butylphthalide (NBP) has shown promise in reducing infarct size in rat cerebral ischaemia-reperfusion (Ji et al., 2024). It is likely that developing a DDAH2 inhibitor will face some of the same challenges that iNOS inhibitor development has met. The DDAH1 selective inhibitor L-257 can cross the blood brain barrier, suggesting that structure activity relationship analysis may be able to guide the development of a DDAH2 selective inhibitor. However, since no compounds have been so far developed for preclinical use, a lot of future work would be needed to match and exceed the benefits of using iNOS inhibitors clinically.

6.3 Limitations

6.3.1 Strengths and limitations of the stroke model

This thesis used the tMCAo model of ischaemia-reperfusion, which mimics stroke with reperfusion and has several strengths. This model closely mimics the pathophysiology of ischaemic stroke followed by reperfusion, such as what occurs in patients receiving thrombolytics or undergoing thrombectomy. It is relatively reliable and reproducible in terms of infarct size and location (typically affecting the striatum and cortex supplied by the MCA). The duration of occlusion is highly adaptable, helping to achieve different severities of ischaemia. The resulting infarcts are visible via a variety of histological and imaging modalities, such as thionin, cresyl violet, or tetrazolium chloride staining, and MRI, facilitating quantitative analysis. The model produces measurable motor and cognitive deficits in animals, which can be assessed behaviourally. Unlike other MCAo models such as the electrocoagulation and the thromboembolic models, an advantage to the intraluminal MCAo is that it does not require craniotomy. The tMCAo model enables the study of ischaemia-reperfusion injury, which is a major aspect of clinical stroke treatment and an important target for therapeutic development. It lends itself well to testing neuroprotective drugs, anti-inflammatory agents, or reperfusion strategies due to its predictable injury profile (Levard et al., 2020, Ma et al., 2020).

A major limitation of this model is that it does not accurately reflect the majority of clinical stroke cases, as only 2.5–11.3% of large vessel stroke patients experience reperfusion (McBride and Zhang, 2017). This likely underpins its relatively low predictive validity for new treatments, as the translatability of findings in preclinical to clinical stroke has been low. An alternative is the permanent MCAo model, which closely replicates malignant stroke, which is however, a rare case of human stroke, as opposed to the smaller size infarcts typically characterised in ischaemic stroke patients. Also, the rapid reperfusion after tMCAo allows for the primary injury to recover and a secondary injury appears in the next 12 hours, which is not seen in human stroke (Fluri et al., 2015). This highlights the differences in the therapeutic time window between clinical stroke (3-6 hours) and in tMCAo (up to 12 hours), perhaps explaining the hugely

unsuccessful development of therapeutics based on pre-clinical findings using this model (Hossmann, 2012).

Additionally, in comparing the results of one study using tMCAo with another, there are several confounding factors that are challenging to control for. For instance, infarct volume is dependent on the patency of the posterior communicating artery, the anatomy of collateral vessels, and may be affected by the transient vessel occlusion of the common carotid artery during the procedure (Howells et al., 2010). Furthermore, hyperthermia exacerbates cell death and inflammation (Schaller and Graf, 2003), signifying that temperature fluctuations may be a source of variability in ischaemic cell death in tMCAo. Despite care being taken to minimise body temperature variations during and after MCAO, it is difficult to monitor the animals' post-operative temperature for hypothalamic-derived hyperthermia without the availability of thermal imaging (Barbosa Pereira et al., 2018). Hypothalamic ischaemia can generate a hyperthermic response that persists for several days after the animal has recovered (Schaller and Graf, 2003). This phenomenon has been reported by others for 40-60 min occlusion durations (Hossmann, 2012), but was not observed in a separate study in this lab group, so it is unlikely to have affected the work presented in Chapter 3 and Chapter 5.

6.3.2 Strengths and limitations of flow cytometry

Since flow cytometry was used in this thesis extensively to immunophenotype many cell types and for verification of isolated cells' identity, the limitations of the technique are hereby appraised. Practical considerations of using this technique, such as cost and complexity, requirement for fresh samples, and spectral overlap have been discussed in Chapter 4 and Chapter 5. A strength of this study was the use of AccuCheck counting beads, since bead-enhanced quantitation has been shown to be superior to other methods of flow cytometric quantification (Montes et al., 2006). While it is a highly robust quantitative method, a major drawback of flow cytometry is the limited morphological information it provides, compared to techniques like immunohistochemistry and immunofluorescence, which is a caveat in interpreting data from markers shared by more than one cell type without assessing their anatomic location and physical features. When dealing with highly heterogeneous cell populations, the ability to distinguish them both phenotypically and morphologically would be of benefit.

Additionally, more precise results could have been obtained by microdissecting the infarct tissue from the rest of the hemisphere, while this method would have required staining the infarct with a dye such as Evans blue that may have interfered with the subsequent cellular fluorescence staining.

6.3.3 The ability of DDAH2 to hydrolyse ADMA

Since the crystal structure of DDAH2 is of yet unresolved, indirect evidence for DDAH2 being a metaboliser of ADMA in macrophages was discussed in the context of controlling macrophage phenotype (cf. General Introduction, Chapter 4, and Chapter 5). Recent evidence has emerged disputing the ability of DDAH2 to hydrolyse ADMA based on observations in homology models using the crystal structure of DDAH1 (Ragavan et al., 2023, Altmann et al., 2012, Nair et al., 2024). The catalytic triad of DDAH1 was first described as Cys249-His162-Glu114 in Pseudomonas aeruginosa (Murray-Rust et al., 2001) and subsequently human DDAH1 was crystallographically resolved to bind ADMA at Cys273-His172-Asp126. The binding of a S atom to a C atom at Cys273 in the substrate was demonstrated as critical to initiate hydrolysis (Leiper et al., 2007). This catalytic triad is conserved across a family of hydrolases, which include arginine deiminases and arginine: glycine amidinotransferases (Leiper et al., 2007). However, Ragavan et al., 2023 used molecular docking and the homology models SWISS-MODEL and AlphaFold to predict that the DDAH2 binding pocket includes a slightly different triad – either Asp125-His171-Leu275 or Asp125-Ser274-Leu275, which they found was an unsuitable fit for the ADMA molecule (Ragavan et al., 2023). A thermophoresis analysis showed unstable binding of ADMA to recombinant DDAH2. The authors then showed a lack of enzymatic activity towards 10 mM of ADMA was evidenced by negligible production of citrulline - the hydrolysis product of ADMA, compared to DDAH1, which exhibited enzymatic activity towards ten times lower ADMA concentration (Ragavan et al., 2023). However, the authors have not specified the exact tissue source used for this assay and any tissue which is optimal for strong activity of DDAH1 towards AMDA is likely not highly expressing DDAH2 and therefore unsuitable to detect metabolism of ADMA by DDAH2. Moreover, ionic concentrations are known to impact macrophage function (Erndt-Marino et al., 2020) and can affect enzymatic rate and saturation (Yang et al., 2008), and therefore the absence of hydrolysis by DDAH2 in this assay could be attributed to it not being optimised for the macrophage intracellular environment. Therefore,

the inability to detect any conversion to citrulline perhaps amounts to absence of evidence, instead of evidence for lack of ADMA hydrolysis by DDAH2 in macrophages.

In major organs that express both DDAH isoforms such as the kidney, brain, and lung, global DDAH1 knockout led to elevated ADMA levels several folds higher than wildtype, and DDAH activity was completely abolished despite a functionally expressed DDAH2 (Hu et al., 2011). The authors have concluded that this is evidence that DDAH2 does not metabolise ADMA. However, it could also mean that DDAH2 is potentially dependent on a concomitant functional expression of DDAH1 or another co-factor to modulate ADMA levels in a more subtle way. Indeed, the contribution of DDAH2 to ADMA metabolism might be more pronounced in the context of disease. For instance, in mice globally deficient in DDAH2, plasma ADMA levels were comparable (0.65 μM) to wildtype mice but were 1.5-fold elevated after a septic challenge (Lambden et al., 2015), potentially because DDAH1 becomes saturated with ADMA and therefore, cannot solely control the increased synthesis of ADMA (4.4 μM in wildtype) in the absence of DDAH2. Moreover, in mice specific for macrophage *Ddah2* deficiency that underwent experimental sepsis, plasma ADMA and SDMA levels, and nitrite/nitrate species, were comparable to littermate floxed controls (Lambden et al., 2015). Both lines of evidence – from the global and the macrophages specific knockouts - indicate that although DDAH2 might be able to hydrolyse ADMA in macrophages, or in other cells to a lesser extent, the systemic effect of its action is masked by the predominant hydrolysis of ADMA and L-NMMA by DDAH1 elsewhere in the body. Since macrophages lack expression of DDAH1, perhaps DDAH2 is dependent on another, yet unidentified ADMA-metabolising enzyme or co-factor.

Nonetheless, in light of this new evidence, an alternative hypothesis could be that DDAH2 has ADMA-independent but NO-mediated effects on immune response (Lambden et al., 2015, Huang et al., 2021). A putative mechanism could involve an interaction with the signalling pathways that control iNOS expression such as NF-κB, STATs, MAPK, and PI3K/Akt, or may be through an epigenetic effect on iNOS activity exerted by microRNAs or histone-modifying enzymes.

6.4 Future work

6.4.1 Optimisation of the isolation of brain macrophages

Preliminary attempts were made to isolate BAMs after tMCAo using florescence activated cell sorting (FACS) for single cell transcriptomic analysis (scRNAseq). Unfortunately, only <10 BAMs were obtained per isolation, which was insufficient for a scRNAseq. Future work would need to optimise the method for brain macrophages isolation, as discussed in Chapter 3, by potentially pooling cells from multiple animals to obtain the higher cellular number. Successful isolation of BAMs and/or microglia from C57BL6/J mice subjected to tMCAo would allow to investigate the effect of ischaemia on gene expression in these macrophages. Additionally, optimisation of RNA isolation and quality control are prerequisite to successful RT-qPCR and scRNAseq analyses. As discussed in Chapter 3, RNA integrity and per reaction amount could be better controlled for. To provide a measure of sensitivity and specificity in RNA-Seq experiments, equal quantity of spike-in RNA controls can be used to bioinformatically normalise the total amount of sequenced reads between samples. Spike RNAs show no sequence similarity to the genome of the studied species, so in this case they need to be different to mouse, and they are added in defined amounts to experimental RNA samples before labelling (Fardin et al., 2007). Issues were encountered with the stability of the housekeeping gene *R18s* and it remains to be explored whether *Rpl13* would be suitable in samples following experimental stroke. An alternative in studying the transcriptome of BAMs is the membrane spanning 4-domains A4A (*Ms4af)*, since it was the only gene found to be stable across health and disease states in mice (Jordão et al., 2019). This can complement the characterisation work of BAMs numbers during different phases after stroke and would offer insights into the functional differences that these cells might display as they adapt to changing post-tMCAo environmental cues.

6.4.2 Examining ADMA metabolism by DDAH2 in macrophages

In line with the above discussed considerations, further work would need to investigate the dose-response to a range of ADMA concentrations [0.1-10 mM] in CNS resident macrophages. Failing a successful isolation of the later, examination of the hydrolysis of ADMA by DDAH2 could be conducted in another model system,

such as RAW264.7 cells, peritoneal macrophages, the murine macrophage line J744.1 or the human monocytic cell line U937. Albeit DDAH1 is known to not be expressed in immune cells, demonstrating a sole expression of DDAH2 in the chosen cell type would strongly complement the specificity of ADMA metabolism by DDAH2 in macrophages.

6.4.3 Regulation of DDAH2 by S-nitrosylation following stroke

The ultimate goal of the experiments in DDAH2 deficient macrophages was to establish a system to investigate the role of DDAH2 in ischaemic stroke outcome through modulation of macrophage function. In this context it would be important to consider potential feedback loops that auto-regulate the DDAH2-ADMA-NOS axis. Increased NO production upon reperfusion, supported by reintroduction of oxygen, can lead to S-nitrosylation of Cys-249 in the catalytic triad of DDAH2, thereby reducing the activity of the endogenous enzyme in floxed controls mice (Leiper et al., 2002). The extent of this reduction in DDAH2 activity may be commensurate with the absence of expression in the knockout, potentially masking any differences in stroke outcomes between the DDAH2 deficient and control mice, as observed in Chapter 5. Assays that examine this post-translational modification in macrophages following stroke could be used to mitigate this effect.

6.4.4 Interplay between BAMs and DDAH2 after stroke

An overarching aim for this thesis and an extension of this work could envisage sorting BAMs and/or microglia from a DDAH2 deficient mouse after tMCAo and studying the effect of the DDAH2-iNOS-NO pathway on BAM and microglia function after stroke. *Lyz2*, which codes for the functional LysM protein used for the macrophage specific knockout, is expressed in both microglia (Zheng et al., 2022) and, to a higher extent, in BAMs (Van Hove et al., 2019). To this end, the expression of Ddah2 in BAMs in naïve mice will need to be verified and subsequently its deletion in the $Ddah2^{Mo-/-}$ mice. RNAseq experiments could investigate the effect of stroke on BAMs transcriptional profile in naïve and in $Ddah2^{Mo-/-}$ mice. If viable, a genetic cross between the monocyte specific Ddah2 mouse and Lyve1Csf1R mice would offer an exciting new tool to study the effect of nitric oxide on BAM function after ischaemic stroke. If the roles of these cells

are found be important and non-redundant in the context of neuroinflammation, an immortalised cell culture of BAMs would allow many further mechanistic studies. The core transcription factor PU.1, which drives maturation of erythromyeloid progenitors into BAMs (Utz et al., 2020), can be used in induced pluripotent stem cells to offer new cell therapies to stroke survivors. What remains to be explored is whether BAMs express *Ddah2, Nos2,* or any of the genes in the NO biosynthesis and signalling pathways. If the genetic machinery is indeed expressed at basal levels in BAMs, it would be valuable to explore the roles of NO at acute, sub-acute and chronic stages after stroke. Given that BAMs are so heterogeneous, it would not be surprising if different subpopulations express NO-related genes differentially.

6.5 Final conclusions

This thesis aimed to characterise the response of a rare and specialised population of CNS border resident macrophages (BAMs) during different phases after experimental stroke. In providing evidence for the accumulation of BAMs into the ischaemic hemisphere of mice following cerebral ischaemia-reperfusion, the reader is invited to an appraisal of the possible mechanisms and functional implications of such accumulation. BAMs are strategically located in niches where they interact with other cell types to elicit their roles in the neuroinflammatory response ensuing stroke, which make them a tentative candidate for cellular therapies. Macrophage function is understood to be controlled by the ubiquitous molecule NO, while the impact of regulation by the enzyme DDAH2 on stroke outcome has not been previously reported. In this thesis the effect of DDAH2 deletion in monocytes and macrophages was examined in the same stroke model that revealed BAMs accumulation. DDAH2 was found to modestly regulate neurological outcomes after stroke, signifying the importance of this enzyme in macrophage function and beyond. Developing robust methods for isolating post-stroke brain macrophages would offer the potential to unravel unique differentially expressed genes and pathways in these enigmatic cell types.

7 Appendix

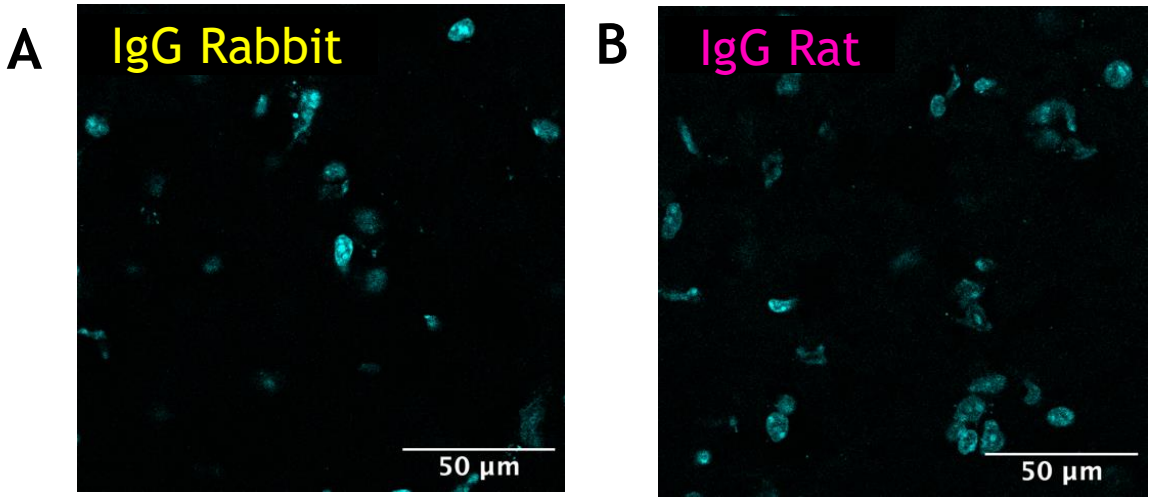

Figure 7-1. The specificity of the detection for immunofluorescence analyses of BAMs localisation was determined by IgG controls. A) Anti-rabbit IgG antibody (Thermo Fisher, 02-6102) was used at the highest equivalent concentration (0.02 µg/ml) as experimentally used anti-Lyve1 and anti-alpha smooth muscle actin antibodies both IgG isotypes and raised in rabbit and B) Anti-rat IgG2a antibody (Thermo Fisher, 02-9688) was used at equivalent concentration (0.025 µg/ml) as experimentally used anti-CD206 antibody, which was an IgG2a isotype and raised in rat.

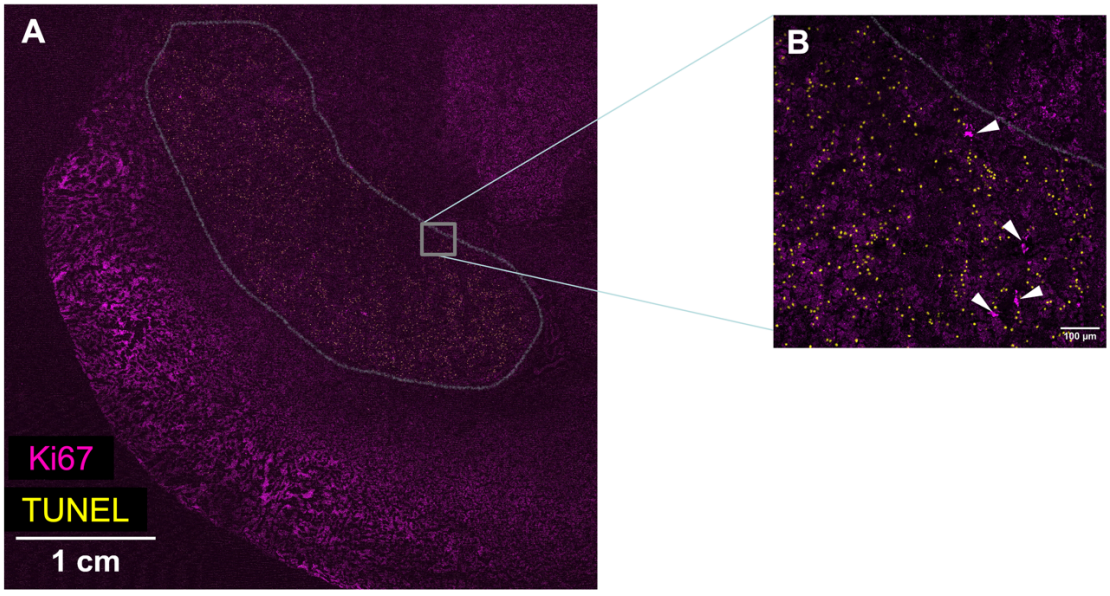

Figure 7-2. Proliferation and DNA strand breaks in the ipsilateral hemisphere of C57BL6/J mice after 60 min of transient middle cerebral artery occlusion (tMCAo). A) A tiled coronal brain section showing expression of the proliferation marker Ki67 in magenta and apoptosis marker terminal deoxynucleotidyl transferase dUTP nick end labelling (TUNEL) in yellow. White line delineates the infarct border. B) A closer magnification showing Ki67^{+} cells are present in the infarct.

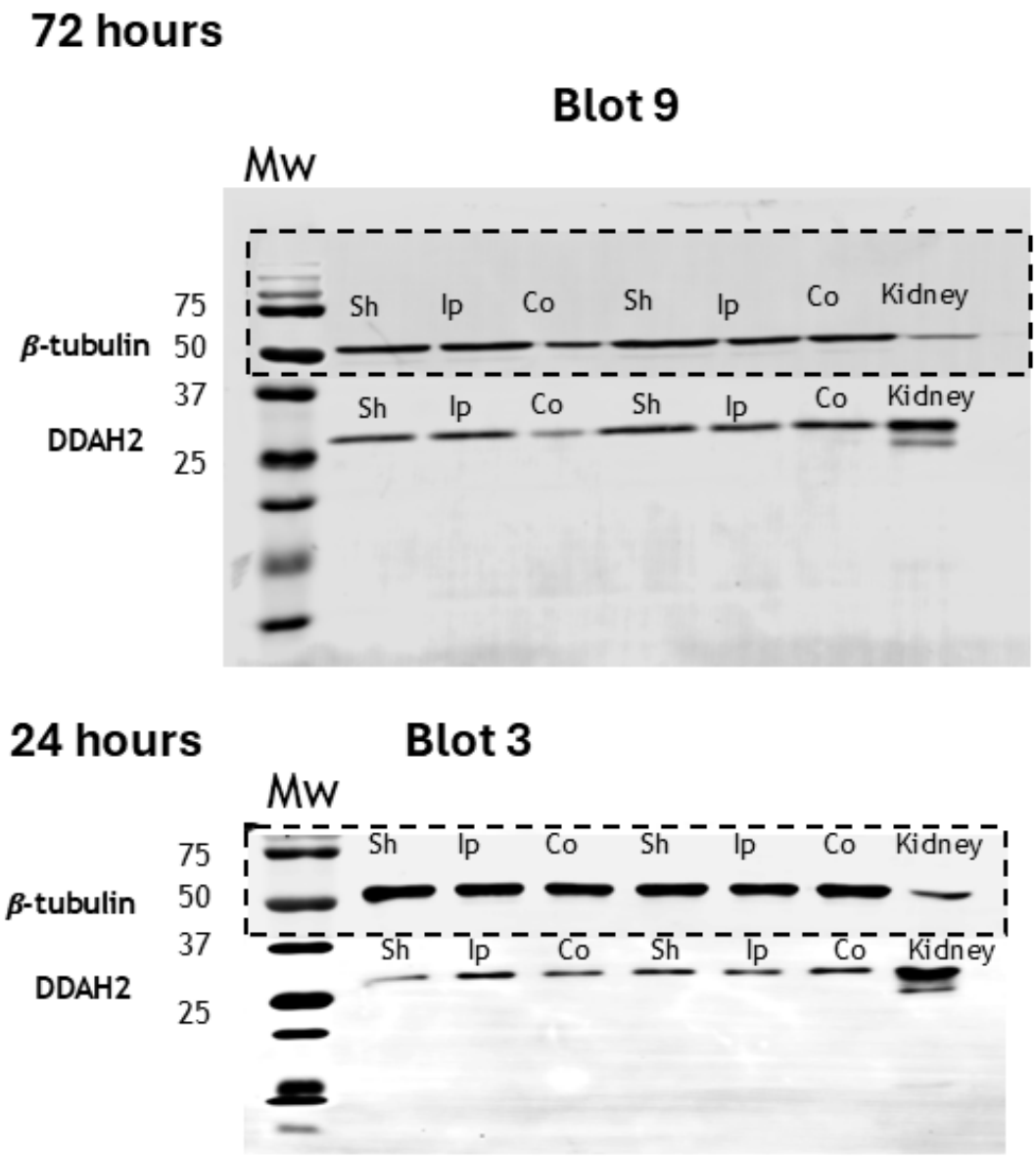

Figure 7-3. Representative blots demonstrating the selectivity of the DDAH2 and ß-tubulin antibodies in mouse brain tissue at two different timepoints following transient middle cerebral artery occlusion (tMCAo). Membranes were routinely cut for concomitant incubation with antibodies for the protein of interest and the housekeeping protein.

Figure 7-4. Starting material for nesting behavioural testing included 3g of nestlet, a wooden chip. A wooden tube was provided for shelter, while other standard enrichment was not provided to encourage animals to build nests.

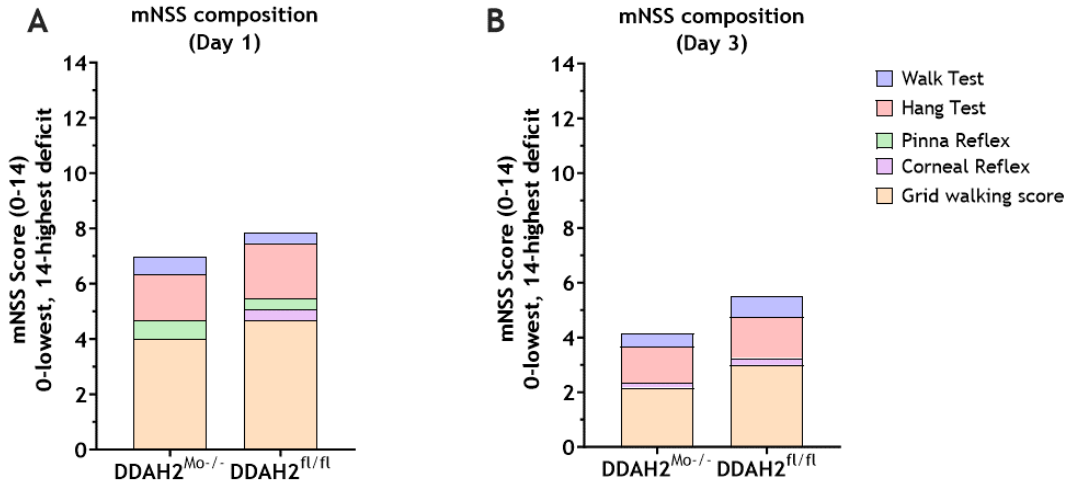

Figure 7-5. A representative composite bar graph of modified Neurological Severity Score (mNNS) in mice from two genotypes measured on day 1 and day 3 after transient middle cerebral artery occlusion. The score comprises of 6 tests and is determined on a scale of 0-14, with 0 indicative of functional normality, while 14 indicates high functional impairment.

List of References

AARTS, M., LIU, Y., LIU, L., BESSHOH, S., ARUNDINE, M., GURD, J. W., WANG, Y.-T., SALTER, M. W. & TYMIANSKI, M. 2002. Treatment of ischemic brain damage by perturbing NMDA receptor-PSD-95 protein interactions. *Science,* 298**,** 846-850.

ABD EL-ALEEM, S. A., MOHAMMED, H. H., SABER, E. A., EMBABY, A. S. & DJOUHRI, L. 2020. Mutual inter-regulation between iNOS and TGF-ß1: Possible molecular and cellular mechanisms of iNOS in wound healing. *Biochimica et Biophysica Acta (BBA) - Molecular Basis of Disease,* 1866**,** 165850.

ABE, T., SHIMAMURA, M., JACKMAN, K., KURINAMI, H., ANRATHER, J., ZHOU, P. & IADECOLA, C. 2010. Key role of CD36 in Toll-like receptor 2 signaling in cerebral ischemia. *Stroke,* 41**,** 898-904.

ABRAM, C. L., ROBERGE, G. L., HU, Y. & LOWELL, C. A. 2014. Comparative analysis of the efficiency and specificity of myeloid-Cre deleting strains using ROSA-EYFP reporter mice. *Journal of immunological methods,* 408**,** 89-100.

ACHAN, V., BROADHEAD, M., MALAKI, M., WHITLEY, G., LEIPER, J., MACALLISTER, R. & VALLANCE, P. 2003. Asymmetric Dimethylarginine Causes Hypertension and Cardiac Dysfunction in Humans and Is Actively Metabolized by Dimethylarginine Dimethylaminohydrolase. *Arteriosclerosis, Thrombosis, and Vascular Biology,* 23**,** 1455-1459.

ADAN, A., ALIZADA, G., KIRAZ, Y., BARAN, Y. & NALBANT, A. 2017. Flow cytometry: basic principles and applications. *Critical reviews in biotechnology,* 37**,** 163-176.

AHMETAJ-SHALA, B. 2013. *The role of nitric oxide synthase inhibitors on macrophage function.* Kingston University.

AJMO JR., C. T., VERNON, D. O. L., COLLIER, L., HALL, A. A., GARBUZOVA-DAVIS, S., WILLING, A. & PENNYPACKER, K. R. 2008. The spleen contributes to stroke-induced neurodegeneration. *Journal of Neuroscience Research,* 86**,** 2227-2234.

AKTAN, F. 2004. iNOS-mediated nitric oxide production and its regulation. *Life Sciences,* 75**,** 639-653.

ALANAZI, S. 2024. *Investigating Asymmetric dimethylarginine (ADMA) and Calcium-sensing receptor (CaSR) signalling in the macrophage*. University of Glasgow.

ALANAZI, S., LEIPER, F. & LEIPER, J. 2022. Dimethylarginine dimethylaminohydrolase (DDAH-2) regulates the macrophage innate response and could be a target for atherosclerotic therapy: High-throughput RNA-seq approach. *Atherosclerosis,* 355**,** 11.

ALBERS, G. W., MARKS, M. P., KEMP, S., CHRISTENSEN, S., TSAI, J. P., ORTEGA-GUTIERREZ, S., MCTAGGART, R. A., TORBEY, M. T., KIM-TENSER, M., LESLIE-MAZWI, T., SARRAJ, A., KASNER, S. E., ANSARI, S. A., YEATTS, S. D., HAMILTON, S., MLYNASH, M., HEIT, J. J., ZAHARCHUK, G., KIM, S., CARROZZELLA, J., PALESCH, Y. Y., DEMCHUK, A. M., BAMMER, R., LAVORI, P. W., BRODERICK, J. P. & LANSBERG, M. G. 2018. Thrombectomy for Stroke at 6 to 16 Hours with Selection by Perfusion Imaging. *New England Journal of Medicine*. Massachussetts Medical Society.

ALEMSEGED, F., NGUYEN, T. N., ALVERNE, F. M., LIU, X., SCHONEWILLE, W. J. & NOGUEIRA, R. G. 2023. Endovascular Therapy for Basilar Artery Occlusion. *Stroke,* 54**,** 1127-1137.

ALEXANDROVA, M. L. & BOCHEV, P. G. 2005. Oxidative stress during the chronic phase after stroke. *Free Radical Biology and Medicine,* 39**,** 297-316.

ALLEN, C. L. & BAYRAKTUTAN, U. 2009. Oxidative stress and its role in the pathogenesis of ischaemic stroke. *International journal of stroke,* 4**,** 461-470.

ALLEN INSTITUE FOR BRAIN SCIENCE, A. 2004. Allen Mouse Brain Atlas [dataset]. .

ALSHUWAYER, N. A. 2024. *Elucidation of the role of methylarginine metabolism in regulation of nitric oxide production and inflammation*. University of Glasgow.

ALTMANN, K. S., HAVEMEYER, A., BEITZ, E. & CLEMENT, B. 2012. Dimethylarginine-Dimethylaminohydrolase-2 (DDAH-2) Does Not Metabolize Methylarginines. *ChemBioChem,* 13**,** 2599-2604.

ANDRABI, S. M., SHARMA, N. S., KARAN, A., SHAHRIAR, S. S., CORDON, B., MA, B. & XIE, J. 2023. Nitric oxide: physiological functions, delivery, and biomedical applications. *Advanced Science,* 10**,** 2303259.

ANDREOU, K. E., SOTO, M. S., ALLEN, D., ECONOMOPOULOS, V., DE BERNARDI, A., LARKIN, J. R. & SIBSON, N. R. 2017. Anti-inflammatory microglia/macrophages as a potential therapeutic target in brain metastasis. *Frontiers in Oncology*. Frontiers Media S.A.

ANFRAY, A., SCHAEFFER, S., HATTORI, Y., SANTISTEBAN, M. M., CASEY, N., WANG, G., STRICKLAND, M., ZHOU, P., HOLTZMAN, D. M., ANRATHER, J., PARK, L. & IADECOLA, C. 2024. A cell-autonomous role for border-associated macrophages in ApoE4 neurovascular dysfunction and susceptibility to white matter injury. *Nature Neuroscience,* 27**,** 2138-2151.

ANTTILA, J. E., WHITAKER, K. W., WIRES, E. S., HARVEY, B. K. & AIRAVAARA, M. 2017. Role of microglia in ischemic focal stroke and recovery: focus on Toll-like receptors. *Progress in neuro-psychopharmacology & biological psychiatry,* 79**,** 3-14.

APPEL, D., SEEBERGER, M., SCHWEDHELM, E., CZORLICH, P., GOETZ, A. E., BÖGER, R. H. & HANNEMANN, J. 2018. Asymmetric and symmetric dimethylarginines are markers of delayed cerebral ischemia and neurological outcome in patients with subarachnoid hemorrhage. *Neurocritical Care,* 29**,** 84-93.

ARBEL-ORNATH, M., HUDRY, E., EIKERMANN-HAERTER, K., HOU, S., GREGORY, J. L., ZHAO, L., BETENSKY, R. A., FROSCH, M. P., GREENBERG, S. M. & BACSKAI, B. J. 2013. Interstitial fluid drainage is impaired in ischemic stroke and Alzheimer's disease mouse models. *Acta neuropathologica,* 126**,** 353-364.

ARNOULT, D., PARONE, P., MARTINOU, J.-C., ANTONSSON, B., ESTAQUIER, J. & AMEISEN, J. C. 2002. Mitochondrial release of apoptosis-inducing factor occurs downstream of cytochrome c release in response to several proapoptotic stimuli. *Journal of Cell Biology,* 159**,** 923-929.

ARUNADEVI, R., RAMTEKE, V. D., KUMAR, S., SHUKLA, M. K., JAGANATHAN, S., KUMAR, D., SHARMA, A. K. & TANDAN, S. K. 2010. Neuroprotective effect of s-methylisothiourea in transient focal cerebral ischemia in rat. *Nitric Oxide,* 22**,** 1-10.

ASAHI, M., HUANG, Z., THOMAS, S., YOSHIMURA, S.-I., SUMII, T., MORI, T., QIU, J., AMIN-HANJANI, S., HUANG, P. L. & LIAO, J. K. 2005. Protective effects of statins involving both eNOS and tPA in focal cerebral ischemia. *Journal of Cerebral Blood Flow & Metabolism,* 25**,** 722-729.

AU, N. P. B., WU, T., KUMAR, G., JIN, Y., LI, Y. Y. T., CHAN, S. L., LAI, J. H. C., CHAN, K. W. Y., YU, K. N., WANG, X. & MA, C. H. E. 2024. Low-dose ionizing radiation promotes motor recovery and brain rewiring by resolving inflammatory response after brain injury and stroke. *Brain, Behavior, and Immunity,* 115**,** 43-63.

AUDOY-RÉMUS, J., RICHARD, J.-F., SOULET, D., ZHOU, H., KUBES, P. & VALLIÈRES, L. 2008. Rod-Shaped Monocytes Patrol the Brain Vasculature and Give Rise to Perivascular Macrophages under the Influence of Proinflammatory Cytokines and Angiopoietin-2. *The Journal of Neuroscience,* 28**,** 10187-10199.

BALKAYA, M., KRÖBER, J. M., REX, A. & ENDRES, M. 2013. Assessing post-stroke behavior in mouse models of focal ischemia. *Journal of Cerebral Blood Flow & Metabolism,* 33**,** 330-338.

BANDERA, E., BOTTERI, M., MINELLI, C., SUTTON, A., ABRAMS, K. R. & LATRONICO, N. 2006. Cerebral Blood Flow Threshold of Ischemic Penumbra and Infarct Core in Acute Ischemic Stroke. *Stroke,* 37**,** 1334-1339.

BARANOVA, I. N., BOCHAROV, A. V., VISHNYAKOVA, T. G., CHEN, Z., KE, Y., BIRUKOVA, A. A., YUEN, P. S., TSUJI, T., STAR, R. A. & BIRUKOV, K. G. 2024. Class B Scavenger Receptor CD36 as a Potential Therapeutic Target in Inflammation Induced by Danger-Associated Molecular Patterns. *Cells,* 13**,** 1992.

BARBOSA PEREIRA, C., KUNCZIK, J., ZIEGLOWSKI, L., TOLBA, R., ABDELRAHMAN, A., ZECHNER, D., VOLLMAR, B., JANSSEN, H., THUM, T. & CZAPLIK, M. 2018. Remote welfare monitoring of rodents using thermal imaging. *Sensors,* 18**,** 3653.

BARKAUSKAS, D. S., EVANS, T. A., MYERS, J., PETROSIUTE, A., SILVER, J. & HUANG, A. Y. 2013. Extravascular CX3CR1+ cells extend intravascular dendritic processes into intact central nervous system vessel lumen. *Microscopy and Microanalysis,* 19**,** 778-790.

BAUMGARDNER, J. E. & OTTO, C. M. 2003. In vitro intermittent hypoxia: challenges for creating hypoxia in cell culture. *Respiratory Physiology & Neurobiology,* 136**,** 131-139.

BECKTEL, D. A., ZBESKO, J. C., FRYE, J. B., CHUNG, A. G., HAYES, M., CALDERON, K., GROVER, J. W., LI, A., GARCIA, F. G. & TAVERA-GARCIA, M. A. 2022. Repeated administration of 2-hydroxypropyl-ß-cyclodextrin (HPßCD) attenuates the chronic inflammatory response to experimental stroke. *Journal of Neuroscience,* 42**,** 325-348.

BELENICHEV, I., POPAZOVA, O., BUKHTIYAROVA, N., SAVCHENKO, D., OKSENYCH, V. & KAMYSHNYI, O. 2024. Modulating Nitric Oxide: Implications for Cytotoxicity and Cytoprotection. *Antioxidants,* 13**,** 504.

BELENKY, S. N., ROBBINS, R. A. & RUBINSTEIN, I. 1993. Nitric oxide synthase inhibitors attenuate human monocyte chemotaxis in vitro. *Journal of Leukocyte Biology,* 53**,** 498-503.

BELOV KIRDAJOVA, D., KRISKA, J., TURECKOVA, J. & ANDEROVA, M. 2020. Ischemia-Triggered Glutamate Excitotoxicity From the Perspective of Glial Cells. *Frontiers in Cellular Neuroscience,* 14.

BENAKIS, C., GARCIA-BONILLA, L., IADECOLA, C. & ANRATHER, J. 2015. The role of microglia and myeloid immune cells in acute cerebral ischemia. *Frontiers in Cellular Neuroscience*. Frontiers Media S.A.

BENJAMIN, E. J., MUNTNER, P., ALONSO, A., BITTENCOURT, M. S., CALLAWAY, C. W., CARSON, A. P., CHAMBERLAIN, A. M., CHANG, A. R., CHENG, S. & DAS, S. R. 2019. Heart disease and stroke statistics—2019 update: a report from the American Heart Association. *Circulation,* 139**,** e56-e528.

BERGE, E., WHITELEY, W., AUDEBERT, H., DE MARCHIS, G. M., FONSECA, A. C., PADIGLIONI, C., DE LA OSSA, N. P., STRBIAN, D., TSIVGOULIS, G. & TURC, G. 2021. European Stroke Organisation (ESO) guidelines on intravenous thrombolysis for acute ischaemic stroke. *Eur Stroke J,* 6**,** I-lxii.

BERNARDO-CASTRO, S., SOUSA, J. A., BRÁS, A., CECÍLIA, C., RODRIGUES, B., ALMENDRA, L., MACHADO, C., SANTO, G., SILVA, F. & FERREIRA, L. 2020. Pathophysiology of blood–brain barrier permeability throughout the different stages of ischemic stroke and its implication on hemorrhagic transformation and recovery. *Frontiers in neurology,* 11**,** 594672.

BEUKER, C., STRECKER, J. K., RAWAL, R., SCHMIDT-POGODA, A., RUCK, T., WIENDL, H., KLOTZ, L., SCHÄBITZ, W. R., SOMMER, C. J., MINNERUP, H., MEUTH, S. G. & MINNERUP, J. 2021. Immune Cell Infiltration into the Brain After Ischemic Stroke in Humans Compared to Mice and Rats: a Systematic Review and Meta-Analysis. *Translational Stroke Research*. Springer.

BHF 2024. British Heart Foundation Heart & Circulatory Disease Statistics, 2024 Compendium.

BI, F., ZHANG, Y., LIU, W. & XIE, K. 2021. Sinomenine activation of Nrf2 signaling prevents inflammation and cerebral injury in a mouse model of ischemic stroke. *Exp Ther Med,* 21**,** 647.

BIEBER, M., GRONEWOLD, J., SCHARF, A.-C., SCHUHMANN, M. K., LANGHAUSER, F., HOPP, S., MENCL, S., GEUSS, E., LEINWEBER, J. & GUTHMANN, J. 2019a. Validity and reliability of neurological scores in mice exposed to middle cerebral artery occlusion. *Stroke,* 50**,** 2875-2882.

BIEBER, M., GRONEWOLD, J., SCHARF, A. C., SCHUHMANN, M. K., LANGHAUSER, F., HOPP, S., MENCL, S., GEUSS, E., LEINWEBER, J., GUTHMANN, J., DOEPPNER, T. R., KLEINSCHNITZ, C., STOLL, G., KRAFT, P. & HERMANN, D. M. 2019b. Validity and Reliability of Neurological Scores in Mice Exposed to Middle Cerebral Artery Occlusion. *Stroke,* 50**,** 2875-2882.

BIJNEN, M., SRIDHAR, S., KELLER, A. & GRETER, M. 2024. Brain macrophages in vascular health and dysfunction. *Trends in Immunology*.

BODHANKAR, S., CHEN, Y., VANDENBARK, A. A., MURPHY, S. J. & OFFNER, H. 2013. IL-10-producing B-cells limit CNS inflammation and infarct volume in experimental stroke. *Metabolic brain disease,* 28**,** 375-386.

BOGOUSSLAVSKY, J., VAN MELLE, G. & REGLI, F. 1988. The Lausanne Stroke Registry: analysis of 1,000 consecutive patients with first stroke. *Stroke,* 19**,** 1083-1092.

BOHLEN, C. J., BENNETT, F. C. & BENNETT, M. L. 2019. Isolation and culture of microglia. *Current protocols in immunology,* 125**,** e70.

BORDT, E. A., BLOCK, C. L., PETROZZIELLO, T., SADRI-VAKILI, G., SMITH, C. J., EDLOW, A. G. & BILBO, S. D. 2020. Isolation of Microglia from Mouse or Human Tissue. *STAR Protocols,* 1**,** 100035.

BORING, L., GOSLING, J., CHENSUE, S. W., KUNKEL, S. L., FARESE, R. V., BROXMEYER, H. E. & CHARO, I. F. 1997. Impaired monocyte migration and reduced type 1 (Th1) cytokine responses in CC chemokine receptor 2 knockout mice. *The Journal of clinical investigation,* 100**,** 2552-2561.

BOSCÁ, L., ZEINI, M., TRAVÉS, P. G. & HORTELANO, S. 2005. Nitric oxide and cell viability in inflammatory cells: a role for NO in macrophage function and fate. *Toxicology,* 208**,** 249-258.

BOUABDALLAOUI, N., TARDIF, J.-C., WATERS, D. D., PINTO, F. J., MAGGIONI, A. P., DIAZ, R., BERRY, C., KOENIG, W., LOPEZ-SENDON, J. & GAMRA, H. 2020. Time-to-treatment initiation of colchicine and cardiovascular outcomes after myocardial infarction in the Colchicine Cardiovascular Outcomes Trial (COLCOT). *European heart journal,* 41**,** 4092-4099.

BRACARD, S., DUCROCQ, X., MAS, J. L., SOUDANT, M., OPPENHEIM, C., MOULIN, T. & GUILLEMIN, F. 2016. Mechanical thrombectomy after intravenous alteplase versus alteplase alone after stroke (THRACE): a randomised controlled trial. *The Lancet Neurology,* 15**,** 1138-1147.

BRAIT, V. H., ARUMUGAM, T. V., DRUMMOND, G. R. & SOBEY, C. G. 2012. Importance of T lymphocytes in brain injury, immunodeficiency, and recovery after cerebral ischemia. *J Cereb Blood Flow Metab,* 32**,** 598-611.

BRAIT, V. H., WRIGHT, D. K., NATEGH, M., OMAN, A., SYEDA, W. T., ERMINE, C. M., O'BRIEN, K. R., WERDEN, E., CHURILOV, L., JOHNSTON, L. A., THOMPSON, L. H., NITHIANANTHARAJAH, J., JACKMAN, K. A. & BRODTMANN, A. 2021. Longitudinal hippocampal volumetric changes in mice following brain infarction. *Scientific Reports,* 11**,** 10269.

BREZOVAKOVA, V. & JADHAV, S. 2020. Identification of Lyve-1 positive macrophages as resident cells in meninges of rats. *Journal of Comparative Neurology,* 528**,** 2021-2032.

BRIOSCHI, S., BELK, J. A., PENG, V., MOLGORA, M., RODRIGUES, P. F., NGUYEN, K. M., WANG, S., DU, S., WANG, W.-L., GRAJALES-REYES, G. E., PONCE, J. M., YUEDE, C. M., LI, Q., BAER, J. M., DENARDO, D. G., GILFILLAN, S., CELLA, M., SATPATHY, A. T. & COLONNA, M. 2023. A Cre-deleter specific for embryo-derived brain macrophages reveals distinct features of microglia and border macrophages. *Immunity,* 56**,** 1027-1045.e8.

BROUNS, R., MARESCAU, B., POSSEMIERS, I., SHEORAJPANDAY, R. & DE DEYN, P. P. 2009. Dimethylarginine levels in cerebrospinal fluid of hyperacute ischemic stroke patients are associated with stroke severity. *Neurochemical research,* 34**,** 1642-1649.

BROWN, G. C. 2010. Nitric oxide and neuronal death. *Nitric Oxide,* 23**,** 153-165.

BROWN, G. C. & COOPER, C. E. 1994. Nanomolar concentrations of nitric oxide reversibly inhibit synaptosomal respiration by competing with oxygen at cytochrome oxidase. *FEBS letters,* 356**,** 295-298.

BUENAVENTURA, R. G., HARVEY, A. C., BURNS, M. P. & MAIN, B. S. 2022. Sequential Isolation of Microglia and Astrocytes from Young and Aged Adult Mouse Brains for Downstream Transcriptomic Analysis. *Methods and Protocols,* 5**,** 77.

CAI, L., GENG, X., HUSSAIN, M., LIU, Z., GAO, Z., LIU, S., DU, H., JI, X. & DING, Y. 2015. Weight loss: indication of brain damage and effect of combined normobaric oxygen and ethanol therapy after stroke. *Neurological Research,* 37**,** 441-446.

CAI, W., DAI, X., CHEN, J., ZHAO, J., XU, M., ZHANG, L., YANG, B., ZHANG, W., ROCHA, M. & NAKAO, T. 2019. STAT6/Arg1 promotes microglia/macrophage efferocytosis and inflammation resolution in stroke mice. *JCI insight,* 4**,** e131355.

CAI, W., LIU, S., HU, M., HUANG, F., ZHU, Q., QIU, W., HU, X., COLELLO, J., ZHENG, S. G. & LU, Z. 2020. Functional dynamics of neutrophils after ischemic stroke. *Translational stroke research,* 11**,** 108-121.

CAMPBELL, B. C., MITCHELL, P. J., CHURILOV, L., YASSI, N., KLEINIG, T. J., DOWLING, R. J., YAN, B., BUSH, S. J., DEWEY, H. M. & THIJS, V. 2018. Tenecteplase versus alteplase before thrombectomy for ischemic stroke. *New England Journal of Medicine,* 378**,** 1573-1582.

CAMPBELL, B. C., MITCHELL, P. J., CHURILOV, L., YASSI, N., KLEINIG, T. J., DOWLING, R. J., YAN, B., BUSH, S. J., THIJS, V. & SCROOP, R. 2020. Effect of intravenous tenecteplase dose on cerebral reperfusion before thrombectomy in patients with large vessel occlusion ischemic stroke: the EXTEND-IA TNK part 2 randomized clinical trial. *Jama,* 323**,** 1257-1265.

CAMPBELL, B. C. V., DE SILVA, D. A., MACLEOD, M. R., COUTTS, S. B., SCHWAMM, L. H., DAVIS, S. M. & DONNAN, G. A. 2019. Ischaemic stroke. *Nature Reviews Disease Primers,* 5**,** 70.

CARMICHAEL, S. T. 2005. Rodent models of focal stroke: Size, mechanism, and purpose. *NeuroRX*. American Society for Experimental Neurotherapeutics.

CARPANESE, E., MORETTO, P., FILPA, V., MARCHET, S., MORO, E., CREMA, F., FRIGO, G. & GIARONI, C. 2014. Antagonism of ionotropic glutamate receptors attenuates chemical ischemia-induced injury in rat primary cultured myenteric ganglia. *PLoS One,* 9**,** e113613.

CHEN, C.-H., ZHAO, J.-F., HSU, C.-P., KOU, Y. R., LU, T.-M. & LEE, T.-S. 2019. The detrimental effect of asymmetric dimethylarginine on cholesterol efflux of macrophage foam cells: Role of the NOX/ROS signaling. *Free Radical Biology and Medicine,* 143**,** 354-365.

CHEN, M., YAN, R., LUO, J., NING, J., ZHOU, R. & DING, L. 2023. The role of PGC-1α-mediated mitochondrial biogenesis in neurons. *Neurochemical research,* 48**,** 2595-2606.

CHEN, S., BENNET, L. & MCGREGOR, A. L. 2015. MacGreen mice: a novel tool to investigate inflammation following experimental stroke. *J. Exp. Stroke Trans. Med,* 8**,** 1-9.

CHEN, S., MARTENS-LOBENHOFFER, J., WEISSENBORN, K., KIELSTEIN, J. T., LICHTINGHAGEN, R., DEB, M., LI, N., TRYC, A. B., GOLDBECKER, A. & DONG, Q. 2012. Association of dimethylarginines and mediators of inflammation after acute ischemic stroke. *Journal of neuroinflammation,* 9**,** 1-9.

CHEN, Z.-Q., MOU, R.-T., FENG, D.-X., WANG, Z. & CHEN, G. 2017. The role of nitric oxide in stroke. *Medical Gas Research*. Medknow Publications.

CHO, D.-I., KIM, M. R., JEONG, H.-Y., JEONG, H. C., JEONG, M. H., YOON, S. H., KIM, Y. S. & AHN, Y. 2014. Mesenchymal stem cells reciprocally regulate the M1/M2 balance in mouse bone marrow-derived macrophages. *Experimental & Molecular Medicine,* 46**,** e70-e70.

CHU, H. X., BROUGHTON, B. R. S., AH KIM, H., LEE, S., DRUMMOND, G. R. & SOBEY, C. G. 2015. Evidence That Ly6C hi Monocytes Are Protective in Acute Ischemic Stroke by Promoting M2 Macrophage Polarization. *Stroke*. Lippincott Williams and Wilkins.

CHU, H. X., KIM, H. A., LEE, S., MOORE, J. P., CHAN, C. T., VINH, A., GELDERBLOM, M., ARUMUGAM, T. V., BROUGHTON, B. R., DRUMMOND, G. R. & SOBEY, C. G. 2014. Immune Cell Infiltration in Malignant Middle Cerebral Artery Infarction: Comparison with Transient Cerebral Ischemia. *Journal of Cerebral Blood Flow & Metabolism,* 34**,** 450-459.

CHUNG, A. G., FRYE, J. B., ZBESKO, J. C., CONSTANTOPOULOS, E., HAYES, M., FIGUEROA, A. G., BECKTEL, D. A., DAY, W. A., KONHILAS, J. P. & MCKAY, B. S. 2018. Liquefaction of the brain following stroke shares a similar molecular and morphological profile with atherosclerosis and mediates secondary neurodegeneration in an osteopontin-dependent mechanism. *eneuro,* 5.

CHUNG, J. W., PARK, S. H., KIM, N., KIM, W. J., PARK, J. H., KO, Y., YANG, M. H., JANG, M. S., HAN, M. K. & JUNG, C. 2014. Trial of ORG 10172 in Acute Stroke Treatment (TOAST) classification and vascular territory of ischemic stroke lesions diagnosed by diffusion – weighted imaging. *Journal of the American Heart Association,* 3, e001119.

CILLERO-PASTOR, B., MATEOS, J., FERNÁNDEZ-LÓPEZ, C., OREIRO, N., RUIZ-ROMERO, C. & BLANCO, F. J. 2012. Dimethylarginine dimethylaminohydrolase 2, a newly identified mitochondrial protein modulating nitric oxide synthesis in normal human chondrocytes. *Arthritis & Rheumatism,* 64, 204-212.

CIRIZA, J., THOMPSON, H., PETROSIAN, R., MANILAY, J. O. & GARCÍA-OJEDA, M. E. 2013. The migration of hematopoietic progenitors from the fetal liver to the fetal bone marrow: lessons learned and possible clinical applications. *Experimental hematology,* 41, 411-423.

CLARKE, D. D. & SOKOLOFF, L. 1999. Circulation and energy metabolism in the brain/Donald D. Clarke and Louis Sokoloff.

CLARKE, S. 1993. Protein methylation. *Current Opinion in Cell Biology,* 5, 977-983.

CLAUSEN, B. E., BURKHARDT, C., REITH, W., RENKAWITZ, R. & FÖRSTER, I. 1999. Conditional gene targeting in macrophages and granulocytes using LysMcre mice. *Transgenic Res,* 8, 265-77.

CONNELLY, L., JACOBS, A. T., PALACIOS-CALLENDER, M., MONCADA, S. & HOBBS, A. J. 2003. Macrophage Endothelial Nitric-oxide Synthase Autoregulates Cellular Activation and Pro-inflammatory Protein Expression *. *Journal of Biological Chemistry,* 278, 26480-26487.

COOKE, J. P. 2005. ADMA: its role in vascular disease. *Vascular Medicine,* 10, S11-S17.

COOPER, M. D. & ALDER, M. N. 2006. The evolution of adaptive immune systems. *Cell,* 124, 815-822.

CROESE, T., CASTELLANI, G. & SCHWARTZ, M. 2021. Immune cell compartmentalization for brain surveillance and protection. *Nature Immunology,* 22, 1083-1092.

CROSS, M., MANGELSDORF, I., WEDEL, A. & RENKAWITZ, R. 1988. Mouse lysozyme M gene: isolation, characterization, and expression studies. *Proceedings of the National Academy of Sciences,* 85, 6232-6236.

CRUM, W. R., GIAMPIETRO, V. P., SMITH, E. J., GORENKOVA, N., STROEMER, R. P. & MODO, M. 2013. A comparison of automated anatomical–behavioural mapping methods in a rodent model of stroke. *Journal of Neuroscience Methods,* 218, 170-183.

CUGURRA, A., MAMULADZE, T., RUSTENHOVEN, J., DYKSTRA, T., BEROSHVILI, G., GREENBERG, Z. J., BAKER, W., PAPADOPOULOS, Z., DRIEU, A., BLACKBURN, S., KANAMORI, M., BRIOSCHI, S., HERZ, J., SCHUETTPELZ, L. G., COLONNA, M., SMIRNOV, I. & KIPNIS, J. 2021. Skull and vertebral bone marrow are myeloid cell reservoirs for the meninges and CNS parenchyma. *Science*, eabf7844.

CUNNINGHAM, C. L., MARTÍNEZ-CERDEÑO, V. & NOCTOR, S. C. 2013. Microglia regulate the number of neural precursor cells in the developing cerebral cortex. *Journal of Neuroscience,* 33, 4216-4233.

CYR, A. R., HUCKABY, L. V., SHIVA, S. S. & ZUCKERBRAUN, B. S. 2020. Nitric oxide and endothelial dysfunction. *Critical care clinics,* 36, 307-321.

DALMAU GASULL, A., GLAVAN, M., SAMAWAR, S. K. R., KAPUPARA, K., KELK, J., RUBIO, M., FUMAGALLI, S., SOROKIN, L., VIVIEN, D. & PRINZ, M. 2024. The niche matters: origin, function and fate of CNS-associated macrophages during health and disease. *Acta Neuropathologica,* 147, 37.

DANI, N., HERBST, R. H., MCCABE, C., GREEN, G. S., KAISER, K., HEAD, J. P., CUI, J., SHIPLEY, F. B., JANG, A., DIONNE, D., NGUYEN, L., RODMAN, C., RIESENFELD, S. J., PROCHAZKA, J., PROCHAZKOVA, M., SEDLACEK, R., ZHANG, F., BRYJA, V.,

ROZENBLATT-ROSEN, O., HABIB, N., REGEV, A. & LEHTINEN, M. K. 2021. A cellular and spatial map of the choroid plexus across brain ventricles and ages. *Cell,* 184**,** 3056-3074.e21.

DANIELISOVA, V., BURDA, J., NEMETHOVA, M. & GOTTLIEB, M. 2011. Aminoguanidine Administration Ameliorates Hippocampal Damage After Middle Cerebral Artery Occlusion in Rat. *Neurochemical Research,* 36**,** 476-486.

DAO, V. T.-V., ELBATREEK, M. H., FUCHS, T., GRÄDLER, U., SCHMIDT, H. H. H. W., SHAH, A. M., WALLACE, A. & KNOWLES, R. 2021. Nitric Oxide Synthase Inhibitors into the Clinic at Last. *In:* SCHMIDT, H. H. H. W., GHEZZI, P. & CUADRADO, A. (eds.) *Reactive Oxygen Species : Network Pharmacology and Therapeutic Applications.* Cham: Springer International Publishing.

DARRA, E., RUNGATSCHER, A., DE PRATI, A. C., PODESSER, B. K., FAGGIAN, G., SCARABELLI, T., MAZZUCCO, A., HALLSTRÖM, S. & SUZUKI, H. 2010. Dual modulation of nitric oxide production in the heart during ischaemia/reperfusion injury and inflammation. *Thrombosis and haemostasis,* 104**,** 200-206.

DAVIES, L. C., ROSAS, M., SMITH, P. J., FRASER, D. J., JONES, S. A. & TAYLOR, P. R. 2011. A quantifiable proliferative burst of tissue macrophages restores homeostatic macrophage populations after acute inflammation. *European Journal of Immunology,* 41**,** 2155-2164.

DAWSON, V. L., DAWSON, T. M., BARTLEY, D. A., UHL, G. R. & SNYDER, S. H. 1993. Mechanisms of nitric oxide-mediated neurotoxicity in primary brain cultures. *Journal of Neuroscience,* 13**,** 2651-2661.

DAWSON, V. L., KIZUSHI, V. M., HUANG, P. L., SNYDER, S. H. & DAWSON, T. M. 1996. Resistance to neurotoxicity in cortical cultures from neuronal nitric oxide synthase-deficient mice. *Journal of Neuroscience,* 16**,** 2479-2487.

DAYAL, S., RODIONOV, R. N., ARNING, E., BOTTIGLIERI, T., KIMOTO, M., MURRY, D. J., COOKE, J. P., FARACI, F. M. & LENTZ, S. R. 2008. Tissue-specific downregulation of dimethylarginine dimethylaminohydrolase in hyperhomocysteinemia. *American Journal of Physiology-Heart and Circulatory Physiology,* 295**,** H816-H825.

DE GENNARO COLONNA, V., BIANCHI, M., PASCALE, V., FERRARIO, P., MORELLI, F., PASCALE, W., TOMASONI, L. & TURIEL, M. 2009. Asymmetric dimethylarginine (ADMA): An endogenous inhibitor of nitric oxide synthase and a novel cardiovascular risk molecule. *Medical Science Monitor,* 15**,** RA91-RA101.

DE SCHEPPER, S., GE, J. Z., CROWLEY, G., FERREIRA, L. S., GARCEAU, D., TOOMEY, C. E., SOKOLOVA, D., RUEDA-CARRASCO, J., SHIN, S.-H. & KIM, J.-S. 2023. Perivascular cells induce microglial phagocytic states and synaptic engulfment via SPP1 in mouse models of Alzheimer's disease. *Nature neuroscience,* 26**,** 406-415.

DEACON, R. M. 2006a. Assessing nest building in mice. *Nature protocols,* 1**,** 1117-1119.

DEACON, R. M. J. 2006b. Assessing nest building in mice. *Nature Protocols,* 1**,** 1117-1119.

DEAKIN, J. E., PAPENFUSS, A. T., BELOV, K., CROSS, J. G., COGGILL, P., PALMER, S., SIMS, S., SPEED, T. P., BECK, S. & GRAVES, J. A. 2006. Evolution and comparative analysis of the MHC Class III inflammatory region. *BMC Genomics,* 7**,** 281.

DEL ÁGUILA, Á., ZHANG, R., YU, X., DANG, L., XU, F., ZHANG, J., JAIN, V., TIAN, J., ZHONG, X.-P., SHENG, H. & YANG, W. 2024. Microglial heterogeneity in the ischemic stroke mouse brain of both sexes. *Genome Medicine,* 16**,** 95.

DELBRIDGE, A. R. D., HUH, D., BRICKELMAIER, M., BURNS, J. C., ROBERTS, C., CHALLA, R., RAYMOND, N., CULLEN, P., CARLILE, T. M., ENNIS, K. A., LIU, M., SUN, C., ALLAIRE, N. E., FOOS, M., TSAI, H.-H., FRANCHIMONT, N., RANSOHOFF, R. M., BUTTS, C. & MINGUENEAU, M. 2020. Organotypic Brain Slice Culture Microglia Exhibit Molecular Similarity to Acutely-Isolated Adult Microglia and Provide a Platform to Study Neuroinflammation. *Frontiers in Cellular Neuroscience,* 14.

DERECKI, N., LOUVEAU, A. & KIPNIS, J. 2015. Dissection and immunostaining of mouse whole-mount meninges. *Protocol Exchange*.

DERMITZAKIS, I., THEOTOKIS, P., EVANGELIDIS, P., DELILAMPOU, E., EVANGELIDIS, N., CHATZISAVVIDOU, A., AVRAMIDOU, E. & MANTHOU, M. E. 2023. CNS Border-Associated Macrophages: Ontogeny and Potential Implication in Disease. *Curr Issues Mol Biol,* 45**,** 4285-4300.

DIENEL, G. A. 2019. Brain glucose metabolism: integration of energetics with function. *Physiological reviews,* 99**,** 949-1045.

DONG, X., ZHANG, X., LI, C., CHEN, J., XIA, S., BAO, X., GE, J., CAO, X. & XU, Y. 2022. γδ T cells aggravate blood–brain-barrier injury via IL-17A in experimental ischemic stroke. *Neuroscience letters,* 776**,** 136563.

DOWSETT, L., HIGGINS, E., ALANAZI, S., ALSHUWAYER, N. A., LEIPER, F. C. & LEIPER, J. 2020. ADMA: a key player in the relationship between vascular dysfunction and inflammation in atherosclerosis. *Journal of Clinical Medicine,* 9**,** 3026.

DOWSETT, L., PIPER, S., SLAVIERO, A., DUFTON, N., WANG, Z., BORUC, O., DELAHAYE, M., COLMAN, L., KALK, E., TOMLINSON, J., BIRDSEY, G., RANDI, A. M. & LEIPER, J. 2015. Endothelial dimethylarginine dimethylaminohydrolase 1 is an important regulator of angiogenesis but does not regulate vascular reactivity or hemodynamic homeostasis. *Circulation.* Lippincott Williams and Wilkins.

DOYLE, K. P., CEKANAVICIUTE, E., MAMER, L. E. & BUCKWALTER, M. S. 2010. TGFβ signaling in the brain increases with aging and signals to astrocytes and innate immune cells in the weeks after stroke. *Journal of Neuroinflammation,* 7**,** 62.

DOYLE, K. P., QUACH, L. N., SOLÉ, M., AXTELL, R. C., NGUYEN, T.-V. V., SOLER-LLAVINA, G. J., JURADO, S., HAN, J., STEINMAN, L., LONGO, F. M., SCHNEIDER, J. A., MALENKA, R. C. & BUCKWALTER, M. S. 2015. B-Lymphocyte-Mediated Delayed Cognitive Impairment following Stroke. *The Journal of Neuroscience,* 35**,** 2133-2145.

DRIEU, A., DU, S., STORCK, S. E., RUSTENHOVEN, J., PAPADOPOULOS, Z., DYKSTRA, T., ZHONG, F., KIM, K., BLACKBURN, S., MAMULADZE, T., HARARI, O., KARCH, C. M., BATEMAN, R. J., PERRIN, R., FARLOW, M., CHHATWAL, J., BROSCH, J., BUCK, J., FARLOW, M., GHETTI, B., ADAMS, S., BARTHELEMY, N., BENZINGER, T., BRANDON, S., BUCKLES, V., CASH, L., CHEN, C., CHUA, J., CRUCHAGA, C., DENNER, D., DINCER, A., DONAHUE, T., FAGAN, A., FELDMAN, B., FLORES, S., FRANKLIN, E., JOSEPH-MATHURIN, N., GONZALEZ, A., GORDON, B., GRAY, J., GREMMINGER, E., GROVES, A., HASSENSTAB, J., HELLM, C., HERRIES, E., HOECHST-SWISHER, L., HOLTZMAN, D., HORNBECK, R., JEROME, G., KEEFE, S., KOUDELIS, D., LI, Y., MARSH, J., MARTINEZ, R., MAWUENYEGA, K., MCCULLOUGH, A., MCDADE, E., MORRIS, J., NORTON, J., SHADY, K., SIGURDSON, W., SMITH, J., WANG, P., WANG, Q., XIONG, C., XU, J., XU, X., ALLEGRI, R., MENDEZ, P. C., EGIDO, N., ARAKI, A., IKEUCHI, T., ISHII, K., KASUGA, K., BECHARA, J., BROOKS, W., SCHOFIELD, P., BERMAN, S., GOLDBERG, S., IKONOMOVIC, S., KLUNK, W., LOPEZ, O., MOUNTZ, J., NADKARNI, N., PATIRA, R., SMITH, L., SNITZ, B., THOMPSON, S., WEAMER, E., BODGE, C., SALLOWAY, S., CARTER, K., DUONG, D., JOHNSON, E., LEVEY, A., PING, L., SEYFRIED, N. T., FITZPATRICK, C., CHUI, H., RINGMAN, J., et al. 2022. Parenchymal border macrophages regulate the flow dynamics of the cerebrospinal fluid. *Nature,* 611**,** 585-593.

DRIEU, A., LANQUETIN, A., LEVARD, D., GLAVAN, M., CAMPOS, F., QUENAULT, A., LEMARCHAND, E., NAVEAU, M., PITEL, A. L., CASTILLO, J., VIVIEN, D. & RUBIO, M. 2020. Alcohol exposure–induced neurovascular inflammatory priming impacts ischemic stroke and is linked with brain perivascular macrophages. *JCI Insight*. American Society for Clinical Investigation.

DURÁN-LAFORET, V., FERNÁNDEZ-LÓPEZ, D., GARCÍA-CULEBRAS, A., GONZÁLEZ-HIJÓN, J., MORAGA, A., PALMA-TORTOSA, S., GARCÍA-YÉBENES, I., VEGA-PÉREZ, A., LIZASOAIN, I. & MORO, M. Á. 2019. Delayed Effects of Acute Reperfusion on Vascular Remodeling and Late-Phase Functional Recovery After Stroke. *Frontiers in Neuroscience,* 13.

EL AMKI, M., GLÜCK, C., BINDER, N., MIDDLEHAM, W., WYSS, M. T., WEISS, T., MEISTER, H., LUFT, A., WELLER, M., WEBER, B. & WEGENER, S. 2020. Neutrophils

Obstructing Brain Capillaries Are a Major Cause of No-Reflow in Ischemic Stroke. *Cell Rep,* 33**,** 108260.

ELTZSCHIG, H. K. & ECKLE, T. 2011. Ischemia and reperfusion—from mechanism to translation. *Nature medicine,* 17**,** 1391-1401.

EMBERSON, J., LEES, K. R., LYDEN, P., BLACKWELL, L., ALBERS, G., BLUHMKI, E., BROTT, T., COHEN, G., DAVIS, S. & DONNAN, G. 2014. Effect of treatment delay, age, and stroke severity on the effects of intravenous thrombolysis with alteplase for acute ischaemic stroke: a meta-analysis of individual patient data from randomised trials. *The Lancet,* 384**,** 1929-1935.

EPELMAN, S., LAVINE, K. J. & RANDOLPH, G. J. 2014. Origin and functions of tissue macrophages. *Immunity,* 41**,** 21-35.

ERNDT-MARINO, J., YEISLEY, D. J., CHEN, H., LEVIN, M., KAPLAN, D. L. & HAHN, M. S. 2020. Interferon-Gamma Stimulated Murine Macrophages In Vitro: Impact of Ionic Composition and Osmolarity and Therapeutic Implications. *Bioelectricity,* 2**,** 48-58.

FABRIEK, B. O., VAN HAASTERT, E. S., GALEA, I., POLFLIET, M. M. J., DÖPP, E. D., VAN DEN HEUVEL, M. M., VAN DEN BERG, T. K., DE GROOT, C. J. A., VAN DER VALK, P. & DIJKSTRA, C. D. 2005. CD163-positive perivascular macrophages in the human CNS express molecules for antigen recognition and presentation. *Glia,* 51**,** 297-305.

FAN, M. M. Y. & RAYMOND, L. A. 2007. N-Methyl-d-aspartate (NMDA) receptor function and excitotoxicity in Huntington's disease. *Progress in Neurobiology,* 81**,** 272-293.

FANG, W., ZHAI, X., HAN, D., XIONG, X., WANG, T., ZENG, X., HE, S., LIU, R., MIYATA, M. & XU, B. 2018. CCR2-dependent monocytes/macrophages exacerbate acute brain injury but promote functional recovery after ischemic stroke in mice. *Theranostics,* 8**,** 3530.

FANN, D. Y.-W., LEE, S.-Y., MANZANERO, S., CHUNDURI, P., SOBEY, C. G. & ARUMUGAM, T. V. 2013. Pathogenesis of acute stroke and the role of inflammasomes. *Ageing Research Reviews,* 12**,** 941-966.

FARACO, G., SUGIYAMA, Y., LANE, D., GARCIA-BONILLA, L., CHANG, H., SANTISTEBAN, M. M., RACCHUMI, G., MURPHY, M., VAN ROOIJEN, N., ANRATHER, J. & IADECOLA, C. 2016. Perivascular macrophages mediate the neurovascular and cognitive dysfunction associated with hypertension. *Journal of Clinical Investigation*. American Society for Clinical Investigation.

FARDIN, P., MORETTI, S., BIASOTTI, B., RICCIARDI, A., BONASSI, S. & VARESIO, L. 2007. Normalization of low-density microarray using external spike-in controls: analysis of macrophage cell lines expression profile. *BMC Genomics,* 8**,** 17.

FEIGIN, V. L., BRAININ, M., NORRVING, B., MARTINS, S., SACCO, R. L., HACKE, W., FISHER, M., PANDIAN, J. & LINDSAY, P. 2022. World Stroke Organization (WSO): global stroke fact sheet 2022. *International Journal of Stroke,* 17**,** 18-29.

FENG, L., HAN, C.-X., CAO, S.-Y., ZHANG, H.-M. & WU, G.-Y. 2020. Deficits in motor and cognitive functions in an adult mouse model of hypoxia-ischemia induced stroke. *Scientific Reports,* 10**,** 20646.

FENG, Y., LIAO, S., WEI, C., JIA, D., WOOD, K., LIU, Q., WANG, X., SHI, F.-D. & JIN, W.-N. 2017. Infiltration and persistence of lymphocytes during late-stage cerebral ischemia in middle cerebral artery occlusion and photothrombotic stroke models. *Journal of neuroinflammation,* 14**,** 1-12.

FISCHER, U., KAESMACHER, J., STRBIAN, D., EKER, O., COGNARD, C., PLATTNER, P. S., BÜTIKOFER, L., MORDASINI, P., DEPPELER, S. & PEREIRA, V. M. 2022. Thrombectomy alone versus intravenous alteplase plus thrombectomy in patients with stroke: an open-label, blinded-outcome, randomised non-inferiority trial. *The Lancet,* 400**,** 104-115.

FLORES, J. J., ZHANG, Y., KLEBE, D. W., LEKIC, T., FU, W. & ZHANG, J. H. 2014. Small molecule inhibitors in the treatment of cerebral ischemia. *Expert Opin Pharmacother,* 15**,** 659-80.

FLURI, F., SCHUHMANN, M. K. & KLEINSCHNITZ, C. 2015. Animal models of ischemic stroke and their application in clinical research. *Drug design, development and therapy*. Dove Medical Press Ltd.

FRANCO, R. & FERNÁNDEZ-SUÁREZ, D. 2015. Alternatively activated microglia and macrophages in the central nervous system. *Progress in Neurobiology,* 131**,** 65-86.

FUHRMANN, M., BITTNER, T., JUNG, C. K., BURGOLD, S., PAGE, R. M., MITTEREGGER, G., HAASS, C., LAFERLA, F. M., KRETZSCHMAR, H. & HERMS, J. 2010. Microglial Cx3cr1 knockout prevents neuron loss in a mouse model of Alzheimer's disease. *Nature neuroscience,* 13**,** 411-413.

GADANI, SACHIN P., WALSH, JAMES T., SMIRNOV, I., ZHENG, J. & KIPNIS, J. 2015. The Glia-Derived Alarmin IL-33 Orchestrates the Immune Response and Promotes Recovery following CNS Injury. *Neuron,* 85**,** 703-709.

GALEA, I., PALIN, K., NEWMAN, T. A., VAN ROOIJEN, N., PERRY, V. H. & BOCHE, D. 2005. Mannose receptor expression specifically reveals perivascular macrophages in normal, injured, and diseased mouse brain. *Glia,* 49**,** 375-384.

GAO, Q., NI, P., WANG, Y., HUO, P., ZHANG, X., WANG, S., XIAO, F., LI, Y., FENG, W. & YUAN, J. 2024. DDAH1 promotes neurogenesis and neural repair in cerebral ischemia. *Acta Pharmaceutica Sinica B,* 14**,** 2097-2118.

GARCIA, R. G., PEREZ, M., MAAS, R., SCHWEDHELM, E., BÖGER, R. H. & LÓPEZ-JARAMILLO, P. 2007. Plasma concentrations of asymmetric dimethylarginine (ADMA) in metabolic syndrome. *International Journal of Cardiology,* 122**,** 176-178.

GARCIA-BONILLA, L., FARACO, G., MOORE, J., MURPHY, M., RACCHUMI, G., SRINIVASAN, J., BREA, D., IADECOLA, C. & ANRATHER, J. 2016. Spatio-temporal profile, phenotypic diversity, and fate of recruited monocytes into the post-ischemic brain. *Journal of Neuroinflammation,* 13**,** 285.

GARCIA-BONILLA, L., MOORE, J. M., RACCHUMI, G., ZHOU, P., BUTLER, J. M., IADECOLA, C. & ANRATHER, J. 2014. Inducible Nitric Oxide Synthase in Neutrophils and Endothelium Contributes to Ischemic Brain Injury in Mice. *The Journal of Immunology,* 193**,** 2531-2537.

GARCIA-BONILLA, L., SHAHANOOR, Z., SCIORTINO, R., NAZARZODA, O., RACCHUMI, G., IADECOLA, C. & ANRATHER, J. 2023. Brain and blood single-cell transcriptomics in acute and subacute phases after experimental stroke. *bioRxiv***,** 2023.03.31.535150.

GASKILL, B. N., KARAS, A. Z., GARNER, J. P. & PRITCHETT-CORNING, K. R. 2013. Nest building as an indicator of health and welfare in laboratory mice. *JoVE (Journal of Visualized Experiments)***,** e51012.

GAUTIER, E. L., SHAY, T., MILLER, J., GRETER, M., JAKUBZICK, C., IVANOV, S., HELFT, J., CHOW, A., ELPEK, K. G., GORDONOV, S., MAZLOOM, A. R., MA'AYAN, A., CHUA, W.-J., HANSEN, T. H., TURLEY, S. J., MERAD, M. & RANDOLPH, G. J. 2012. Gene-expression profiles and transcriptional regulatory pathways that underlie the identity and diversity of mouse tissue macrophages. *Nature Immunology,* 13**,** 1118-1128.

GEISSMANN, F., JUNG, S. & LITTMAN, D. R. 2003. Blood monocytes consist of two principal subsets with distinct migratory properties. *Immunity,* 19**,** 71-82.

GELDERBLOM, M., LEYPOLDT, F., STEINBACH, K., BEHRENS, D., CHOE, C.-U., SILER, D. A., ARUMUGAM, T. V., ORTHEY, E., GERLOFF, C., TOLOSA, E. & MAGNUS, T. 2009. Temporal and Spatial Dynamics of Cerebral Immune Cell Accumulation in Stroke. *Stroke,* 40**,** 1849-1857.

GIBSON, C. L., BATH, P. M. & MURPHY, S. P. 2005. G-CSF Reduces Infarct Volume and Improves Functional Outcome after Transient Focal Cerebral Ischemia in Mice. *Journal of Cerebral Blood Flow & Metabolism,* 25**,** 431-439.

GINHOUX, F., GRETER, M., LEBOEUF, M., NANDI, S., SEE, P., GOKHAN, S., MEHLER, M. F., CONWAY, S. J., NG, L. G., STANLEY, E. R., SAMOKHVALOV, I. M. & MERAD, M. 2010. Fate mapping analysis reveals that adult microglia derive from primitive macrophages. *Science,* 330**,** 841-5.

GLIEM, M., KRAMMES, K., LIAW, L., VAN ROOIJEN, N., HARTUNG, H. P. & JANDER, S. 2015. Macrophage – derived osteopontin induces reactive astrocyte polarization and promotes re – establishment of the blood brain barrier after ischemic stroke. *Glia,* 63**,** 2198-2207.

GLIEM, M., MAUSBERG, A. K., LEE, J. I., SIMIANTONAKIS, I., VAN ROOIJEN, N., HARTUNG, H. P. & JANDER, S. 2012. Macrophages prevent hemorrhagic infarct transformation in murine stroke models. *Ann Neurol,* 71**,** 743-52.

GOLDMANN, T., WIEGHOFER, P., JORDÃO, M. J. C., PRUTEK, F., HAGEMEYER, N., FRENZEL, K., AMANN, L., STASZEWSKI, O., KIERDORF, K., KRUEGER, M., LOCATELLI, G., HOCHGERNER, H., ZEISER, R., EPELMAN, S., GEISSMANN, F., PRILLER, J., ROSSI, F. M. V., BECHMANN, I., KERSCHENSTEINER, M., LINNARSSON, S., JUNG, S. & PRINZ, M. 2016. Origin, fate and dynamics of macrophages at central nervous system interfaces. *Nature Immunology*. Nature Publishing Group.

GOMEZ PERDIGUERO, E., KLAPPROTH, K., SCHULZ, C., BUSCH, K., AZZONI, E., CROZET, L., GARNER, H., TROUILLET, C., DE BRUIJN, M. F., GEISSMANN, F. & RODEWALD, H.-R. 2015. Tissue-resident macrophages originate from yolk-sac-derived erythro-myeloid progenitors. *Nature*. Nature Publishing Group.

GOURIOU, Y., DEMAUREX, N., BIJLENGA, P. & DE MARCHI, U. 2011. Mitochondrial calcium handling during ischemia-induced cell death in neurons. *Biochimie,* 93**,** 2060-2067.

GROSS, A., SCHOENDUBE, J., ZIMMERMANN, S., STEEB, M., ZENGERLE, R. & KOLTAY, P. 2015. Technologies for single-cell isolation. *International journal of molecular sciences,* 16**,** 16897-16919.

GROSS, T. J., KREMENS, K., POWERS, L. S., BRINK, B., KNUTSON, T., DOMANN, F. E., PHILIBERT, R. A., MILHEM, M. M. & MONICK, M. M. 2014. Epigenetic silencing of the human NOS2 gene: rethinking the role of nitric oxide in human macrophage inflammatory responses. *The Journal of Immunology,* 192**,** 2326-2338.

GROSSMANN, R., STENCE, N., CARR, J., FULLER, L., WAITE, M. & DAILEY, M. E. 2002. Juxtavascular microglia migrate along brain microvessels following activation during early postnatal development. *Glia,* 37**,** 229-240.

GUERRIERO, J. L. 2019. Macrophages: their untold story in T cell activation and function. *International Review of Cell and Molecular Biology,* 342**,** 73-93.

GULYÁS, B., TÓTH, M., SCHAIN, M., AIRAKSINEN, A., VAS, Á., KOSTULAS, K., LINDSTRÖM, P., HILLERT, J. & HALLDIN, C. 2012. Evolution of microglial activation in ischaemic core and peri-infarct regions after stroke: a PET study with the TSPO molecular imaging biomarker [11C] vinpocetine. *Journal of the neurological sciences,* 320**,** 110-117.

HACKE, W., KASTE, M., FIESCHI, C., VON KUMMER, R., DAVALOS, A., MEIER, D., LARRUE, V., BLUHMKI, E., DAVIS, S. & DONNAN, G. 1998. Randomised double-blind placebo-controlled trial of thrombolytic therapy with intravenous alteplase in acute ischaemic stroke (ECASS II). *The Lancet,* 352**,** 1245-1251.

HAJIBABAIE, F., ABEDPOOR, N. & MOHAMADYNEJAD, P. 2023. Types of Cell Death from a Molecular Perspective. *Biology,* 12**,** 1426.

HALEY, M. J., WHITE, C. S., ROBERTS, D., O'TOOLE, K., CUNNINGHAM, C. J., RIVERS-AUTY, J., O'BOYLE, C., LANE, C., HEANEY, O. & ALLAN, S. M. 2020. Stroke induces prolonged changes in lipid metabolism, the liver and body composition in mice. *Translational stroke research,* 11**,** 837-850.

HAMADA, T., DUARTE, S., TSUCHIHASHI, S., BUSUTTIL, R. W. & COITO, A. J. 2009. Inducible nitric oxide synthase deficiency impairs matrix metalloproteinase-9 activity and disrupts leukocyte migration in hepatic ischemia/reperfusion injury. *The American journal of pathology,* 174**,** 2265-2277.

HAMMOND, T. R., DUFORT, C., DISSING-OLESEN, L., GIERA, S., YOUNG, A., WYSOKER, A., WALKER, A. J., GERGITS, F., SEGEL, M., NEMESH, J., MARSH, S. E., SAUNDERS, A., MACOSKO, E., GINHOUX, F., CHEN, J., FRANKLIN, R. J. M., PIAO, X., MCCARROLL, S. A. & STEVENS, B. 2019. Single-Cell RNA Sequencing of Microglia throughout the Mouse Lifespan and in the Injured Brain Reveals Complex Cell-State Changes. *Immunity,* 50**,** 253-271.e6.

HANNOCKS, M.-J., PIZZO, M. E., HUPPERT, J., DESHPANDE, T., ABBOTT, N. J., THORNE, R. G. & SOROKIN, L. 2018. Molecular characterization of perivascular drainage pathways in the murine brain. *Journal of Cerebral Blood Flow & Metabolism,* 38**,** 669-686.

HARARI, O. & LIAO, J. K. 2004. Inhibition of MHC II gene transcription by nitric oxide and antioxidants. *Current pharmaceutical design,* 10**,** 893-898.

HARRISON, J. K., JIANG, Y., CHEN, S., XIA, Y., MACIEJEWSKI, D., MCNAMARA, R. K., STREIT, W. J., SALAFRANCA, M. N., ADHIKARI, S. & THOMPSON, D. A. 1998. Role for neuronally derived fractalkine in mediating interactions between neurons and CX3CR1-expressing microglia. *Proceedings of the National Academy of Sciences,* 95**,** 10896-10901.

HASEGAWA, K., WAKINO, S., KIMOTO, M., MINAKUCHI, H., FUJIMURA, K., HOSOYA, K., KOMATSU, M., KANEKO, Y., KANDA, T., TOKUYAMA, H., HAYASHI, K. & ITOH, H. 2013. The hydrolase DDAH2 enhances pancreatic insulin secretion by transcriptional regulation of secretagogin through a Sirt1-dependent mechanism in mice. *Faseb j,* 27**,** 2301-15.

HASEGAWA, K., WAKINO, S., TANAKA, T., KIMOTO, M., TATEMATSU, S., KANDA, T., YOSHIOKA, K., HOMMA, K., SUGANO, N., KURABAYASHI, M., SARUTA, T. & HAYASHI, K. 2006. Dimethylarginine Dimethylaminohydrolase 2 Increases Vascular Endothelial Growth Factor Expression Through Sp1 Transcription Factor in Endothelial Cells. *Arteriosclerosis, Thrombosis, and Vascular Biology*. Arterioscler Thromb Vasc Biol.

HAWKES, C. A. & MCLAURIN, J. 2009. Selective targeting of perivascular macrophages for clearance of -amyloid in cerebral amyloid angiopathy. *Proceedings of the National Academy of Sciences,* 106**,** 1261-1266.

HAZELL, A. S. 2007. Excitotoxic mechanisms in stroke: An update of concepts and treatment strategies. *Neurochemistry International,* 50**,** 941-953.

HE, H., MACK, J. J., GÜÇ, E., WARREN, C. M., SQUADRITO, M. L., KILARSKI, W. W., BAER, C., FRESHMAN, R. D., MCDONALD, A. I. & ZIYAD, S. 2016. Perivascular macrophages limit permeability. *Arteriosclerosis, thrombosis, and vascular biology,* 36**,** 2203-2212.

HEMMEN, T. M. & LYDEN, P. D. 2009. Hypothermia after acute ischemic stroke. *J Neurotrauma,* 26**,** 387-91.

HERING, D., PISKUNOWICZ, M. & MANIOS, E. 2024. Hypertension, Ischaemic Stroke and Transient Ischaemic Attack. *In:* COCA, A. (ed.) *Hypertension and Brain Damage*. Cham: Springer International Publishing.

HERISSON, F., FRODERMANN, V., COURTIES, G., ROHDE, D., SUN, Y., VANDOORNE, K., WOJTKIEWICZ, G. R., MASSON, G. S., VINEGONI, C., KIM, J., KIM, D. E., WEISSLEDER, R., SWIRSKI, F. K., MOSKOWITZ, M. A. & NAHRENDORF, M. 2018. Direct vascular channels connect skull bone marrow and the brain surface enabling myeloid cell migration. *Nat Neurosci,* 21**,** 1209-1217.

HOLFELDER, K., SCHITTENHELM, J., TRAUTMANN, K., HAYBAECK, J., MEYERMANN, R. & BESCHORNER, R. 2011. De novo expression of the hemoglobin scavenger receptor CD163 by activated microglia is not associated with hemorrhages in human brain lesions. *Histology and Histopathology, vol. 26, nº8, 2011.*

HOLMSTEDT, C. A., TURAN, T. N. & CHIMOWITZ, M. I. 2013. Atherosclerotic intracranial arterial stenosis: risk factors, diagnosis, and treatment. *Lancet Neurol,* 12**,** 1106-14.

HOSSMANN, K.-A. 2012. The two pathophysiologies of focal brain ischemia: implications for translational stroke research. *Journal of Cerebral Blood Flow & Metabolism,* 32**,** 1310-1316.

HOWELLS, D. W., PORRITT, M. J., REWELL, S. S., O'COLLINS, V., SENA, E. S., VAN DER WORP, H. B., TRAYSTMAN, R. J. & MACLEOD, M. R. 2010. Different strokes for different folks: the rich diversity of animal models of focal cerebral ischemia. *Journal of Cerebral Blood Flow & Metabolism,* 30**,** 1412-1431.

HU, X., ATZLER, D., XU, X., ZHANG, P., GUO, H., LU, Z., FASSETT, J., SCHWEDHELM, E., BÖGER, R. H., BACHE, R. J. & CHEN, Y. 2011. Dimethylarginine

Dimethylaminohydrolase-1 Is the Critical Enzyme for Degrading the Cardiovascular Risk Factor Asymmetrical Dimethylarginine. *Arteriosclerosis, Thrombosis, and Vascular Biology,* 31**,** 1540-1546.

HU, X., LI, P., GUO, Y., WANG, H., LEAK, R. K., CHEN, S., GAO, Y. & CHEN, J. 2012. Microglia/macrophage polarization dynamics reveal novel mechanism of injury expansion after focal cerebral ischemia. *Stroke,* 43**,** 3063-70.

HU, X., XU, X., ZHU, G., ATZLER, D., KIMOTO, M., CHEN, J., SCHWEDHELM, E., LUNEBURG, N., BÖGER, R. H. & ZHANG, P. 2009. Vascular endothelial-specific dimethylarginine dimethylaminohydrolase-1–deficient mice reveal that vascular endothelium plays an important role in removing asymmetric dimethylarginine. *Circulation,* 120**,** 2222-2229.

HU, X. M., LEAK, R. K., SHI, Y. J., SUENAGA, J., GAO, Y. Q., ZHENG, P. & CHEN, J. 2015. Microglial and macrophage polarization -new prospects for brain repair. *Nature Reviews Neurology,* 11**,** 56-64.

HUANG, J., UPADHYAY, U. M. & TAMARGO, R. J. 2006. Inflammation in stroke and focal cerebral ischemia. *Surgical Neurology.* Surg Neurol.

HUANG, S., LI, Z., WU, Z., LIU, C., YU, M., WEN, M., ZHANG, L. & WANG, X. 2021. DDAH2 suppresses RLR-MAVS–mediated innate antiviral immunity by stimulating nitric oxide–activated, Drp1-induced mitochondrial fission. *Science Signaling,* 14**,** eabc7931.

HUANG, Z., HOFFMANN, F. W., FAY, J. D., HASHIMOTO, A. C., CHAPAGAIN, M. L., KAUFUSI, P. H. & HOFFMANN, P. R. 2012. Stimulation of Unprimed Macrophages with Immune Complexes Triggers a Low Output of Nitric Oxide by Calcium-dependent Neuronal Nitric-oxide Synthase *. *Journal of Biological Chemistry,* 287**,** 4492-4502.

HUGHES, P. M., BOTHAM, M. S., FRENTZEL, S., MIR, A. & PERRY, V. H. 2002. Expression of fractalkine (CX3CL1) and its receptor, CX3CR1, during acute and chronic inflammation in the rodent CNS. *Glia,* 37**,** 314-327.

HÜTTEMANN, M., HELLING, S., SANDERSON, T. H., SINKLER, C., SAMAVATI, L., MAHAPATRA, G., VARUGHESE, A., LU, G., LIU, J. & RAMZAN, R. 2012. Regulation of mitochondrial respiration and apoptosis through cell signaling: cytochrome c oxidase and cytochrome c in ischemia/reperfusion injury and inflammation. *Biochimica et Biophysica Acta (BBA)-Bioenergetics,* 1817**,** 598-609.

IADECOLA, C. 1997. Bright and dark sides of nitric oxide in ischemic brain injury. *Trends in Neurosciences.* Elsevier Ltd.

IADECOLA, C. & ANRATHER, J. 2011. The immunology of stroke: from mechanisms to translation. *Nat Med,* 17**,** 796-808.

IADECOLA, C., ZHANG, F., XU, S., CASEY, R. & ROSS, M. E. 1995. Inducible Nitric Oxide Synthase Gene Expression in Brain following Cerebral Ischemia. *Journal of Cerebral Blood Flow & Metabolism,* 15**,** 378-384.

IWASAKI, A. & MEDZHITOV, R. 2015. Control of adaptive immunity by the innate immune system. *Nature immunology,* 16**,** 343-353.

IYONAGA, T., SHINOHARA, K., MASTUURA, T., HIROOKA, Y. & TSUTSUI, H. 2020. Brain perivascular macrophages contribute to the development of hypertension in stroke-prone spontaneously hypertensive rats via sympathetic activation. *Hypertension Research,* 43**,** 99-110.

JACKMAN, K. A., MILLER, A. A. A., DE SILVA, T. M., CRACK, P. J., DRUMMOND, G. R. G. & SOBEY, C. G. 2009. Reduction of cerebral infarct volume by apocynin requires pretreatment and is absent in Nox2-deficient mice. *British Journal of Pharmacology.* John Wiley & Sons, Ltd.

JAIS, A., SOLAS, M., BACKES, H., CHAURASIA, B., KLEINRIDDERS, A., THEURICH, S., MAUER, J., STECULORUM, SOPHIE M., HAMPEL, B., GOLDAU, J., ALBER, J., FÖRSTER, CAROLA Y., EMING, SABINE A., SCHWANINGER, M., FERRARA, N., KARSENTY, G. & BRÜNING, JENS C. 2016. Myeloid-Cell-Derived VEGF Maintains Brain Glucose Uptake and Limits Cognitive Impairment in Obesity. *Cell,* 165**,** 882-895.

JAYARAJ, R. L., AZIMULLAH, S., BEIRAM, R., JALAL, F. Y. & ROSENBERG, G. A. 2019. Neuroinflammation: friend and foe for ischemic stroke. *Journal of Neuroinflammation,* 16**,** 142.

JI, D., JIN, C., TAO, M., SUN, Y., CHEN, H., LI, H., QU, X., YE, H., ZHANG, L., HUANG, Z., ZHANG, Y., KONG, T. & WU, J. 2024. Design, synthesis, and biological evaluation of novel iNOS inhibitors as potent neuroprotective agents for ischemic stroke. *European Journal of Medicinal Chemistry,* 280**,** 116907.

JIANG, M. Q., ZHAO, Y.-Y., CAO, W., WEI, Z. Z., GU, X., WEI, L. & YU, S. P. 2017. Long-term survival and regeneration of neuronal and vasculature cells inside the core region after ischemic stroke in adult mice. *Brain Pathology,* 27**,** 480-498.

JICKLING, G. C., LIU, D., STAMOVA, B., ANDER, B. P., ZHAN, X., LU, A. & SHARP, F. R. 2014. Hemorrhagic transformation after ischemic stroke in animals and humans. *Journal of Cerebral Blood Flow & Metabolism,* 34**,** 185-199.

JIN, L., ZHU, Z., HONG, L., QIAN, Z., WANG, F. & MAO, Z. 2023. ROS-responsive 18ß-glycyrrhetic acid-conjugated polymeric nanoparticles mediate neuroprotection in ischemic stroke through HMGB1 inhibition and microglia polarization regulation. *Bioactive materials,* 19**,** 38-49.

JIRKOF, P. 2014. Burrowing and nest building behavior as indicators of well-being in mice. *Journal of Neuroscience Methods,* 234**,** 139-146.

JORDÃO, M. J. C., SANKOWSKI, R., BRENDECKE, S. M., SAGAR, LOCATELLI, G., TAI, Y.-H., TAY, T. L., SCHRAMM, E., ARMBRUSTER, S. & HAGEMEYER, N. 2019. Single-cell profiling identifies myeloid cell subsets with distinct fates during neuroinflammation. *Science,* 363**,** eaat7554.

JURCAU, A. & ARDELEAN, A. I. 2022. Oxidative Stress in Ischemia/Reperfusion Injuries following Acute Ischemic Stroke. *Biomedicines,* 10**,** 574.

KANAZAWA, M., MIURA, M., TORIYABE, M., KOYAMA, M., HATAKEYAMA, M., ISHIKAWA, M., NAKAJIMA, T., ONODERA, O., TAKAHASHI, T. & NISHIZAWA, M. 2017a. Microglia preconditioned by oxygen-glucose deprivation promote functional recovery in ischemic rats. *Scientific reports,* 7**,** 42582.

KANAZAWA, M., NINOMIYA, I., HATAKEYAMA, M., TAKAHASHI, T. & SHIMOHATA, T. 2017b. Microglia and Monocytes/Macrophages Polarization Reveal Novel Therapeutic Mechanism against Stroke. *International Journal of Molecular Sciences,* 18**,** 2135.

KANDARAKOV, O., BELYAVSKY, A. & SEMENOVA, E. 2022. Bone marrow niches of hematopoietic stem and progenitor cells. *International Journal of Molecular Sciences,* 23**,** 4462.

KANG, L., YU, H., YANG, X., ZHU, Y., BAI, X., WANG, R., CAO, Y., XU, H., LUO, H. & LU, L. 2020. Neutrophil extracellular traps released by neutrophils impair revascularization and vascular remodeling after stroke. *Nature communications,* 11**,** 2488.

KASHFI, K., KANNIKAL, J. & NATH, N. 2021. Macrophage reprogramming and cancer therapeutics: role of iNOS-derived NO. *Cells,* 10**,** 3194.

KAWABORI, M. & YENARI, M. 2015. Inflammatory Responses in Brain Ischemia. *Current Medicinal Chemistry,* 22**,** 1258-1277.

KELLY, B. & O'NEILL, L. A. 2015. Metabolic reprogramming in macrophages and dendritic cells in innate immunity. *Cell research,* 25**,** 771-784.

KERKHOFS, D., VAN HAGEN, B. T., MILANOVA, I. V., SCHELL, K. J., VAN ESSEN, H., WIJNANDS, E., GOOSSENS, P., BLANKESTEIJN, W. M., UNGER, T., PRICKAERTS, J., BIESSEN, E. A., VAN OOSTENBRUGGE, R. J. & FOULQUIER, S. 2020. Pharmacological depletion of microglia and perivascular macrophages prevents Vascular Cognitive Impairment in Ang II-induced hypertension. *Theranostics,* 10**,** 9512-9527.

KHAN, M., SEKHON, B., GIRI, S., JATANA, M., GILG, A. G., AYASOLLA, K., ELANGO, C., SINGH, A. K. & SINGH, I. 2005. S-Nitrosoglutathione reduces inflammation and protects brain against focal cerebral ischemia in a rat model of experimental stroke. *Journal of Cerebral Blood Flow & Metabolism,* 25**,** 177-192.

KIDA, S., STEART, P. V., ZHANG, E. T. & WELLER, R. O. 1993. Perivascular cells act as scavengers in the cerebral perivascular spaces and remain distinct from pericytes, microglia and macrophages. *Acta Neuropathol,* 85**,** 646-52.

KILKENNY, C., BROWNE, W. J., CUTHILL, I. C., EMERSON, M. & ALTMAN, D. G. 2010. Improving bioscience research reporting: the ARRIVE guidelines for reporting animal research. *PLoS Biol,* 8**,** e1000412.

KIM, J.-S., KOLESNIKOV, M., PELED-HAJAJ, S., SCHEYLTJENS, I., XIA, Y., TRZEBANSKI, S., HAIMON, Z., SHEMER, A., LUBART, A., VAN HOVE, H., CHAPPELL-MAOR, L., BOURA-HALFON, S., MOVAHEDI, K., BLINDER, P. & JUNG, S. 2021a. A Binary Cre Transgenic Approach Dissects Microglia and CNS Border-Associated Macrophages. *Immunity.* Cell Press.

KIM, M., KIM, S.-D., KIM, K. I., JEON, E. H., KIM, M. G., LIM, Y.-R., LKHAGVA-YONDON, E., OH, Y., NA, K. & CHUNG, Y. C. 2021b. Dynamics of T lymphocyte between the periphery and the brain from the acute to the chronic phase following ischemic stroke in mice. *Experimental Neurobiology,* 30**,** 155.

KIM, M., KIM, S. D., KIM, K. I., JEON, E. H., KIM, M. G., LIM, Y. R., LKHAGVA-YONDON, E., OH, Y., NA, K., CHUNG, Y. C., JIN, B. K., SONG, Y. S. & JEON, M. S. 2021c. Dynamics of T Lymphocyte between the Periphery and the Brain from the Acute to the Chronic Phase Following Ischemic Stroke in Mice. *Exp Neurobiol,* 30**,** 155-169.

KITAMURA, T., TERASHIMA, T., KATAGI, M., OHASHI, N., NOZAKI, K. & TSUJI, A. 2023. Bone marrow-derived mononuclear cells ameliorate neurological function in chronic cerebral infarction model mice via improvement of cerebral blood flow. *Cytotherapy,* 25**,** 1186-1199.

KLEINSCHNITZ, C., SCHWAB, N., KRAFT, P., HAGEDORN, I., DREYKLUFT, A., SCHWARZ, T., AUSTINAT, M., NIESWANDT, B., WIENDL, H. & STOLL, G. 2010. Early detrimental T-cell effects in experimental cerebral ischemia are neither related to adaptive immunity nor thrombus formation. *Blood,* 115**,** 3835-42.

KLUGE, M. G., ABDOLHOSEINI, M., ZALEWSKA, K., ONG, L. K., JOHNSON, S. J., NILSSON, M. & WALKER, F. R. 2019. Spatiotemporal analysis of impaired microglia process movement at sites of secondary neurodegeneration post-stroke. *Journal of Cerebral Blood Flow & Metabolism,* 39**,** 2456-2470.

KOBAYASHI, E. H., SUZUKI, T., FUNAYAMA, R., NAGASHIMA, T., HAYASHI, M., SEKINE, H., TANAKA, N., MORIGUCHI, T., MOTOHASHI, H., NAKAYAMA, K. & YAMAMOTO, M. 2016. Nrf2 suppresses macrophage inflammatory response by blocking proinflammatory cytokine transcription. *Nature Communications,* 7**,** 11624.

KOIZUMI, J. 1986. Experimental studies of ischemic brain edema. 1. A new experimental model of cerebral embolism in rats in which recirculation can be introduced in the ischemic area. *Jpn. J. Stroke.,* 8**,** 1-8.

KOIZUMI, S., SHIGEMOTO-MOGAMI, Y., NASU-TADA, K., SHINOZAKI, Y., OHSAWA, K., TSUDA, M., JOSHI, B. V., JACOBSON, K. A., KOHSAKA, S. & INOUE, K. 2007. UDP acting at P2Y6 receptors is a mediator of microglial phagocytosis. *Nature,* 446**,** 1091-1095.

KONCZ, G., JENEI, V., TÓTH, M., VÁRADI, E., KARDOS, B., BÁCSI, A. & MÁZLÓ, A. 2023. Damage-mediated macrophage polarization in sterile inflammation. *Frontiers in Immunology,* 14**,** 1169560.

KOZLOVA, A. A., RAGAVAN, V. N., JARZEBSKA, N., LUKIANOVA, I. V., BIKMURZINA, A. E., RUBETS, E., SUZUKI-YAMAMOTO, T., KIMOTO, M., MANGONI, A. A., GAINETDINOV, R. R., WEISS, N., BAUER, M., MARKOV, A. G., RODIONOV, R. N. & BERNHARDT, N. 2021. Divergent Dimethylarginine Dimethylaminohydrolase Isoenzyme Expression in the Central Nervous System. *Cellular and Molecular Neurobiology.*

KRIEGLSTEIN, K., STRELAU, J., SCHOBER, A., SULLIVAN, A. & UNSICKER, K. 2002. TGF-ß and the regulation of neuron survival and death. *Journal of Physiology-Paris,* 96**,** 25-30.

KRUMENACKER, J. S., HANAFY, K. A. & MURAD, F. 2004. Regulation of nitric oxide and soluble guanylyl cyclase. *Brain research bulletin,* 62**,** 505-515.

KU, J. M., TAHER, M., CHIN, K. Y., BARSBY, T., AUSTIN, V., WONG, C. H. Y., ANDREWS, Z. B., SPENCER, S. J. & MILLER, A. A. 2016. Protective actions of des-acylated ghrelin on brain injury and blood–brain barrier disruption after stroke in mice. *Clinical Science*. Portland Press Ltd.

KUZAN, A., KOZAK-SYKAŁA, A., FIEDOROWICZ, A., KAŁAS, W., STRZĄDAŁA, L. & GAMIAN, A. 2024. Advanced Glycation End-Products in Blood Serum—Novel Ischemic Stroke Risk Factors? Implication for Diabetic Patients. *Journal of Clinical Medicine,* 13**,** 443.

LAI, T. W., ZHANG, S. & WANG, Y. T. 2014. Excitotoxicity and stroke: Identifying novel targets for neuroprotection. *Progress in Neurobiology,* 115**,** 157-188.

LAKHAN, S. E., KIRCHGESSNER, A., TEPPER, D. & LEONARD, A. 2013. Matrix metalloproteinases and blood-brain barrier disruption in acute ischemic stroke. *Frontiers in neurology,* 4**,** 32.

LAMBDEN, S. 2016. *Monocyte dimethylarginine dimethylaminohydrolase 2 is regulated by pathological stress and plays a critical role in the immune response to sepsis*, Imperial College London.

LAMBDEN, S., KELLY, P., AHMETAJ-SHALA, B., WANG, Z., LEE, B., NANDI, M., TORONDEL, B., DELAHAYE, M., DOWSETT, L., PIPER, S., TOMLINSON, J., CAPLIN, B., COLMAN, L., BORUC, O., SLAVIERO, A., ZHAO, L., OLIVER, E., KHADAYATE, S., SINGER, M., ARRIGONI, F. & LEIPER, J. 2015. Dimethylarginine Dimethylaminohydrolase 2 Regulates Nitric Oxide Synthesis and Hemodynamics and Determines Outcome in Polymicrobial Sepsis. *Arteriosclerosis, Thrombosis, and Vascular Biology*. Lippincott Williams and Wilkins.

LAMBDEN, S., MARTIN, D., VANEZIS, K., LEE, B., TOMLINSON, J., PIPER, S., BORUC, O., MYTHEN, M. & LEIPER, J. 2016. Hypoxia causes increased monocyte nitric oxide synthesis which is mediated by changes in dimethylarginine dimethylaminohydrolase 2 expression in animal and human models of normobaric hypoxia. *Nitric Oxide,* 58**,** 59-66.

LANGE, C., MOWAT, F., SAYED, H., MEHAD, M., DULUC, L., PIPER, S., LUHMANN, U., NANDI, M., KELLY, P., SMITH, A., ALI, R., LEIPER, J. & BAINBRIDGE, J. 2016. Dimethylarginine dimethylaminohydrolase-2 deficiency promotes vascular regeneration and attenuates pathological angiogenesis. *Experimental Eye Research*. Academic Press.

LANGHORNE, P., COUPAR, F. & POLLOCK, A. 2009. Motor recovery after stroke: a systematic review. *The Lancet Neurology,* 8**,** 741-754.

LAPENNA, A., DE PALMA, M. & LEWIS, C. E. 2018. Perivascular macrophages in health and disease. *Nature Reviews Immunology*.

LAUDER, L., MAHFOUD, F., AZIZI, M., BHATT, D. L., EWEN, S., KARIO, K., PARATI, G., ROSSIGNOL, P., SCHLAICH, M. P., TEO, K. K., TOWNSEND, R. R., TSIOUFIS, C., WEBER, M. A., WEBER, T. & BÖHM, M. 2022. Hypertension management in patients with cardiovascular comorbidities. *European Heart Journal,* 44**,** 2066-2077.

LEE, E., EO, J. C., LEE, C. & YU, J. W. 2021. Distinct Features of Brain-Resident Macrophages: Microglia and Non-Parenchymal Brain Macrophages. *Mol Cells,* 44**,** 281-291.

LEE, S., KIM, J., YOU, J. S., HYUN, Y.-M., KIM, J. Y. & LEE, J. E. 2024. Ischemic stroke outcome after promoting CD4+ CD25+ Treg cell migration through CCR4 overexpression in a tMCAO animal model. *Scientific reports,* 14**,** 10201.

LEE, S. H., OH, C. W., HAN, J. H., KIM, C.-Y., KWON, O.-K., SON, Y.-J., BAE, H.-J., HAN, M.-K. & CHUNG, Y. S. 2010. The effect of brain atrophy on outcome after a large cerebral infarction. *Journal of Neurology, Neurosurgery & Psychiatry,* 81**,** 1316-1321.

LEIPER, J., MURRAY-RUST, J., MCDONALD, N. & VALLANCE, P. 2002. S-nitrosylation of dimethylarginine dimethylaminohydrolase regulates enzyme activity: further interactions between nitric oxide synthase and dimethylarginine dimethylaminohydrolase. *Proceedings of the National Academy of Sciences,* 99**,** 13527-13532.

LEIPER, J. & NANDI, M. 2011. The therapeutic potential of targeting endogenous inhibitors of nitric oxide synthesis. *Nature Reviews Drug Discovery,* 10**,** 277-291.

LEIPER, J., NANDI, M., TORONDEL, B., MURRAY-RUST, J., MALAKI, M., O'HARA, B., ROSSITER, S., ANTHONY, S., MADHANI, M., SELWOOD, D., SMITH, C., WOJCIAK-STOTHARD, B., RUDIGER, A., STIDWILL, R., MCDONALD, N. Q. & VALLANCE, P. 2007. Disruption of methylarginine metabolism impairs vascular homeostasis. *Nature Medicine*. Nat Med.

LEIPER, J. M., SANTA MARIA, J., CHUBB, A., MACALLISTER, R. J., CHARLES, I. G., WHITLEY, G. S. J. & VALLANCE, P. 1999. Identification of two human dimethylarginine dimethylaminohydrolases with distinct tissue distributions and homology with microbial arginine deiminases. *Biochemical Journal,* 343**,** 209-209.

LEVARD, D., BUENDIA, I., LANQUETIN, A., GLAVAN, M., VIVIEN, D. & RUBIO, M. 2020. Filling the gaps on stroke research: Focus on inflammation and immunity. *Brain, Behavior, and Immunity*. Academic Press Inc.

LEVARD, D., SEILLIER, C., BELLEMAIN-SAGNARD, M., FOURNIER, A. P., LEMARCHAND, E., DEMBECH, C., RIOU, G., MCDADE, K., SMITH, C., MCQUAID, C., MONTAGNE, A., AMANN, L., PRINZ, M., VIVIEN, D. & RUBIO, M. 2024. Central nervous system-associated macrophages modulate the immune response following stroke in aged mice. *Nature Neuroscience,* 27**,** 1721-1733.

LEWIS, C. R. A. 2014. Cerebral Blood Flow: Determinants. *In:* FREEMAN, B. S. & BERGER, J. S. (eds.) *Anesthesiology Core Review: Part One Basic Exam*. New York, NY: McGraw-Hill Education.

LI, H. Y., SU, Y. Y., ZHANG, Y. F., LIU, Z. Q. & HUA, B. J. 2016. Involvement of peroxisome proliferator activated receptor-γ in the anti-inflammatory effects of atorvastatin in oxygen-glucose deprivation/reperfusion-stimulated RAW264. 7 murine macrophages. *Molecular Medicine Reports,* 14**,** 4055-4062.

LI, T., XU, T., ZHAO, J., GAO, H. & XIE, W. 2022. Depletion of iNOS-positive inflammatory cells decelerates neuronal degeneration and alleviates cerebral ischemic damage by suppressing the inflammatory response. *Free Radical Biology and Medicine,* 181**,** 209-220.

LI, Y., TAN, L., YANG, C., HE, L., LIU, L., DENG, B., LIU, S. & GUO, J. 2023. Distinctions between the Koizumi and Zea Longa methods for middle cerebral artery occlusion (MCAO) model: a systematic review and meta-analysis of rodent data. *Scientific Reports,* 13**,** 10247.

LI, Z., LI, W., LI, Q. & TANG, M. 2013. Extracellular nucleotides and adenosine regulate microglial motility and their role in cerebral ischemia. *Acta Pharmaceutica Sinica B,* 3**,** 205-212.

LI, Z., ZHAO, Z.-J., ZHU, X.-Q., REN, Q.-S., NIE, F.-F., GAO, J.-M., GAO, X.-J., YANG, T.-B., ZHOU, W.-L. & SHEN, J.-L. 2012. Differences in iNOS and arginase expression and activity in the macrophages of rats are responsible for the resistance against T. gondii infection. *PloS one,* 7**,** e35834.

LIBERALE, L., DIAZ-CAÑESTRO, C., BONETTI, N. R., PANENI, F., AKHMEDOV, A., BEER, J. H., MONTECUCCO, F., LÜSCHER, T. F. & CAMICI, G. G. 2018. Post-ischaemic administration of the murine Canakinumab-surrogate antibody improves outcome in experimental stroke. *European heart journal,* 39**,** 3511-3517.

LIESZ, A., DALPKE, A., MRACSKO, E., ANTOINE, D. J., ROTH, S., ZHOU, W., YANG, H., NA, S. Y., AKHISAROGLU, M., FLEMING, T., EIGENBROD, T., NAWROTH, P. P., TRACEY, K. J. & VELTKAMP, R. 2015a. DAMP signaling is a key pathway inducing immune modulation after brain injury. *J Neurosci,* 35**,** 583-98.

LIESZ, A., DALPKE, A., MRACSKO, E., ROTH, S., ZHOU, W., YANG, H., NA, S.-Y., AKHISAROGLU, M., FLEMING, T., EIGENBROD, T., NAWROTH, P. P., TRACEY, K. J. & VELTKAMP, R. 2015b. DAMP Signaling is a Key Pathway Inducing Immune Modulation after Brain Injury. *The Journal of Neuroscience,* 35**,** 583-598.

LINDGREN, C., HULTIN, M., KOSKINEN, L.-O. D., LINDVALL, P., BOROTA, L. & NAREDI, S. 2014. ADMA levels and arginine/ADMA ratios reflect severity of disease and

extent of inflammation after subarachnoid hemorrhage. *Neurocritical care,* 21, 91-101.
LIPPMANN, E. S., AZARIN, S. M., KAY, J. E., NESSLER, R. A., WILSON, H. K., AL-AHMAD, A., PALECEK, S. P. & SHUSTA, E. V. 2012. Derivation of blood-brain barrier endothelial cells from human pluripotent stem cells. *Nat Biotechnol,* 30, 783-91.
LIU, C., CHU, D., KALANTAR-ZADEH, K., GEORGE, J., YOUNG, H. A. & LIU, G. 2021a. Cytokines: From Clinical Significance to Quantification. *Advanced Science,* 8, 2004433.
LIU, C., WU, C., YANG, Q., GAO, J., LI, L., YANG, D. & LUO, L. 2016. Macrophages Mediate the Repair of Brain Vascular Rupture through Direct Physical Adhesion and Mechanical Traction. *Immunity,* 44, 1162-1176.
LIU, D.-L., HONG, Z., LI, J.-Y., YANG, Y.-X., CHEN, C. & DU, J.-R. 2021b. Phthalide derivative CD21 attenuates tissue plasminogen activator-induced hemorrhagic transformation in ischemic stroke by enhancing macrophage scavenger receptor 1-mediated DAMP (peroxiredoxin 1) clearance. *Journal of Neuroinflammation,* 18.
LIU, F. & MCCULLOUGH, L. D. 2014. The Middle Cerebral Artery Occlusion Model of Transient Focal Cerebral Ischemia. *In:* MILNER, R. (ed.) *Cerebral Angiogenesis: Methods and Protocols.* New York, NY: Springer New York.
LIU, X., FASSETT, J., WEI, Y. & CHEN, Y. 2013. Regulation of DDAH1 as a potential therapeutic target for treating cardiovascular diseases. *Evidence – Based Complementary and Alternative Medicine,* 2013, 619207.
LIU, X., XU, X., SHANG, R. & CHEN, Y. 2018. Asymmetric dimethylarginine (ADMA) as an important risk factor for the increased cardiovascular diseases and heart failure in chronic kidney disease. *Nitric Oxide,* 78, 113-120.
LIU, Z. Q., BOHATSCHEK, M., PFEFFER, K., BLUETHMANN, H. & RAIVICH, G. 2005. Major histocompatibility complex (MHC2+) perivascular macrophages in the axotomized facial motor nucleus are regulated by receptors for interferon-γ (IFNγ) and tumor necrosis factor (TNF). *Neuroscience,* 131, 283-292.
LLUFRIO, E. M., WANG, L., NASER, F. J. & PATTI, G. J. 2018. Sorting cells alters their redox state and cellular metabolome. *Redox biology,* 16, 381-387.
LONGA, E. Z., WEINSTEIN, P. R., CARLSON, S. & CUMMINS, R. 1989. Reversible middle cerebral artery occlusion without craniectomy in rats. *stroke,* 20, 84-91.
LOURENÇO, C. F. & LARANJINHA, J. 2021. Nitric Oxide Pathways in Neurovascular Coupling Under Normal and Stress Conditions in the Brain: Strategies to Rescue Aberrant Coupling and Improve Cerebral Blood Flow. *Frontiers in Physiology,* Volume 12 - 2021.
LOURENÇO, C. F., SANTOS, R. M., BARBOSA, R. M., CADENAS, E., RADI, R. & LARANJINHA, J. 2014. Neurovascular coupling in hippocampus is mediated via diffusion by neuronal-derived nitric oxide. *Free Radical Biology and Medicine,* 73, 421-429.
LU, C.-W., GUO, Z., FENG, M., WU, Z.-Z., HE, Z.-M. & XIONG, Y. 2010. Ex vivo gene transferring of human dimethylarginine dimethylaminohydrolase-2 improved endothelial dysfunction in diabetic rat aortas and high glucose-treated endothelial cells. *Atherosclerosis,* 209, 66-73.
LU, G., ZHANG, R., GENG, S., PENG, L., JAYARAMAN, P., CHEN, C., XU, F., YANG, J., LI, Q. & ZHENG, H. 2015. Myeloid cell-derived inducible nitric oxide synthase suppresses M1 macrophage polarization. *Nature communications,* 6, 6676.
LUO, W., LIU, T., LI, S., WEN, H., ZHOU, F., ZAFONTE, R., LUO, X., XU, M., BLACK-SCHAFFER, R. & WOOD, L. J. 2019. The serum BDNF level offers minimum predictive value for motor function recovery after stroke. *Translational stroke research,* 10, 342-351.
LUO, Z., ASLAM, S., WELCH, W. J. & WILCOX, C. S. 2015. Activation of nuclear factor erythroid 2–related factor 2 coordinates dimethylarginine dimethylaminohydrolase/PPAR-γ/endothelial nitric oxide synthase pathways that enhance nitric oxide generation in human glomerular endothelial cells. *Hypertension,* 65, 896-902.

LYU, J., XIE, D., BHATIA, T. N., LEAK, R. K., HU, X. & JIANG, X. 2021. Microglial/Macrophage polarization and function in brain injury and repair after stroke. *CNS Neuroscience & Therapeutics,* 27**,** 515-527.

MA, M., MA, Y., YI, X., GUO, R., ZHU, W., FAN, X., XU, G., FREY, W. H. & LIU, X. 2008. Intranasal delivery of transforming growth factor-beta1 in mice after stroke reduces infarct volume and increases neurogenesis in the subventricular zone. *BMC neuroscience,* 9**,** 1-10.

MA, R., XIE, Q., LI, Y., CHEN, Z., REN, M., CHEN, H., LI, H., LI, J. & WANG, J. 2020. Animal models of cerebral ischemia: A review. *Biomedicine & Pharmacotherapy,* 131**,** 110686.

MA, Y., LI, Y., JIANG, L., WANG, L., JIANG, Z., WANG, Y., ZHANG, Z. & YANG, G.-Y. 2016. Macrophage depletion reduced brain injury following middle cerebral artery occlusion in mice. *Journal of Neuroinflammation*. BioMed Central.

MA, Y., WANG, J., WANG, Y. & YANG, G. Y. 2017. The biphasic function of microglia in ischemic stroke. *Prog Neurobiol,* 157**,** 247-272.

MAKSOUD, M. J. E., TELLIOS, V., XIANG, Y.-Y. & LU, W.-Y. 2020. Nitric oxide signaling inhibits microglia proliferation by activation of protein kinase-G. *Nitric Oxide,* 94**,** 125-134.

MANI, S., MUTHA, P. K., PRZYBYLA, A., HAALAND, K. Y., GOOD, D. C. & SAINBURG, R. L. 2013. Contralesional motor deficits after unilateral stroke reflect hemisphere-specific control mechanisms. *Brain,* 136**,** 1288-1303.

MANNINO, G. C., PEZZILLI, S., AVERTA, C., FUOCO, A., SPIGA, R., MANCUSO, E., DI FATTA, C., PERTICONE, F., PRUDENTE, S., TRISCHITTA, V., ANDREOZZI, F. & SESTI, G. 2019. A functional variant of the dimethylarginine dimethylaminohydrolase-2 gene is associated with myocardial infarction in type 2 diabetic patients. *Cardiovascular Diabetology,* 18.

MANOHAR, S. M., SHAH, P. & NAIR, A. 2021. Flow cytometry: principles, applications and recent advances. *Bioanalysis,* 13**,** 181-198.

MANTOVANI, A., SICA, A. & LOCATI, M. 2005. Macrophage polarization comes of age. *Immunity,* 23**,** 344-6.

MAO, M., HUA, Y., JIANG, X., LI, L., ZHANG, L. & MU, D. 2006. Expression of tumor necrosis factor α and neuronal apoptosis in the developing rat brain after neonatal stroke. *Neuroscience letters,* 403**,** 227-232.

MĂRGĂRITESCU, O., MOGOANTĂ, L., PIRICI, I., PIRICI, D., CERNEA, D. & MĂRGĂRITESCU, C. 2009. Histopathological changes in acute ischemic stroke. *Rom J Morphol Embryol,* 50**,** 327-39.

MARINO, S., MARANI, L., NAZZARO, C., BEANI, L. & SINISCALCHI, A. 2007. Mechanisms of sodium azide-induced changes in intracellular calcium concentration in rat primary cortical neurons. *NeuroToxicology,* 28**,** 622-629.

MARTI, H. J., BERNAUDIN, M., BELLAIL, A., SCHOCH, H., EULER, M., PETIT, E. & RISAU, W. 2000. Hypoxia-induced vascular endothelial growth factor expression precedes neovascularization after cerebral ischemia. *The American journal of pathology,* 156**,** 965-976.

MARTIN, E., BERKA, V., TSAI, A. L. & MURAD, F. 2005. Soluble guanylyl cyclase: the nitric oxide receptor. *Methods in enzymology,* 396**,** 478-492.

MARTIN, E., EL-BEHI, M., FONTAINE, B. & DELARASSE, C. 2017a. Analysis of Microglia and Monocyte-derived Macrophages from the Central Nervous System by Flow Cytometry. *J Vis Exp*.

MARTIN, E., EL-BEHI, M., FONTAINE, B. & DELARASSE, C. 2017b. Analysis of microglia and monocyte-derived macrophages from the central nervous system by flow cytometry. *Journal of visualized experiments: JoVE*.

MARTINEZ-POMARES, L. 2012. The mannose receptor. *Journal of Leukocyte Biology*. Wiley-Blackwell.

MASUDA, T., AMANN, L., SANKOWSKI, R., STASZEWSKI, O., LENZ, M., D´ERRICO, P., SNAIDERO, N., COSTA JORDÃO, M. J., BÖTTCHER, C., KIERDORF, K., JUNG, S., PRILLER, J., MISGELD, T., VLACHOS, A., LUEHMANN, M. M., KNOBELOCH, K. P. &

PRINZ, M. 2020. Novel Hexb-based tools for studying microglia in the CNS. *Nature Immunology*. Nature Research.
MCBRIDE, D. W. & ZHANG, J. H. 2017. Precision stroke animal models: the permanent MCAO model should be the primary model, not transient MCAO. *Translational stroke research,* 8**,** 397-404.
MCCABE, C., ARROJA, M. M., REID, E. & MACRAE, I. M. 2018. Animal models of ischaemic stroke and characterisation of the ischaemic penumbra. *Neuropharmacology,* 134**,** 169-177.
MCCULLOUGH, L. D. & MORO, M. A. 2021. Translational Interdisciplinary Science—Immune Cell Niches: Possible Targets for Stroke Therapy? *Stroke,* 52**,** 3692-3695.
MCFALL, A., HIETAMIES, T. M., BERNARD, A., AIMABLE, M., ALLAN, S. M., BATH, P. M., BREZZO, G., CARARE, R. O., CARSWELL, H. V., CLARKSON, A. N., CURRIE, G., FARR, T. D., FOWLER, J. H., GOOD, M., HAINSWORTH, A. H., HALL, C., HORSBURGH, K., KALARIA, R., KEHOE, P., LAWRENCE, C., MACLEOD, M., MCCOLL, B. W., MCNEILLY, A., MILLER, A. A., MINERS, S., MOK, V., O'SULLIVAN, M., PLATT, B., SENA, E. S., SHARP, M., STRANGWARD, P., SZYMKOWIAK, S., TOUYZ, R. M., TRUEMAN, R. C., WHITE, C., MCCABE, C., WORK, L. M. & QUINN, T. J. 2020. UK consensus on pre-clinical vascular cognitive impairment functional outcomes assessment: Questionnaire and workshop proceedings. *Journal of Cerebral Blood Flow and Metabolism*. SAGE Publications Ltd.
MEYER-LINDEMANN, U., MAUERSBERGER, C., SCHMIDT, A.-C., MOGGIO, A., HINTERDOBLER, J., LI, X., KHANGHOLI, D., HETTWER, J., GRÄSSE, C. & DUTSCH, A. 2022. Colchicine impacts leukocyte trafficking in atherosclerosis and reduces vascular inflammation. *Frontiers in immunology,* 13**,** 898690.
MILDE, S. & BROWN, G. C. 2022. Knockout of the P2Y6 receptor prevents peri-infarct neuronal loss after transient, focal ischemia in mouse brain. *International Journal of Molecular Sciences,* 23**,** 2304.
MILDNER, A., SCHLEVOGT, B., KIERDORF, K., BÖTTCHER, C., ERNY, D., KUMMER, M. P., QUINN, M., BRÜCK, W., BECHMANN, I., HENEKA, M. T., PRILLER, J. & PRINZ, M. 2011. Distinct and non-redundant roles of microglia and myeloid subsets in mouse models of Alzheimer's disease. *J Neurosci,* 31**,** 11159-71.
MILLS, C. 2012. M1 and M2 macrophages: oracles of health and disease. *Critical Reviews™ in Immunology,* 32.
MILTENYI, S., MÜLLER, W., WEICHEL, W. & RADBRUCH, A. 1990. High gradient magnetic cell separation with MACS. *Cytometry: The Journal of the International Society for Analytical Cytology,* 11**,** 231-238.
MIRZAYANS, R. & MURRAY, D. 2020. Do TUNEL and Other Apoptosis Assays Detect Cell Death in Preclinical Studies? *Int J Mol Sci,* 21.
MIYANISHI, M., TADA, K., KOIKE, M., UCHIYAMA, Y., KITAMURA, T. & NAGATA, S. 2007. Identification of Tim4 as a phosphatidylserine receptor. *Nature,* 450**,** 435-439.
MOHAMMADI, M. T. 2016. Overproduction of nitric oxide intensifies brain infarction and cerebrovascular damage through reduction of claudin-5 and ZO-1 expression in striatum of ischemic brain. *Pathology-Research and Practice,* 212**,** 959-964.
MØLLGÅRD, K., BEINLICH, F. R. M., KUSK, P., MIYAKOSHI, L. M., DELLE, C., PLÁ, V., HAUGLUND, N. L., ESMAIL, T., RASMUSSEN, M. K., GOMOLKA, R. S., MORI, Y. & NEDERGAARD, M. 2023. A mesothelium divides the subarachnoid space into functional compartments. *Science,* 379**,** 84-88.
MONTES, M., JAENSSON, E. A., OROZCO, A. F., LEWIS, D. E. & CORRY, D. B. 2006. A general method for bead-enhanced quantitation by flow cytometry. *Journal of Immunological Methods,* 317**,** 45-55.
MONTEZANO, A. C. & TOUYZ, R. M. 2012. Reactive oxygen species and endothelial function–role of nitric oxide synthase uncoupling and Nox family nicotinamide adenine dinucleotide phosphate oxidases. *Basic & clinical pharmacology & toxicology,* 110**,** 87-94.
MORAIS, A., IMAI, T., JIN, X., LOCASCIO, J. J., BOISSERAND, L., HERMAN, A. L., CHAUHAN, A., LAMB, J., NAGARKATTI, K., DINIZ, M. A., KUMSKOVA, M.,

DHANESHA, N., KAMAT, P. K., BADRUZZAMAN KHAN, M., DHANDAPANI, K. M., PATEL, R. B., SUTARIYA, B., SHI, Y., VAN LEYEN, K., KIMBERLY, W. T., HESS, D. C., ARONOWSKI, J., LEIRA, E. C., KOEHLER, R. C., CHAUHAN, A. K., SANSING, L. H., LYDEN, P. D. & AYATA, C. 2024. Biological and Procedural Predictors of Outcome in the Stroke Preclinical Assessment Network (SPAN) Trial. *Circulation Research,* 135**,** 575-592.

MORRISON, H. W. & FILOSA, J. A. 2013. A quantitative spatiotemporal analysis of microglia morphology during ischemic stroke and reperfusion. *J Neuroinflammation,* 10**,** 4.

MOSKOWITZ, M. A., LO, E. H. & IADECOLA, C. 2010. The science of stroke: mechanisms in search of treatments. *Neuron,* 67**,** 181-198.

MOSTAJERAN, M., EDVINSSON, L., AHNSTEDT, H., ARKELIUS, K. & ANSAR, S. 2022. Repair-related molecular changes during recovery phase of ischemic stroke in female rats. *BMC Neuroscience,* 23**,** 23.

MRDJEN, D., PAVLOVIC, A., HARTMANN, F. J., SCHREINER, B., UTZ, S. G., LEUNG, B. P., LELIOS, I., HEPPNER, F. L., KIPNIS, J., MERKLER, D., GRETER, M. & BECHER, B. 2018. High-Dimensional Single-Cell Mapping of Central Nervous System Immune Cells Reveals Distinct Myeloid Subsets in Health, Aging, and Disease. *Immunity.* Cell Press.

MUNRO, D. A. D., BRADFORD, B. M., MARIANI, S. A., HAMPTON, D. W., VINK, C. S., CHANDRAN, S., HUME, D. A., PRIDANS, C. & PRILLER, J. 2020. CNS macrophages differentially rely on an intronic Csf1r enhancer for their development. *Development (Cambridge),* 147.

MURPHY, R. B., TOMMASI, S., LEWIS, B. C. & MANGONI, A. A. 2016. Inhibitors of the Hydrolytic Enzyme Dimethylarginine Dimethylaminohydrolase (DDAH): Discovery, Synthesis and Development. *Molecules,* 21**,** 615.

MURRAY-RUST, J., LEIPER, J., MCALISTER, M., PHELAN, J., TILLEY, S., MARIA, J. S., VALLANCE, P. & MCDONALD, N. 2001. Structural insights into the hydrolysis of cellular nitric oxide synthase inhibitors by dimethylarginine dimethylaminohydrolase. *Nature Structural Biology,* 8**,** 679-683.

NAGATA, S. 2018. Apoptosis and clearance of apoptotic cells. *Annual review of immunology,* 36**,** 489-517.

NAIR, P. C., MANGONI, A. A. & RODIONOV, R. N. 2024. Redefining the biological and pathophysiological role of dimethylarginine dimethylaminohydrolase 2. *Trends in Molecular Medicine,* 30**,** 552-561.

NAITO, H., NOJIMA, T., FUJISAKI, N., TSUKAHARA, K., YAMAMOTO, H., YAMADA, T., AOKAGE, T., YUMOTO, T., OSAKO, T. & NAKAO, A. 2020. Therapeutic strategies for ischemia reperfusion injury in emergency medicine. *Acute Med Surg,* 7**,** e501.

NAN, W., ZHONGHANG, X., KEYAN, C., TONGTONG, L., WANSHU, G. & ZHONGXIN, X. 2018. Epigallocatechin – 3 – gallate reduces neuronal apoptosis in rats after middle cerebral artery occlusion injury via PI3K/AKT/eNOS signaling pathway. *BioMed research international,* 2018**,** 6473580.

NAYAK, D., ZINSELMEYER, B. H., CORPS, K. N. & MCGAVERN, D. B. 2012. In vivo dynamics of innate immune sentinels in the CNS. *IntraVital,* 1**,** 95-106.

NEGOESCU, A., LORIMIER, P., LABAT-MOLEUR, F., DROUET, C., ROBERT, C., GUILLERMET, C., BRAMBILLA, C. & BRAMBILLA, E. 1996. In situ apoptotic cell labeling by the TUNEL method: improvement and evaluation on cell preparations. *Journal of Histochemistry & Cytochemistry,* 44**,** 959-968.

NIDORF, S. M., FIOLET, A. T., EIKELBOOM, J. W., SCHUT, A., OPSTAL, T. S., BAX, W. A., BUDGEON, C. A., TIJSSEN, J. G., MOSTERD, A. & CORNEL, J. H. 2019. The effect of low-dose colchicine in patients with stable coronary artery disease: the LoDoCo2 trial rationale, design, and baseline characteristics. *American heart journal,* 218**,** 46-56.

NIJVELDT, R. J., TEERLINK, T., VAN DER HOVEN, B., SIROEN, M. P. C., KUIK, D. J., RAUWERDA, J. A. & VAN LEEUWEN, P. A. M. 2003. Asymmetrical dimethylarginine (ADMA) in critically ill patients: high plasma ADMA

concentration is an independent risk factor of ICU mortality. *Clinical Nutrition,* 22**,** 23-30.

NINDS 1995. National Institute of Neurological Disorders

Stroke rt-PA Stroke Study Group: Tissue plasminogen activator for acute ischemic stroke. *New England Journal of Medicine,* 333**,** 1581-1588.

NOGUEIRA, R. G., JADHAV, A. P., HAUSSEN, D. C., BONAFE, A., BUDZIK, R. F., BHUVA, P., YAVAGAL, D. R., RIBO, M., COGNARD, C., HANEL, R. A., SILA, C. A., HASSAN, A. E., MILLAN, M., LEVY, E. I., MITCHELL, P., CHEN, M., ENGLISH, J. D., SHAH, Q. A., SILVER, F. L., PEREIRA, V. M., MEHTA, B. P., BAXTER, B. W., ABRAHAM, M. G., CARDONA, P., VEZNEDAROGLU, E., HELLINGER, F. R., FENG, L., KIRMANI, J. F., LOPES, D. K., JANKOWITZ, B. T., FRANKEL, M. R., COSTALAT, V., VORA, N. A., YOO, A. J., MALIK, A. M., FURLAN, A. J., RUBIERA, M., AGHAEBRAHIM, A., OLIVOT, J.-M., TEKLE, W. G., SHIELDS, R., GRAVES, T., LEWIS, R. J., SMITH, W. S., LIEBESKIND, D. S., SAVER, J. L. & JOVIN, T. G. 2018. Thrombectomy 6 to 24 Hours after Stroke with a Mismatch between Deficit and Infarct. *New England Journal of Medicine*. Massachussetts Medical Society.

O'SHEA, T. M., AO, Y., WANG, S., REN, Y., CHENG, A. L., KAWAGUCHI, R., SHI, Z., SWARUP, V. & SOFRONIEW, M. V. 2024. Derivation and transcriptional reprogramming of border-forming wound repair astrocytes after spinal cord injury or stroke in mice. *Nature Neuroscience,* 27**,** 1505-1521.

OGAWA, T., KIMOTO, M. & SASAOKA, K. 1989. Purification and properties of a new enzyme, NG, NG-dimethylarginine dimethylaminohydrolase, from rat kidney. *Journal of Biological Chemistry,* 264**,** 10205-10209.

OHAB, J. J., FLEMING, S., BLESCH, A. & CARMICHAEL, S. T. 2006. A neurovascular niche for neurogenesis after stroke. *Journal of neuroscience,* 26**,** 13007-13016.

OLNEY, J. W. 1971. Glutamate-induced neuronal necrosis in the infant mouse hypothalamus: an electron microscopic study. *Journal of Neuropathology & Experimental Neurology,* 30**,** 75-90.

OLVEDA, G. E., BARASA, M. N. & HILL, R. A. 2024. Microglial phagocytosis of single dying oligodendrocytes is mediated by CX3CR1 but not MERTK. *Cell Reports,* 43.

ORECCHIONI, M., GHOSHEH, Y., PRAMOD, A. B. & LEY, K. 2019. Macrophage polarization: different gene signatures in M1 (LPS+) vs. classically and M2 (LPS–) vs. alternatively activated macrophages. *Frontiers in immunology,* 10**,** 1084.

ORTHGIESS, J., GERICKE, M., IMMIG, K., SCHULZ, A., HIRRLINGER, J., BECHMANN, I. & EILERS, J. 2016. Neurons exhibit Lyz2 promoter activity in vivo: Implications for using LysM-Cre mice in myeloid cell research. *European Journal of Immunology,* 46**,** 1529-1532.

PALMIERI, E. M., GONZALEZ-COTTO, M., BASELER, W. A., DAVIES, L. C., GHESQUIÈRE, B., MAIO, N., RICE, C. M., ROUAULT, T. A., CASSEL, T., HIGASHI, R. M., LANE, A. N., FAN, T. W. M., WINK, D. A. & MCVICAR, D. W. 2020. Nitric oxide orchestrates metabolic rewiring in M1 macrophages by targeting aconitase 2 and pyruvate dehydrogenase. *Nature Communications,* 11**,** 698.

PAN, J. & WAN, J. 2020. Methodological comparison of FACS and MACS isolation of enriched microglia and astrocytes from mouse brain. *Journal of Immunological Methods,* 486**,** 112834.

PAN, J., XU, G. & YEUNG, S.-C. J. 2001. Cytochrome c release is upstream to activation of caspase-9, caspase-8, and caspase-3 in the enhanced apoptosis of anaplastic thyroid cancer cells induced by manumycin and paclitaxel. *The Journal of Clinical Endocrinology & Metabolism,* 86**,** 4731-4740.

PARK, L., UEKAWA, K., GARCIA-BONILLA, L., KOIZUMI, K., MURPHY, M., PISTIK, R., YOUNKIN, L., YOUNKIN, S., ZHOU, P., CARLSON, G., ANRATHER, J. & IADECOLA, C. 2017. Brain Perivascular Macrophages Initiate the Neurovascular Dysfunction of Alzheimer Aß Peptides. *Circulation Research,* 121**,** 258-269.

PARSONS, M. W., YOGENDRAKUMAR, V., CHURILOV, L., GARCIA-ESPERON, C., CAMPBELL, B. C., RUSSELL, M. L., SHARMA, G., CHEN, C., LIN, L. & CHEW, B. L. 2024. Tenecteplase versus alteplase for thrombolysis in patients selected by use of perfusion imaging within 4· 5 h of onset of ischaemic stroke (TASTE): a

multicentre, randomised, controlled, phase 3 non-inferiority trial. *The Lancet Neurology*.

PATEL, S. C., JAIN, R. & WAGNER, S. 2008. The Vasculature of the Human Brain. *In:* CONN, P. M. (ed.) *Neuroscience in Medicine*. Totowa, NJ: Humana Press.

PEDRAGOSA, J., MIRÓ-MUR, F., OTXOA-DE-AMEZAGA, A., JUSTICIA, C., RUÍZ-JAÉN, F., PONSAERTS, P., PASPARAKIS, M. & PLANAS, A. M. 2020. CCR2 deficiency in monocytes impairs angiogenesis and functional recovery after ischemic stroke in mice. *J Cereb Blood Flow Metab,* 40**,** S98-s116.

PEDRAGOSA, J., SALAS-PERDOMO, A., GALLIZIOLI, M., CUGOTA, R., MIRÓ-MUR, F., BRIANSÓ, F., JUSTICIA, C., PÉREZ-ASENSIO, F., MARQUEZ-KISINOUSKY, L., URRA, X., GIERYNG, A., KAMINSKA, B., CHAMORRO, A. & PLANAS, A. M. 2018. CNS-border associated macrophages respond to acute ischemic stroke attracting granulocytes and promoting vascular leakage. *Acta Neuropathologica Communications,* 6**,** 76-76.

PEI, L., SHANG, Y., JIN, H., WANG, S., WEI, N., YAN, H., WU, Y., YAO, C., WANG, X. & ZHU, L.-Q. 2014. DAPK1–p53 interaction converges necrotic and apoptotic pathways of ischemic neuronal death. *Journal of Neuroscience,* 34**,** 6546-6556.

PEI, Z., PANG, S. F. & CHEUNG, R. T. F. 2003. Administration of Melatonin After Onset of Ischemia Reduces the Volume of Cerebral Infarction in a Rat Middle Cerebral Artery Occlusion Stroke Model. *Stroke,* 34**,** 770-775.

PEKAROVA, M., KUBALA, L., MARTISKOVA, H., BINO, L., TWAROGOVA, M., KLINKE, A., RUDOLPH, T. K., KUCHTOVA, Z., KOLAROVA, H., AMBROZOVA, G., KUCHTA, R., KADLEC, J. & LOJEK, A. 2013. Asymmetric dimethylarginine regulates the lipopolysaccharide-induced nitric oxide production in macrophages by suppressing the activation of NF-kappaB and iNOS expression. *European Journal of Pharmacology,* 713**,** 68-77.

PERCIE DU SERT, N., HURST, V., AHLUWALIA, A., ALAM, S., AVEY, M. T., BAKER, M., BROWNE, W. J., CLARK, A., CUTHILL, I. C., DIRNAGL, U., EMERSON, M., GARNER, P., HOLGATE, S. T., HOWELLS, D. W., KARP, N. A., LAZIC, S. E., LIDSTER, K., MACCALLUM, C. J., MACLEOD, M., PEARL, E. J., PETERSEN, O. H., RAWLE, F., REYNOLDS, P., ROONEY, K., SENA, E. S., SILBERBERG, S. D., STECKLER, T. & WÜRBEL, H. 2020. The ARRIVE guidelines 2.0: Updated guidelines for reporting animal research. *PLOS Biology,* 18**,** e3000410-e3000410.

PEREGO, C., FUMAGALLI, S. & DE SIMONI, M.-G. 2011. Temporal pattern of expression and colocalization of microglia/macrophage phenotype markers following brain ischemic injury in mice. *Journal of neuroinflammation,* 8**,** 1-20.

PÉREZ, S. & RIUS-PÉREZ, S. 2022. Macrophage Polarization and Reprogramming in Acute Inflammation: A Redox Perspective. *Antioxidants,* 11**,** 1394.

PEREZ-DE-PUIG, I., MIRÓ-MUR, F., FERRER-FERRER, M., GELPI, E., PEDRAGOSA, J., JUSTICIA, C., URRA, X., CHAMORRO, A. & PLANAS, A. M. 2015. Neutrophil recruitment to the brain in mouse and human ischemic stroke. *Acta Neuropathol,* 129**,** 239-57.

PETROVA, E. 2024. *Deciphering the Role of Border-Associated Macrophages in Glioblastoma Development by Using Novel CD206-Transgenic Mouse Models.* University of Zurich.

PEZZI, H. M., NILES, D. J., SCHEHR, J. L., BEEBE, D. J. & LANG, J. M. 2018. Integration of Magnetic Bead-Based Cell Selection into Complex Isolations. *ACS Omega,* 3**,** 3908-3917.

PIAZZA, M., GUILLEMETTE, J. G. & DIECKMANN, T. 2015. Dynamics of nitric oxide synthase–calmodulin interactions at physiological calcium concentrations. *Biochemistry,* 54**,** 1989-2000.

PIKULA, A., BØGER, R. H., BEISER, A. S., MAAS, R., DECARLI, C., SCHWEDHELM, E., HIMALI, J. J., SCHULZE, F., AU, R. & KELLY-HAYES, M. 2009. Association of plasma ADMA levels with MRI markers of vascular brain injury: Framingham offspring study. *Stroke,* 40**,** 2959-2964.

PILIPENKO, V., UPITE, J., REVINA, B. L. & JANSONE, B. 2024. Long-Term Alterations in Motor Skills, Neurogenesis and Astrocyte Numbers following Transient Cerebral Ischemia in Mice. *Medicina,* 60**,** 658.

PIVOVAROVA, N. B. & ANDREWS, S. B. 2010. Calcium – dependent mitochondrial function and dysfunction in neurons. *The FEBS journal,* 277**,** 3622-3636.

PLANAS, A. M. 2018. Role of Immune Cells Migrating to the Ischemic Brain. *Stroke*. Lippincott Williams and Wilkins.

POLFLIET, M. M. J., GOEDE, P. H., VAN KESTEREN-HENDRIKX, E. M. L., VAN ROOIJEN, N., DIJKSTRA, C. D. & VAN DEN BERG, T. K. 2001. A method for the selective depletion of perivascular and meningeal macrophages in the central nervous system. *Journal of Neuroimmunology*. Elsevier.

PÖSEL, C., MÖLLER, K., BOLTZE, J., WAGNER, D.-C. & WEISE, G. 2016. Isolation and Flow Cytometric Analysis of Immune Cells from the Ischemic Mouse Brain. *Journal of Visualized Experiments*.

POSSEL, H., NOACK, H., PUTZKE, J., WOLF, G. & SIES, H. 2000. Selective upregulation of inducible nitric oxide synthase (iNOS) by lipopolysaccharide (LPS) and cytokines in microglia: in vitro and in vivo studies. *Glia,* 32**,** 51-59.

POWERS, W. J., RABINSTEIN, A. A., ACKERSON, T., ADEOYE, O. M., BAMBAKIDIS, N. C., BECKER, K., BILLER, J., BROWN, M., DEMAERSCHALK, B. M. & HOH, B. 2018. 2018 guidelines for the early management of patients with acute ischemic stroke: a guideline for healthcare professionals from the American Heart Association/American Stroke Association. *stroke,* 49**,** e46-e99.

PRICE, C., MENON, D., PETERS, A., BALLINGER, J., BARBER, R., BALAN, K., LYNCH, A., XUEREB, J., FRYER, T. & GUADAGNO, J. 2004. Cerebral neutrophil recruitment, histology, and outcome in acute ischemic stroke: an imaging-based study. *Stroke,* 35**,** 1659-1664.

PRINZ, M., ERNY, D. & HAGEMEYER, N. 2017. Ontogeny and homeostasis of CNS myeloid cells. *Nat Immunol,* 18**,** 385-392.

PRINZ, M., JUNG, S. & PRILLER, J. 2019. Microglia Biology: One Century of Evolving Concepts. *Cell,* 179**,** 292-311.

PULIDO-SALGADO, M., VIDAL-TABOADA, J. M., BARRIGA, G. G.-D., SOLÀ, C. & SAURA, J. 2018. RNA-Seq transcriptomic profiling of primary murine microglia treated with LPS or LPS + IFNγ. *Scientific Reports,* 8**,** 16096.

RAGAVAN, V. N., NAIR, P. C., JARZEBSKA, N., ANGOM, R. S., RUTA, L., BIANCONI, E., GROTTELLI, S., TARAROVA, N. D., RYAZANSKIY, D. & LENTZ, S. R. 2023. A multicentric consortium study demonstrates that dimethylarginine dimethylaminohydrolase 2 is not a dimethylarginine dimethylaminohydrolase. *Nature communications,* 14**,** 3392.

RAJAN, W. D., WOJTAS, B., GIELNIEWSKI, B., MIRÓ-MUR, F., PEDRAGOSA, J., ZAWADZKA, M., PILANC, P., PLANAS, A. M. & KAMINSKA, B. 2020. Defining molecular identity and fates of CNS-border associated macrophages after ischemic stroke in rodents and humans. *Neurobiology of Disease*. Academic Press Inc.

RAMOS-CABRER, P., CAMPOS, F., SOBRINO, T. & CASTILLO, J. 2011. Targeting the ischemic penumbra. *Stroke,* 42**,** S7-S11.

RANSOHOFF, R. M. & CARDONA, A. E. 2010. The myeloid cells of the central nervous system parenchyma. *Nature,* 468**,** 253-262.

RATOVITSKI, E. A., BAO, C., QUICK, R. A., MCMILLAN, A., KOZLOVSKY, C. & LOWENSTEIN, C. J. 1999. An Inducible Nitric-oxide Synthase (NOS)-associated Protein Inhibits NOS Dimerization and Activity *. *Journal of Biological Chemistry,* 274**,** 30250-30257.

RAVINDRAN, A. V., KILLINGSWORTH, M. C. & BHASKAR, S. 2021. Cerebral collaterals in acute ischaemia: Implications for acute ischaemic stroke patients receiving reperfusion therapy. *European Journal of Neuroscience,* 53**,** 1238-1261.

REED, M., KERNDT, C. C. & NICOLAS, D. 2025. Alteplase. *StatPearls*. Treasure Island (FL) ineligible companies. Disclosure: Connor Kerndt declares no relevant financial

relationships with ineligible companies. Disclosure: Diala Nicolas declares no relevant financial relationships with ineligible companies.: StatPearls Publishing Copyright © 2025, StatPearls Publishing LLC.

REICHARD, A. & ASOSINGH, K. 2019. Best Practices for Preparing a Single Cell Suspension from Solid Tissues for Flow Cytometry. *Cytometry Part A,* 95**,** 219-226.

RICOTE, M., HUANG, J. T., WELCH, J. S. & GLASS, C. K. 1999. The peroxisome proliferator-activated receptorγ (PPARγ) as a regulator of monocyte/macrophage function. *Journal of Leukocyte Biology,* 66**,** 733-739.

RIDKER, P. M., EVERETT, B. M., THUREN, T., MACFADYEN, J. G., CHANG, W. H., BALLANTYNE, C., FONSECA, F., NICOLAU, J., KOENIG, W. & ANKER, S. D. 2017. Antiinflammatory therapy with canakinumab for atherosclerotic disease. *New England journal of medicine,* 377**,** 1119-1131.

RITZEL, R. M., PATEL, A. R., GRENIER, J. M., CRAPSER, J., VERMA, R., JELLISON, E. R. & MCCULLOUGH, L. D. 2015. Functional differences between microglia and monocytes after ischemic stroke. *Journal of neuroinflammation,* 12**,** 1-12.

RIVA, M., PAPPADÀ, G. B., PAPADAKIS, M., CUCCIONE, E., CARONE, D., MENENDEZ, V. R., SGANZERLA, E. P. & BERETTA, S. 2012. Hemodynamic monitoring of intracranial collateral flow predicts tissue and functional outcome in experimental ischemic stroke. *Experimental Neurology,* 233**,** 815-820.

RODRIGO, R., FERNANDEZ-GAJARDO, R., GUTIÉRREZ, R., MANUEL MATAMALA, J., CARRASCO, R., MIRANDA-MERCHAK, A. & FEUERHAKE, W. 2013. Oxidative stress and pathophysiology of ischemic stroke: novel therapeutic opportunities. *CNS & Neurological Disorders-Drug Targets (Formerly Current Drug Targets-CNS & Neurological Disorders),* 12**,** 698-714.

ROJO, R., RAPER, A., OZDEMIR, D. D., LEFEVRE, L., GRABERT, K., WOLLSCHEID-LENGELING, E., BRADFORD, B., CARUSO, M., GAZOVA, I. & SÁNCHEZ, A. 2019. Deletion of a Csf1r enhancer selectively impacts CSF1R expression and development of tissue macrophage populations. *Nature communications,* 10**,** 3215.

ROSENZWEIG, S. & CARMICHAEL, S. T. 2013. Age-Dependent Exacerbation of White Matter Stroke Outcomes. *Stroke,* 44**,** 2579-2586.

ROSSITER, S., SMITH, C. L., MALAKI, M., NANDI, M., GILL, H., LEIPER, J. M., VALLANCE, P. & SELWOOD, D. L. 2005. Selective Substrate-Based Inhibitors of Mammalian Dimethylarginine Dimethylaminohydrolase. *Journal of Medicinal Chemistry,* 48**,** 4670-4678.

ROUSSELET, E., KRIZ, J. & SEIDAH, N. 2012. Mouse model of intraluminal MCAO: cerebral infarct evaluation by cresyl violet staining. *Journal of visualized experiments : JoVE,* 69.

RUAN, J. & YAO, Y. 2020. Behavioral tests in rodent models of stroke. *Brain Hemorrhages,* 1**,** 171-184.

RUDI, K. T., HEATHER, L. S., ROBERT, I. W. & PETER, R. D. 2004. The Identification and Characterization of Excitotoxic Nerve-endings in Alzheimer Disease. *Current Alzheimer Research,* 1**,** 11-25.

RUSSO, M. V., LATOUR, L. L. & MCGAVERN, D. B. 2018. Distinct myeloid cell subsets promote meningeal remodeling and vascular repair after mild traumatic brain injury. *Nature immunology,* 19**,** 442-452.

SALIM, T., SERSHEN, C. L. & MAY, E. E. 2016. Investigating the role of TNF-α and IFN-γ activation on the dynamics of iNOS gene expression in LPS stimulated macrophages. *PloS one,* 11**,** e0153289.

SANTISTEBAN, M. M., AHN, S. J., LANE, D., FARACO, G., GARCIA-BONILLA, L., RACCHUMI, G., POON, C., SCHAEFFER, S., SEGARRA, S. G., KÖRBELIN, J., ANRATHER, J. & IADECOLA, C. 2020. Endothelium-Macrophage Crosstalk Mediates Blood-Brain Barrier Dysfunction in Hypertension. *Hypertension.* Lippincott Williams & Wilkins Hagerstown, MD.

SANTISTEBAN, M. M., SCHAEFFER, S., ANFRAY, A., FARACO, G., BREA, D., WANG, G., SOBANKO, M. J., SCIORTINO, R., RACCHUMI, G., WAISMAN, A., PARK, L.,

ANRATHER, J. & IADECOLA, C. 2024. Meningeal interleukin-17-producing T cells mediate cognitive impairment in a mouse model of salt-sensitive hypertension. *Nature Neuroscience,* 27**,** 63-77.
SANZ-MORENO, A., DA SILVA-BUTTKUS, P., TERWEE, C. B., RAESS, M., FUCHS, H., GAILUS-DURNER, V. & HRABĚ DE ANGELIS, M. 2024. Assessment of quality of life and wellbeing in mouse preclinical research – A scoping review. *Neuroscience Applied,* 3**,** 104058.
SARKAR, C. & LIPINSKI, M. M. 2024. Autophagy in neuroinflammation after traumatic brain injury. *Neural Regeneration Research,* 19**,** 951-952.
SAVAGE, C. D., LOPEZ-CASTEJON, G., DENES, A. & BROUGH, D. 2012. NLRP3-inflammasome activating DAMPs stimulate an inflammatory response in glia in the absence of priming which contributes to brain inflammation after injury. *Frontiers in immunology,* 3**,** 288.
SCHAAR, K. L., BRENNEMAN, M. M. & SAVITZ, S. I. 2010. Functional assessments in the rodent stroke model. *Experimental & translational stroke medicine,* 2**,** 1-11.
SCHAEFFER, S. & IADECOLA, C. 2021. Revisiting the neurovascular unit. *Nature Neuroscience,* 24**,** 1198-1209.
SCHALLER, B. & GRAF, R. 2003. Hypothermia and stroke: the pathophysiological background. *Pathophysiology,* 10**,** 7-35.
SCHILLING, M., BESSELMANN, M., LEONHARD, C., MUELLER, M., RINGELSTEIN, E. B. & KIEFER, R. 2003. Microglial activation precedes and predominates over macrophage infiltration in transient focal cerebral ischemia: a study in green fluorescent protein transgenic bone marrow chimeric mice. *Experimental neurology,* 183**,** 25-33.
SCHITTENHELM, L., HILKENS, C. M. & MORRISON, V. L. 2017. ß2 integrins as regulators of dendritic cell, monocyte, and macrophage function. *Frontiers in immunology,* 8**,** 1866.
SCHMITTGEN, T. D. & LIVAK, K. J. 2008. Analyzing real-time PCR data by the comparative CT method. *Nature Protocols,* 3**,** 1101-1108.
SCHONHOFF, A., FIGGE, D., WILLIAMS, G., JURKUVENAITE, A., GALLUPS, N., CHILDERS, G., WEBSTER, J., STANDAERT, D., GOLDMAN, J. & HARMS, A. 2023. Border-associated macrophages mediate the neuroinflammatory response in an alpha-synuclein model of Parkinson disease. *Nature communications,* 14**,** 3754.
SCHROETER, C. B., HERRMANN, A. M., BOCK, S., VOGELSANG, A., EICHLER, S., ALBRECHT, P., MEUTH, S. G. & RUCK, T. 2021. One Brain—All Cells: A Comprehensive Protocol to Isolate All Principal CNS-Resident Cell Types from Brain and Spinal Cord of Adult Healthy and EAE Mice. *Cells,* 10**,** 651.
SCHROETER, M., JANDER, S., WITTE, O. W. & STOLL, G. 1994. Local immune responses in the rat cerebral cortex after middle cerebral artery occlusion. *Journal of neuroimmunology,* 55**,** 195-203.
SCHUHMANN, M. K., KOLLIKOWSKI, A. M., MÄRZ, A. G., BIEBER, M., PHAM, M. & STOLL, G. 2021a. Danger-associated molecular patterns are locally released during occlusion in hyper-acute stroke. *Brain, Behavior, & Immunity-Health,* 15**,** 100270.
SCHUHMANN, M. K., KOLLIKOWSKI, A. M., MÄRZ, A. G., BIEBER, M., PHAM, M. & STOLL, G. 2021b. Danger-associated molecular patterns are locally released during occlusion in hyper-acute stroke. *Brain, Behavior, & Immunity - Health,* 15**,** 100270.
SCHULZE, J., ZIERATH, D., TANZI, P., CAIN, K., SHIBATA, D., DRESSEL, A. & BECKER, K. 2013. Severe stroke induces long-lasting alterations of high-mobility group box 1. *Stroke,* 44**,** 246-248.
SEIFERT, H. A., BENEDEK, G., LIANG, J., NGUYEN, H., KENT, G., VANDENBARK, A. A., SAUGSTAD, J. A. & OFFNER, H. 2017. Sex differences in regulatory cells in experimental stroke. *Cellular immunology,* 318**,** 49-54.
SEKERDAG, E., SOLAROGLU, I. & GURSOY-OZDEMIR, Y. 2018. Cell death mechanisms in stroke and novel molecular and cellular treatment options. *Current neuropharmacology,* 16**,** 1396-1415.

SELVARAJ, U. M., UJAS, T. A., KONG, X., KUMAR, A., PLAUTZ, E. J., ZHANG, S., XING, C., SUDDUTH, T. L., WILCOCK, D. M., TURCHAN-CHOLEWO, J., GOLDBERG, M. P. & STOWE, A. M. 2021. Delayed diapedesis of CD8 T cells contributes to long-term pathology after ischemic stroke in male mice. *Brain, Behavior, and Immunity,* 95**,** 502-513.

SERBINA, N. V., SALAZAR-MATHER, T. P., BIRON, C. A., KUZIEL, W. A. & PAMER, E. G. 2003. TNF/iNOS-producing dendritic cells mediate innate immune defense against bacterial infection. *Immunity,* 19**,** 59-70.

SERDAR, C. C., CIHAN, M., YÜCEL, D. & SERDAR, M. A. 2021. Sample size, power and effect size revisited: simplified and practical approaches in pre-clinical, clinical and laboratory studies. *Biochem Med (Zagreb),* 31**,** 010502.

SERHAN, C. N. & SAVILL, J. 2005. Resolution of inflammation: the beginning programs the end. *Nature Immunology,* 6**,** 1191-1197.

SERRATS, J., SCHILTZ, J. C., GARCÍA-BUENO, B., VAN ROOIJEN, N., REYES, T. M. & SAWCHENKO, P. E. 2010. Dual Roles for Perivascular Macrophages in Immune-to-Brain Signaling. *Neuron.*

SHABAN, A., AL KASAB, S., CHALHOUB, R. M., BASS, E., MAIER, I., PSYCHOGIOS, M.-N., ALAWIEH, A., WOLFE, S. Q., ARTHUR, A. S., DUMONT, T. M., KAN, P., KIM, J.-T., DE LEACY, R., OSBUN, J. W., RAI, A. T., JABBOUR, P., PARK, M. S., CROSA, R. J., MASCITELLI, J. R., LEVITT, M. R., POLIFKA, A. J., CASAGRANDE, W., YOSHIMURA, S., MATOUK, C., WILLIAMSON, R., GORY, B., MOKIN, M., FRAGATA, I., ROMANO, D. G., CHOWDHRY, S. A., MOSS, M., BEHME, D., LIMAYE, K., SPIOTTA, A. M. & SAMANIEGO, E. A. 2023. Mechanical thrombectomy for large vessel occlusion strokes beyond 24 hours. *Journal of NeuroInterventional Surgery,* 15**,** e331-e336.

SHAHID, J., KASHIF, A. & SHAHID, M. K. 2023. A Comprehensive Review of Physical Therapy Interventions for Stroke Rehabilitation: Impairment-Based Approaches and Functional Goals. *Brain Sciences,* 13**,** 717.

SHAPOURI – MOGHADDAM, A., MOHAMMADIAN, S., VAZINI, H., TAGHADOSI, M., ESMAEILI, S. A., MARDANI, F., SEIFI, B., MOHAMMADI, A., AFSHARI, J. T. & SAHEBKAR, A. 2018. Macrophage plasticity, polarization, and function in health and disease. *Journal of cellular physiology,* 233**,** 6425-6440.

SHENG, J., RUEDL, C. & KARJALAINEN, K. 2015. Most Tissue-Resident Macrophages Except Microglia Are Derived from Fetal Hematopoietic Stem Cells. *Immunity.* Cell Press.

SHI, J., HUA, L., HARMER, D., LI, P. & REN, G. 2018. Cre Driver Mice Targeting Macrophages. *In:* ROUSSELET, G. (ed.) *Macrophages: Methods and Protocols.* New York, NY: Springer New York.

SHI, K., TIAN, D.-C., LI, Z.-G., DUCRUET, A. F., LAWTON, M. T. & SHI, F.-D. 2019. Global brain inflammation in stroke. *The Lancet Neurology,* 18**,** 1058-1066.

SHIMADA, I. S., PETERSON, B. M. & SPEES, J. L. 2010. Isolation of Locally Derived Stem/Progenitor Cells From the Peri-Infarct Area That Do Not Migrate From the Lateral Ventricle After Cortical Stroke. *Stroke,* 41**,** e552-e560.

SHOEIBI, S., MAHDIPOUR, E., MOHAMMADI, S., MOOHEBATI, M. & GHAYOUR-MOBARHAN, M. 2021. Treatment of atherosclerosis through transplantation of endothelial progenitor cells overexpressing dimethylarginine dimethylaminohydrolase (DDAH) in rabbits. *International Journal of Cardiology,* 331**,** 189-198.

SIENEL, R. I., KATAOKA, H., KIM, S.-W., SEKER, F. B. & PLESNILA, N. 2022. Adhesion of Leukocytes to Cerebral Venules Precedes Neuronal Cell Death and Is Sufficient to Trigger Tissue Damage After Cerebral Ischemia. *Frontiers in Neurology,* 12.

SIRET, C. 2021. Identification and characterization of a non-conventional CD45 negative perivascular macrophage population within the mouse brain.

SOZMEN, E. G., ROSENZWEIG, S., LLORENTE, I. L., DITULLIO, D. J., MACHNICKI, M., VINTERS, H. V., HAVTON, L. A., GIGER, R. J., HINMAN, J. D. & CARMICHAEL, S. T. 2016. Nogo receptor blockade overcomes remyelination failure after white matter stroke and stimulates functional recovery in aged mice. *Proc Natl Acad Sci U S A,* 113**,** E8453-e8462.

STREMMEL, C., SCHUCHERT, R., WAGNER, F., THALER, R., WEINBERGER, T., PICK, R., MASS, E., ISHIKAWA-ANKERHOLD, H., MARGRAF, A. & HUTTER, S. 2018. Yolk sac macrophage progenitors traffic to the embryo during defined stages of development. *Nature communications,* 9**,** 75.

STROBEL, J., MÜLLER, F., ZOLK, O., ENDRES, B., KÖNIG, J., FROMM, M. F. & MAAS, R. 2013. Transport of asymmetric dimethylarginine (ADMA) by cationic amino acid transporter 2 (CAT2), organic cation transporter 2 (OCT2) and multidrug and toxin extrusion protein 1 (MATE1). *Amino acids,* 45**,** 989-1002.

STUBBE, T., EBNER, F., RICHTER, D., ENGEL, O., KLEHMET, J., ROYL, G., MEISEL, A., NITSCH, R., MEISEL, C. & BRANDT, C. 2013. Regulatory T cells accumulate and proliferate in the ischemic hemisphere for up to 30 days after MCAO. *J Cereb Blood Flow Metab,* 33**,** 37-47.

SUN, J., KE, Z., YIP, S. P., HU, X.-L., ZHENG, X.-X. & TONG, K.-Y. 2014. Gradually increased training intensity benefits rehabilitation outcome after stroke by BDNF upregulation and stress suppression. *BioMed research international,* 2014**,** 925762.

SUN, P., ZHANG, K., HASSAN, S. H., ZHANG, X., TANG, X., PU, H., STETLER, R. A., CHEN, J. & YIN, K.-J. 2020. Endothelium-Targeted Deletion of microRNA-15a/16-1 Promotes Poststroke Angiogenesis and Improves Long-Term Neurological Recovery. *Circulation Research,* 126**,** 1040-1057.

SUNDARAM, K., MATHER, ANDREW R., MARIMUTHU, S., SHAH, PARAG P., SNIDER, ASHLEY J., OBEID, LINA M., HANNUN, YUSUF A., BEVERLY, LEVI J. & SISKIND, LEAH J. 2016. Loss of neutral ceramidase protects cells from nutrient- and energy -deprivation-induced cell death. *Biochemical Journal,* 473**,** 743-755.

SUOFU, Y., CLARK, J., BRODERICK, J., WAGNER, K. R., TOMSICK, T., SA, Y. & LU, A. 2010. Peroxynitrite decomposition catalyst prevents matrix metalloproteinase activation and neurovascular injury after prolonged cerebral ischemia in rats. *Journal of neurochemistry,* 115**,** 1266-1276.

SZUBA, A. & PODGÓRSKI, M. 2006. Asymmetric dimethylarginine (ADMA) a novel cardiovascular risk factor--evidence from epidemiological and prospective clinical trials. *Pharmacol Rep,* 58 Suppl**,** 16-20.

T'JONCK, W., GUILLIAMS, M. & BONNARDEL, J. 2018. Niche signals and transcription factors involved in tissue-resident macrophage development. *Cellular Immunology,* 330**,** 43-53.

TAN, I., DEMCHUK, A., HOPYAN, J., ZHANG, L., GLADSTONE, D., WONG, K., MARTIN, M., SYMONS, S., FOX, A. & AVIV, R. 2009. CT angiography clot burden score and collateral score: correlation with clinical and radiologic outcomes in acute middle cerebral artery infarct. *American Journal of Neuroradiology,* 30**,** 525-531.

TANNAHILL, G., CURTIS, A., ADAMIK, J., PALSSON-MCDERMOTT, E., MCGETTRICK, A., GOEL, G., FREZZA, C., BERNARD, N., KELLY, B. & FOLEY, N. 2013. Succinate is an inflammatory signal that induces IL-1ß through HIF-1α. *Nature,* 496**,** 238-242.

TAROZZO, G., CAMPANELLA, M., GHIANI, M., BULFONE, A. & BELTRAMO, M. 2002. Expression of fractalkine and its receptor, CX3CR1, in response to ischaemia – reperfusion brain injury in the rat. *European Journal of Neuroscience,* 15**,** 1663-1668.

TEERLINK, T., LUO, Z., PALM, F. & WILCOX, C. S. 2009. Cellular ADMA: Regulation and action. *Pharmacological Research,* 60**,** 448-460.

TEN DONKELAAR, H. J., CÖMERT, A., VAN DER VLIET, T., VAN DOMBURG, P. & WESSELING, P. 2020. Vascularization of the Brain and Spinal Cord. *Clinical Neuroanatomy: Brain Circuitry and Its Disorders.* Cham: Springer International Publishing.

THOMALLA, G., SIMONSEN, C. Z., BOUTITIE, F., ANDERSEN, G., BERTHEZENE, Y., CHENG, B., CHERIPELLI, B., CHO, T.-H., FAZEKAS, F. & FIEHLER, J. 2018. MRI-guided thrombolysis for stroke with unknown time of onset. *New England Journal of Medicine,* 379**,** 611-622.

THORED, P., HELDMANN, U., GOMES – LEAL, W., GISLER, R., DARSALIA, V., TANEERA, J., NYGREN, J. M., JACOBSEN, S. E. W., EKDAHL, C. T. & KOKAIA, Z. 2009. Long – term accumulation of microglia with proneurogenic phenotype concomitant with persistent neurogenesis in adult subventricular zone after stroke. *Glia,* 57**,** 835-849.

TOJO, A., WELCH, W. J., BREMER, V., KIMOTO, M., KIMURA, K., OMATA, M., OGAWA, T., VALLANCE, P. & WILCOX, C. S. 1997. Colocalization of demethylating enzymes and NOS and functional effects of methylarginines in rat kidney. *Kidney international,* 52**,** 1593-1601.

TRAN, C. T. L., FOX, M. F., VALLANCE, P. & LEIPER, J. M. 2000. Chromosomal Localization, Gene Structure, and Expression Pattern of DDAH1: Comparison with DDAH2 and Implications for Evolutionary Origins. *Genomics*. Academic Press Inc.

TRAN, C. T. L., LEIPER, J. M. & VALLANCE, P. 2003. The DDAH/ADMA/NOS pathway. *Atherosclerosis Supplements,* 4**,** 33-40.

TSAO, P. S., WANG, B.-Y., BUITRAGO, R., SHYY, J. Y.-J. & COOKE, J. P. 1997. Nitric oxide regulates monocyte chemotactic protein-1. *Circulation,* 96**,** 934-940.

TSOU, C. L., PETERS, W., SI, Y., SLAYMAKER, S., ASLANIAN, A. M., WEISBERG, S. P., MACK, M. & CHARO, I. F. 2007. Critical roles for CCR2 and MCP-3 in monocyte mobilization from bone marrow and recruitment to inflammatory sites. *J Clin Invest,* 117**,** 902-9.

TUO, Q.-Z., ZHANG, S.-T. & LEI, P. 2022. Mechanisms of neuronal cell death in ischemic stroke and their therapeutic implications. *Medicinal Research Reviews,* 42**,** 259-305.

TURNER, R. C., DIPASQUALE, K., LOGSDON, A. F., TAN, Z., NASER, Z. J., HUBER, J. D., ROSEN, C. L. & LUCKE-WOLD, B. P. 2016. The role for infarct volume as a surrogate measure of functional outcome following ischemic stroke. *J Syst Integr Neurosci,* 2.

UEDA, S., KATO, S., MATSUOKA, H., KIMOTO, M., OKUDA, S., MORIMATSU, M. & IMAIZUMI, T. 2003. Regulation of cytokine-induced nitric oxide synthesis by asymmetric dimethylarginine: role of dimethylarginine dimethylaminohydrolase. *Circulation research,* 92**,** 226-233.

UNAL-CEVIK, I., KILINÇ, M., CAN, A., GÜRSOY-ÖZDEMIR, Y. & DALKARA, T. 2004. Apoptotic and necrotic death mechanisms are concomitantly activated in the same cell after cerebral ischemia. *Stroke,* 35**,** 2189-2194.

URRA, X., MIRÓ, F., CHAMORRO, A. & PLANAS, A. M. 2014. Antigen-specific immune reactions to ischemic stroke. *Front Cell Neurosci,* 8**,** 278.

UTZ, S. G., SEE, P., MILDENBERGER, W., THION, M. S., SILVIN, A., LUTZ, M., INGELFINGER, F., RAYAN, N. A., LELIOS, I., BUTTGEREIT, A., ASANO, K., PRABHAKAR, S., GAREL, S., BECHER, B., GINHOUX, F. & GRETER, M. 2020. Early Fate Defines Microglia and Non-parenchymal Brain Macrophage Development. *Cell*. Cell Press.

VALLANCE, P., LEONE, A., CALVER, A., COLLIER, J. & MONCADA, S. 1992. Endogenous Dimethylarginine as an Inhibitor of Nitric Oxide Synthesis. *Journal of Cardiovascular Pharmacology,* 20**,** S60-S62.

VAN DEN BOSSCHE, J., BAARDMAN, J., OTTO, N. A., VAN DER VELDEN, S., NEELE, A. E., VAN DEN BERG, S. M., LUQUE-MARTIN, R., CHEN, H.-J., BOSHUIZEN, M. C. & AHMED, M. 2016. Mitochondrial dysfunction prevents repolarization of inflammatory macrophages. *Cell reports,* 17**,** 684-696.

VAN HOVE, H., MARTENS, L., SCHEYLTJENS, I., DE VLAMINCK, K., POMBO ANTUNES, A. R., DE PRIJCK, S., VANDAMME, N., DE SCHEPPER, S., VAN ISTERDAEL, G., SCOTT, C. L., AERTS, J., BERX, G., BOECKXSTAENS, G. E., VANDENBROUCKE, R. E., VEREECKE, L., MOECHARS, D., GUILLIAMS, M., VAN GINDERACHTER, J. A., SAEYS, Y. & MOVAHEDI, K. 2019. A single-cell atlas of mouse brain macrophages reveals unique transcriptional identities shaped by ontogeny and tissue environment. *Nature Neuroscience*.

VEGA-AVILA, E. & PUGSLEY, M. K. An overview of colorimetric assay methods used to assess survival or proliferation of mammalian cells. Proc West Pharmacol Soc, 2011. 4.

VELLY, L., BOUMAZA, D. & SIMEONE, P. 2018. Cerebral Ischemia: Pathophysiology, Diagnosis, and Management. *In:* ICHAI, C., QUINTARD, H. & ORBAN, J.-C. (eds.) *Metabolic Disorders and Critically Ill Patients: From Pathophysiology to Treatment*. Cham: Springer International Publishing.

VERMA, M., WILLS, Z. & CHU, C. T. 2018. Excitatory Dendritic Mitochondrial Calcium Toxicity: Implications for Parkinson's and Other Neurodegenerative Diseases. *Frontiers in Neuroscience,* 12.

VILLALTA, S. A., NGUYEN, H. X., DENG, B., GOTOH, T. & TIDBALL, J. G. 2009. Shifts in macrophage phenotypes and macrophage competition for arginine metabolism affect the severity of muscle pathology in muscular dystrophy. *Human molecular genetics,* 18**,** 482-496.

VINDEGAARD, N., MUÑOZ-BRIONES, C., EL ALI, H. H., KRISTENSEN, L. K., RASMUSSEN, R. S., JOHANSEN, F. F. & HASSELDAM, H. 2017. T-cells and macrophages peak weeks after experimental stroke: Spatial and temporal characteristics. *Neuropathology,* 37**,** 407-414.

VOLDEN, T. A., REYELTS, C. D., HOKE, T. A., ARIKKATH, J. & BONASERA, S. J. 2015. Validation of Flow Cytometry and Magnetic Bead-Based Methods to Enrich CNS Single Cell Suspensions for Quiescent Microglia. *Journal of Neuroimmune Pharmacology,* 10**,** 655-665.

WAN, H., BRATHWAITE, S., AI, J., HYNYNEN, K. & MACDONALD, R. L. 2021. Role of perivascular and meningeal macrophages in outcome following experimental subarachnoid hemorrhage. *Journal of cerebral blood flow and metabolism : official journal of the International Society of Cerebral Blood Flow and Metabolism*. SAGE PublicationsSage UK: London, England.

WANBY, P., TEERLINK, T., BRUDIN, L., BRATTSTRÖM, L., NILSSON, I., PALMQVIST, P. & CARLSSON, M. 2006. Asymmetric dimethylarginine (ADMA) as a risk marker for stroke and TIA in a Swedish population. *Atherosclerosis,* 185**,** 271-277.

WANG, H.-R., CHEN, M., WANG, F.-L., DAI, L.-H., FEI, A.-H., LIU, J.-F., LI, H.-J., SHEN, S., LIU, M. & PAN, S.-M. 2015. Comparison of therapeutic effect of recombinant tissue plasminogen activator by treatment time after onset of acute ischemic stroke. *Scientific Reports,* 5**,** 1-6.

WANG, L., YAO, C., CHEN, J., GE, Y., WANG, C., WANG, Y., WANG, F., SUN, Y., DAI, M. & LIN, Y. 2022. γδ T cell in cerebral ischemic stroke: characteristic, immunity-inflammatory role, and therapy. *Frontiers in neurology,* 13**,** 842212.

WANG, L., ZHENG, J., ZHAO, S., WAN, Y., WANG, M., BOSCO, D. B., KUAN, C.-Y., RICHARDSON, J. R. & WU, L.-J. 2024. CCR2⁺ monocytes replenish border-associated macrophages in the diseased mouse brain. *Cell Reports,* 43.

WANG, R., LIU, Y., YE, Q., HASSAN, S. H., ZHAO, J., LI, S., HU, X., LEAK, R. K., ROCHA, M., WECHSLER, L. R., CHEN, J. & SHI, Y. 2020a. RNA sequencing reveals novel macrophage transcriptome favoring neurovascular plasticity after ischemic stroke. *Journal of Cerebral Blood Flow & Metabolism,* 40**,** 720-738.

WANG, R., PU, H., YE, Q., JIANG, M., CHEN, J., ZHAO, J., LI, S., LIU, Y., HU, X., ROCHA, M., JADHAV, A. P., CHEN, J. & SHI, Y. 2020b. Transforming Growth Factor Beta-Activated Kinase 1–Dependent Microglial and Macrophage Responses Aggravate Long-Term Outcomes After Ischemic Stroke. *Stroke,* 51**,** 975-985.

WANG, S., ZHANG, H. & XU, Y. 2016. Crosstalk between microglia and T cells contributes to brain damage and recovery after ischemic stroke. *Neurological research,* 38**,** 495-503.

WATTANANIT, S., TORNERO, D., GRAUBARDT, N., MEMANISHVILI, T., MONNI, E., TATARISHVILI, J., MISKINYTE, G., GE, R., AHLENIUS, H., LINDVALL, O., SCHWARTZ, M. & KOKAIA, Z. 2016. Monocyte-Derived Macrophages Contribute to Spontaneous Long-Term Functional Recovery after Stroke in Mice. *The Journal of Neuroscience,* 36**,** 4182-4195.

WEITBRECHT, L., BERCHTOLD, D., ZHANG, T., JAGDMANN, S., DAMES, C., WINEK, K., MEISEL, C. & MEISEL, A. 2021. CD4+ T cells promote delayed B cell responses in the ischemic brain after experimental stroke. *Brain, Behavior, and Immunity,* 91**,** 601-614.

WEN, R. X., SHEN, H., HUANG, S. X., WANG, L. P., LI, Z. W., PENG, P., MAMTILAHUN, M., TANG, Y. H., SHEN, F. X. & TIAN, H. L. 2020. P2Y6 receptor inhibition aggravates ischemic brain injury by reducing microglial phagocytosis. *CNS Neuroscience & Therapeutics,* 26**,** 416-429.

WETZEL, M. D., GAO, T., STANLEY, K., COOPER, T. K., MORRIS, S. M. & AWAD, A. S. 2020. Enhancing kidney DDAH-1 expression by adenovirus delivery reduces ADMA and ameliorates diabetic nephropathy. *American Journal of Physiology-Renal Physiology,* 318**,** F509-F517.

WIEROŃSKA, J. M., CIEŚLIK, P. & KALINOWSKI, L. 2021. Nitric oxide-dependent pathways as critical factors in the consequences and recovery after brain ischemic hypoxia. *Biomolecules,* 11**,** 1097.

WINKLER, I. G., SIMS, N. A., PETTIT, A. R., BARBIER, V., NOWLAN, B., HELWANI, F., POULTON, I. J., VAN ROOIJEN, N., ALEXANDER, K. A. & RAGGATT, L. J. 2010. Bone marrow macrophages maintain hematopoietic stem cell (HSC) niches and their depletion mobilizes HSCs. *Blood, The Journal of the American Society of Hematology,* 116**,** 4815-4828.

WLODARCZYK, A., LØBNER, M., CÉDILE, O. & OWENS, T. 2014. Comparison of microglia and infiltrating CD11c+ cells as antigen presenting cells for T cell proliferation and cytokine response. *Journal of Neuroinflammation,* 11**,** 57.

WOO, M.-S., YANG, J., BELTRAN, C. & CHO, S. 2016a. Cell Surface CD36 Protein in Monocyte/Macrophage Contributes to Phagocytosis during the Resolution Phase of Ischemic Stroke in Mice. *The Journal of biological chemistry,* 291**,** 23654-23661.

WOO, M.-S., YANG, J., BELTRAN, C. & CHO, S. 2016b. Cell Surface CD36 Protein in Monocyte/Macrophage Contributes to Phagocytosis during the Resolution Phase of Ischemic Stroke in Mice*. *Journal of Biological Chemistry,* 291**,** 23654-23661.

WORTHMANN, H., CHEN, S., MARTENS-LOBENHOFFER, J., LI, N., DEB, M., TRYC, A. B., GOLDBECKER, A., DONG, Q., KIELSTEIN, J. T. & BODE-BÖGER, S. M. 2011. High plasma dimethylarginine levels are associated with adverse clinical outcome after stroke. *Journal of Atherosclerosis and Thrombosis,* 18**,** 753-761.

WU, C.-H., CHEN, T.-L., CHEN, T.-G., HO, W.-P., CHIU, W.-T. & CHEN, R.-M. 2003. Nitric Oxide Modulates Pro- and Anti-inflammatory Cytokines in Lipopolysaccharide-Activated Macrophages. *Journal of Trauma and Acute Care Surgery,* 55**,** 540-545.

WYNN, T. A. & VANNELLA, K. M. 2016. Macrophages in tissue repair, regeneration, and fibrosis. *Immunity,* 44**,** 450-462.

XIE, L., LI, W., HERSH, J., LIU, R. & YANG, S.-H. 2019a. Experimental ischemic stroke induces long-term T cell activation in the brain. *Journal of Cerebral Blood Flow & Metabolism,* 39**,** 2268-2276.

XIE, M., WANG, Q., WU, T. H., SONG, S. K. & SUN, S. W. 2011. Delayed axonal degeneration in slow Wallerian degeneration mutant mice detected using diffusion tensor imaging. *Neuroscience,* 197**,** 339-47.

XIE, Q.-W., CHO, H. J., CALAYCAY, J., MUMFORD, R. A., SWIDEREK, K. M., LEE, T. D., DING, A., TROSO, T. & NATHAN, C. 1992. Cloning and Characterization of Inducible Nitric Oxide Synthase from Mouse Macrophages. *Science,* 256**,** 225-228.

XIE, W., ZHU, T., DONG, X., NAN, F., MENG, X., ZHOU, P., SUN, G. & SUN, X. 2019b. HMGB1-triggered inflammation inhibition of notoginseng leaf triterpenes against cerebral ischemia and reperfusion injury via MAPK and NF-κB signaling pathways. *Biomolecules,* 9**,** 512.

XING, C., ARAI, K., LO, E. H. & HOMMEL, M. 2012. Pathophysiologic cascades in ischemic stroke. *International Journal of Stroke,* 7**,** 378-385.

XIONG, X.-Y., LIU, L. & YANG, Q.-W. 2016. Functions and mechanisms of microglia/macrophages in neuroinflammation and neurogenesis after stroke. *Progress in neurobiology,* 142**,** 23-44.

YAGHI, S., WILLEY, J. Z., CUCCHIARA, B., GOLDSTEIN, J. N., GONZALES, N. R., KHATRI, P., KIM, L. J., MAYER, S. A., SHETH, K. N. & SCHWAMM, L. H. 2017. Treatment and outcome of hemorrhagic transformation after intravenous alteplase in acute ischemic stroke: a scientific statement for healthcare professionals from the American Heart Association/American Stroke Association. *Stroke,* 48**,** e343-e361.

YAN, T., CHOPP, M. & CHEN, J. 2015. Experimental animal models and inflammatory cellular changes in cerebral ischemic and hemorrhagic stroke. *Neuroscience bulletin,* 31**,** 717-734.

YANG, D., YANG, L., CAI, J., HU, X., LI, H., ZHANG, X., ZHANG, X., CHEN, X., DONG, H. & NIE, H. 2021. A sweet spot for macrophages: focusing on polarization. *Pharmacological Research***,** 105576.

YANG, T., GUO, R. & ZHANG, F. 2019. Brain perivascular macrophages: Recent advances and implications in health and diseases. *CNS Neuroscience & Therapeutics*. Blackwell Publishing Ltd.

YANG, Y., SALAYANDIA, V. M., THOMPSON, J. F., YANG, L. Y., ESTRADA, E. Y. & YANG, Y. 2015. Attenuation of acute stroke injury in rat brain by minocycline promotes blood-brain barrier remodeling and alternative microglia/macrophage activation during recovery. *Journal of Neuroinflammation*. BioMed Central Ltd.

YANG, Z., YUE, Y.-J., HUANG, W.-C., ZHUANG, X.-M., CHEN, Z.-T. & XING, M. 2008. Importance of the Ionic Nature of Ionic Liquids in Affecting Enzyme Performance. *The Journal of Biochemistry,* 145**,** 355-364.

YAO, Q., CUI, Q., LIU, J., XIE, X., JIANG, T., WANG, H., ZHAO, Z., ZHAO, W., DU, X., LAI, B., XIAO, L. & WANG, N. 2023. Free fatty acids stabilize integrin β₁ via S-nitrosylation to promote monocyte–endothelial adhesion. *Journal of Biological Chemistry,* 299.

YI, J.-H. & HAZELL, A. S. 2006. Excitotoxic mechanisms and the role of astrocytic glutamate transporters in traumatic brain injury. *Neurochemistry international,* 48**,** 394-403.

YILMAZ, G., ARUMUGAM, T. V., STOKES, K. Y. & GRANGER, D. N. 2006. Role of T Lymphocytes and Interferon-γ in Ischemic Stroke. *Circulation,* 113**,** 2105-2112.

YILMAZ, G. & GRANGER, D. N. 2008. Cell adhesion molecules and ischemic stroke. *Neurological research,* 30**,** 783-793.

YILMAZ, G. & GRANGER, D. N. 2010. Leukocyte recruitment and ischemic brain injury. *Neuromolecular Med,* 12**,** 193-204.

YU, N., ZHAO, Y., WANG, P., ZHANG, F., WEN, C. & WANG, S. 2025. Changes in border-associated macrophages after stroke: Single-cell sequencing analysis. *Neural Regeneration Research,* 21**,** 346-356.

YUAN, D., LIU, C., WU, J. & HU, B. 2018. Nest – building activity as a reproducible and long – term stroke deficit test in a mouse model of stroke. *Brain and behavior,* 8**,** e00993.

ZACHRISON, K. S., SCHWAMM, L. H., XU, H., MATSOUAKA, R., SHAH, S., SMITH, E. E., XIAN, Y., FONAROW, G. C. & SAVER, J. 2021. Frequency, Characteristics, and Outcomes of Endovascular Thrombectomy in Patients With Stroke Beyond 6 Hours of Onset in US Clinical Practice. *Stroke,* 52**,** 3805-3814.

ZARRUK, J. G., GREENHALGH, A. D. & DAVID, S. 2018. Microglia and macrophages differ in their inflammatory profile after permanent brain ischemia. *Experimental Neurology,* 301**,** 120-132.

ZBESKO, J. C., STOKES, J., BECKTEL, D. A. & DOYLE, K. P. 2023. Targeting foam cell formation to improve recovery from ischemic stroke. *Neurobiology of Disease,* 181**,** 106130.

ZEISEL, A., MUNOZ-MANCHADO, A. B., CODELUPPI, S., LONNERBERG, P., LA MANNO, G., JUREUS, A., MARQUES, S., MUNGUBA, H., HE, L., BETSHOLTZ, C., ROLNY, C., CASTELO-BRANCO, G., HJERLING-LEFFLER, J. & LINNARSSON, S. 2015. Cell types

in the mouse cortex and hippocampus revealed by single-cell RNA-seq. *Science*. American Association for the Advancement of Science.

ZHANG, Q., JIA, M., WANG, Y., WANG, Q. & WU, J. 2022. Cell death mechanisms in cerebral ischemia–reperfusion injury. *Neurochemical research,* 47**,** 3525-3542.

ZHANG, W., ZHAO, J., WANG, R., JIANG, M., YE, Q., SMITH, A. D., CHEN, J. & SHI, Y. 2019. Macrophages reprogram after ischemic stroke and promote efferocytosis and inflammation resolution in the mouse brain. *CNS Neuroscience & Therapeutics,* 25**,** 1329-1342.

ZHANG, Y., PARK, Y. S. & KIM, I.-B. 2023. A distinct microglial cell population expressing both CD86 and CD206 constitutes a dominant type and executes phagocytosis in two mouse models of retinal degeneration. *International Journal of Molecular Sciences,* 24**,** 14236.

ZHAO, Y., MA, X., ZHOU, Y., XIE, J., LIU, X. & ZHAO, Y. 2021. DDAH-1, via regulation of ADMA levels, protects against ischemia-induced blood-brain barrier leakage. *Laboratory Investigation,* 101**,** 808-823.

ZHAO, Y., WEI, Z. Z., LEE, J. H., GU, X., SUN, J., DIX, T. A., WEI, L. & SHAN, P. Y. 2020. Pharmacological hypothermia induced neurovascular protection after severe stroke of transient middle cerebral artery occlusion in mice. *Experimental Neurology,* 325**,** 113133.

ZHENG, K., LIN, L., JIANG, W., CHEN, L., ZHANG, X., ZHANG, Q., REN, Y. & HAO, J. 2021. Single-cell RNA-seq reveals the transcriptional landscape in ischemic stroke. *Journal of Cerebral Blood Flow & Metabolism***,** 0271678X211026770.

ZHENG, L., DING, J., WANG, J., ZHOU, C. & ZHANG, W. 2016. Effects and mechanism of action of inducible nitric oxide synthase on apoptosis in a rat model of cerebral ischemia – reperfusion injury. *The Anatomical Record,* 299**,** 246-255.

ZHENG, Z., WANG, S., WU, C., CAO, Y., GU, Q., ZHU, Y., ZHANG, W. & HU, W. 2022. Gut microbiota dysbiosis after traumatic brain injury contributes to persistent microglial activation associated with upregulated Lyz2 and shifted tryptophan metabolic phenotype. *Nutrients,* 14**,** 3467.

ZHOU, L., LI, F., XU, H.-B., LUO, C.-X., WU, H.-Y., ZHU, M.-M., LU, W., JI, X., ZHOU, Q.-G. & ZHU, D.-Y. 2010. Treatment of cerebral ischemia by disrupting ischemia-induced interaction of nNOS with PSD-95. *Nature medicine,* 16**,** 1439-1443.

ZHU, Z.-D., YE, J.-M., FU, X.-M., WANG, X.-C., YE, J.-Y., WU, X.-R., HUA, P., LIAO, Y.-Q., XUAN, W. & DUAN, J.-L. 2019. DDAH2 alleviates myocardial fibrosis in diabetic cardiomyopathy through activation of the DDAH/ADMA/NOS/NO pathway in rats. *International Journal of Molecular Medicine,* 43**,** 749-760.

ZIS, O., ZHANG, S., DOROVINI-ZIS, K., WANG, L. & SONG, W. 2015. Hypoxia signaling regulates macrophage migration inhibitory factor (MIF) expression in stroke. *Molecular neurobiology,* 51**,** 155-167.